CARPATHIAN JOURNAL OF FOOD SCIENCE AND TECHNOLOGY

CJFST 17(3)
2025

Technical University of Cluj Napoca
U.T.Press Publishing House

Carpathian Journal of Food Science and Technology

Print : ISSN 2066-6845
Online : ISSN 2344-5459
ISSN-L 2066-6845

Vol. 17, Nr.(3) 2025

UNIVERSITATEA TEHNICĂ DIN CLUJ-NAPOCA

Technical University of Cluj Napoca
U.T.Press Publishing House

CARPATHIAN JOURNAL OF FOOD SCIENCE AND TECHNOLOGY
ISSN-L 2066 -6845

journal homepage: **http://chimie-biologie.ubm.ro/carpathian_journal/index.html**

CARPATHIAN JOURNAL OF FOOD SCIENCE AND TECHNOLOGY

journal homepage: **http://chimie-biologie.ubm.ro/carpathian_journal/index.html**

CONTENT

CARPATHIAN JOURNAL OF FOOD SCIENCE AND TECHNOLOGY

journal homepage: **http://chimie-biologie.ubm.ro/carpathian_journal/index.html**

Research Article

NUTRITIONAL ANALYSIS, *IN VITRO* AND *IN SILICO* STUDIES ON ANTIOXIDANT AND ANTI-DIABETIC POTENTIAL OF *COCCINIA GRANDIS* L. FRUIT

Manikandaselvi, S[1], Surya, M[1], Thinagarbabu, R[2], and Vadivel, V[3]✉

[1]PG & Research Department of Biochemistry, Sengamala Thayaar Educational Trust Women's College (Autonomous, Affiliated to Bharathidasan University, Tiruchirappalli), Mannargudi, Tamilnadu, India.
[2]Department of Chemistry, School of Chemical and Biotechnology, SASTRA Deemed University, Thanjavur, Tamilnadu, India.
[3]Chemical Biology Lab (ASK-II-409), School of Chemical and Biotechnology, SASTRA Deemed University, Thanjavur, Tamilnadu, India.
✉vadivel@carism.sastra.ac.in

https://doi.org/10.34302/crpjfst/2025.17.3.1

Article history:
Received:
March 10th , 2025
Accepted:
August 23th, 2025

Keywords:
Coccinia grandis;
Nutrients, Antioxidant;
Anti-diabetic;
HPTLC;
In silico.

ABSTRACT

Coccinia, commonly known as ivy gourd (Coccinia grandis L.), is a medicinal food plant with numerous health benefits. It is widely used in traditional medicine, particularly in Ayurveda and folk medicine, for managing conditions such as inflammation and oxidative stress. The precise biochemical mechanisms through which Coccinia exerts its therapeutic effects are not yet fully understood, and there is limited research on its long-term safety and potential side effects. Investigating these lesser-reported aspects of Coccinia is crucial for filling the knowledge gaps, developing natural therapeutics, and validating its role in modern healthcare. The aim of this study was to evaluate the nutritional profile, antioxidant activity, and the anti-diabetic potential of the fruit of Coccinia grandis L. through in vitro and in silico approaches. From the study, the fruit extract of C. grandis possesses a good nutritional profile like protein (1.2 g/100 g) and fiber (1.2 g/100 g). There are 38 ± 0.45 µg/g of total alkaloids, 84 ± 0.25 µg/g of total phenols and 98 ± 0.31 µg/g of total flavonoids in the fruit extract. When compared to standard (butylated hydroxytoluene), the extract exhibits the strong antioxidant activity of 94.4% at 250 µg/mL. The results of the in vitro assay highlighted that the extract has low inhibition activity on α-amylase (4.6% at 250 µg/mL) and moderate inhibition against α-glucosidase (53% at 250 µg/mL) when compared to the standard acarbose. The phytoconstituent quercetin was quantified in the fruit extract (0.06 % w/w) using HPTLC method. Further, the computational in silico analysis of quercetin binding affinity with alpha amylase (-15.866 kcal/mol) and alpha glucosidase glucosidase (-14.147 kcal/mol) enzymes and the in silico results are consistent with in vitro experimental data. The study concluded that the fruit of C. grandis presents a good source of nutrients with antioxidant and anti-diabetic potentials.

1. Introduction

Coccinia grandis L., commonly known as ivy gourd or scarlet gourd, has been studied for its medicinal and nutritional properties. Earlier studies have reported that it is rich in vitamins such as vitamin A, C, and B-complex, along with essential minerals like iron, calcium, phosphorus, and potassium. It also contains dietary fiber and essential amino acids, making it a valuable functional food (Tardy *et al*., 2020). The fruit is known to contain various phytochemicals, including flavonoids, alkaloids, terpenoids, saponins, tannins, and phenolics. Additionally, it has a high content of β-carotene, lutein, and lycopene, contributing to its antioxidant properties (Lee and Joo, 2022). Pharmacologically, *C. grandis* exhibits significant antioxidant activity due to the presence of polyphenols and flavonoids, which contribute to its free-radical scavenging ability. Studies have also shown its anti-diabetic potential, as it helps lower blood glucose levels by enhancing insulin sensitivity. Furthermore, the fruit possesses anti-inflammatory and hepatoprotective properties, helping to reduce oxidative stress-related inflammation. It also demonstrates antimicrobial activity against various pathogens, making it a promising candidate for medicinal applications (Pekamwar *et al*., 2013).

Despite the existing research on *C. grandis*, further studies are necessary to provide a more comprehensive understanding of its health benefits. There is a need for detailed nutritional profiling to validate its role as a functional food. *In vitro* and *in silico* studies will help assess its antioxidant and anti-diabetic potential more precisely. *In vitro* studies will evaluate antioxidant properties, along with anti-diabetic potential through α-amylase and α-glucosidase inhibition assays. *In silico* studies will include molecular docking and computational analysis to predict the interaction of bioactive compounds with diabetic and oxidative stress-related targets.

Moreover, many traditional uses of *C. grandis* lack scientific validation, creating a gap between traditional knowledge and scientific evidence. This study aims to bridge that gap by providing robust scientific data supporting its medicinal applications. Additionally, identifying bioactive compounds in the fruit could lead to the development of natural antioxidant and anti-diabetic supplements, contributing to pharmaceutical and nutraceutical advancements. By conducting nutritional analysis, *in vitro*, and *in silico* studies, this work aims to establish *C. grandis* as a scientifically validated functional food with significant antioxidant and anti-diabetic properties.

The International Diabetes Federation published statistics in 2021 that showed 1 in 11 persons in Southeast Asia had diabetes mellitus (DM), with over half (46 million) going untreated. By 2045, it is expected that there will be 152 million diabetics, underscoring the urgent need for all-encompassing regional action. With an 8.3% prevalence rate, one in seven (90 million) persons worldwide have diabetes in India alone (IDF, 2024). According to the WHO report in 2021, noncommunicable diseases accounted for seven out of the ten top causes of death worldwide. DM is one of the seven noncommunicable diseases (WHO, 2024). DM is a group of metabolic disorders of carbohydrates, proteins, and lipids. It is characterized by hyperglycemia resulting from a defect in beta cells of the pancreas. This leads to affect insulin secretion, failure of insulin action, or both. Untreated conditions, DM can cause microvascular complications such as damage to the eye, which can cause retinopathy; damage to the kidney, which leads to nephropathy; and damage to the nerve, which results in neuropathy. It can also cause macrovascular complications such as myocardial infarction, cerebrovascular accident, thrombosis, and atherosclerosis (Deshpande *et al*., 2008). DM is categorized into two types: insulin-dependent (IDDM) and non-insulin-dependent (NIDDM) DM. IDDM is called type I DM, and NIDDM is known as type II DM (CDC, 2024). Due to immunological reactions occurring in type I DM, beta cells are selectively destroyed. There

is no insulinogenic stimuli that causes hypoinsulinemia. Juvenile suffering from type I DM. The imbalance between blood sugar absorption and insulin secretion causes type II DM. Type II DM is controlled by delaying postprandial hyperglycemia via secretion of insulin from beta cells, optimizing insulin action, lowering glucogenesis and gluconeogenesis, interfering with carbohydrate metabolism, blocking ATP-gated potassium channels, stimulating peroxisome proliferator-activated receptor activity (PPAR), and modifying glucagon-like peptide-1 (GLP-1) (Casa-Villegas *et al*., 2018). In the present study, therapeutic approaches for controlling postprandial hyperglycemia are designed to inhibit gastrointestinal carbohydrate-hydrolyzing enzymes alpha amylase and alpha glucosidase. Alpha amylase has the property of cleaving the glycosidic linkage of alpha (1,4) in homo- and heteropolysaccharides to produce oligosaccharides (Ogunyemi *et al*., 2022).

Alpha-glucosidase breaks the alpha 1,4-glycosidic linkage in oligosaccharides to produce monosaccharides (Patil *et al*., 2017). Only monosaccharides are absorbed via the intestinal mucosa cells. When carbohydrate-hydrolyzing enzymes are blocked, blood glucose concentrations fall, diminishing the insulin requirement (Ekor, 2014), which can assist to prevent the production of Advanced Glycation End-Products (AGEs). AGEs are a risk factor for complications of DM. Most of the pharmacotherapeutics reveal that DM is not a cure because the rising prevalence causes difficulties. The use of phytotherapeutics as a supplement to existing pharmaceuticals to control DM and its complications (Bharti *et al*., 2018). Many herbs have anti-diabetic properties. *Coccinia grandis* (Cucurbitaceae), also have revealed that this plant is capable of acting as an antipyretic, analgesic, antibacterial, anti-inflammatory, antidiabetic, antioxidant, antidyslipidemic, antituberculosis, antieczema, antiulcer, hepatoprotective, anticancer, and antitussive agent (DAF, 2016). There are few studies on the phytoconstituents that are responsible for suppressing the carbohydrate-digesting enzymes that control DM. A balanced diet throughout life supports growth, development, and aging while also lowering the risk of chronic disease, resulting in general health and well-being (Patil *et al*., 2017). Experimental screening processes are time-consuming and expensive; computational screening has received a lot of attention in recent years. Hence, in this present study, the anti-diabetic effect of a flavonoid compound identified by HPTLC from the fruits of *C. grandis* L. was determined by an experimental *in vitro* and *in silico* approach to explore the antidiabetic targets by inhibiting alpha amylase and alpha glucosidase enzymes.

2. Materials and methods

2.1. Collection of plant material

Fruits of *C. grandis* L. were collected from Thanjavur, Tamil Nadu, India. To get rid of contaminants, the collected fruits cleaned several times with distilled water. After being, sliced fruits were spread out on plain paper and allowed to dry in the shade for ten days at room temperature, then ground into a fine powder using a grinder mixture. Powered materials used in further work.

2.2. Preparation of the extract

The 100 g of powdered material of *C. grandis* fruit was extracted with 1 L sterile distilled water at room temperature for 24 h, filtered using Whatman 42 filter paper and freeze dried. The powder was dissolved in 80 percent hydro-alcohol with a know concentration, again filterd and used for further experiments.

2.3. Determination of moisture content

The moisture content of a sample was determined by weighing the sample before and after drying in a preheated oven at 105°C for 6 hours. The sample was first weighed along with the crucible, and then after drying, it was cooled in a desiccator to prevent moisture absorption. The moisture content was calculated by comparing the weight loss, which

corresponds to the amount of water evaporated from the sample.

2.4. Determination of total ash

The crucible was weighed and placed over the electric burner and the crucible was partially opened. The sample was charred with initial expulsion of smoke and the crucible was placed in a muffle furnace and heated to 600^{o}C and kept for 2 hours. Organic matter in the sample burnt to left the minerals. The crucible was removed from the furnace and cooled it in a dessicator to room temperature and weighed.

2.5. Nutritional profile

Determination of total carbohydrates (Morris, 1948), total proteins (Lowry *et al.,* 1952), total lipids (Bligh and Dyer, 1959), total energy value (Sands, 1974) and total fibers (Maynard, 1970) were carried out in the *C. grandis* fruit sample. The total carbohydrate content was determined using the anthrone method. In the presence of sulfuric acid, carbohydrates undergo hydrolysis into simple sugars, which further dehydrate to form furfural derivatives. These derivatives react with anthrone to produce a blue-green complex that was measured spectrophotometrically at 620 nm.

The Lowry method is based on the reaction of protein molecules with the Folin–Ciocalteu reagent. The method involves two steps: first, proteins react with copper ions under alkaline conditions (Biuret reaction), forming a complex; second, the complex undergoes reduction by the Folin-Ciocalteu reagent, producing a blue color that was measured spectrophotometrically at 660 nm. The intensity of the color was proportional to the protein concentration in the sample. The Bligh and Dyer method was used as solvent extraction technique for determining total lipids in *C. grandis* fruit. Chloroform-methanol-water system was employed to efficiently extract lipids while minimizing non-lipid contaminants. Lipids were extracted into the chloroform phase, separated from the aqueous phase, and quantified gravimetrically. The total lipid content was calculated by the formula: Total Lipid Content (%) = (Weight of lipids / Weight of sample) x 100. Total energy value was calculated using the formula: Total Energy (kcal/100g) = (Carbohydrates x 4) + (Proteins x 4) + (Lipids x 9).

The determination of total fibre was done by the Maynard method (1970), which involves sequential digestion of the sample with acid and alkali to remove digestible components, leaving behind the indigestible fiber fraction. First, a weighed sample (2-5 g) was boiled in 1.25% sulfuric acid for 30 minutes, maintaining a constant volume by adding hot distilled water as needed. The mixture was then filtered through Whatman No. 41 filter paper or a sintered glass crucible, and the residue was washed thoroughly with hot distilled water. The residue was then transferred to a beaker containing 1.25% sodium hydroxide and boiled for another 30 minutes before being filtered and washed again with hot distilled water, 95% ethanol, and acetone to remove non-fiber components. The purified residue was dried at 105°C for 6 hours, cooled in a desiccator, and weighed (W_1). To determine the fiber content, the dried residue was ashed in a muffle furnace at 550°C for 4–5 hours, cooled in a desiccator, and reweighed (W_2). The total fiber content was calculated using the formula: Total Fiber Content (%) = ((W1−W2) / Sample weight) x 100.

2.6. Phytochemical analysis

Alkaloids content of aqeous fruit extract was estimated by Evans (2002) method. Phenol content was determined using modified Folin-Ciocalteu's method described by Singleton and Rossi (1965). Flavonoid content measured through aluminium chloride method observed by Chang et al. (2002).

2.7. *In vitro* assays

The antioxidant capacity of the fruit sample is tested based on the procedure described by Evans (1991), which utilizes the DPPH method. In this method, a 0.1 mM DPPH solution was prepared and mixed with the fruit

extract. The DPPH radical, initially violet in color, was reduced by antioxidants present in the sample, leading to a color change towards colorlessness or light yellow. After incubating the mixture for 30 minutes at room temperature, the absorbance was measured at 517 nm using a spectrophotometer. The degree of scavenging activity was calculated by comparing the decrease in absorbance to a control.

The alpha-amylase inhibitory activity of the fruit sample was determined by using 4-nitrophenyl α-D-glucopyranoside (CNPG) as a substrate (Gella et al., 1997). The method involves incubating the fruit extract with alpha-amylase, followed by the addition of CNPG. If the enzyme is inhibited, the hydrolysis of CNPG was reduced, leading to a lower production of 4-nitrophenol. The amount of 4-nitrophenol released was measured spectrophotometrically, and the inhibition of alpha-amylase was quantified by comparing the absorbance with a control sample. The percentage inhibition was calculated using the formula:

$$\text{Inhibition Percentage} = \frac{\text{Absorbance of control} - \text{Absorbance of sample}}{\text{Absorbance of control}} \times 100$$

The inhibition of alpha-glucosidase was evaluated by measuring the ability of the fruit extract to inhibit the hydrolysis of p-nitrophenyl-α-D-glucopyranoside (p-NPG) (Dewi et al., 2007). The fruit extract was incubated with alpha-glucosidase and p-NPG, and the resulting release of p-nitrophenol was measured at a specific wavelength of 405 nm. A decrease in the amount of p-nitrophenol indicates the inhibition of the enzyme. The percentage inhibition of alpha-glucosidase was calculated by comparing the absorbance values.

2.8. HPTLC analysis

Hydrochloroform extract was prepared for HPTLC analysis to identify both hydrophilic and lipophilic compounds present in the sample. The aqueous extract was used to obtain hydrophilic bioactive compounds, such as polyphenols and flavonoids, which are often responsible for the observed antioxidant and anti-diabetic activity. Analyzing the aqueous extract was used in the *in vitro* assays and hence HPTLC test is crucial because it allows for the identification and profiling of the compounds responsible for the biological effects observed, such as alpha-amylase, alpha-glucosidase inhibition and free radical scavenging. This analysis not only helps correlate the chemical composition with the bioactivity but also ensures the quality control and standardization of the extract by providing a chemical fingerprint.

The test sample (0.5 g) was taken in a fractional funnel with 50 mL of water and added chloroform to extract. After shaking, the chloroform fraction was collected and dried and the dried sample was dissolved in chloroform again. The standard quercetin sample was prepared using 20 mg of quercetin in 10 mL of methanol and 1 mL of standard was diluted to 10 mL. Linomat5 (CAMAG) applicator was used for applying 1 to 4 µL of standard and 5 to 25 µL of sample to a precoated silica gel 60 F254 HPTLC plates (Merck) with a uniform thickness of 0.2 mm. The plate was developed in the Toluene: Ethyl acetate: Formic acid (5:4:1) solvent system to a distance of 8 cm. CAMAG TLC Scanner3 was used to scan the plate at 254 nm and CAMAG REPROSTAR3 was used to observe the plate under UV light at 254 nm and 366 nm.

2.9. *In silico* studies (molecular docking)

GalaxyDockWeb (2024), an online web tool was used for flexible docking study. The structure of the identified compound (Quercetin; $C_{15}H_{10}O_7$; M.W: 302.23) by HPTLC in the fruit extract taken as a ligand and its 3D coordinate was downloaded (Figure1) from the PubChem database to check the binding affinity with the carbohydrate hydrolyzing enzymes of alpha-amylase and alpha-glucosidase. The 3D crystal structures of alpha-amylase (PDB ID: 2QV4) and alpha-glucosidase (PDB ID: 5NN5) were downloaded from the PDB database. Using Biovia Discovery Studio Client 2021, the target

proteins were prepared by eliminating ligands and other non-receptor entities that might occupy surrounding space. Water was removed from the crystal structures to refine them. In the Discovery Studio Visualiser (DSV), 3D structures of protein targets created and saved in PDB format. The number and bond length of hydrogen bonds and binding amino acid residues were visualized in the form of a 2D interaction using the Discovery studio visualizer after docking.

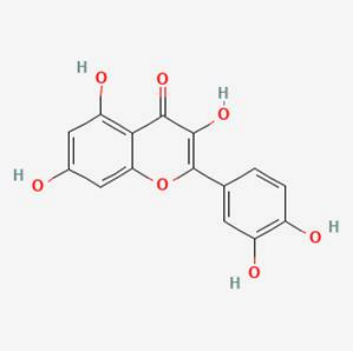

Figure 1. Chemical structure of quercetin (PubChem ID: 5280343).

3. Results and discussion

3.1. Nutritional profile

The rate of absorption and the quality of food are determined by the amount of moisture available in the food. The reported moisture value (3.2%) indicates that the fruits could be stored at room temperature for a long time (Table 1). The amount of minerals likely to be found in food substances is largely determined by the amount of ash present in the food. The reported value of ash (2.8 g/100 g) indicated that *C. grandis* fruit is a good source of minerals. Protein-rich diets are shown to be an effective weight-loss tool, hence sustained satiety is essential for promoting weight loss and inducing a negative energy balance (Moon and Koh, 2020). According to the analysis report, the current test sample of *C. grandis* fruits contains proteins (1.2 g/100 g), lipids (0.2 g/100 g) and carbohydrates (3.1 g/100 g). In addition, *C. grandis* is also identified to contain high-fiber sources (1.2 g/100 g). Increased fiber consumption has also been linked to a lower risk of metabolic syndrome and factors that raise the risk of heart disease and diabetes (Lattimer and Haub, 2010). Hence, *C. grandis* fruit may be added to our daily diets to reduce the risk of diseases like heart and diabetes.

Table 1. Proximate and Nutritional profiles in the extract.

S. No.	Constituents	Quantity
1.	Moisture	3.2 %
2.	Ash	2.8 g/100 g
3.	Proteins	1.2 g/100 g
4.	Lipids	0.2 g/100 g
5.	Carbohydrates	3.1 g/100 g
6.	Fibre	1.2 g/100 g
7.	Energy	19 kcal

Table 2. Organic constituents present in the extract. Values are mean ± S.D (n = 3).

S. No.	Organic constituents	Quantity (µg/g)
1.	Total alkaloids	38 ± 0.45
2.	Total flavonoids	98 ± 0.31
3.	Total phenols	84 ± 0.25

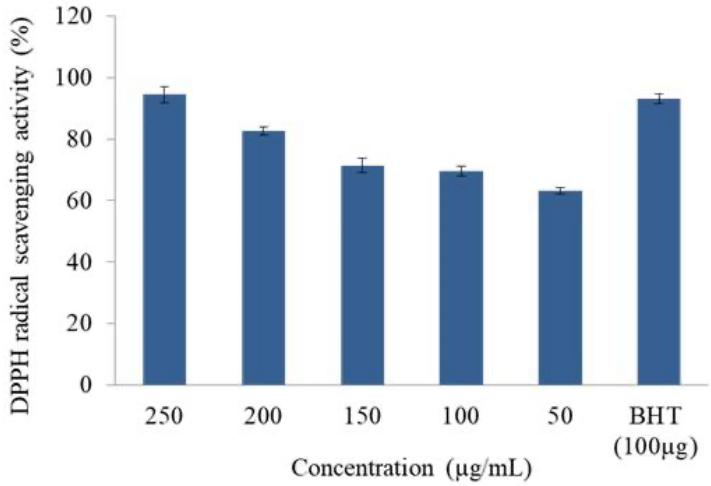

Figure 2. Free radical-scavenging capacities of the *C. grandis* fruit extract.

3.2. Phytochemical analysis

Total alkaloids, phenolics, and flavonoids content showed in Table 2. Heavy metal atoms in Dragendorff reagents bind with the nitrogen atoms of alkaloids to produce ionic complex. Thiourea and bismuth of nitric acid medium form a yellow bismuth complex with the ionic compound (Raal *et al.,* 2020). Based on the fact, alkaloid content reported as (38 ± 0.45 µg/g) and it can contribute to various health benefits, such as anti-inflammatory, analgesic and anti-cancer properties. Some alkaloids also have the potential to regulate blood sugar levels, improve digestion and support the immune system. However, while alkaloids can provide therapeutic effects, they must be consumed in controlled amounts, as excessive intake can lead to toxicity. Phenolics reacts with Folin-Ciocalteu reagent to form blue chromophore that was quantitatively measured and the maximum absorption of chromophore based on pholic concentration found in the extract (84 ± 0.25 µg/g). C-4 keto groups of flavonoid reacts with aluminium chloride to forms acid stable yellow complex (Pérez *et al.*, 2023). Consider these mechanism, *C. grandis* fruit extract showed profound amount of flavonoids (98 ± 0.31 µg/g). Phenolic acid and flavonoids are antioxidants found in plants. These antioxidants can nutralize the activity of free radicals to produce chelated metal complex.

3.3. *In vitro* antioxidant assay

The phenolic compounds act as reducing agents, hydrogen donors and singlet oxygen quenchers and have the redox property which are crucial role for their antioxidant activity and they also can chelate metals (Deshpande *et al*., 2008). The DPPH method used to unraveling the free radical scavenging activity of *C. grandis* L. fruit extract. Depends on electron-transfer reaction, DPPH (2,2-diphenyl-1-picryl-hydrazyl-hydrate) produces violet colour in alcohol. This free radicals reduced in the presence of phonolics and flavonoids in the fruit extract to form yellow solution, which comprehensively indicates the free radicals are quenched (Baliyan *et al.,* 2022). The absorpance of the extract observed and reported

in Figure 2 as the percent in dry weight extract µg/mL. When compared to BHT (93.1% at 100 µg/mL), the extract exhibited the significant free radical scavenging activity at 250 µg/mL of 94.4%. At 250 µg/mL, the extract had the significant total phenolics and flavonoids content, as well as the highest free radical-scavenging activity of 94.4%. Hence, this delved study strongly proved that *C. grandis* L fruit extract possesses efficient antioxidant properties.

3.4. *In vitro* anti-diabetic assay

At 250 µg/mL, the extract had 4.6% inhibition against α-amylase and its inhibitory activity on alpha-amylase was comparable to that of standard acarbose (3.6% at 100 µg/mL) (Table 3). The phenolic and flavonoid compounds in the *C. grandis* fruit extract competatively inhibit the alpha-amylase activity by competitively binding to its active site, preventing the enzyme from breaking down starch, and potentially altering its structure, thereby reducing starch digestion. Alpha-amylase involved in several biological activities, including the digestion of carbohydrates. Many crude drugs reduce alpha-amylase activity (Kalita *et al*., 2018). Natural α-amylase inhibitors slow down the digestion of carbohydrates, which lowers blood glucose absorption and consequently leads to postprandial hyperglycemia. Polyphenolic compounds are abundant in plants and have attracted a lot of attention because of their inhibitory activity against digestive enzymes, which is achieved by the presence of hydroxyl groups in polyphenolic structures (Grundy *et al*., 2016). Two mechanistic pathways have been proposed for alpha-amylase inhibition: (i) the formation of an enzyme-inhibitor complex and (ii) reducing the rate of glucose diffusion from the active site by slowing the digestion and absorption of carbohydrates and viscous water-soluble dietary fibres (Alqahtani *et al*., 2019). The inhibitory activity of *C. grandis* fruit extract against alpha-amylase enzyme is represented in Table 3. Inhibition of alpha-amylase activity found to be increasing in a dose-dependent manner.

Table 3. Alpha-amylase inhibition assay of the extract. Values are mean ± S.D (n = 3)

S. No.	Concentration (µg /mL)	% Inhibition
1	250	4.6 ± 0.7
2	200	4.4 ± 1.7
3	150	3.4 ± 1.0
4	100	2.1 ± 0.7
5	50	1.6 ± 0.6
6	Acarbose (100 µg)	3.6 ± 1.5

Table 4. Alpha-glucosidase inhibition assay of the extract. Values are mean ± S.D (n = 3)

S. No.	Concentration (µg /mL)	% Inhibition
1	250	53 ± 0.67
2	200	45 ± 0.43
3	150	37 ± 0.46
4	100	26 ± 0.62
5	50	13 ± 0.15
6	Acarbose (100 µg)	44 ± 0.47

Alpha-glucosidase is a membrane-bound enzyme that catalyses the conversion of oligosaccharides to glucose and is found in the epithelium of the small intestine. Inhibition of the alpha-glucosidase enzyme essential for the control the conversion of glucose from oligosaccharides. The conversion committed for the control of diabetes (Gong *et al*., 2020). Inhibition of alpha-glucosidase enzyme depends on the hydrogen scavenging capacity because the hydrogen is required for hydrolysis of the alpha-(1→4)-glycosidic linkage. As a result, the inhibitors prevent the binding of hydrogen ion to the catalytic site of the enzyme (Alqahtani *et al*., 2019; Ansari and Khodagholi, 2013). The α-glucosidase inhibitory activity of the aqueous extract of *C. grandis* L. fruits extract shown in Table 4. As a result, the fruit extract found to have moderate inhibitory activity against the alpha-glucosidase enzyme. The percentage inhibition of *C. grandis* fruit extract at 50-250 µg/mL concentrations showed a dose-dependent increase in percentage inhibition (13-53%). Hence, the inhibition activity of fruit extract of *C. grandis* against alpha-glucosidase would delay carbohydrate degradation that results in a decrease glucose absorption and a reduction in the postprandial blood glucose level. Standard acarbose (100 µg/mL) showed 44% α-glucosidase inhibitory activity. In comparison to acarbose, this study indicates that the extract of *C.grandis* possesses a very formidable inhibitor activity against the enzymes alpha-amylase and alpha-glucosidase.

3.5. HPTLC analysis

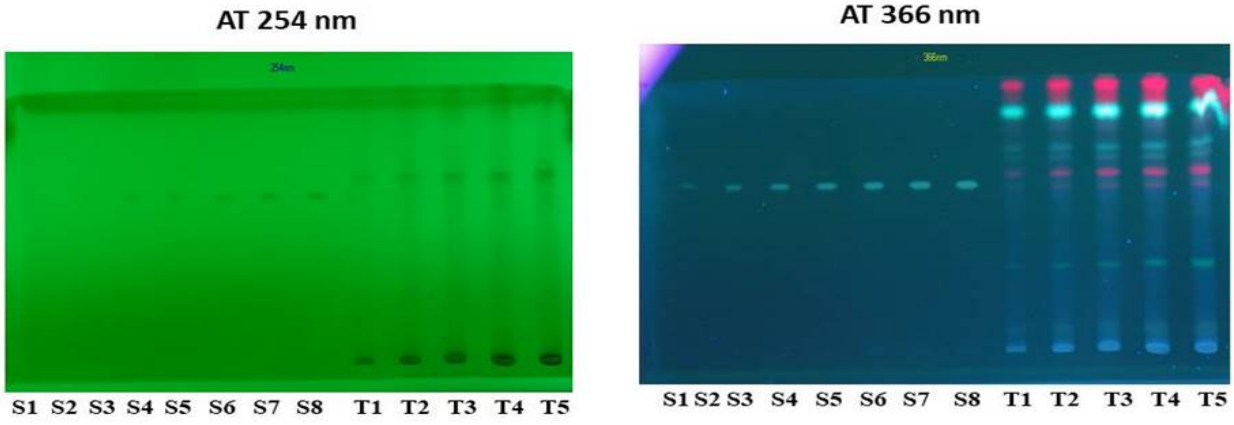

S1-S8: 1 to 4µl of Standard Quercetin; T1-T5: 5 to 25µl of sample Solution

A band R_f value of 0.61 corresponding to Quercetin is visible in test solution tracks

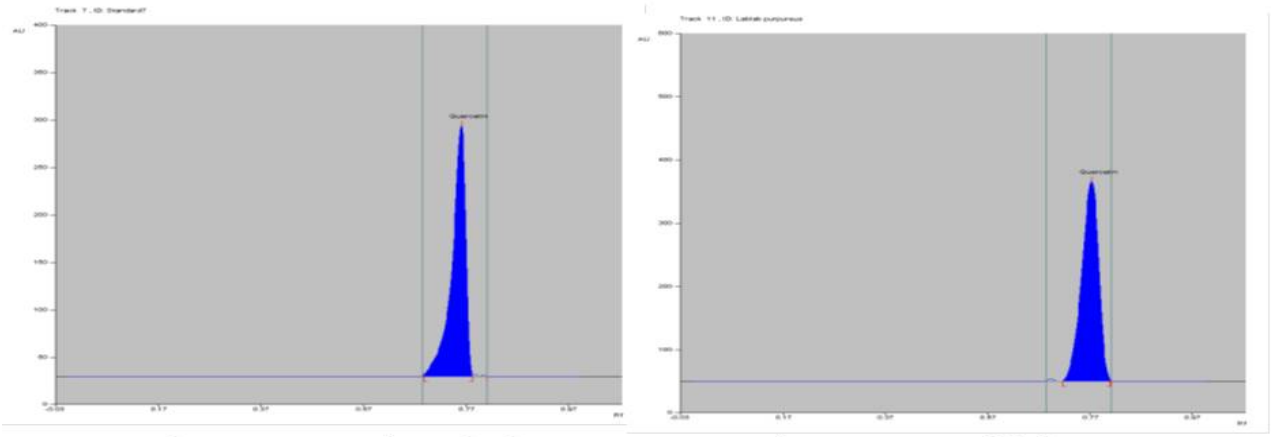

Chromatogram of standard

Chromatogram of fruit extract

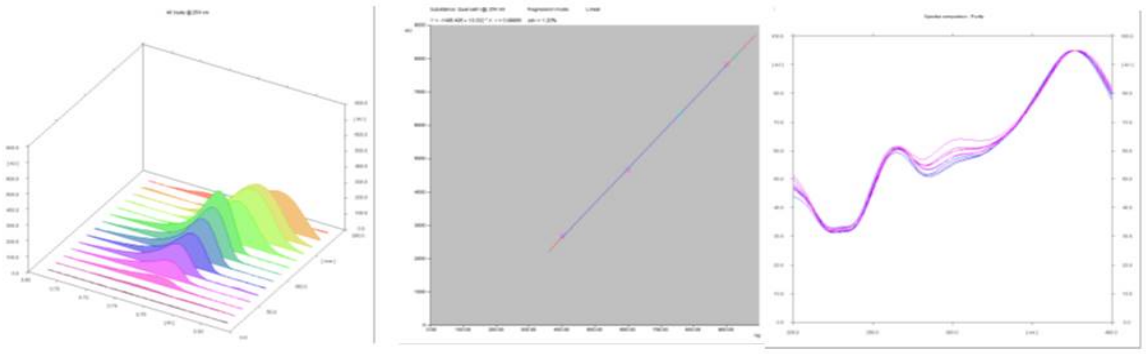

Figure 3. Identification and quantification of quercetin in *C. grandis* fruit extract.

The mobile phase used for the HPTLC investigation was Toluene: Ethyl acetate: Formic acid with the 5:4:1 ratio found to be suitable to furnish sharp, compact and intense peak at R_f = 0.60 (Figure 3). This analysis helped to separate the most abundant compound, quercetin in the extract. The peaks of the standard and the extract compared by aligning each other at wavelength 254 nm. The regression/correlation coefficient (r) were obtained as Regression via Height, Y = -27.8 + 0.2; r = 0.99 & sdv = 1.4; Regression via Area, Y = -501.2 + 3.8; r = 0.99 & sdv = 0.46. The (%) recovery for quercetin in the extract was found as 0.06% w/w.

3.6. Molecular docking studies

Cartoon diagrams of quercetin bound alpha-amylase and alpha-glucosidase structures and 2D representation of various interactions between the quercetin and active site residues of enzymes are shown in Figures 4a & b and Figures 6a & b, respectively. The drug quercetin exhibited good inhibitory binding affinities against two human carbohydrate metabolic enzymes alpha-amylase (-15.866 kcal/mol) and alpha-glucosidase (-14.147 kcal/mol). The binding pose of the quercetin molecule and its interacting residues within the catalytic site of alpha-amylase is shown in Figure 5c. Based on the previous research report of alpha-amylase crystal structure, it possesses three important catalytic residues, Asp197, Glu233, and Asp300 in the active site of alpha-amylase. According to a computational docking study, the alpha-amylase showed six hydrogen bond interactions between the amino acid residues including the catalytic residues reported earlier and the quercetin drug. The donor hydroxy groups of quercetin molecule showed hydrogen bond interactions with the residues of Thr163, Lys200, Asp300, and Glu233 with the distances of 2.98, 2.90, 3.07, and 2.72 & 3.1 Å, respectively. The quercetin molecule also involved as an acceptor to have hydrogen bond interaction with a distance of 3.48Å to amino acid Lys200. Proença *et al.*(2019), reported similar hydrogen bond interactions for other flavonoid compounds with alpha-amylase in his study. Apart from these interactions, quercetin molecule identified as hydrophobic core owing to its aromatic rings present in the basic skeleton of the structure and also it contributed significantly to have the interactions at the active site by contacting the residues of Trp58,Trp59, Tyr62,Tyr151, His299, Arg195, Ser199, and Val234. Interesting to note that few special type interactions like π…alkyl interactions (Drug…Leu162, Leu165, and Ala198), π…π T-shaped interactions (His201), π…sigma interactions (Ile235) and π…Anion interactions (Glu233) also contributed significantly to the drug binding affinity and stabilize the drug molecule at the active site of alpha-amylase.

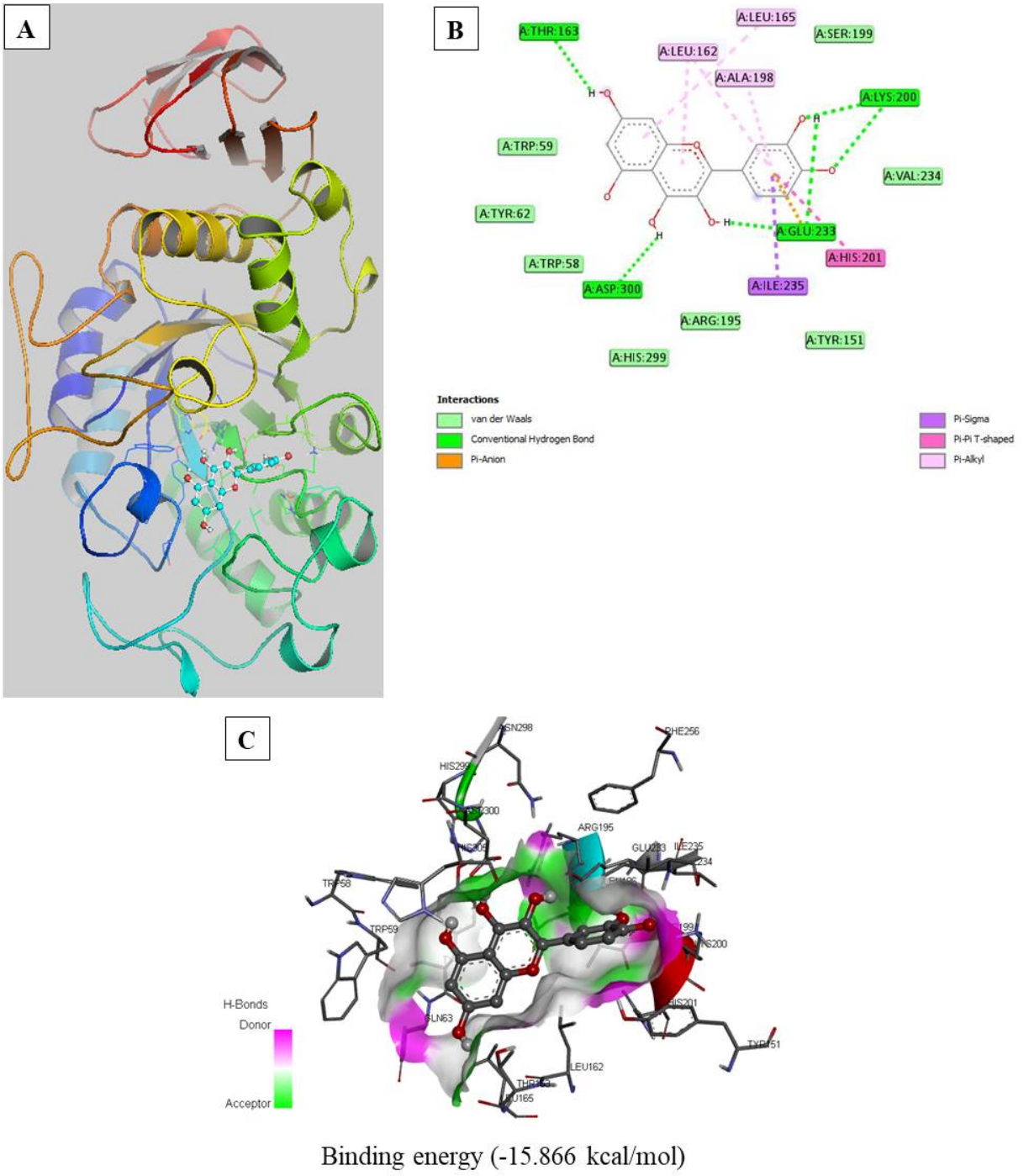

Figure 4. (a) Binding pose of quercetin in the catalytic site of alpha-amylase. (b) Two dimensional representation of quercetin with interacting residues of alpha-amylase. (c) Binding mode of quercetin along with active residues of alpha-amylase at the active site. Here pink, green and white colours represent the donor, acceptor, and hydrophobic regions, respectively.

A similar computational docking study for quercetin against the alpha-glucosidase enzyme, which is another carbohydrate metabolic enzyme secreted in the intestine was also done. The docked pose of quercetin in the active site of alpha-glucosidase is shown in Figure 5a and a two-dimensional representation of various intermolecular interactions between the quercetin and alpha-glucosidase is shown in Figure 5b. Observation of docked pose in the

alpha-glucosidase active site showed five hydrogen bonds with various receptor residues (Asp282, Asp404, Asp616, and Arg600).

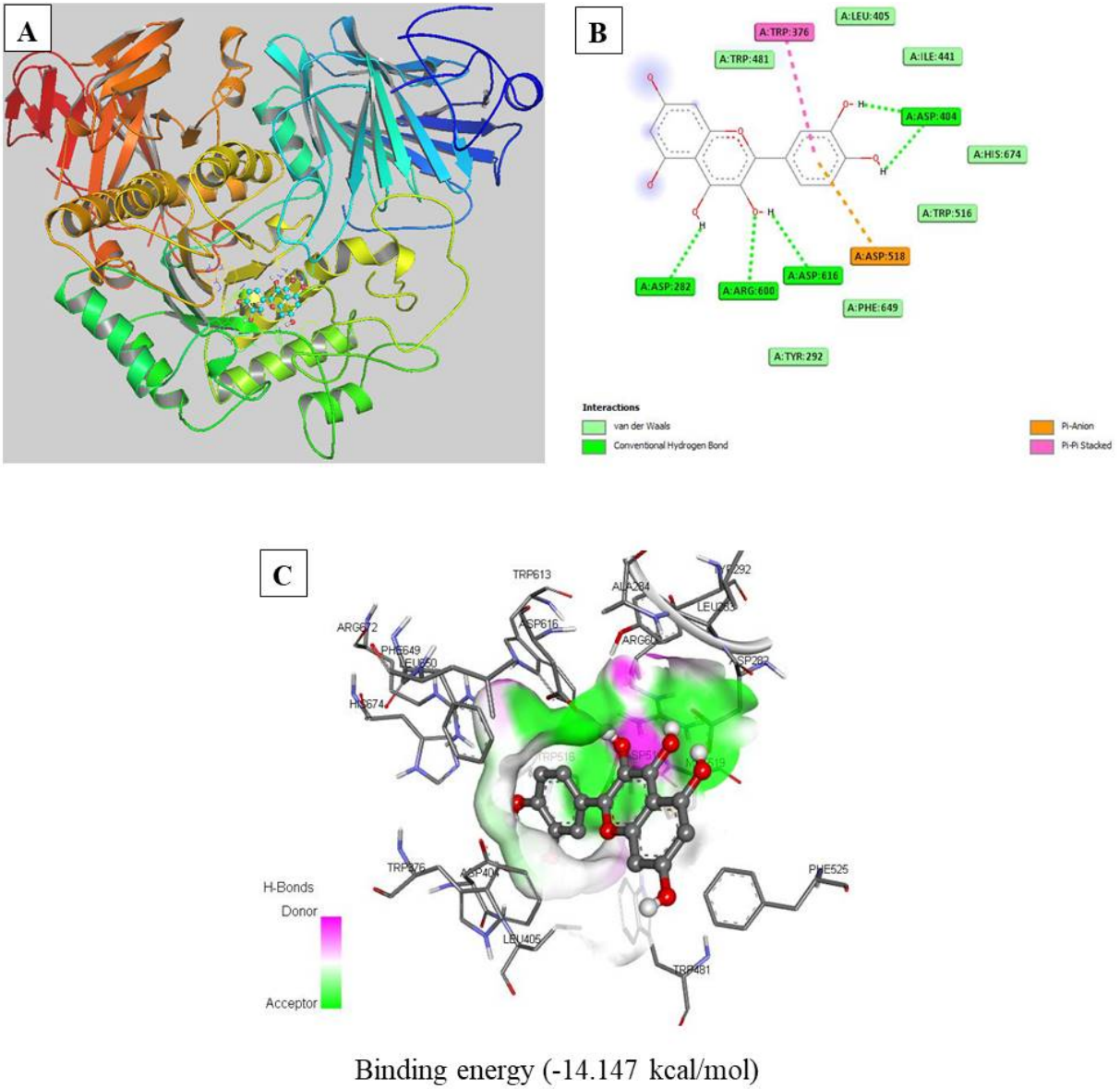

Figure 5. (a) Binding pose of quercetin in the catalytic site of alpha-glucosidase. (b) Two-dimensional representation of quercetin with interacting residues of alpha-glucosidase. (c) Binding mode of quercetin along with active residues of alpha- glucosidase at the active site. Here, pink, green, and white colours represent the donor, acceptor, and hydrophobic regions, respectively

Many hydroxy groups of quercetin donate the hydrogens to form hydrogen bonds by interacting the alpha-glucosidase residues of Asp282, Asp616, and Asp404 with the distances of 2.52, 2.71, and 2.50 & 2.72Å, respectively. Similarly, quercetin also accepts two hydrogen bonds from the residues of Arg600 and His674 with distances of 2.7 and 3.3Å, respectively. Apart from these non-bonded interactions, a few residues of alpha-glucosidase namely Tyr292, Phe649, Trp516, His674, Ile441, Leu405, and Trp481 are also contributing vander Waals short contacts with the quercetin molecule and helps to fit the drug well at the active site. Interestingly, few special types of interactions π…anion (between drug &

Asp518) and π…π stacking interaction (between drug & Trp376) also significantly contribute the energy to drug stability and anti-diabetic activity. Hence, the drug quercetin extracted from *C. grandis* fruit demonstrated significant inhibitory activity against human carbohydrate metabolic enzymes alpha-amylase and alpha-glucosidase and it was actively pronounced as an anti-diabetic agent through *in vitro* and *in-silico* molecular docking studies.

4. Conclusions

The comprehensive study proved that *C. grandis*, is one of the highest nutrient such as carbohydrates, proteins and lipids containing fruit which possess the most valuable phytochemical Quercetin with the high medicinal potency. From the study, the fruit extract of *C. grandis* possesses a good nutritional profile such as nutrients, ash and fibre content. The amounts of individual phytoconstituents, alkaloids, phenols, and flavonoids were identified as rich in the *C. grandis* fruit extract. The extract exhibits the strong free radical scavenging ability due to the presence of active phytoconstituents such as phenols and flavonoids. The *in vitro* assay highlighted that the the extract has inhibition activity on alpha-amylase and alpha-glucosidase. The antioxidants reduce oxidative stress and inflammation, improve insulin sensitivity, and helps to regulate blood sugar level. As the results of present meticulous studies, phytoconstituents quercetin molecule in the *C. grandis* fruit extract was proved to possess the strong inhibitory activity against alpha-amylase and alpha-glucosidase enzymes by *in-silico* approach. Thus, quercetin present in the current plant extract proved to possess the *in vitro* anti-diabetic activity and in these aspects are also taken into account while developing novel alpha-amylase and alpha-glucosidase inhibitors.

5. References

Alqahtani, A.S., Hidayathulla, S., Rehman, M.T., ElGamal, A.A., Al-Massarani, S., Razmovski-Naumovski, V., Alqahtani, M.S., El Dib, R.A., AlAjmi, M.F. (2019). Alpha-amylase and Alpha-glucosidase enzyme inhibition and antioxidant potential of 3-oxolupenal and katononic acid isolated from *Nuxiaoppositi folia*. *Biomolecules*, 10 (1), 61. DOI: 10.3390/biom10010061.

Ansari, N., Khodagholi, F. (2013). Natural products as promising drug candidates for the treatment of Alzheimer's disease: molecular mechanism aspect. *Current Neuropharmacology*. 11 (4), 414–429. DOI: 10.2174/1570159X11311040005.

Baliyan, S., Mukherjee, R., Priyadarshini, A., Vibhuti, A., Gupta, A., Pandey, R.P., Chang, C.M. (2022). Determination of antioxidants by DPPH radical scavenging activity and quantitative phytochemical analysis of *Ficus religiosa*. *Molecules* (Basel). 27 (4), 1326. DOI: 10.3390/molecules27041326.

Bharti, S. K., Krishnan, S., Kumar, A., Kumar, A. (2018). Anti-diabetic phytoconstituents and their mode of action on metabolic pathways. *Therapeutic Advances in Endocrinology and Metabolism*, 9 (3), 81–100. DOI: 10.1177/2042018818755019.

Bligh, E. G., Dyer, W. J. (1959). A repid method of total lipid extraction and purification. *Canadian Journal of Biochemistry and Physiology*, 8 (37), 911-917.

Casa-Villegas, M., Marín-Navarro, J., Polaina, J. (2018). Amylases and related glycoside hydrolases with transglycosylation activity used for the production of isomalt oligosaccharides. *Amylase*, 2 (1), 17-29. DOI: 10.1515/amylase-2018-0003.

CDC, 2024. Available online at www.cdc.gov/diabetes/php/data-research.

Chang, C., Yang, M., Wen, H., Chern, J. (2002). Estimation of total flavonoid content in propolis by two complementary colorimetric methods. *Journal of Food Drug Analaysis*, 10, 178-182.

DAF (2016). Accessed from online: https://www.daf.qld.gov.au/__data/assets/pdf_file/0009/68616/IPA-Ivy-Gourd-

Risk_Assessment.pdf, accessed on 12-02-2025.

Deshpande, A.D., Harris-Hayes, M., Schootman, M. (2008). Epidemiology of diabetes and diabetes-related complications. *Physical Therapy*, 88 (11), 1254–1264. DOI: 10.2522/ptj.20080020.

Dewi, R.T., Iskandar, Y.M., Hanafi, M., Kardono, L.B., Angelina, M., Dewijanti, I.D., Banjarnahor, S.D. (2007). Inhibitory effect of koji *Aspergillus terreus* on alpha-glucosidase activity and postprandial hyperglycemia. *Pakistan Journal of Biological Sciences*, 10 (18), 3131–3135. DOI: 10.3923/pjbs.2007.3131.3135.

GalaxyDockWeb (2024). Avaialble online at http://galaxy.seoklab.org/cgi-bin/submit.cgi?type=DOCK.

Ekor, M. (2014). The growing use of herbal medicines: Issues relating to adverse reactions and challenges in monitoring safety. *Frontiers in Pharmacology*, 4, 177. DOI: 10.3389/fphar.2013.00177.

Evans, W.C. Trease and Evans Pharmacognosy, 15th Ed. Edinburgh, UK: WB Saunders, 2002.

Gella, F.J., Gubern, G., Vidal, R., Canalias, F. (1997). Determination of total and pancreatic a-amylase in human serum with 2-chloro-4- nitrophenyl-a-D-maltotrioside as substrate. *Clinica Chimica Acta*, 259, 147–160.

Gong, L., Feng, D., Wang, T., Ren, Y., Liu, Y., Wang, J. (2020). Inhibitors of α-amylase and α-glucosidase: Potential linkage for whole cereal foods on prevention of hyperglycemia. Food Science & Nutrition, 8 (12), 6320–6337. DOI: 10.1002/fsn3.1987.

Grundy, M.M., Edwards, C.H., Mackie, A.R., Gidley, M.J., Butterworth, P.J., Ellis, P.R. (2016). Re-evaluation of the mechanisms of dietary fibre and implications for macronutrient bioaccessibility, digestion, and postprandial metabolism. *The British Journal of Nutrition*, 116 (5), 816–833. DOI: 10.1017/S0007114516002610.

IDF (2024). Available online at https://idf.org/news/who-searo-wdd24-event.

Kalita, D., Holm, D.G., LaBarbera, D.V., Petrash, J.M., Jayanty, S.S. (2018). Inhibition of α-glucosidase, α-amylase, and aldose reductase by potato polyphenolic compounds. *PloS one*, 13 (1), e0191025. DOI: 10.1371/journal.pone.0191025.

Lattimer, J.M., Haub, M.D. (2010). Effects of dietary fiber and its components on metabolic health. *Nutrients*, 2 (12), 1266–1289. DOI: 10.3390/nu2121266.

Lee, I.Y., Joo, N. (2022). Identification and quantification of key phytochemicals, phytohormones, and antioxidant properties in *Coccinia grandis* during fruit ripening. *Antioxidants (Basel)*, 11 (11), 2218. DOI: 10.3390/antiox11112218.

Lowry, O.H., Rosebrough, N.J., Farr, A.L., Randall, R.J. (1952). Protein measurement with the Folin-phenol reagent. *Journal Biological Chemistry*, 193, 265-275.

Maynard, A.J. (Ed). 1970. Methods in Food Analysis Academic Press New York p 176.

Moon, J., Koh, G. (2020). Clinical evidence and mechanisms of high-protein diet-induced weight loss. Journal of Obesity & Metabolic Syndrome, 29 (3), 166–173. DOI: 10.7570/jomes20028.

Morris, D.L. (1948). Quantitative determination of carbohydrates with Dreywood's anthrone reagent. *Science*, 107 (2775), 254-255. DOI: 10.1126/science.107.2775.254.

Ogunyemi, O.M., Gyebi, G.A., Saheed, A., Paul, J., Nwaneri-Chidozie, V., Olorundare, O., Adebayo, J., Koketsu, M., Aljarba, N., Alkahtani, S., Batiha, G.E., Olaiya, C.O. (2022). Inhibition mechanism of alpha-amylase, a diabetes target, by a steroidal pregnane and pregnane glycosides derived from *Gongronema latifolium* Benth. *Frontiers in Molecular Biosciences*, 9, 866719. DOI: 10.3389/fmolb.2022.866719.

Patil, M., Anand, T., Ilaiyaraja, N., Khanum, F. (2017). *In-vitro* antioxidant and anti-obesity

properties of *Bauhinia variegata*. *Defense Life Science Journal*, 2 (2), 128-132. DOI: 10.14429/dlsj.2.11355.

Pekamwar, S.S., Kalyankar, T.M., Kokate, S.S. (2013). Pharmacological activities of *Coccinia grandis*: Review. *Journal of Applied Pharmaceutical Science*, 3 (05), 114-119.

Pérez, M., Dominguez-López, I., Lamuela-Raventós, R.M. (2023). The chemistry behind the Folin-Ciocalteu method for the estimation of (poly)phenol content in food: Total phenolic intake in a Mediterranean dietary pattern. *Journal of Agricultural and Food Chemistry*, 71 (46), 17543–17553. DOI: 10.1021/acs.jafc.3c04022.

Proença, C., Freitas, M., Ribeiro, D., Tomé, S.M., Oliveira, E., Viegas, M.F., Araújo, A.N., Ramos, M.J., Silva, A., Fernandes, P.A., Fernandes, E. (2019). Evaluation of a flavonoids library for inhibition of pancreatic α-amylase towards a structure-activity relationship. *Journal of Enzyme Inhibition and Medicinal Chemistry*, 34 (1), 577–588. DOI: 10.1080/14756366.2018.1558221.

Raal, A., Meos, A., Hinrikus, T., Heinämäki, J., Romāne, E., Gudienė, V., Jak Tas, V., Koshovyi, O., Kovaleva, A., Fursenco, C., Chiru, T., Nguyen, H.T. (2020). Dragendorff's reagent: Historical perspectives and current status of a versatile reagent introduced over 150 years ago at the University of Dorpat, Tartu, Estonia. *Die Pharmazie*, 75 (7), 299–306. DOI: 10.1691/ph.2020.0438

Sands, R. (1974). Rapid method for calculating energy value of food components. *Food Technology*, 29-40.

Singleton, V.L., Rossi, J.A. (1965). Colorimetry of total phenolics with phosphomolybdic-phosphotungstic acid reagents. *American Journal of Enology and Viticulture*, 16, 144–158.

Tardy, A.L., Pouteau, E., Marquez, D., Yilmaz, C., Scholey, A. (2020). Vitamins and minerals for energy, fatigue and cognition: A narrative review of the biochemical and clinical evidence. *Nutrients*, 12 (1), 228. DOI: 10.3390/nu12010228.

WHO (2024). Available online at https://www.who.int/en/news-room/fact-sheets/detail/the-top-10-causes-of-death.

Funding statement:

This research work was not supported by any Governmental / Non-Governmental / Public / Private funding agencies.

Ethical statement:

There are no animal studies involved in the reported work.

Consent for publication:

All authors have given consent to publish the paper.

Availability of data and material:

Data will be made available upon request.

Authors' contributions:

All authors contributed to the design and implementation of the research, to the analysis of the results and to the writing of the manuscript.

Acknowledgements:

Authors SM & MS are thankful to the Management and Administrative authorities of Sengamala Thayaar Educational Trust Women's College (Autonomous), Mannargudi, Tamilnadu while RT & VV are grateful to SASTRA Deemed University, Thanjavur, Tamilnadu for their encouragement and support.

Conflict of interest:

The authors declare no conflict of interest.

CARPATHIAN JOURNAL OF FOOD SCIENCE AND TECHNOLOGY

journal homepage: **http://chimie-biologie.ubm.ro/carpathian_journal/index.html**

Research Article

CULTIVATION AND ANTIOXIDANT PROPERTIES OF WILD *SCHIZOPHYLLUM COMMUNE* PRODUCED ON DIFFERENT AGRO-INDUSTRIAL WASTES

Noor Aisyah Md Noordin[1], Nur Ain Izzati Mohd Zainudin[1,2]✉, Nurul Shazini Ramli[3] and Nor Azwady Abd Aziz[1]

[1]*Department of Biology, Faculty of Science, Universiti Putra Malaysia, 43400 Serdang, Selangor, Malaysia*
[2]*Laboratory of Sustainable Agronomy and Crop Protection, Institute of Plantation Studies, Universiti Putra Malaysia, 43400 Serdang, Selangor, Malaysia*
[3]*Department of Food Science, Faculty of Food Science and Technology, Universiti Putra*
✉*ainizzati@upm.edu.my*

https://doi.org/10.34302/2025.17.3.2

Article history:
Received:
December 17th, 2024
Accepted:
October 15th, 2025

Keywords:
Spilt-gill;
Mushroom;
Wild mushroom;
Bioactive compound;
Natural antioxidant;

ABSTRACT

This study explores the cultivation and antioxidant properties of *Schizophyllum commune*, commonly known as the split-gill mushroom, as a sustainable natural food source. The growth performance of *S. commune* was evaluated on two lignocellulosic substrates, which are rubber wood and cocopeat. Key antioxidant activities include 2,2-diphenyl-1- (2,4,6-trinitrophenyl) hydrazyl stable free radical (DPPH), 2,2'-azino-bis (3-ethylbenzothiazoline-6-sulfonic acid (ABTS), ferric reducing antioxidant (FRAP) assays were analyzed to assess the bioactive potential of the mushrooms. The highest inhibition in rubber wood samples was recorded in 100% sawdust (55%), with the lowest inhibition concentration (IC_{50}) value being 0.957 µg/ml in ABTS, while 75% inhibition in DPPH. Rubberwood substrates yielded superior growth and higher levels of antioxidant activity, suggesting that the substrate can optimize both biomass and bioactive compound production. This research highlights *S. commune* as a viable alternative food source with significant antioxidant potential, promoting sustainability and contributing to the search for natural supplements and antioxidant sources for food.

1.Introduction

Increment of global demand for natural food sources and bioactive compounds has driven interest in the sustainable cultivation of edible wild mushrooms. *Schizophyllum commune*, commonly known as split-gill mushroom, is a widely distributed fungus found in diverse ecosystems. It has gained attention for its potential as a sustainable natural food source due to its ease of cultivation and rich nutritional profile (Suwannarach *et al.,* 2022).

Schizophyllum commune is a good source of protein, fiber, and bioactive compounds, particularly antioxidants (Wunjuntuk *et al.,* 2021). Antioxidants can neutralize harmful free

radicals in the body, thus helping to prevent oxidative stress-related diseases (Roncero-Ramos & Delgado-Andrade, 2017).

Mushroom cultivation not only provides an eco-friendly food source but also utilizes agricultural by-products as substrates, reducing waste and promoting sustainability (Basso *et al.,* 2020). Cultivation of *S. commune* is relatively simple, making it an attractive option for low-cost food production, especially in regions where food security is a concern. However, optimizing the choice of substrate can significantly influence both the growth and bioactive compound production of cultivated fungi, which can affect their nutritional value.

To address this, the present study evaluates the growth performance and antioxidant properties of *S. commune* cultivated on two lignocellulosic substrates: rubber wood and cocopeat. By employing key antioxidant assays such as DPPH, ABTS, and FRAP, the study aims to determine the bioactive potential of the mushrooms across different growth substrates. The findings contribute to the optimization of cultivation practices, emphasizing the importance of substrate selection for enhancing biomass yield and antioxidant capacity. This research not only emphasizes the value of *S. commune* as a natural food source with high antioxidant potential but also aligns with the global movement towards sustainable and health-promoting dietary alternatives.

2. Materials and methods

2.1. Fungal sampling and isolation

Sporocarps of *S. commune* were sampled in Sultan Idris Shah Forest Education Centre (SISFEC), UPM, Selangor on 16 March 2022. The samples were kept in paper bags for identification and cultivation. Fruiting bodies of the wild *S. commune* were surface sterilized using 10% Clorox and rinsed using sterile distilled water. *Schizophyllum commune* tissue was thereafter aseptically broken with the aid of sterile forceps. A small piece of 2 × 2 mm of the fruiting body tissue was aseptically transferred onto plates containing PDA. The formed fungal mycelium was subsequently transferred onto fresh PDA plates and incubated at room temperature. The pure fungal culture is ready for spawn inoculation.

2.2. Fungal identification

Schizophyllum commune was identified based on morphological characteristics and Internal Transcribed Spacer (ITS) sequence analysis. Morphological characteristics include stipe, pileus, and lamella arrangement of sporocarps were observed.

For molecular identification, the samples were cut into small pieces and ground using liquid nitrogen, and proceeded to DNA extraction using the Ultra Clean® Microbial DNA isolation kit (MO-BIO, Carlsbad, CA, USA) by following the manufacturer's guidelines.

PCR amplification of the ITS region was completed using a Professional Standard Thermocycler (Biometra Company, USA). A total of 50 µl reaction master mix containing 5× Green *GoTaq* Buffer, 2 mM dNTPs, 25 mM $MgCl_2$, 10 mM primer ITS1, 10 mM primer ITS4, Taq Polymerase, sterile distilled water (Promega, Madison, WI, USA). The quality of extracted gDNA was assessed by subjecting it to agarose gel electrophoresis. To amplify the ITS region of macrofungi, ITS1 (5'-TCCGTAGGTGAACCTGCGG-3') and ITS4 (5'- TCCTCCGCTTATTGATATGC-3') were applied (White *et al.,* 1990). PCR was run with the following cycle: initial denaturation at 95 ºC for 30 seconds, followed by 35 cycles of denaturation, annealing and extension at 95 ºC for 10 seconds, 59 ºC for 15 seconds and 72 ºC for 30 seconds, respectively. The final extension was running at 72 ºC for 5 minutes.

The PCR product undergoes the gel electrophoresis process by using 1% agarose gel consisting of 1× TBE buffer composed of 5.5 g of boric acid, 1 L of sterilized distilled water, 10.8 g of Tris-acetate and 0.93 g of Ethylenediaminetetraacetic acid disodium salt dihydrate. FloroSafe DNA was used to stain the amplified band. The produced band was observed under ultraviolet light using the Labnet Enduro TM Gel Documentation System (LABNET, USA). After obtaining a good DNA quality, it was processed for ITS sequencing by

the Nextgene Company using a Sanger dideoxy sequencer, 3730xl DNA Analyzer.

The sequences were aligned using BioEdit software. The aligned DNA sequences were blasted using the Basic Local Alignment Search Tool (BLAST) (www.ncbi.nlm.gov) against sequences in GenBank to determine the closest matched sequence from the database. For depositing, the ITS sequences were prepared in FASTA format. Then, the document was submitted through the GenBank submission portal (https://submit.ncbi.nlm.nih.gov/subs/genbank/).

2.3. Cultivation of *S. commune*

2.3.1 Mushroom spawn preparation

Mushroom spawn was prepared with slight modifications to the volume and type of substrates following. Corn grains (500 g) were washed with running water to remove debris and soaked in water for 8 hours. Then, the grains were drained and left to air-dry overnight. The grains were mixed with 1% limestone (based on dry weight), and 250 g of the mixture was packed into a polypropylene spawn bag (13 x 6 cm). The bags were sealed with a plastic neck and cap before being autoclaved. The sterile corn grains were inoculated with a pure fungal culture. The inoculated spawn bags were incubated for 14 days.

2.3.2. *Mushroom substrate preparation and inoculation*

The mushroom substrate was prepared following the method of Hassan *et al.* (2022), with modifications based on the treatment sets. The ratios of rubber sawdust : cocopeat : cornbran : $CaCO_3$ were adjusted as follows: Treatment 1 (100:0:50:1), Treatment 2 (90:10:50:1), Treatment 3 (60:40:50:1), Treatment 4 (30:70:50:1), and Treatment 5 (0:100:50:1).

The corn grains that spawned with full mycelial growth were poured adequately, capped tightly in the inoculated substrate bag, and stored in an incubation room, 28 ± 2°C with an 8-hour photoperiod and 70-85% relative humidity. A total of five vertical notches were made on a bag of ripe mushrooms to allow the fruiting bodies to mature. Fungal growth was observed weekly until the bags were completely coated at 30-35 days after inoculation. After seven to 10 days of primordial creation, mushrooms were harvested. After 12-14 days from the first flush, a second flush was performed, and the same schedule was followed for subsequent flushes, or depending on the commencement of the mushroom primordia. Harvested fruiting bodies from this cultivation were used as mushroom samples in the antioxidant analysis. The biological efficiencies of mushroom specimens were calculated according to De Siquiera *et al.* (2011).

$$\text{Biological efficiency (\%)} = \frac{\text{Fresh fruiting body (g) x 100}}{\text{Dry substrate (g)}} \quad (1)$$

2.3.3. Mushroom extraction for antioxidant bioassay

Mushroom samples were prepared for antioxidant tests according to Tsai (2009). The moisture content of fresh fruiting bodies was calculated by weighing them. Mushrooms were sliced and lyophilized for 3 days (0,045 mBar, -51°C, Labconco, Missouri) before being milled into a fine powder using a blender. By subtracting the fresh and lyophilized weights of mushroom fruiting bodies, the moisture content was estimated. Mushroom powder (10 g) was extracted with 100 mL of distilled water and filtered through Whatman No. 1 filter paper using a water bath shaker (3.25 hours, 42.5°C, 160 rpm). The mixture was centrifuged for 10 min at 4000 rpm. The supernatant was collected and passed through Whatman No. 1 filter paper supernatant was collected and passed through Whatman No.1filter paper. All aqueous extracts were then freeze-dried and diluted for further analysis.

2.4. Scavenging activity towards 2,2-diphenyl-1- (2,4,6-trinitrophenyl) hydrazyl (DPPH) radical

With slight modification on a series of concentrations, the DPPH assay was carried out

according to Bloise's technique (Kebaili *et al.,* 2021). Fresh DPPH solution was made by dissolving 5 mg DPPH crystals in 2 ml ethanol, sealing it in aluminum foil, and keeping it at 4°C. In 96-well microtiter plates, extracts were diluted to generate a series of concentrations (0.13-1.00 µg/ml, volume 100 µL). Each well was filled with a 5 µL DPPH solution and left to react in the dark for 30 minutes. A microplate reader set to 515 nm was used to measure absorbance (MultiskanSky 1530-80079, Sweden) 8. All test analyses were averaged after at least three replicates. As standard antioxidants, ascorbic acid (Sigma) was utilised. To determine the blank absorbance, methanol was utilised instead of the mushroom extract. The extracts' antioxidant potential was determined using the equation below (Mwangi et al., 2022):

$$\text{Scavenging activity (\%)} = \frac{(\Delta A_{\text{blank}} - \Delta A_{\text{extract}})\text{x } 100\%}{\Delta A_{blank}} \quad (2)$$

Where:

$\Delta \boldsymbol{A_{blank}}$ = Average of blank absorbance (t=30 min)

$\Delta \boldsymbol{A_{sample}}$= Average of extract absorbance (t=30 min)

2.5. Ferric reducing antioxidant (FRAP) assay

With few adjustments, the FRAP test of mushroom extracts were adapted from Oyaizu (1986). Phosphate buffer (1 ml, 0.2 M, pH 6.6) and CNFeKz were combined with different quantities of extract (0.125 µl, 1 µ g/L) (1 L,1 percent). The mixture was incubated for 20 minutes at 50°C before being cooled on ice. $CHC_{13}O_2$ (1 ml, 10%) aliquots were added to the mixture and centrifuged (6000 rpm) for 10 minutes for the upper layer of the solution (2 ml) to react with distilled water (2 ml) and $FeCl_3$ solution (1 ml, 0.1 percent). The solution's absorbance was measured at 593 nm according to Madhanraj *et al.* (2017).

2.6. Determination of total phenolic content (TPC)

The total phenolic contents (TPC) of *S. commune* were determined by the Folin–Ciocalteau method developed by Singleton and Rossi (1965). The extract with distilled water (1200 ml), NaCO; (450 L) and Folin-Ciocalteu reagent (450 µl). The mixture was agitated and allowed to stand for 90 min. Absorbance of the blue coloration mixture were determined at 760 nm by using a UV visible spectrophotometer. Results were expressed as mg/g gallic acid equivalent (GAE) as followed, based on the calibration curve y=0.0007x+0.1886, RP=0.9865 (Liu *et al.,* 2017).

Total phenolic content = (mg TAE/g) – CXV x df/M (3)

Where,

C-concentration of tannic acid established from calibration curve (mg/ml)

V = volume of extraction solvent (ml)

df=dilution factor

M=weight of plant material (g)

2.7. Determination of 2,2′-Azinobis-(3-ethylbenzothiazoline-6-sulfonic acid (ABTS)

ABTS was formed by creating a mixture of 7 mM ABTS stock solution combined with 2.45 mM potassium persulfate (1/1, v/v) (Wongaem *et al.,* 2020). The mixture was permitted to stand at room temperature in complete darkness for 12 h prior to use. The mixture was allowed to stand for 4–16 h to ensure that the reaction has been completed, and a state of stable absorbance achieved. Distilled water was used to dilute the ABTS solution such that the level of absorbance measured 0.7 ± 0.02 at 734 nm. 750 µL sample of the ABTS solution was collected for the photometric assay with test samples of 25 µL which underwent vortexing for 5s before the absorbance was recorded at A 734 nm after being allowed to stand for 10 min. The reference compound chosen for this assay was ascorbic acid.

3. Results and discussions

3.1. Identification of *S. commune*

Schizophyllum commune is a distinctive basidiomycete fungus known for its unique fan-shaped fruit bodies, which are small in the range 3-5 cm with a pubescent, hairy upper surface (Figure 1B). The fruit bodies are typically grayish to brown. It has intercalcated lamellae and the stipe sessile (Figure 1A). *Schizophyllum commune* can be found on dead wood in a cluster form (Figure 1C). A hallmark feature of *S. commune* is its split-gills which are bifurcated.

Figure 1. *Schizophyllum commune* that found in Ayer Hitam Reserve Forest Selangor. (A) intercalcated lamellae; (B) hairy top surface; (C) attach to dead wood. (D) on PDA culture plate. Scale bar: 1 cm

Table 1. Moisture content and total extraction yield, quantity and quality fruiting bodies of *Schizophyllum commune* from rubber tree substrate

*Treatment	Moisture content (%)	Dry weight (g)	Number of fruiting bodies	Length of cap (mm)	Width of cap (mm)
T1	58.55 ± 0.007	40.16 ± 0.023	413	15-65	3-45
T2	53.96 ± 0.156	36.82 ± 0.157	399	15-41	10-52
T3	60.69 ± 0.018	35.80 ± 0.062	104	5-50	7-56
T4	67.47 ± 0.004	28.88 ± 0.027	94	15-40	5-40
T5	63.27 ± 0.004	25.28 ± 0.042	62	10-36	4-35

*Composition treatments: the ratios of rubber sawdust : cocopeat : cornbran : $CaCO_3$ were adjusted as follows: T1 (100:0:50:1), T2 (90:10:50:1), T3 (60:40:50:1), T4 (30:70:50:1), and T5 (0:100:50:1).

To verify the identification of the fungus species utilized in this investigation, the ITS region was sequenced as it is commonly recognized as the universal DNA barcode for fungi (White *et al.,* 1990). Following sequencing, species identification was verified by comparing the ITS sequences with reference sequences in GenBank using the BLAST program. A strong resemblance (99.84%) with *S. commune* was found in the analysis, supporting the samples' classification as a species. The obtained sequence was deposited in GenBank with the accession number OR178483

3.2. Growth and yield of *S. commune*

The moisture content of *S. commune* varied less significantly across treatments, though the highest content (67.47%) was observed in T4, while T2 exhibited the lowest (53.96%) (Table 1). The increased moisture in T4 suggests that the substrate or treatment applied enhanced the water-retention capacity. Moisture levels in

mushrooms are crucial for their physiological processes, as higher water content supports growth, development, and amplification (Dawadi *et al.,* 2022).

The moderate moisture content observed in the T1 group (58.55%) aligns with findings that untreated substrates typically provide a baseline for water availability in fungal cultivation (Muswati et al., 2021). The differences in moisture content across treatments imply that the physical and chemical properties of the rubber sawdust substrates were altered by treatment applications, affecting water retention and absorption efficiency. Substrate composition and environmental modifications are known to influence the microenvironment, thus impacting temperatures, and oxygen availability (Shakir *et al.,* 2023).

The T1 produces the highest number of fruiting bodies (413), suggesting that the untreated substrate provides optimal conditions for mushroom growth (Figure 2).

As treatments are introduced, particularly from T3 to T5, there is a significant decrease in the number of fruiting bodies, with T5 showing only 62 fruiting bodies. The size of the fruiting bodies, indicated by cap length and width, also decreases with more intense treatments. However, T2 exhibits the largest cap sizes, ranging from 15-41 mm in length and 10-52 mm in width, while T5 shows the smallest cap sizes, ranging from 10-36 mm in length and 4-35 mm in width.

Regarding extraction yield, the T1 group exhibited the highest yield (40.16%), indicating that untreated mushrooms were more efficient in providing extractable bioactive compounds. This observation supports previous studies that suggest excessive substrate modifications may reduce the availability of target metabolites, pH of substrate block, and available minerals that affect mycelial density (Khoo *et al.,* 2021). As more intensive treatments are applied, the extraction yield decreases, with T5 showing the lowest yield (25.28%).

Figure 2. Formation of fruiting bodies of *Schizophyllum commune* based on different substrate composition with the rations of rubber sawdust : cocopeat : cornbran : CaCO3 . A) T1 (100:0:50:1), B) T2 (90:10:50:1), C) T3 (60:40:50:1), D) T4 (30:70:50:1), and E) T5 (0:100:50:1).

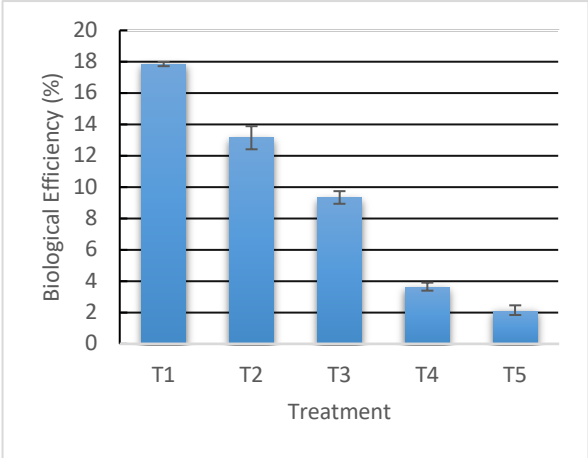

Figure 3. Biological efficiency of substrates on rubber dead wood at different treatments. Composition treatments: the ratios of rubber sawdust : cocopeat : cornbran : $CaCO_3$ were adjusted as follows: T1 (100:0:50:1), T2 (90:10:50:1), T3 (60:40:50:1), T4 (30:70:50:1), and T5 (0:100:50:1).

3.3. Biological Efficiency Ratio (BER) of *S. commune*

The Biological Efficiency Ratio (BER) reflects how efficiently a substrate is converted into mushroom biomass. The high BE in the T1 group, when compared to all treatments, raises the possibility that either the rubber wood substrate is more biologically efficient in its original state or that the treatments are preventing growth. The slow drop in BE from T2 to T5 may indicate that the modifications made to these treatments gradually impacted biological efficiency, perhaps by changing substrate structure, pH, or nutrient availability in ways that were detrimental to biological growth. BE in mushrooms can be impacted by changing the substrate's composition (Hoa *et al.,* 2015). Nitrogen and carbon supplementation are essential for mycelial growth and fruiting body formation (Singh *et al.,* 2021) is one example of how improper nutrition levels can hinder growth and decrease efficiency.

3.4. Antioxidant Properties of *S. commune*

Phenolic compounds contribute significantly to the antioxidant properties of mushrooms. Mushrooms grown on rubber dead trunk substrates show higher total phenolic content (TPC), particularly in the T2 (10% cocopeat) treatment, which achieves a TPC of 1924.57 GAE/g (Table 2). This high TPC value suggests that the rubber dead trunk substrate, especially when mixed with cocopeat, is effective in promoting the accumulation of phenolic compounds in the mushrooms. T2 treatment had the highest TPC value, suggesting specialized treatments can increase fungi's phenolic content, potentially influencing the formation of phenolic compounds linked to secondary metabolism or stress reactions (Ao & Deb, 2019).

For DPPH inhibition, T1 (100% sawdust) and T3 (40% cocopeat) show the best results, with inhibition percentages of 75% and 78%, respectively, and high IC_{50} values of 0.654 and 0.741 µg/ml, respectively. These values indicate that these treatments produce mushrooms with strong antioxidant properties, capable of effectively neutralizing free radicals. The ABTS assay, another method for measuring antioxidant activity, also shows moderate inhibition values for mushrooms grown on rubber dead trunk substrates. Treatment 1 (100% sawdust) again performs best with 55% inhibition and an IC_{50} of 0.957 µg/ml. This consistency across different antioxidant assays reinforces the conclusion that rubber dead trunk substrates support the production of mushrooms with strong antioxidant properties. The consistent performance of T1 across both assays suggests that 100% sawdust is particularly effective at supporting the production of compounds such as gallic acid, p-hydroxybenzoic acid, and protocatechuic that can neutralize free radicals (Abdelshafy *et al.,* 2021). The FRAP assay measures the antioxidant power in terms of the ability to reduce ferric ions. Interestingly, the T4 (30:70:50:1) treatment shows the highest FRAP value at 4217.90 GAE/g.

Table 2. Antioxidant properties of *Schizophyllum commune* in different treatments

Treatment	TPC (GAE/g)	DDPH inhibition activity		ABTS inhibition activity		FRAP (GAE/g)
		Inhibition (%) at 1 g/ml	IC_{50} (ug/ml)	Inhibition (%) at 1 ug/ml	IC_{50} (ug/ml)	
T1	1795.05	75	0.654	55	0.957	2521.40
T2	1924.57	74	0.686	49	1.032	2562.03
T3	1556.32	78	0.741	43	1.011	2577.27
T4	1439.49	64	0.827	37	1.047	4217.90
T5	1670.60	66	0.814	33	1.095	3864.89
Ascorbic acid	-	63.68	0.991	66	0.891	-

*Composition treatments: the ratios of rubber sawdust:cocopeat:cornbran:CaCO3 were adjusted as follows: T1 (100:0:50:1), T2 (90:10:50:1), T3 (60:40:50:1), T4 (30:70:50:1), and T5 (0:100:50:1).

Schizophyllum commune produces a polysaccharide known as schizophyllan which has various properties and applications, such as stimulating the immune system (Zhang *et al.,* 2013). It also possesses specialized enzymes, such as lignin peroxidases and laccases, that can break down lignin. The degradation of lignin can lead to the release of phenolic compounds, which are known for their antioxidant properties. Therefore, while lignin poses a challenge, it also offers an opportunity to produce valuable bioactive compounds. The lignocellulosic composition of rubber wood, which includes a moderate amount of lignin, creates an optimal environment for mushroom growth (Kumla *et al.,* 2020). The balance between cellulose, hemicellulose, and lignin in rubber wood ensures that the substrate is not only nutritious but also capable of supporting the complex metabolic processes required for the synthesis of bioactive compounds. The higher phenolic content in mushrooms grown on rubber wood is linked to increased antioxidant activity, as demonstrated by tests such as DPPH (2,2-diphenyl-1-picrylhydrazyl) and ABTS (2,2'-azinobis-(3-ethylbenzothiazoline-6-sulfonic acid) assays (Boonthatui *et al.,* 2021).

Fungal enzymes, such as cellulases, break down cellulose into glucose, which is then utilized by the fungus for energy and growth (Kumla *et al.,* 2020). The high cellulose content in rubber wood makes it an ideal substrate for mushrooms like *S. commune,* as it provides a steady and sufficient supply of carbon. An optimal C:N ratio is crucial for maintaining a balance between fungal growth and the production of bioactive compounds. If the ratio is too high (excess carbon), the fungus may grow rapidly but produce fewer bioactive compounds. Conversely, if the ratio is too low (excess nitrogen), the growth of the fungus may be stunted, leading to a lower yield. Rubber wood, with its high cellulose content, provides a rich carbon source, while the addition of nitrogen supplements can help achieve the desired C:N ratio. This balance ensures that the fungus not only grows well but also produces a high concentration of bioactive compounds, making rubber wood an ideal substrate for mushroom cultivation.

4. Conclusions

This study demonstrates the potential of *S. commune* as an alternative natural food source with promising antioxidant properties. The results highlight that the choice of substrate significantly impacts both the growth and antioxidant activity of the mushrooms. Rubberwood substrates support optimal mycelial development and higher antioxidant activity, as indicated by superior DPPH, ABTS, and FRAP assay results. The use of sustainable cultivation practices for *S. commune* could provide a cost-effective, environmentally friendly food source with functional health benefits, contributing to food security and the development of natural antioxidants.

5. References

Abdelshafy, A. M., Belwal, T., Liang, Z., Wang, L., Li, D., Luo, Z., & Li, L. (2021). A comprehensive review on phenolic compounds from edible mushrooms: Occurrence, biological activity, application and future prospective. *Critical Reviews in Food Science and Nutrition,* 62(22), 6204–6224. https://doi.org/10.1080/10408398.2021.1898335

Ao, T., & Deb, C. R. (2019). Nutritional and antioxidant potential of some wild edible mushrooms of Nagaland, India. *Journal of Food Science and Technology,* 56(2), 1084–1089. https://doi.org/10.1007/s13197-018-03557-w

Basso, V., Schiavenin, C., Mendonça, S., De Siqueira, F. G., Salvador, M., & Camassola, M. (2020). Chemical features and antioxidant profile by *Schizophyllum commune* produced on different agroindustrial wastes and by products of biodiesel production. *Food Chemistry, 329,* 127089. https://doi.org/10.1016/j.foodchem.2020.127089

Boonthatui, Y., Chongsuwat, R., & Kittisakulnam, S. (2021). Production of

Antioxidant bioactive compounds during mycelium growth of *Schizophyllum commune* on different cereal media. *Chiang Mai University Journal of Natural Sciences,* 20(2). https://doi.org/10.12982/cmujns.2021.032

Dawadi, E., Magar, P. B., Sagar, B., Subash, S., Suraj, S., & Jiban, S. (2022). Nutritional and post-harvest quality preservation of mushrooms: A review. *Heliyon,* 8(12): e12093. https://doi.org/10.1016/j.heliyon.2022.e12093

De Siqueira, F. G., Martos, E. T., Da Silva, E. G., Da Silva, R., & Dias, E. S. (2011). Biological efficiency of *Agaricus brasiliensis* cultivated in compost with nitrogen concentrations. *Horticultura Brasileira,* 29(2), 157–161. https://doi.org/10.1590/S0102-05362011000200004

Hassan, S. A. M., Ting, S. S., Zulkepli, N. N., & Kasim, F. H. (2022). Physicochemical characterization of rubberwood sawdust, mushroom spent medium, rice husk, and rice husk ash as potential growth substrates for wild *Schizophyllum commune* cultivation. *Malaysian Journal of Microscopy*, 18(2), 225-236. https://malaysianjournalofmicroscopy.org/ojs/index.php/mjm/article/view/665/364

Kebaili, F. F., Tahar, N., Esseddik, T. M., Redouane, R., Chawki, B., Pablo, A., & Massimiliano, P. (2021). Antioxidant activity and phenolic content of extracts of wild Algerian Lingzhi or Reishi medicinal mushroom, *Ganoderma lucidum* (Agaricomycetes). *International Journal of Medicinal Mushrooms*, 23(6), 79–88. https://doi.org/10.1615/intjmedmushrooms.2021038424

Khoo, S. C., Ling, N., MA, Peng, W. X., Ng, K. K., Goh, M. S., Chen, H. L., Tan, S. H., Lee, C. H., Luang-In, V., & Sonne, C. (2021). Valorisation of biomass and diaper waste into a sustainable production of the medical mushroom Lingzhi *Ganoderma lucidum*. *Chemosphere*, 286, 131477. https://doi.org/10.1016/j.chemosphere.2021.131477

Kumla, J., Suwannarach, N., Sujarit, K., Penkhrue, W., Kakumyan, P., Jatuwong, K., Vadthanarat, S., & Lumyong, S. (2020). Cultivation of mushrooms and their lignocellulolytic enzyme production through the utilization of agro-industrial waste. *Molecules,* 25(12), 2811. https://doi.org/10.3390/molecules25122811

Liu, K., Xiao, X., Wang, J., Chen, C. O., & Hu, H. (2017). Polyphenolic composition and antioxidant, antiproliferative, and antimicrobial activities of mushroom Inonotus sanghuang. *LWT - Food Science and Technology*, 82, 154–161. https://doi.org/10.1016/j.lwt.2017.04.041

Madhanraj, R., Eyini, M., & Balaji, P. (2017). Antioxidant Assay of Gold and Silver Nanoparticles from Edible Basidiomycetes Mushroom Fungi. *Free Radicals and Antioxidants*, 7(2), 137–142. https://doi.org/10.5530/fra.2017.2.20

Muswati, C., Simango, K., Tapfumaneyi, L., Mutetwa, M., Ngezimana. W. (2021). The Effects of different substrate combinations on growth and yield of oyster mushroom (*Pleurotus ostreatus*). *International Journal of Agronomy,* 2021: 1-10. https://doi.org/10.1155/2021/9962285

Oyaizu, M. (1986). Studies on products of browning reaction. Antioxidative activities of products of browning reaction prepared from glucosamine. *The Japanese Journal of Nutrition and Dietetics,* 44(6), 307–315. https://doi.org/10.5264/eiyogakuzashi.44.307

Roncero-Ramos, I., & Delgado-Andrade, C. (2017). The beneficial role of edible mushrooms in human health. *Current Opinion in Food Science,* 14, 122–128. https://doi.org/10.1016/j.cofs.2017.04.002

Shakir, M.A., Ahmad, M.I., Yusup, Y. et al. From waste to wealth: converting rubber wood sawdust into green mycelium-based composite. *Biomass Conversion and Biorefinery,* (2023): https://doi.org/10.1007/s13399-023-05113-9

Singh, S., Raj, C., Singh, H. K., Avasthe, R. K., Said, P., Balusamy, A., Sharma, S. K., Lepcha, S. C., & Kerketta, V. (2021). Characterization and development of cultivation technology of wild split gill *Schizophyllum commune* mushroom in India. *Scientia Horticulturae,* 289, 110399. https://doi.org/10.1016/j.scienta.2021.110399

Singleton, V. L., & Rossi, J. A., (1965). Colorimetry of total phenolics with phosphomolybdic phosphotungstic acid reagents. *American Journal of Enology and Viticulture,* 16, 144–158

Suwannarach, N., Kumla, J., Zhao, Y. Kakumyan, P. (2022). Impact of cultivation substrate and microbial community on improving mushroom productivity: A review. *Biology,* 11(4), 569; https://doi.org/10.3390/biology11040569

Tsai, S., Tsai, H., & Mau, J. (2009). Antioxidant properties of Coprinus comatus. *Journal of Food Biochemistry,* 33(3), 368–389. https://doi.org/10.1111/j.1745-4514.2009.00224.x

White, T., Bruns, T., Lee, S., & Taylor, J. (1990). Amplification and direct sequencing of fungal ribosomal RNA genes for phylogenetics. In: PCR Protocols A Guide to Methods and Applications. Academic Press, Inc. https://doi.org/10.1016/B978-0-12-372180-8.50042-1

Wongaem, A., Reamtong, O., Srimongkol, P., Sangtanoo, P., Saisavoey, T., & Karnchanatat, A. (2020). Antioxidant properties of peptides obtained from the split gill mushroom (*Schizophyllum commune). Journal of Food Science and Technology,* 58(2), 680–691. https://doi.org/10.1007/s13197-020-04582-4

Wunjuntuk, K., Ahmad, M., Techakriengkrai, T., Chunhom, R., Jaraspermsuk, E., Chaisri, A., Kiwwongngam, R., Wuttimongkolkul, S., & Charoenkiatkul, S. (2021). Proximate composition, dietary fibre, beta-glucan content, and inhibition of key enzymes linked to diabetes and obesity in cultivated and wild mushrooms. *Journal of Food Composition and Analysis,* 105, 104226. https://doi.org/10.1016/j.jfca.2021.104226

Zhang, Y., Kong, H., Fang, Y., Nishinari, K., & Phillips, G. O. (2013). Schizophyllan: A review on its structure, properties, bioactivities and recent developments. *Bioactive Carbohydrates and Dietary Fibre,* 1(1), 53–71. https://doi.org/10.1016/j.bcdf.2013.01.002

Acknowledgment

This work was supported by a grant of the IPS Putra Grant, (grant no: GP-IPS/2022/9729200). Nor Aisyah was sponsored by the Graduate Research Fund GRF-UPM. The authors thank the Department of Biology, Faculty of Science, UPM for providing the technical support and laboratory to make this study possible.

CARPATHIAN JOURNAL OF FOOD SCIENCE AND TECHNOLOGY

journal homepage: **http://chimie-biologie.ubm.ro/carpathian_journal/index.html**

Research article

DEVELOPMENT OF RESISTANT STARCH TYPE-5 AND ITS UTILIZATION IN COOKIE-PREPARATION

Betül Oskaybaş-Emlek[1]✉, Ayşe Özbey[1], Kevser Kahraman[2]

[1]Department of Food Engineering, Engineering Faculty, Niğde Ömer Halisdemir University, Niğde, Türkiye
[2] Department of Nanotechnology Engineering, Engineering Faculty, Abdullah Gül University, Kayseri, Türkiye
✉Corresponding author: Betül Oskaybaş-Emlek, Department of Food Engineering, Engineering Faculty, Niğde Ömer Halisdemir University,
✉betuloskaybas@ohu.edu.tr
ORCID Number: 0000-0002-0238-8948

https://doi.org/10.34302/2025.17.3.3

Article history:
Received:
April 6th, 2025
Accepted:
October 15th, 2025

Keywords
Lauric acid;
Resistant starch;
Starch-fatty acid complex;
Tapioca starch.

Abstract
The objective of this study was the production of resistant starch type-5 (RS-5), its characterization, and utilization in cookie making. In first part of the study, the effects of starch-fatty acid complex formation (RS-5) between tapioca starch and lauric acid on the structure, digestibility, thermal and morphological properties of tapioca starch were investigated. X-ray diffraction revealed that the RS-5 had a V-type crystalline pattern. FT-IR analysis showed that a distinctive peak at 2846 cm-1 was only observed in RS-5. The resistant starch (RS) content of native starch increased from 22.76% to 28.02% with RS-5 formation. In the second part of the study, the RS-5 was added as a replacement for wheat flour with 10%, 20%, and 30% compared to control sample made with 100% wheat flour in cookie-making. The effects of RS-5 replacement of cookie samples on some physicochemical, estimated glycemic index (eGI) value, physical, and hardness properties were determined. Compared to control cookie, the cookie samples included RS-5 had lower hardness value, higher spread ratio. The eGI value of cookie samples was slightly decreased with the replacement with RS-5. The results demonstrated that the RS-5 has good potential for developing softer cookie with no adverse impact on eGI value.

1. Introduction

Starch, a storage compound in plants, consists of two polysaccharides which are amylose and amylopectin (Li *et al.*, 2021). Three categories of starch are distinguished by their digestibility characteristics: Rapidly Digestible Starch (RDS), Slowly Digestible Starch (SDS), and Resistant Starch (RS) (Oskaybaş-Emlek *et al.*, 2022a). RS consists of complex carbohydrates, which can resist digestion and absorption in the small intestine (Stewart and Zimmer, 2017). It is classified into five groups according to structural properties. RS-1 is physically inaccessible starch, RS-2 is granular starch with B- or C-XRD pattern, retrograded starches are RS-3, and modified starches with chemical agents are RS-4. In addition, RS-5 is formed the starch-

fatty acid complex (Stewart and Zimmer, 2017).

The starch-fatty acid complex can be naturally present in starch or formed during starch gelatinization in the presence of lipids (Garcia *et al.*, 2016). It was known that the apolar chains of fatty acid molecules can interact with the hydrophobic cavity of amylose through hydrophobic interaction resulting in starch-fatty acid complexes. Many types of starch have been used in the formation of amylose lipid complexes, such as corn (Sun *et al.*, 2021), buckwheat (Oskaybaş-Emlek *et al.*, 2022b), wheat (S. Wang *et al.*, 2016), rice, potato and tapioca starch (Ramos-Villacob *et al.*). Besides, based on previous studies about starch-fatty acid complex, very little information concerning the tapioca starch-lauric acid complex is available (Ramos-Villacob *et al.*). Additionally, this RS-5 was formed with tapioca starch and lauric acid at the temperature below the gelatinization temperature (60°C) (Ramos-Villacob *et al.*). There are various studies in the literature that the starch-lipid complex formed at a temperature below (Chang *et al.*, 2013; D'Silva *et al.*, 2011) and also above the pasting temperature (Ai *et al.*, 2013; Reddy *et al.*, 2018). However, Seo *et al.* (2015) reported that the complex formation at a relatively low temperature leads to less-ordered complexes. The reaction temperature of complex formation affects the digestibility properties of starch-fatty acid complex samples (Oskaybaş-Emlek *et al.*, 2022a). Therefore, the reaction temperature used in the production of the complex may affect the beneficial effects of the complex on human health.

Resistant starch is known as beneficial functions in human physiology, such as reducing the risk of diabetes (Rojhani *et al.*, 2022), preventing the development of colon cancer, having beneficial effect on blood lipid levels (Sharma *et al.*, 2008), and protecting against the obesity (Han *et al.*, 2023). Additionally, Zheng *et al.* (2020) reported that the higher RS-5 level may have contributed to the significant reduction in body weight and healing in serum-lipid profiles and liver function of rats under a high-fat diet. In addition to the health benefits of RS, it has many techno-functional properties, giving advantages to food products. Milašinović Šeremešić *et al.* (2013) reported that the adding RS to various confectionery products led to an improvement in softness structure. RSs can be used to give the final product the desired texture and appropriate crispness in food products. Besides, RSs improve the flavor, color, and aroma of some foods (Milašinović Šeremešić *et al.*, 2013). The existence of starch-fatty acid complexes (RS-5) in starch supports the development of new starch-based products with appropriate structure and functionality (Sengupta *et al.*, 2023). Adding starch- fatty acid complexes (RS-5) to food products decreases starch's retrogradation, i.e., it delays the staling process (Luo *et al.*, 2020; Sengupta *et al.*, 2023). The RSs have many advantages in terms of the physiology of humans and technological aspects of the food industry. Therefore, RSs practically can be utilized in many bakery products.

Cookies are among the most widely consumed snack foods due to their low cost, convenience, and long shelf life (Rojhani *et al.*, 2022). There are many studies in the literature on cookie enrichment with dietary fiber and RS (Aparicio-Saguilán *et al.*, 2007; Giuberti *et al.*, 2017; Kahraman *et al.*, 2019; Rojhani *et al.*, 2022). However, RS is a more preferred alternative compared to dietary fiber due to the cookies with higher dietary fiber content having a coarser and denser structure (Rojhani *et al.*, 2022). Additionally, RS has no negative effects on the sensory properties of food such as texture, appearances because it has small particle size, bland flavor, and white color (Rojhani *et al.*, 2022). However, in the literature, there are very little information about the utilization of RS-5 in cookie-making (X.-H. Chen *et al.*, 2022; Xiaohan Chen and Wang, 2024; Garzóan *et al.*, 2003). On the other hand, to the best of our knowledge, there is no information regarding the use of the RS-5 complexation between lauric acid and tapioca starch in the cookie production.

In this study, the RS-5 was formed (>60°C) by the complexation between tapioca starch and lauric acid and the impact of complex formation on the morphological, FT-IR structure, XRD pattern, and digestibility properties of tapioca starch was examined. Additionally, another purpose of this study was to investigate some physico-chemical (pH, aw, color), physical (spread ratio) and texture characteristics of cookies prepared using RS-5 as a replacement for 10%, 20% and 30% of wheat flour as compared to a control made with 100% wheat flour.

2. Materials and methods

2.1. Materials

Lauric acid (C12:0), pancreatin (P7545) and pepsin (P7000) were bought from Sigma Aldrich (Sigma-Aldrich, ABD). Tapioca starch and sodium acetate were purchased from Tito Gıda (Turkey) and Merck Millipore Corporation (Germany), respectively. Glucose oxidase-peroxidase (GOPOD) reagent was supplied from Megazyme International (Ireland). Ingredients used in cookie production were purchased from a local store in Nigde, Turkey..

2.2. Methods

2.2.1 Production of Resistant Starch Type-5 (RS-5)

The RS-5 was produced using a Rapid Visco-Analyzer (RVA 4500, Perten Instruments, Sydney, Australia) according to S. Wang *et al.* (2017) with slight modifications. For this purpose, 3.5 g (14% moisture, db) and lauric acid (350 mg) were mixed with deionized water to make a total weight of 28 g. To produce the RS-5 between tapioca starch and lauric acid, the STD 1 profile provided with RVA was performed. The obtained RS-5 was freeze-dried, then grounded with a laboratory mill (<212 μm). The RS-5 sample and native tapioca starch were stored (+4°C) until further analyses.

2.2.2 Characterization of RS-5

The complex index value (CI) of RS-5 was determined according to method described by S. Wang *et al*. (2016).

The rapidly digestible starch (RDS), slowly digestible starch (SDS) and resistant starch (RS) content of native tapioca starch and RS-5 were determined according to Oskaybaş-Emlek *et al.* (2022a).

The XRD patterns of native tapioca starch and RS-5 were obtained using Bruker AXS D8 X-Ray diffractometer (Karlsruhe, Germany) with CuKα radiation (λ = 0.15405 nm) operating at a voltage current of 40 kV and 30 mA. Data were collected from 2θ of 5°-40°.

The structural properties of native tapioca starch and RS-5 were investigated with Thermo Nicolet Avatar 370 Fourier Transformed Infrared Spectrometer (FT-IR) (Madison, WI, USA). The wavenumber range was determined as 4000–400 cm−1 and scanning time was 32 for each sample

The morphological properties of native tapioca starch and RS-5 was analyzed using a scanning electron microscope (Zeiss Sigma 300 Field Emission SEM, Oberkochen, Germany). Prior the analysis, the samples coated with a thin layer of gold. Images were taken at 15.00 kV.

Thermogravimetric analysis was conducted with a STA TG-DSC/DTA PT1600 (Linseis, Germany) The operation was performed from 20 °C to 700 °C at a heating rate of 10 °C/min under nitrogen.

2.2.3 Preparation of cookies

In the cookie production, RS-5 was replaced with wheat flour at different ratios (0, 10, 20 and 30%). The cookies were prepared according to the method of Oskaybaş-Emlek *et al.* (2021) with slight modifications. The water content of cookie dough preparation was 30 mL. After baking, the cookies were cooled to room temperature (23°C), then they were packaged in polyethylene bags, until used.

2.2.4 Cookie characterization

The estimated in-vitro glycemic index value (eGI) of cookie samples were determined according to method described by Kahraman *et al.* (2019).

The physical properties of the baked cookies were determined were thickness, diameter and spread ratio (Diameter/Thickness). The thickness and

diameter of cookies were measured using digital caliper.

The color properties of cookies were determined using colorimeter (Konica Minolta CR 400, Japan) (Oskaybaş-Emlek *et al.*, 2021). The results were expressed in terms of L* (lightness/ darkness), α* (redness/greenness) and b* (yellowness/blueness)

The Texture Analyzer (TA.XT Plus Texture Analyzer, Godalming, UK) using with a three-point bending jig was used to determine the textural properties of cookies in terms of break strength. The analysis was performed after baking 24 h. Test parameters were determined as test speed of 3.0 mm/s and strain value of 10.0%.

The water activity values (aw) of cookie samples were measured with a water activity meter (Novasina Labswift, Switzerland). Scanning electron microscope system (Jeol JSM-6480LV, Japan) was used to examine morphological of dried powder before and after enzyme treatment.

The pH value of grounded cookie samples (10% (w/v) suspension in distilled water) was determined with a pH meter (Hanna Instruments, Malaysia).

2.3. Data analysis

Independent t-test ($p_{value} < 0.05$) was performed to compare the data of native tapioca starch and RS-5 samples. Data of cookie samples were analyzed using IBM SPSS Statistics version 24.0 (SPSS Inc., Chicago, IL) with analysis of variance with Duncan's test multiple comparison ($p_{value} < 0.05$) between treatments.

3. Results and discussions

3.1. Some characteristic properties of RS-5

Some characteristic properties of RS-5 are shown in Table 1. The complex index value (CI) is determined by the ratio of free amylose components in starch-lauric acid complex to iodine complexation compared to untreated starch. In other words, this value means the percentage complex formation of tapioca starch with lauric acid (D'Silva *et al.*, 2011). The CI value of RS-5 was 90.16%.

Table 1. The properties of native tapioca starch and Resistant starch type-5 (RS-5)

Parameters	Samples	
	Native starch	**RS-5**
Complex index value (CI%)	-	90,16
Rapidly digestible starch (%)	43,03*	40,28*
Slowly digestible starch (%)	33,20	30,71
Resistant starch (%)	22,76*	28,02*

*: Means within each row are significantly different according to independent t-test ($p_{value} < 0.05$).

The rapidly digestible starch (RDS), slowly digestible starch (SDS) and resistant starch (RS) content of native tapioca starch and RS-5 samples are displayed in Table 1. The RDS, SDS and RS content of native tapioca starch were 43.03%, 33.20% and 22.76%, respectively. In literature, there are various studies on the RDS, SDS, and RS content of tapioca starch. For example, Corgneau *et al.* (2019) reported that the RDS, SDS, and RS content of native tapioca starch were 19.6%, 37.8% and 42.7%, respectively. Mei *et al.* (2015) showed that the RDS, SDS and RS content of native tapioca starch were approximately 85%, 8%, and 5%, respectively. Different digestibility properties can be influenced by several factors, including the ratio of amylose to amylopectin, the degree of crystallinity of the starch, the structure of the starch molecule, the length of the amylopectin chains, the particle size, and the protein content of the starch, among others (Xu Chen *et al.*, 2017; Farooq *et al.*, 2018; Kim *et al.*, 2017; Oskaybaş-Emlek *et al.*, 2022a). The complex formation of tapioca starch with lauric acid led to decrease in RDS (40.28%) and SDS

(30.71%). However, complex formation resulted in increase in RS (28.02%) content. This situation was revealed that the complex formation between tapioca starch and lauric acid led to increase in starch's resistance to digestible enzymes. Similarly, Ramos-Villacob *et al.* observed that digestible properties of native tapioca starch and tapioca starch-lauric acid complex. They reported that RDS, SDS and RS content of native tapioca starch were 72.98%, 17.06%, and 9.96%, respectively. In addition to these, they observed that RDS, SDS and RS content of tapioca starch-lauric acid complex ranged from 36.48 to 75.61%; 10.87 to 44.61%; 11.00 to 18.90%. The starch-fatty acid complex may form an insoluble film on the starch granule. This structure has the potential to block the transportation of enzymes into the granule, thereby enhancing resistance to digestion (Oskaybaş-Emlek *et al.*, 2022a). According to Y.-S. Wang *et al.* (2020), the complex formation led to develop a more structure form, which enhanced its decrease in susceptibility of starch to digestion enzymes.

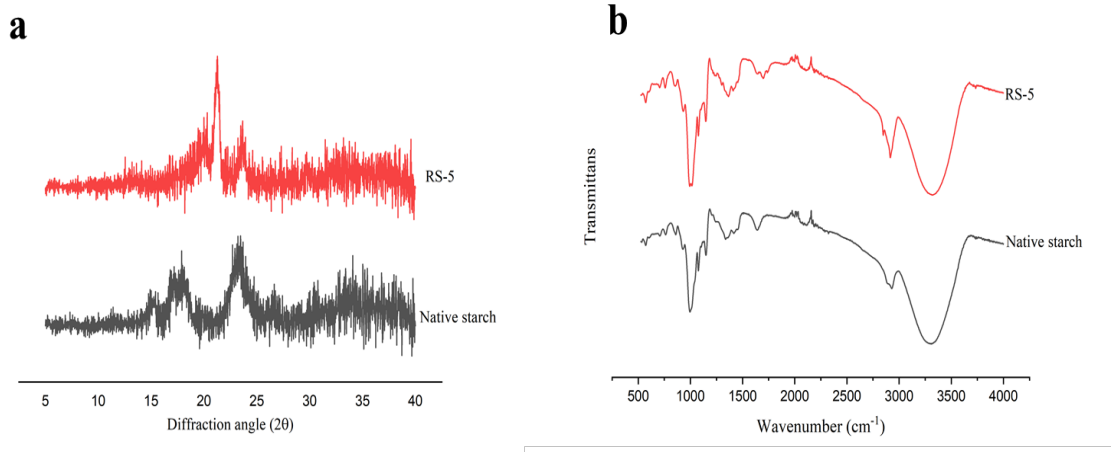

Figure 1.a- X-ray diffraction (XRD) patterns and **b-** FT-IR spectra of starch samples. RS-5; Resistant starch type-5.

The X-Ray diffraction patterns of native tapioca starch and RS-5 are shown in Figure 1a. Native tapioca starch had a typical A-type crystalline pattern with peaks at 15°, 17°,18°, ve 23° (Xia *et al.*, 2015). The complex formation of native tapioca starch with lauric acid led to emergence of a distinct diffraction at 19.9°, which can be attributed to the starch-fatty acid complex (S. Wang *et al.*, 2016). In addition, the diffraction angle at 21.6° found in the starch-lipid complex pattern belongs to the crystal form of free fatty acids (S. Wang *et al.*, 2016).

FTIR spectroscopy was utilized to verify the change in the chemical structures of tapioca starch molecules resulting from resistant starch formation. The FTIR spectra of native tapioca starch and RS-5 sample are shown in Figure 1b. In the spectrum of native tapioca starch and RS-5, the peaks at 3300 and 1600 cm^{-1} correspond to OH groups, i.e, these peaks were related to water molecule found in starch (Oskaybaş-Emlek *et al.*, 2022b; Yun *et al.*, 2020). Additionally, in two starch samples (native starch and RS-5), there was a strong absorption band at 2900 cm^{-1}, which were attributed to stretching vibration of C-H bond (Mendes *et al.*, 2021). The peaks at between 1340 and 1400 cm^{-1} was attributed to stretching of OH groups (Oskaybaş-Emlek *et al.*, 2021). The region between the 800 and 1200 cm^{-1} bands is associated with intermolecular hydrogen bonds of the double helices of amylose and amylopectin or amylose-amylopectin complexes (Oskaybaş-Emlek *et al.*, 2022b). Compared to native starch, RS-5 had a absorption band at 2848 cm^{-1}. This band was related to asymmetric stretching vibration of CH_3 and CH_2 of fatty acids. In literature, the band at 2848 was observed in starch-fatty acid

complexes compared to native starch (Sun *et al.*, 2021; S. Wang *et al.*, 2016).

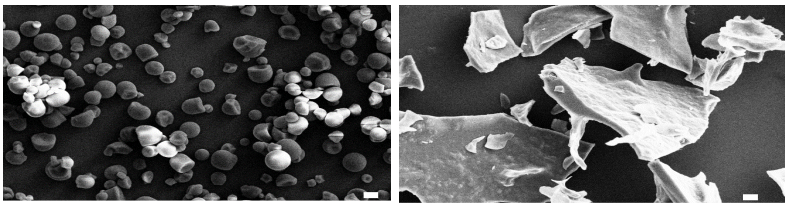

Figure 2. Scanning electronic microscope (SEM) images of **a-** Native tapioca starch **b-**RS-5. Magnification 1.0 Kx. RS-5; Resistant starch type-5.

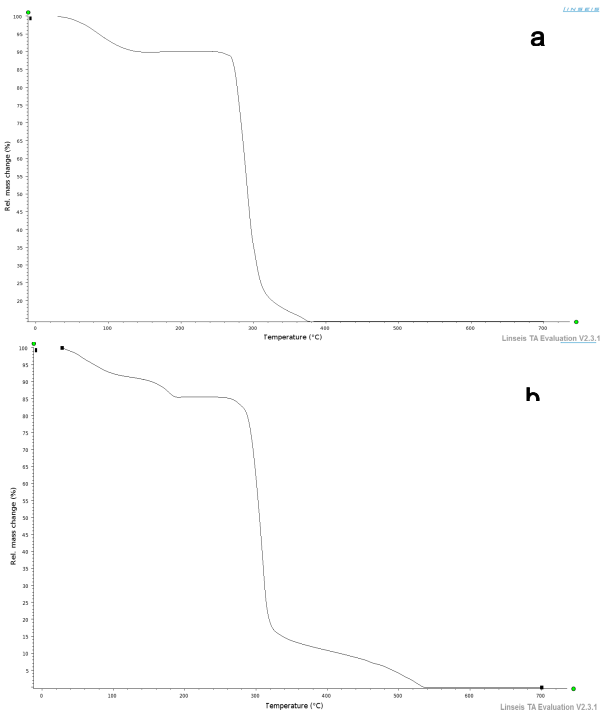

Fig. 3. TGA curves of starch samples **a-** Native tapioca starch **b-**RS-5. RS-5; Resistant starch type-5.

The scanning electron microscopy of the native tapioca starch and RS-5 are given in Figure 2. The SEM of tapioca starch (Figure.2a) exhibited a spherical granules with smooth surface. Similar observation was reported by (Xia *et al.*, 2015). However, the granule structure of tapioca starch was obviously changed by RS-5 formation between native tapioca starch and lauric acid. During RS-5 production, the starch granules swelled and ruptured, therefore the original structure was destroyed. After RS-5 formation, starch granule was disintegrated and aggregated, and thus, it became irregular. In Figure. 2b, microcrystals in the shape of protruding spherulites formed on the particle surface as a result of the RS-5 formation (Wu *et al.*, 2022). Additionally, RS-5 have larger granule size compared to native tapioca starch, as also reported by Z. Chen *et al.* (2024).

The TGA curves of native tapioca starch and RS-5 are presented in Figure 3. According to Figure 3, the thermal decomposition process of starch showed three stages in the temperature range of 20-700°C. The first stage occurred between 20-120°C and 20-200°C for native tapioca starch and RS-5, respectively, which was related to the weight loss of water evaporation (Rodríguez-Huezo *et al.*, 2018). The second stage for native tapioca starch and RS-5 occurred at approximately 120-350°C and 200-350°C, respectively. In this stage, the thermal weight loss was associated with starch degradation and degradation of guest molecules (Liu *et al.*, 2022). The weight loss in the last stage appeared at 320°C-380°C for tapioca starch, while this temperature reached 540°C for RS-5. The weight loss was ascribed to the decomposition of the ash (Liu *et al.*, 2022). According to TGA curves (Figure.4), the temperature value required for the degradation of RS-5 was approximately 140°C higher than the native starch. This situation revealed that the thermal stability of starch improved with the formation of the RS-5 sample.

3.2. Some characteristic properties of cookie samples

Table 2 shows the characteristics of cookie samples. The highest aw value belonged to cookie with 30% RS-5 replacement level (0.48) (p_{value} <0.05). This increase was related to the higher water binding capacity of the RS-5 than that of wheat flour (Water absorption capacity data of wheat flour and starch samples were not shown). The aw value is crucial in assessing food safety regarding microbial risks. The aw values suitable for the development of most bacteria, yeasts and molds are in the range of 1-0.87, 0.91-0.87 and 0.87-0.65, respectively (Oskaybaş-Emlek *et al*., 2021).

Table 2. The properties of cookie samples

Parameters	Cookie samples			
	Control	**10% RS-5**	**20% RS-5**	**30% RS-5**
a_w	0,41[b]	0,44[ab]	0,47[ab]	0,48[a]
pH	6,77[a]	6,69[b]	6,62[c]	6,61[c]
*L**	78,44[a]	78,10[a]	77,81[a]	76,84[a]
*α**	-0,24[a]	-0,56[b]	-0,65[c]	-0,93[d]
*b**	27,29[a]	24,19[b]	25,00[b]	22,28[c]
eGI	149,75[a]	147,62[a]	144,41[a]	143,37[a]
Diameter (mm)	59,75[a]	56,5[b]	55,5[c]	55,25[c]
Thickness (mm)	7,75[a]	7,75[a]	7,00[b]	7,25[ab]
Spread ratio	7,72[ab]	7,30[b]	7,96[a]	7,63[ab]
Hardness (g)	12363,87[a]	8184,52[b]	7048,89[c]	4724,42[d]

The L*, α* and b* values were determined within the scope of the color properties of cookie samples. The L* value represents lightness-darkness and that value is in the range of 100-0 (Bawa *et al.*, 2020). The L* value of control cookie was 78.44, and it slightly decreased to 76.84 with RS-5

[a-d] Mean values in the same row with different superscript letters differ significantly (p_{value} < 0.05)

RS-5; Resistant starch type-5, aw; water activity, eGI; estimated glycemic index value.

According to these aw values, the risk of microbial growth in the cookie samples produced within this study is very low. The pH value of cookie samples was significantly decreased by replacement of RS-5. The cookie samples including 30% RS-5 had the lowest pH value (6.61). The decrease in pH may be due to the fact that RS-5 contained lauric acid, i.e, the increase in replacement of RS-5 led to increase in lauric acid content in cookie.

replacement levels (P>0.05). According to Table 2, the RS-5 replacement led to less yellow (lower b*) and more green-looking cookie ($-\alpha$*: greenness) (p_{value} <0.05). Additionally, the images of the cookies were shown in Figure.5.

The estimated glycemic index (eGI) value of control cookie sample was 149.75. The eGI value of cookies decreased with the replacement of wheat flour with RS-5. However, there were no significant difference among the eGI of cookie samples (p_{value} >0.05). It may be due to the fact that the replacement level is not sufficient to decrease in eGI. These unexpected results could be due to the fact that the replacement ratio with wheat flour is not sufficient. Additionally, the eGI value of cookie made with the replacement of wheat flour with RS-5 may not have significantly decreased because of properties of wheat flour such as amylose content, relative crystallinity value (Kunyanee and Luangsakul, 2020), protein content (Jimenez-Pulido *et al*., 2022).

The cookie with 20% RS-5 replacement level had the highest spread ratio. However, there were no significant difference among spread ratio values of control sample, cookie with 20% and 30% RS-5 replacement level (p_{value}>0.05). According to Mudgil *et al*. (2017), the spread ratio is related to the quality of the cookie. A higher spread ratio is an indicator of a desirable cookie.

The hardness value of cookie samples ranged from 4724.42 g to 12362.87 g (p_{value} <0.05). The hardness value decreased with an increase in the RS-5 replacement level. The decrease in cookie hardness with the increase in RS-5 can be associated with a decrease in protein content. In other words, the increase in the RS-5 replacement level reduced the protein from wheat flour in cookie samples (Khouryieh and Aramouni, 2012). Similarly, Bae *et al*. (2013), observed that the hardness value of cookie samples diminished with increasing resistant starch content.

4. Conclusions

The complex formation of tapioca starch with lauric acid greatly affected the digestibility, crystallinity, and thermal properties of starch. V-type crystalline pattern was formed between tapioca starch and lauric acid. With complex formation, RS content of starch (from 22.75% to 42.70%) and thermal stability of starch enhanced. Morphological properties of tapioca starch were significantly affected with RS-5 formation. Additionally, the cookie samples with RS-5 replacement had a softer texture compared to the control sample, which is among the desired cookie characteristics. The eGI of cookie was not affected by the replacement of wheat flour with RS-5. This situation revealed that there are many factors affecting eGI value in addition to RS content. This study has also shown that the RS-5 produced with buckwheat starch and lauric acid is an applicable option that the increase in spread ratio. The results were especially good at the 20% substitution level when evaluating the general physical and textural characteristics of the cookie samples with RS-5 substitution.

5. References

Ai, Y., Hasjim, J., Jane, J.-l. (2013). Effects of lipids on enzymatic hydrolysis and physical properties of starch. *Carbohydrate polymers, 92*(1), 120-127. DOI: 10.1016/j.carbpol.2012.08.092.

Aparicio-Saguilán, A., Sáyago-Ayerdi, S. G., Vargas-Torres, A., Tovar, J., Ascencio-Otero, T. E., Bello-Pérez, L. A. (2007). Slowly digestible cookies prepared from resistant starch-rich lintnerized banana starch. *Journal of Food Composition and Analysis, 20*(3-4), 175-181. DOI: 10.1016/j.jfca.2006.07.005.

Bae, C.-H., Park, G.-H., Kang, W.-W., Park, H.-D. (2013). Quality characteristics of cookies added with RS4 type resistant corn starch. *Korean Journal of Food Preservation, 20*(4), 539-545. DOI: 10.11002/kjfp.2013.20.4.539.

Bawa, M., Songsermpong, S., Kaewtapee, C., Chanput, W. (2020). Effects of microwave and hot air oven drying on the nutritional, microbiological load, and color parameters of the house crickets (Acheta domesticus). *Journal of Food Processing and Preservation, 44*(5), e14407. DOI: 10.1111/jfpp.14407.

Chang, F., He, X., Huang, Q. (2013). Effect of lauric acid on the V-amylose complex distribution and properties of swelled normal cornstarch granules. *Journal of Cereal Science, 58*(1), 89-95. DOI: 10.1016/j.jcs.2013.03.016.

Chen, X.-H., Chen, S., Chen, X., Zou, S.-Y., Qiu, H.-X. (2022). Effects of maize starch-lipid complexes on in vitro digestion and glycemic index of cookies. *Journal of Food Safety and Quality*, 13(8), 2680-2686.

Chen, X., He, X., Fu, X., Zhang, B., Huang, Q. (2017). Complexation of rice starch/flour and maize oil through heat moisture treatment: Structural, in vitro digestion and physicochemical properties. *International journal of biological macromolecules, 98*, 557-564.

Chen, X., Wang, W. (2024). The lipid-amylose complexes enhance resistant starch content in candelilla wax-based oleogels cookies. *International journal of biological macromolecules, 278*, 134804. DOI:10.1016/j.ijbiomac.2024.134804.

Chen, Z., Hu, A., Ihsan, A., Zheng, J. (2024). The formation, structure, and physicochemical characteristics of starch-lipid complexes and the impact of ultrasound on their properties: A review. *Trends in Food Science & Technology*, 104515. DOI: 10.1016/j.tifs.2024.104515.

Corgneau, M., Gaiani, C., Petit, J., Nikolova, Y., Banon, S., Ritié-Pertusa, L., Le, D. T. L., Scher, J. (2019). Digestibility of common native starches with reference to starch granule size, shape and surface features towards guidelines for starch-containing food products. *International Journal of Food Science & Technology, 54*(6), 2132-2140. DOI: 10.1111/ijfs.14120.

D'Silva, T. V., Taylor, J. R., Emmambux, M. N. (2011). Enhancement of the pasting properties of teff and maize starches through wet–heat processing with added stearic acid. *Journal of Cereal Science, 53*(2), 192-197. DOI: 10.1016/j.jcs.2010.12.002.

Farooq, A. M., Dhital, S., Li, C., Zhang, B., Huang, Q. (2018). Effects of palm oil on structural and in vitro digestion properties of cooked rice starches. *International journal of biological macromolecules, 107*, 1080-1085. DOI: 10.1016/j.ijbiomac.2017.09.089.

Garcia, M., Pereira-da-Silva, M., Taboga, S., Franco, C. (2016). Structural characterization of complexes prepared with glycerol monoestearate and maize starches with different amylose contents. *Carbohydrate polymers, 148*, 371-379. DOI: 10.1016/j.carbpol.2016.04.067.

Garzóan, G., Gaines, C., Palmquist, D. (2003). Use of wheat flour-lipid and waxy maize starch-lipid composites in wire-cut formula cookies. *Journal of Food Science, 68*(2), 654-659. DOI: 10.1111/j.1365-2621.2003.tb05726.x.

Giuberti, G., Marti, A., Fortunati, P., Gallo, A. (2017). Gluten free rice cookies with resistant starch ingredients from modified waxy rice starches: Nutritional aspects and textural characteristics. *Journal of Cereal Science, 76*, 157-164. DOI: 10.1016/j.jcs.2017.06.008.

Han, J., Wu, J., Liu, X., Shi, J., Xu, J. (2023). Physiological effects of resistant starch and its applications in food: a review. *Food Production, Processing and Nutrition, 5*(1), 48. DOI: 10.1186/s43014-023-00156-x.

Jimenez-Pulido, I. J., Daniel, R., Perez, J., Martínez-Villaluenga, C., De Luis, D., Martín Diana, A. B. (2022). Impact of protein content on the antioxidants, anti-inflammatory properties and glycemic index of wheat and wheat bran. *Foods, 11*(14), 2049. DOI: 10.3390/foods11142049.

Kahraman, K., Aktas-Akyildiz, E., Ozturk, S., Koksel, H. (2019). Effect of different resistant starch sources and wheat bran on dietary fibre content and in vitro glycaemic index values of cookies. *Journal of Cereal Science, 90*, 102851. DOI: 10.1016/j.jcs.2019.102851.

Khouryieh, H., Aramouni, F. (2012). Physical and sensory characteristics of cookies prepared with flaxseed flour. *Journal of the science of food and agriculture, 92*(11), 2366-2372. DOI: 10.1002/jsfa.5642.

Kim, H. I., Kim, H. R., Choi, S. J., Park, C.-S., Moon, T. W. (2017). Preparation and characterization of the inclusion complexes between amylosucrase-treated waxy starch and palmitic acid. *Food science and biotechnology, 26*(2), 323-329. DOI: 10.1007/s10068-017-0044-z.

Kunyanee, K., Luangsakul, N. (2020). The effects of ultrasound–assisted recrystallization followed by chilling to produce the lower glycemic index of rice with different amylose content. *Food Chemistry, 323*, 126843. DOI: 10.1016/j.foodchem.2020.126843.

Li, L., Liu, Z., Zhang, W., Xue, B., Luo, Z. (2021). Production and applications of amylose-lipid complexes as resistant starch: recent approaches. *Starch-Stärke, 73*(5-6), 2000249. DOI: 10.1002/star.202000249.

Liu, P., Dong, Y., Gao, W., Wu, Z., Yu, B., Yuan, C., Cui, B. (2022). Effects of water/ionic liquid ratios on the physicochemical properties of high amylose maize starch-lauric acid complex. *Food Hydrocolloids*, 108134. DOI: 10.1016/j.foodhyd.2022.108134.

Luo, S., Zeng, Z., Mei, Y., Huang, K., Wu, J., Liu, C., Hu, X. (2020). Improving ordered arrangement of the short-chain amylose-lipid complex by narrowing molecular weight distribution of short-chain amylose. *Carbohydrate polymers, 240*, 116359. DOI: 10.1016/j.carbpol.2020.116359.

Mei, J.-Q., Zhou, D.-N., Jin, Z.-Y., Xu, X.-M., Chen, H.-Q. (2015). Effects of citric acid esterification on digestibility, structural and physicochemical properties of cassava starch. *Food Chemistry, 187*, 378-384. DOI: 10.1016/j.foodchem.2015.04.076.

Mendes, D. d. C. S., Asquieri, E. R., Batista, R. D., de Morais, C. C., Ascheri, D. P. R., de Macêdo, I. Y. L., de Souza Gil, E. (2021). Microencapsulation of jabuticaba extracts (Myrciaria cauliflora): Evaluation of their bioactive and thermal properties in cassava starch biscuits. *LWT, 137*, 110460. DOI: 10.1016/j.lwt.2020.110460.

Milašinović Šeremešić, M., Dokić, L., Nikolić, I., Radosavljević, M., Šoronja Simović, D. (2013). Rheological and textural properties of short (cookie) dough made with two types of resistant starch. *Journal of texture studies, 44*(2), 115-123. DOI: 10.1111/jtxs.12003.

Mudgil, D., Barak, S., Khatkar, B. (2017). Cookie texture, spread ratio and sensory acceptability of cookies as a function of soluble dietary fiber, baking time and different water levels. *LWT, 80*, 537-542. DOI: 10.1016/j.lwt.2017.03.009.

Oskaybaş-Emlek, B., Özbey, A., Aydemir, L. Y., Kahraman, K. (2022a). Buckwheat Starch-Myristic Acid Complex Formation: Effect Of Reaction Temperature And Myristic Acid Concentration On Digestibility Properties. *Gıda, 47*(6), 1168-1179. DOI: 10.15237/gida.GD22116.

Oskaybaş-Emlek, B., Özbey, A., Aydemir, L. Y., Kahraman, K. (2022b). Production of buckwheat starch-myristic acid complexes and effect of reaction conditions on the physicochemical properties, X-ray pattern and FT-IR spectra. *International journal of*

biological macromolecules, 207, 978-989. DOI: 10.1016/j.ijbiomac.2022.03.189.

Oskaybaş-Emlek, B., Özbey, A., Kahraman, K. (2021). Effects of germination on the physicochemical and nutritional characteristics of lentil and its utilization potential in cookie-making. *Journal of Food Measurement and Characterization*, 1-11. DOI: 10.1007/s11694-021-00958-y.

Oskaybaş-Emlek, V., Figueroa-Flórez, J., Salcedo-Mendoza, J., Hernandez-Ruydíaz, J., Romero-Verbel, L. Development of modified cassava starches by ultrasound-assisted amylose/lauric acid complex formation Desarrollo de almidones modificados de yuca mediante la formación de complejos amilosa/ácido láurico asistido por ultrasonido. *Revista Mexicana de Ingeniería Química*, 23(1), 2024. DOI: 10.24275/rmiq/Alim24109.

Reddy, C. K., Choi, S. M., Lee, D.-J., Lim, S.-T. (2018). Complex formation between starch and stearic acid: Effect of enzymatic debranching for starch. *Food Chemistry, 244*, 136-142. DOI: 10.1016/j.foodchem.2017.10.040.

Rodríguez-Huezo, M. E., Flores-Silva, P. C., Garcia-Diaz, S., Meraz, M., Vernon-Carter, E. J., Alvarez-Ramirez, J. (2018). Effect of fat type on starch and protein digestibility of traditional tamales. *Starch-Stärke, 70*(5-6), 1700286. DOI: 10.1002/star.201700286.

Rojhani, A., Naranjo, J., Ouyang, P. (2022). Physiochemical properties and sensory characteristics of resistant starch enriched cookies. *Nutrition & Food Science, 52*(5), 791-800. DOI: 10.1108/NFS-07-2021-0231.

Sengupta, A., Chakraborty, I., Mazumder, N. (2023). An insight into the physicochemical characterisation of starch-lipid complex and its importance in food industry. *Food Reviews International, 39*(7), 4198-4212. DOI: 10.1080/87559129.2021.2021936.

Seo, T.-R., Kim, J.-Y., Lim, S.-T. (2015). Preparation and characterization of crystalline complexes between amylose and C18 fatty acids. *LWT-Food Science and Technology, 64*(2), 889-897. DOI: 10.1016/j.lwt.2015.06.021.

Sharma, A., Yadav, B. S., Ritika. (2008). Resistant starch: physiological roles and food applications. *Food Reviews International, 24*(2), 193-234. DOI: 10.1080/87559120801926237.

Stewart, M. L., Zimmer, J. P. (2017). A high fiber cookie made with resistant starch type 4 reduces post-prandial glucose and insulin responses in healthy adults. *Nutrients, 9*(3), 237. DOI: 10.3390/nu9030237.

Sun, S., Jin, Y., Hong, Y., Gu, Z., Cheng, L., Li, Z., Li, C. (2021). Effects of fatty acids with various chain lengths and degrees of unsaturation on the structure, physicochemical properties and digestibility of maize starch-fatty acid complexes. *Food Hydrocolloids, 110*, 106224. DOI:10.1016/j.foodhyd.2020.106224.

Wang, S., Wang, J., Yu, J., Wang, S. (2016). Effect of fatty acids on functional properties of normal wheat and waxy wheat starches: a structural basis. *Food Chemistry, 190*, 285-292. DOI: 10.1016/j.foodchem.2015.05.086.

Wang, S., Zheng, M., Yu, J., Wang, S., Copeland, L. (2017). Insights into the formation and structures of starch–protein–lipid complexes. *Journal of agricultural and food chemistry, 65*(9), 1960-1966. DOI: 10.1021/acs.jafc.6b05772.

Wang, Y.-S., Liu, W.-H., Zhang, X., Chen, H.-H. (2020). Preparation of VII-type normal cornstarch-lauric acid complexes with high yield and stability using a combination treatment of debranching and different complexation temperatures. *International journal of biological macromolecules, 154*, 456-465. DOI: 10.1016/j.ijbiomac.2020.03.142.

Wu, X., Yu, H., Bao, G., Luan, M., Wang, C. (2022). Preparation of adzuki bean starch-lipid complexes and their anti-digestion mechanism. *Journal of Food Measurement and Characterization*, 1-12. DOI: 10.1007/s11694-021-01222-z.

Xia, W., Wang, F., Li, J., Wei, X., Fu, T., Cui, L., Li, T., Liu, Y. (2015). Effect of high speed jet on the physical properties of tapioca starch. *Food Hydrocolloids, 49*, 35-41. DOI: 10.1016/j.foodhyd.2015.03.010.

Yun, P., Devahastin, S., Chiewchan, N. (2020). Physical properties, microstructure and digestion behavior of amylose-lipid powder complexes prepared using conventional and spray-drying based methods. *Food Bioscience, 37*, 100724. DOI: 10.1016/j.fbio.2020.100724.

Zheng, B., Wang, T., Wang, H., Chen, L., Zhou, Z. (2020). Studies on nutritional intervention of rice starch-oleic acid complex (resistant starch type V) in rats fed by high-fat diet. *Carbohydrate polymers, 246*, 116637. DOI: 10.1016/j.carbpol.2020.116637.

Acknowledgements

This project was financially supported by the Scientific Research Commission of Niğde Ömer Halisdemir University (Project No: TGT 2019/4-BAGEP). The authors are grateful for the support.

CARPATHIAN JOURNAL OF FOOD SCIENCE AND TECHNOLOGY

journal homepage: **http://chimie-biologie.ubm.ro/carpathian_journal/index.html**

Research article

DEVELOPMENT OF A MATHEMATICAL MODEL TO DETERMINE THE MOISTURE DIFFUSIVITY OF AN INFINITE FLAT SLAB DRYING MATERIAL: APPLICATION TO FREEZE-DRYING OF YOGURT

Van Doanh Pham[1], Hoan Pham Thi[1], Dung Dang Thi Ngoc[1], Khanh Dung Pham[1], Liviu Giurgiulescu[2], Dzung Tan Nguyen[1]✉

[1]Department of Food Technology, Faculty of Chemical and Food Technology, HCMC University of Technology and Education, No 01-Vo Van Ngan Street, Thu Duc City, Ho Chi Minh City, Viet Nam.
[2]Chemistry-Biology Department, Technical University of Cluj Napoca, North Universitary Center of Baia Mare, Romania,
✉tandzung072@hcmute.edu.vn

https://doi.org/10.34302/2025.17.3.4

Article history:
Received:
June 5th, 2025
Accepted:
Novemebre 1st, 2025

Keywords:
Freeze-drying;
Yogurt;
Mass Transfer during Freeze-drying;
Mathematical model;
Moisture diffusivity;
Moisture diffusion coefficient.

ABSTRACT

In the study of freeze-drying engineering and technology, one of the key factors is the development and solution of a mathematical modeling problem to describe the drying kinetics, thereby determining the optimal technological parameters. The ultimate goal is to ensure that the dried product meets high quality standards, achieves the desired moisture content, and minimizes energy consumption. However, this modeling and optimization process cannot be effectively carried out without first determining the characteristic moisture diffusion coefficient of the material. In particular, the characteristic moisture diffusivity coefficient of the material depends on the temperature and pressure of the freeze-drying environment, which, until now, has not been addressed in any research work. Therefore, this study presents a mathematical model for determining the effective moisture diffusivity of yogurt during the freeze-drying process: $D = (0.284 + 0.05\times X_1 + 0.123\times X_2 + 0.144\times X_1\times X_2)\times 10^{-11}$, m^2/s, with the maximum error of 1.11% for the mathematical model and the correlation coefficient $R^2 = 0.9979$. Based on this model, when the freeze-drying temperature $X_1 = T = (30\div 40)^0C$ and the pressure $X_2 = P = (0.01\div 0.1)$mmHg the effective moisture diffusivity of yogurt during freeze-drying was determined to range from 1.822×10^{-11} to 2.864×10^{-11} m^2/s.

1. Introduction

Over the past two decades, freeze-drying technology and engineering have developed rapidly worldwide and are now considered to have reached a high level of maturity (Fellows, 2000; Dzung et al., 2022). This advancement has made significant contributions to the development of various fields such as pharmaceuticals, food processing, biotechnology, and related industries.

Freeze-drying is conducted under low-pressure and low-temperature conditions, specifically below the triple point of

water O (0.0098∘C; 4.58 mmHg). This means that the temperature of the drying material remains below 0.0098∘C and the ambient drying pressure stays below 4.58 mmHg. As a result, the dried product retains almost all of the original natural characteristics of the raw material: proteins are neither hydrolyzed nor denatured, carbohydrates are not hydrolyzed or gelatinized, lipids are not oxidized; color and flavor are preserved; bioactive compounds and vitamins remain intact; and trace minerals are conserved (Anandharamakrishnan, C., 2017; Dzung, N.T and et al., 2024).

In addition, the final product structure is porous, with no shrinkage or surface cracking, and exhibits excellent rehydration capability—superior to that of products dried using conventional methods (Bhushani & Anandharamakrishnan, 2017; Athanasios, I. Liapis and Roberto Bruttini, 2020; Dzung et al., 2022). Therefore, freeze-drying is considered one of the most advanced drying technologies available today. Many years of experimentation have shown that freeze-drying is highly suitable for drying yogurt.

Yogurt is a dairy product fermented mainly by lactic acid bacteria such as Lactobacillus delbrueckii subsp. bulgaricus and Streptococcus thermophilus. Nutritionally, yogurt contains a high level of easily digestible proteins, calcium, B vitamins (particularly B2 and B12), as well as various essential minerals. Importantly, during the fermentation process, lactose in milk is converted into lactic acid, making yogurt more tolerable for individuals with lactose intolerance (Dzung et al., 2024).

In addition to its nutritional value, yogurt is also considered a probiotic food. Beneficial bacteria in yogurt, such as Lactobacillus and Bifidobacterium, can help balance the gut microbiota, inhibit the growth of harmful microorganisms, and stimulate the immune system. Numerous clinical studies have demonstrated that the consumption of probiotic yogurt improves digestion, enhances nutrient absorption, reduces the risk of gastrointestinal disorders, and supports overall health, (Dzung et al., 2024).

The studies by Dzung et al. (2024) have demonstrated that no drying method other than freeze-drying can preserve the structure, nutritional composition, and probiotic content of yogurt.

Due to the high energy costs associated with the freeze-drying process, this method is typically suitable only for raw materials with high economic value. Therefore, it is essential to optimize the drying process to ensure that the final product achieves the highest possible quality, meets the required moisture content for extended shelf life and marketability, and minimizes energy consumption. Only under such conditions can freeze-drying provide a competitive advantage (Athanasios I. Liapis and Roberto Bruttini, 2020; Mawilai, P., Chaloeichitratham, N., and Pornchaloempong, P., 2019).

However, the modeling and optimization of the freeze-drying process are far from straightforward. This is not only due to the inherently complex nature of simultaneous heat and mass transfer phenomena, but also because the effective moisture diffusivity of the drying material—a critical parameter required to solve the mathematical model—has not yet been determined (G. Wilhelm-Oetjen and Peter Haseley, 2004; Bhushani and Anandharamakrishnan, 2017; Dzung et al., 2022).

To date, numerous studies have reported the determination of effective moisture diffusivity for various types of drying materials, such as: Effective

moisture diffusivity of plain yogurt undergoing microwave vacuum drying (Suk Shin Kim, Santi R. Bhowmik, 1995); Dehydration characteristics of papaya (Carica pubenscens): determination of equilibrium moisture content and diffusion coefficient (R. Lemus-Mondaca et al., 2007); Dependence of the effective diffusion coefficient of moisture on thickness and temperature in convective drying of sliced materials. A study on slices of banana, cassava and pumpkin (W.J.N. Fernando, H.C. Low, A.L. Ahmad, 2011). However, the specific determination of moisture diffusivity in frozen yogurt in the form of flat slabs—intended for application in freeze-drying—has not yet received sufficient attention (Lim, Y., Hong, S., Shin, Y. K. Kang, S. H., and Center D., 2015). Therefore, the objective of this study is to develop a mathematical model for determining the effective moisture diffusivity of drying materials in general, and frozen yogurt slabs in particular. The findings of this research will serve as a basis for the modeling and optimization of the freeze-drying process (Bhushani and Anandharamakrishnan, 2017; Dzung N.T., Chuyen H.V., Linh V.T.K., et al., 2022; Liviu Giurgiulescu, Phong Le Thanh, Linh T.K. Do, and Tan Dzung Nguyen., 2024).

2. Development of a Mathematical Model for Freeze-Drying of Yogurt

2.1. Initial Assumptions for Developing the Mathematical Model

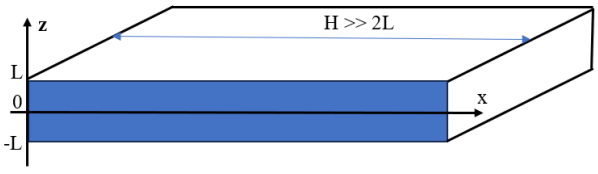

Figure 1a. Physical model of frozen yogurt in flat slab form

Frozen yogurt is cast into flat slab molds with length H (m), width h (m), and thickness a = 2L (m). Since H and h are much larger than the thickness a = 2L (i.e., H, h ≫ a = 2L), the flat slab can be considered as infinite in the length and width directions, (Dzung et al., 2022).

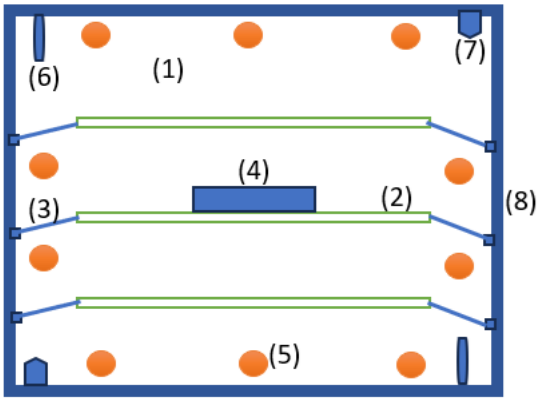

Figure 1b. Experimental freeze-drying chamber

(1)- freeze-drying chamber; (2)- The grid frame for placing the freeze-drying samples, made of 304 stainless steel, is connected to the load cell lever arm; (3)- The lever arm connects the sample grid to the vertically moving slider of the load cell to determine the change in sample mass during the drying process; (4) The yogurt samples, pre-frozen for freeze-drying; (5)- Infrared lamps provide heat to ensure uniform temperature within the drying chamber; (6)- Temperature sensor; (7)- Pressure sensor; (8)- Drying chamber wall with a hole connecting to the freezing chamber and vacuum pump.

The flat slab-shaped yogurt is frozen until the surface temperature reaches -37°C and the core temperature reaches -33°C. At this point, the average temperature of the frozen yogurt slab is approximately -35°C. At this temperature, the water within the frozen yogurt slab is completely solidified, preparing the sample for the subsequent freeze-drying stage, (Hoan Thi Pham, Linh T.K. Do, Tuan Thanh Chau, Dzung Tan Nguyen, 2023).

The initial moisture content of the frozen yogurt flat slab is W_0 (%) and is uniformly distributed throughout the entire sample.

The moisture content of the freeze-dried yogurt product reaches the desired level W_e (%) corresponding to the drying time $t = t_e$ (seconds).

The frozen yogurt flat slab is placed into the freeze-drying chamber with the drying environment set at a temperature T = 30 to 40°C and pressure P = 0.01 to 0.1 mmHg, which is below 4.58 mmHg. Freeze-drying experiments are conducted under these conditions to investigate and determine the moisture diffusivity coefficient, (Duan, X., Yang, X., Ren, G., Pang, Y., Liu, L., and Liu, Y., 2016; Liviu Giurgiulescu, et al., 2024).

2.2. Development of a Mathematical Model Describing Mass Transfer During Freeze-Drying

Since H, h >> a = 2L (see Figure 1), the Fick's second law model describing the sublimation of frozen water can be expressed as follows (Dzung N.T., Chuyen H.V., Linh V.T.K., et al., 2022):

$$\frac{\partial W}{\partial t} = D\frac{\partial^2 W}{\partial z^2};\ t \geq 0;\ -L \leq z \leq L \qquad (1)$$

- Initial condition:

At t = 0, the moisture content is uniformly distributed:

$$W(z, 0) = W_o = \text{const} \qquad (2)$$

- Boundary conditions:

At z = 0 and z = L and at time t = t_e:

$$W(0, t_e) = W(L, t_e) = W_e = \text{const} \qquad (3)$$

2.3. Solving the Mathematical Model to Determine the Moisture Diffusivity of the Drying Material

Introduce a new function to homogenize the initial and boundary conditions for solving the system of equations (1), (2), and (3), (Nguyen Tan Dzung., 2017):

$$u(z, t) = W(z, t) - W_e \qquad (4)$$

$$\Rightarrow \begin{cases} u(z,0) = W_o - W_e \\ u(0,t) = u(L,t) = 0 \end{cases} \qquad (5)$$

Substituting equation (4) into equation (1) yields:

$$\begin{cases} \dfrac{\partial u(z,t)}{\partial t} = D\dfrac{\partial^2 u(z,t)}{\partial z^2} \\ u(z,t) = u_o = W_o - W_e \\ u(0,t) = 0 \\ u(L,t) = 0 \end{cases} \qquad (6)$$

$$\text{Let } u(z, t) = Z(z).T(t) \qquad (7)$$

Substituting equation (7) into equation (6) yields:

$$\frac{1}{D}\frac{T'(t)}{T(t)} = \frac{Z''(z)}{Z(z)} = -k, (k > 0) \qquad (8)$$

$$(8) \Rightarrow \begin{cases} T'(t) + kD.T(t) = 0 \\ Z''(z) + k\,Z(z) = 0 \end{cases} \qquad (9)$$

Solving system of equations (9) yields the solution:

$$\begin{cases} T(t) = B.\exp(-kDt) \\ Z(z) = C_1 \sin\left(z\sqrt{k}\right) + C_2 \cos\left(z\sqrt{k}\right) \end{cases} \qquad (10)$$

Substituting equation (10) into equation (7) yields the solution of equation (6):

$$u(z,t) = Z(z).T(t) = \left[C_1 \sin\left(z\sqrt{k}\right) + C_2 \cos\left(z\sqrt{k}\right)\right] B.\exp(-kDt) \qquad (11)$$

From equation (11), it follows that:

$$u(0,t) = 0 \Rightarrow C_2 = 0 \qquad (12)$$

Substituting equation (12) into equation (11) yields:

$$u(z,t) = \left[C_1 \sin\left(z\sqrt{k}\right)\right] B.\exp(-kDt) \qquad (13)$$

From equation (13), it follows that:

$$u(L, t) = 0 \Rightarrow \sin\left(L\sqrt{k}\right) = 0$$

$$\Rightarrow L\sqrt{k} = n\pi \Rightarrow k = \left(\frac{n\pi}{L}\right)^2 \qquad (14)$$

Let A = B.C_1, since n = 1 $\rightarrow \infty$ the solution (13) can be rewritten in the form of the following series:

$$u(z,t)=\sum_{n=1}^{\infty}A_n\sin\left(\frac{n\pi}{L}z\right).\exp\left[-D.\left(\frac{n\pi}{L}\right)^2 t\right] \quad (15)$$

The coefficients A_n are determined according to the initial condition:

$$u(z,0)=u_o=W_o-W_e=\text{const} \quad (16)$$

From equation (15), it follows that:

$$u_o=\sum_{n=1}^{\infty}A_n\sin\left(\frac{n\pi}{L}z\right)\Leftrightarrow$$

$$2u_o\sum_{n=1}^{\infty}\sin\left(\frac{n\pi}{L}z\right)=\sum_{n=1}^{\infty}2A_n\sin^2\left(\frac{n\pi}{L}z\right)$$

$$\Leftrightarrow A_n\int_0^L 2\sin^2\left(\frac{n\pi}{L}z\right)dz=2u_o\int_0^L\sin\left(\frac{n\pi}{L}z\right)dz$$

$$\Leftrightarrow A_n\int_0^L\left[1-\cos\left(\frac{2n\pi}{L}z\right)\right]dz=$$

$$2u_o\left[-\frac{L}{n\pi}\cos\left(\frac{n\pi}{L}z\right)\right]_0^L$$

$$\Leftrightarrow A_n\left[z-\frac{L}{2n\pi}\sin\left(\frac{2n\pi}{L}z\right)\right]_0^L=$$

$$2u_o\frac{L}{n\pi}\left(1-\cos(n\pi)\right),n=2m+1$$

$$\Leftrightarrow A_n=\frac{4u_o}{n\pi} \quad (17)$$

With: $n=2m+1$

Substituting equation (17) into equation (15) yields the solution:

$$u(z,t)=u_0\sum_{\substack{m=0\\n=2m+1}}^{\infty}\frac{4}{n\pi}\sin\left(\frac{n\pi}{L}z\right).\exp\left[-D.\left(\frac{n\pi}{L}\right)^2 t\right] \quad (18)$$

Equation (18) is rewritten as follows:

$$W(z,t)=W_e+$$

$$\left(W_o-W_e\right)\sum_{\substack{m=0\\n=2m+1}}^{\infty}\frac{4}{n\pi}\sin\left(\frac{n\pi}{L}z\right).\exp\left[-D.\left(\frac{n\pi}{L}\right)^2 t\right] \quad (19)$$

Since the moisture content in the drying material is non-uniformly distributed, it is necessary to calculate the average moisture content. The average moisture content of the drying material is determined by the following equation (Nguyen Tan Dzung., 2017):

$$\overline{W}(z,t)=\frac{1}{L}\int_0^L W(z,t)dz=\frac{1}{L}\left[\int_0^L W_e dz+\right.$$

$$\left.\int_0^L\left(W_o-W_e\right)\sum_{\substack{m=0\\n=2m+1}}^{\infty}\frac{4}{n\pi}\sin\left(\frac{n\pi}{L}z\right).\exp\left[-D.\left(\frac{n\pi}{L}\right)^2 t\right]dz\right] \quad (20)$$

Calculating equation (20) yields:

$$\overline{W}(z,t)=W_e+\frac{\left(W_o-W_e\right)}{L}\times$$

$$\sum_{\substack{m=1\\n=2m+1}}^{\infty}\frac{4L}{(n\pi)^2}\left[-\cos\left(\frac{n\pi}{L}z\right)\right]_0^L.\exp\left[-D.\left(\frac{n\pi}{L}\right)^2 t\right]$$

$$\Rightarrow\frac{\overline{W}(z,t)-W_e}{W_o-W_e}=\sum_{\substack{m=0\\n=2m+1}}^{\infty}\frac{8}{(n\pi)^2}.\exp\left[-D.\left(\frac{n\pi}{L}\right)^2.t\right] \quad (21)$$

Since the series (21) converges rapidly when $m \geq 1$, in practice, only the term with $m = 0$ is considered in calculations. Therefore, equation (21) is rewritten as follows:

$$\frac{\overline{W}(z,t)-W_e}{W_o-W_e}=\frac{8}{\pi^2}\times\exp\left[-\frac{\pi^2 D}{L^2}.t\right] \quad (22)$$

Let: $MR=\dfrac{\overline{W}(z,t)-W_e}{W_o-W_e}$ (23)

Rewriting from equations (22) and (23):

$$\ln(MR)=\ln\left(\frac{8}{\pi^2}\right)-\left(\frac{\pi^2 D}{L^2}\right).t \quad (24)$$

Let: $A=\dfrac{8}{\pi^2}=0.8106;\ b=\dfrac{\pi^2 D}{L^2}$ (25)

Rewriting from equations (24) and (25):

$$\ln(MR)=-bt+\ln(A) \quad (26)$$

Equation (26) serves as the basis for determining the coefficient b, which is then used to experimentally determine the moisture diffusion coefficient of the drying material.

$$D = \frac{L^2 b}{\pi^2},\ m^2/s \qquad (27)$$

3. Materials and methods

3.1. Raw material

Sample Preparation: The raw material used is yogurt with an initial moisture content W_o = 83% = 0.83. The mold is designed to ensure uniform shape and thickness among samples, facilitating the drying process and subsequent moisture kinetics analysis. The sample is poured into a flat plate mold with the following dimensions (Figure 2):

- Thickness: a = 2L = 4mm = 0.004m; half-thickness: L = 2mm = 0.002m
- Width: h = 30mm = 0.03m
- Length: H = 60mm = 0.06m

Freezing the Sample: The entire mold filled with yogurt is placed in a freezing environment at a temperature of −50°C. The freezing process continues until the surface temperature of the flat plate reaches -37^0C and the temperature at the center of the flat plate reaches -33^0C. At this point, the average temperature of the flat yogurt sample is approximately -35^0C. At this temperature, the water in the sample is completely frozen, ensuring suitable conditions for proceeding to the freeze-drying stage.

Storage of the Frozen Sample: After the freezing process is complete, the flat yogurt sample is removed from the mold and stored in a stable environment at a temperature of -35^0C. Maintaining this temperature helps preserve the frozen state of the sample, ensuring the necessary initial conditions for the freeze-drying process (Athanasios, I. Liapis and Roberto Bruttini, 2020).

Thus, the sample preparation process has been completed and is ready for the subsequent steps in the study.

Note: The samples were frozen separately to the required temperature before being placed into the freeze-drying chamber. Prior to loading the samples, the chamber was also pre-cooled to approximately the average temperature of the samples. This procedure helps minimize experimental errors.

Moisture Content Requirement of the Freeze-Dried Product: For freeze-dried yogurt products, the technical requirement is that the final moisture content must not exceed 3%. This moisture level is considered the necessary equilibrium moisture content to ensure long-term preservation, inhibit microbial growth, and maintain the sensory and nutritional properties of the product. Therefore, in this study, the post-drying moisture content is selected as W_e = 3% = 0.03 (Yildiz, F., 2010).

3.2. Equipment

The main equipment used in this study is the DS-12 Freeze Drying System, which was designed, and fabricated by the research team of Associate Professor Dr. Dzung N.T from the Department of Chemical and Food Technology, Ho Chi Minh City University of Technology and Education, Vietnam (Dzung, N.T and et al., 2024).

Figure 2. The DS-12 Freeze Drying System automatically measured and controlled by compute

3.3. Methods

3.3.1. Freeze-drying experiment of yogurt

The yogurt samples were frozen and stored at a stable temperature of -35^0C. These samples

were then transferred into the freeze-drying chamber of the DS-12 freeze-dryer system to conduct the experiment.

The drying ambient temperature was set at T = (30 ÷ 40) ^oC and the drying ambient pressure at P = (0.01 ÷ 0.1) mmHg, which is below 4.58 mmHg, see Table 2 and Table 3. Temperature and pressure were automatically measured and controlled through sensors connected to a computer, with the data displayed on the control panel. The measurement of time was obtained directly from the computer system.

Freeze-drying was carried out to investigate the change in moisture content of yogurt ($\overline{W}(z,t)$) over drying time, t (seconds).

3.3.2. Moisture content of the product

The moisture content of the product ($\overline{W}(z,t)$, %) was determined using the following formula (Dzung, N.T and et al., 2024):

$$\overline{W}(z,t) = 100 - \frac{G_o}{G_j}(100 - W_o), (\%) \quad (28)$$

Where: G_0 = 10g represents the initial mass of yogurt before drying; G_j (g) represents the mass of yogurt after drying; W_0 represents the initial moisture content of yogurt (%).

In which, W_0 represents the initial moisture content of yogurt (%) was determined using the convective drying method in a drying oven, as described in AOAC – 927.05. Accurately weighed G_0 = 10g of finely ground sample was placed in a clean, dry, pre-weighed aluminum dish. The sample was then subjected to the drying cabinet at a temperature of 105 °C until a constant mass was achieved (AOAC International, 2000);

G_0 = 10g was determined by gravimetric measurement;

G_j (g) was measured using a specially designed mass sensor located inside the drying chamber to monitor the sample's weight changes throughout the drying process, with the data displayed on the control panel.

3.3. Experimental data processing and analysis

For experimental data processing in this study, only Microsoft Excel 2024 combined with statistical theory was used. The Excel Solver function was applied to determine the maximum and minimum values.

In addition, this study employed Matlab 2024 software to simulate the variation of the diffusion coefficient as a function of the temperature and pressure of the freeze-drying environment.

4. Results and Discussion

4.1.Some necessary thermophysical parameters for calculating the moisture diffusion coefficient of yogurt

The frozen yogurt material in flat sheet form has thermophysical properties presented in Table 1.

Table 1. Thermophysical Properties of Yogurt Material

Parameters	Symbol	Unit	Value
Half-thickness	L	m	0.002
Width	b	m	0.03
Length	H	m	0.06
Moisture content of the material	W_0	%	83
Moisture content of the product	W_e	%	3

These thermophysical parameters are essential for calculating the variation of Ln(MR) with drying time *t*, as presented in Equation (26). From this, the coefficient *b* in the linear relationship of Equation (26) can be determined. Subsequently, by applying Equation (27), the effective moisture diffusivity of yogurt during the freeze-drying process can be accurately calculated.

4.2. Determination of the moisture diffusivity of freeze-dried yogurt

The experiment was conducted by freeze-drying yogurt using the DS-12 system at a freeze-drying ambient temperature of T = 30°C and an ambient pressure of P = 0.1 mmHg to investigate

the moisture content changes of the material over drying time. Based on this, the moisture ratio (MR) as a function of drying time was calculated. Equation (28) was used to determine $\overline{W}(z,t)$, and equation (23) was applied to calculate the moisture ratio (MR) and Ln(MR). The experimental results and the calculated values are summarized and presented in Table 2.

Table 2. Variation of moisture content ($\overline{W}(z,t)$, %) and moisture ratio (MR) and Ln(MR) over drying time t (s)

t (h)	t (s)	$\overline{W}(z,t)$ %	MR	Ln(MR)-Ln(A)
0	0	0.8300	1.0000	0.2100
1	3600	0.7240	0.8675	0.0678
2	7200	0.6140	0.7300	-0.1047
3	10800	0.4640	0.5425	-0.4016
4	14400	0.3260	0.3700	-0.7843
5	18000	0.2690	0.2988	-0.9982
6	21600	0.2380	0.2600	-1.1371
7	25200	0.2160	0.2325	-1.2489
8	28800	0.1740	0.1800	-1.5048
9	32400	0.1510	0.1513	-1.6788
10	36000	0.1316	0.1270	-1.8536
11	39600	0.1138	0.1048	-2.0462
12	43200	0.1080	0.0975	-2.1179
13	46800	0.0892	0.0740	-2.3937
14	50400	0.0786	0.0608	-2.5910
15	54000	0.0721	0.0526	-2.7346
16	57600	0.0617	0.0396	-3.0183
17	61200	0.0568	0.0335	-3.1862
18	64800	0.0531	0.0289	-3.3348
19	68400	0.0487	0.0234	-3.5461
20	72000	0.0465	0.0206	-3.6713
21	75600	0.0432	0.0164	-3.8982
22	79200	0.0409	0.0136	-4.0859
23	82800	0.0387	0.0109	-4.3113
24	86400	0.0368	0.0085	-4.5577
25	90000	0.0363	0.0078	-4.6420
26	93600	0.0353	0.0066	-4.8126
27	97200	0.0343	0.0053	-5.0254
28	100800	0.0335	0.0044	-5.2219
29	104400	0.0332	0.0040	-5.3115
30	108000	0.0330	0.0038	-5.3760

Based on the data in Table 2 describing the relationship between Ln(MR/A) and t. the least squares method was applied to minimize the sum of squared deviations between experimental values and those calculated from the mathematical model. At the same time, the significance of the model coefficients was tested using the Student's t-test, and the goodness of fit of the mathematical model was evaluated by the Fisher's F-test. The resulting mathematical model was determined as follows:

$$Ln(MR/A) = -5.5\times10^{-5}\times t \quad (29)$$

With $A = \frac{8}{\pi^2} = 0.8106$, it follows that:

$$Ln(A) = -0.201$$

Equation (29) is rewritten as follows:

$$Ln(MR) = -5.5\times10^{-5}\times t - 0.201 \quad (30)$$

The simulation of the relationship between Ln(MR) and drying time (t) using the experimental data in Table 2 and the mathematical model (30) is presented in Figure 3. The correlation coefficient of $R^2 = 0.9945$ indicates a very strong relationship between Ln(MR) and drying time (t).

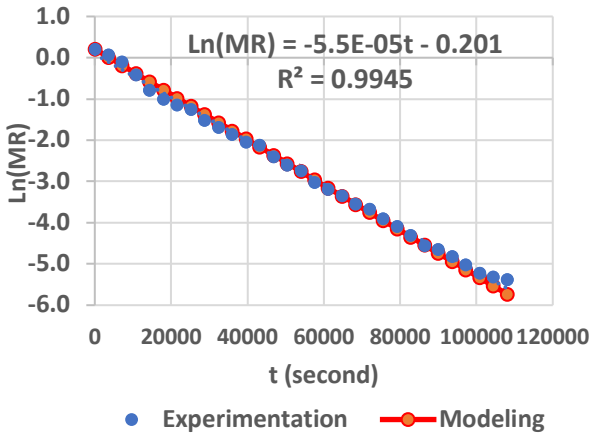

Figure 3. The relationship between Ln(MR) and drying time (t)

From Figure 3, the simulation results as well as the compatibility test of the mathematical model (29) according to the Fisher criterion ($F < F_{1-p}(f_1, f_2)$; $p = 0.05$) demonstrate that the mathematical model (30), which describes the relationship between Ln(MR) and drying time (t), fits the experimental data very well.

Therefore, model (30) can be applied to determine the moisture diffusion coefficient of yogurt during freeze drying. Based on this model, the drying kinetics of yogurt freeze drying can be further analyzed.

From the mathematical model (30), the coefficient b in equation (26) has been determined:

$Ln(MR) = -5.5\times10^{-5}\times t - 0.201 = -bt - 0.201$

It follows that: $b = 5.5\times10^{-5}$ (31)

From equations (27) and (31), the following can be determined:

$$D = \frac{L^2 b}{\pi^2} = \frac{0.002^2 \times 5.5\times10^{-5}}{\pi^2} \quad (32)$$

$D = 2.2313\times10^{-11}$ m^2/s

The calculation results showed that, at a sublimation drying environment temperature of $X_1 = T = 30°C$ and a drying environment pressure of $X_2 = P = 0.1$ mmHg, the experiment determined the moisture diffusion coefficient of yogurt during the freeze-drying process to be $D = 2.2313\times10^{-11}$ m^2/s.

Although there is no available data on the moisture diffusion coefficient of yogurt during freeze-drying from other studies for direct comparison, the calculated value is fully consistent with the experimental data and aligns well with previously published research (Athanasios I. Liapis and Roberto Bruttini, 2020; Dzung N. T. (Ed), Chuyen H. Van, Linh V. T. K, Nhiem L.T., Hoan P. T., Linh D.T.K, Quang N.D., Duyen N.D.M, Tung P.T., 2022). Typically, materials subjected to freeze-drying have moisture diffusion coefficients in the range of 10^{-10} to 10^{-12} m^2/s.

The experiment showed that when the temperature and pressure of the freeze-drying environment change, the moisture diffusion coefficient of yogurt during the freeze-drying process also varies accordingly. For details, see the experimental results and calculated values presented in Table 3.

4.3.Build a mathematical model to determine the moisture diffusion coefficient of yogurt during the freeze-drying process

The freeze-drying experiments of yogurt, which were previously frozen during the sample preparation step, were arranged as presented in Table 3. Each experiment used a different set of temperature and pressure parameters for the freeze-drying environment.

The freeze-drying experiments of yogurt were conducted using the sets of temperature and pressure parameters of the drying environment as presented in Table 3. The calculations were performed similarly to those in section 4.2, and the moisture diffusion coefficients of yogurt during the freeze-drying process were determined, compiled, and presented in Table 3.

Table 3. Relationship between the moisture diffusion coefficient of yogurt (D) and the temperature (T) and pressure (P) of the freeze-drying environment

T $T = X_1$ (^oC)	P $P = X_2$ (mmHg)	D (m^2/s) $Y_E = D\times10^{11}$ (m^2/s)
30	0.10	2.231
32	0.08	2.246
34	0.06	2.261
36	0.04	2.273
38	0.02	2.297
40	0.01	2.332
30	0.01	1.830
32	0.02	1.967
34	0.04	2.178
36	0.06	2.422
38	0.08	2.615
40	0.10	2.868

Let $X_1 = T$ (^oC) be the drying environment temperature; $X_2 = P$ (mmHg) be the drying environment pressure; $Y\times10^{11} = D$ (m^2/s) be the moisture diffusion coefficient of yogurt. Therefore, $Y_E = D\times10^{11}$ (m^2/s).

Based on the experimental data in Table 3, the relationship pattern between the moisture diffusion coefficient of yogurt during freeze-

drying and the temperature and pressure of the drying environment can be predicted as follows:

$$Y_M = b_o + b_1X_1 + b_2X_2 + b_{12}X_1X_2 \quad (33)$$

The mathematical model (33) was established based on the experimental data presented in Table 3. Simulation of these data using Matlab 2024 indicated that the relationship between Y_M and X_1, X_2 follows a planar rather than a curved surface. Furthermore, no existing models were adopted in this study, as they are not suitable for the specific case where yogurt serves as the drying material.

From the predictive mathematical model (33) and the experimental data in Table 3, the root means square error (RMSE) function representing the total squared deviation between the calculated values from the model and the experimental data is constructed as follows:

$$RMSE = \sqrt{\frac{1}{N-1}\sum_{j=1}^{N}\left(Y_{Mj} - Y_{Ej}\right)^2} = (b_0, b_1, b_2, b_{12}) \quad (34)$$

Trong đó: N is the number of experiments (in Table 3, N = 12); j is the index of the j-th experimen; Y_{Mj} is the value calculated from the mathematical model (33) for the j-th experiment; Y_{Ej} is the value determined from the j-th experimental result.

The mathematical model (33) is considered appropriate when the values calculated from the model (Y_M) are equal to or approximately equal to the experimental values (Y_E). Therefore, when the RMSE value reaches its minimum, the model Y_M can be regarded as closely approximating Y_E, from which the model parameters b_0, b_1, b_2, and b_{12} can be determined.

Using Excel – Solver 2024, the following parameters were determined: when $b_0 = 0.284$; $b_1 = 0.05$; $b_2 = 0.123$ and $b_{12} = 0.144$, the minimum value of the Root Mean Square Error (RMSE) was determined to be 0.0124

$\Leftrightarrow RMSE_{min} = 0.0124$

The results of the calculations can be seen in Table 4.

Table 4. Calculation of the model values (Equation 33) and the Root Mean Square Error (RMSE)

X_1	X_2	Y_E	Y_M	$(Y_M - Y_E)^2$	δ_E (%)
30	0.10	2.231	2.222	0.0001	0.41
32	0.08	2.246	2.256	0.0001	0.43
34	0.06	2.261	2.278	0.0003	0.75
36	0.04	2.273	2.289	0.0002	0.69
38	0.02	2.297	2.288	0.0001	0.40
40	0.01	2.332	2.334	0.0000	0.07
30	0.01	1.830	1.822	0.0001	0.43
32	0.02	1.967	1.972	0.0000	0.26
34	0.04	2.178	2.177	0.0000	0.01
36	0.06	2.422	2.395	0.0007	**1.11**
38	0.08	2.615	2.624	0.0001	0.33
40	0.10	2.868	2.864	0.0000	0.14
	∑	**27.519**	**RMSE**	**0.0124**	

Based on the calculation results in Table 4, the minimum value of the RMSE function was determined, from which the mathematical model (Equation 33) was established as follows:

$$Y_M = D\times10^{11} = 0.284 + 0.05\times X_1 + 0.123\times X_2 + 0.144\times X_1\times X_2 \quad (35)$$

Now, it is necessary to verify the compatibility of the mathematical model (35) with the experimental data. In freeze-drying technology, the maximum allowable relative error of the mathematical model must be less than 5%, that is:

$$\delta_{E\,max} = Max\left\{\frac{|Y_{Mj} - Y_{Ej}|}{Y_{Ej}}\times100\right\} \le 5\% \quad (36)$$

From Table 4, it is shown that the maximum relative error, $\delta_{Emax} = 1.11$, is less than 5%. Therefore, the mathematical model (35) is compatible with the experimental data. Thus, this model can be used to determine the moisture diffusion coefficient of yogurt during the freeze-drying process, to calculate the drying kinetics, to develop optimal technological conditions, as

well as to support the calculation and design of freeze-drying systems.

Once again, to demonstrate the strong relationship between Y_M and X_1 and X_2 in the mathematical model (35), it is necessary to determine the correlation coefficient R^2. The correlation coefficient R^2 is determined as follows:

$$R^2 = 1 - \frac{RSS}{TSS} \quad (37)$$

In which, N = 12: Number of experiments;

$RSS = \sum_{i=1}^{N} (Y_{Ei} - Y_{Mi}) =$ 0.0017: Residual Sum of Squares;

$TSS = \sum_{i=1}^{N} (Y_{Ei} - \overline{Y}) =$ 0.7944: Total Sum of Squares;

$\overline{Y} = \frac{1}{N} \sum_{i=1}^{N} Y_{Ei} =$ 2.293: average value of Y_E;

Therefore, the correlation coefficient R^2 is determined as follows:

$$R^2 = 1 - \frac{RSS}{TSS} = 1 - \frac{0.0017}{0.7944} = 0.9979$$

The correlation coefficient of R^2 = 0.9979 indicates a very strong relationship between Y_M and X_1 and X_2.

According to the study by Suk Shin Kim and Santi R. Bhowmik (1995) on Effective moisture diffusivity of plain yogurt undergoing microwave vacuum drying, the diffusivity coefficient was found to be primarily influenced by microwave power; R. Lemus-Mondaca et al. (2007). Dehydration characteristics of papaya (Carica pubenscens): determination of diffusion coefficient. The results of the study established the relationship between the effective moisture diffusivity and the drying air temperature; W.J.N. Fernando, H.C. Low, A.L. Ahmad, (2011). The study was conducted on slices of banana, cassava, and pumpkin to determine the dependence of the effective moisture diffusivity on thickness and temperature during convective drying of sliced materials.

The results of the above studies have shown that the effective moisture diffusivity of drying materials depends on many factors and usually ranges from 10^{-12} to 10^{-8} m²/s, which is consistent with the findings of this publication. However, none of the previous studies have established a relationship between moisture diffusivity and the temperature and pressure of the freeze-drying environment for yogurt. Therefore, the development of the mathematical model (37), which describes the relationship between moisture diffusivity and the temperature and pressure of the freeze-drying environment for yogurt, is a completely novel contribution. It plays a significant role in addressing the problem of simultaneous heat and mass transfer in freeze-drying yogurt, thereby determining the drying kinetics and optimizing the technological drying conditions.

The simulation of mathematical model (35) on a 3D coordinate system is presented in Figure 4.

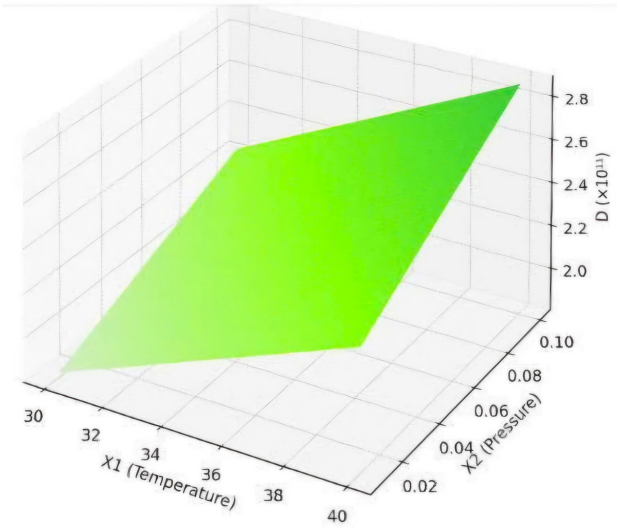

Figure 4. Relationship between the moisture diffusion coefficient of yogurt and the temperature and pressure of the freeze-drying environment.

Looking at the 3D graph, it is evident that the relationship between the temperature and pressure of the freeze-drying environment and the moisture diffusion coefficient of yogurt is linear. This can be considered a novel finding that has not been reported in previous studies. This linear relationship facilitates solving coupled heat and mass transfer problems using numerical methods such as the finite difference method and the finite element method.

From equation (35), it can be rewritten as:

$$D = (0.284 + 0.05\times X_1 + 0.123\times X_2 + 0.144\times X_1\times X_2)\times 10^{-11},\ m^2/s \quad (38)$$

Where:

$$30\ ^oC \le X_1 = T \le 40\ ^oC$$

$$0.01\ mmHg \le X_2 = P \le 0.1\ mmHg$$

The method for constructing the mathematical model (38) to determine the moisture diffusion coefficient of yogurt during freeze-drying, although applied to a specific material—yogurt—essentially generalizes into a universal approach. This is because the method can be applied to any drying material to determine its corresponding moisture diffusion coefficient. This is the core value of this research.

5. Conclusions

This study has proposed a method to determine the moisture diffusion coefficient specifically for yogurt and, more generally, for other drying materials during the freeze-drying process.

Based on this method, the moisture diffusion coefficient of yogurt during the freeze-drying process has been determined through the mathematical model (38). This is an important issue that must be resolved prior to modeling and optimizing the freeze-drying process in order to establish an appropriate technological regime.

6. References

Anandharamakrishnan, C., (2017). Handbook of drying for dairy products. John Wiley & Sons, Ltd, 2017. doi: 10.1002/9781118930526.

AOAC International, AOAC-927.05 Moisture in Dried Milk. 2000.

Athanasios, I. Liapis and Roberto Bruttini, (2020). "Freeze drying," in Handbook of industrial drying, 4th ed.CRC press, pp. 309–343, 2020.

Bhushani, A. and Anandharamakrishnan, C., (2017). "Freeze Drying," in Handbook of Drying for Dairy Products, John Wiley & Sons, pp. 95–121, 2017.

Dzung, N.T and et al., (2024). "Mathematical model study to optimize the freeze drying process for production of dried yogurt," *Carpathian Journal of Food Science and Technology*, 16(4), pp. 151–163, 2024, https://doi.org/10.34302/crpjfst/2024.16.4.12.

Dzung, N. T. (Ed)., Chuyen, H. Van, Linh, V. T. K, Nhiem, L.T., Hoan, P. T., Linh, D.T.K, Quang, N.D., Duyen N.D.M, Tung, P.T., (2022) Freeze drying. VNU-HCM Press, pp. 187-192, 2022.

Nguyen Tan Dzung., (2017). Study dynamics of the freeze drying process of royal jelly in viet nam. *Carpathian Journal of Food Science and Technology 2017, 9(3), 17-29.*

Duan, X., Yang, X., Ren, G., Pang, Y., Liu, L., and Liu, Y., (2016). "Technical aspects in freeze-drying of foods," *Drying Technology*, vol. 34, no. 11. 2016. doi: 10.1080/07373937.2015.1099545.

Fellows, P., (2000). *Food Proccesing Technology*, 2nd ed. Woodhead Publishing Limited and CRC Press LLC, 2000.

G.Wilhelm, Oetjen, and Peter Haseley, Freeze-drying. Wiley-VCH, 2004.

Hoan Thi Pham, Linh T.K. Do, Tuan Thanh Chau, Dzung Tan Nguyen, (2023). "Study on determining the freezing mode of frozen fillet bigeye tuna (thunnus obesus)" *Carpathian Journal of Food Science and Technology, 2023, 15(3),17-25*. https://doi.org/10.34302/crpjfst/2023.15.3.2

Lim, Y., Hong, S., Shin, Y. K. Kang, S. H., and Center D., (2015). "Changes in the viability of lactic acid bacteria during storage of freeze-dried yogurt snacks," *Journal of Dairy Science and Biotechnology*, vol. 33, no. 3, p. 203, 2015.

Liviu Giurgiulescu, Phong Le Thanh, Linh T.K. Do, and Tan Dzung Nguyen., (2024). Study on designing and manufacturing the DS-12 freeze - drying system using infrared radiation heating process, *JTE*, Volume 19, Issue 03, PP. 1-14, 2024. https://doi.org/10.54644/jte.2024.1579

Mawilai, P., Chaloeichitratham, N., and Pornchaloempong, P., (2019). "Processing feasibility and qualities of freeze dried mango powder for SME scale," in IOP Conference Series: *Earth and Environmental Science*, 2019. doi: 10.1088/1755-1315/301/1/012059.

R. Lemus-Mondaca et al., (2007). Dehydration characteristics of papaya (Carica pubenscens): determination of equilibrium moisture content and diffusion coefficient. *Journal of Food Process Engineering*, 32(5):645 – 663.

Suk Shin Kim, Santi R. Bhowmik., (1995). Effective moisture diffusivity of plain yogurt undergoing microwave vacuum drying. *Journal of Food Engineering*, Volume 24, Issue 1, 1995, Pages 137-148.

W.J.N. Fernando, H.C. Low, A.L. Ahmad, (2011). Dependence of the effective diffusion coefficient of moisture on thickness and temperature in convective drying of sliced materials. A study on slices of banana, cassava and pumpkin, *Journal of Food Engineering*, Volume 102, Issue 4, February 2011, Pages 310-316.

Yildiz, F., (2010). Development and manufacture of yogurt and other functional dairy products. CRC Press/Taylor & Francis, 2010.

Conflict of interest

The author declares no conflict of interest.

Acknowledgments

This research is supported by Ho Chi Minh City University of Technology and Education (HCMUTE), Vietnam.

The authors thank the Head of Food Engineering and Technology Lab, Department of Food Technology, Faculty of Chemical and Food Technology, HCMC University of Technical Education, Viet Nam, for their support and help to carry out the experiments.

CARPATHIAN JOURNAL OF FOOD SCIENCE AND TECHNOLOGY

journal homepage: **http://chimie-biologie.ubm.ro/carpathian_journal/index.html**

Research article

TOTAL PHENOLIC CONTENT, RADICAL SCAVENGING, AND ANTIBACTERIAL ACTIVITY OF THREE DIFFERENT FRACTIONS OF *PARIJOTO* FRUIT (*MEDINILLA SPECIOSA BLUME*)

Nurdyansyah, F.[1], Qulub, A. S[1]., Widyastuti, D. A.[2]✉, Mona, N. [2], Bhakti Etza Setiani[3], Ganwarige Sumali N Fernando[4], Fariz Nurmita Aziz[3]

[1] *Department of Food Technology, Universitas PGRI Semarang, Semarang 50125, Indonesia*
[2] *Department of Biology Education, Universitas PGRI Semarang, Semarang 50125, Indonesia*
[3] *Department of Food Technology, Universitas Diponegoro, Semarang 50275, Indonesia*
[4]*Department of Food Science and Technology, Faculty of Agriculture, University of Ruhuna, Sri Lanka*
✉*dyah.ayu@upgris.ac.id*
https://orcid.org/0009-0004-3422-9986

https://doi.org/10.34302/2025.17.3.5

Article history:
Received:
March 6th, 2025
Accepted:
Novembre 10th , 2025

Keywords:
Antibacterial activity;
DPPH radical scavenging activity;
Medinilla speciosa;
Antioxidant activity;
Phenoliccontent

ABSTRACT

Parijoto (*Medinilla speciosa Blume*), a traditional Indonesian medicinal plant, requires further scientific investigation. This study explored the total phenolic content, antioxidant activity, and antibacterial properties of three *Parijoto* fruit fractions. Understanding these variations helps identify the most potent fraction for functional food development. Methanol extract was fractionated into n-hexane (PNF), ethyl acetate (PEF), and methanol fractions (PMF). Total phenolic content was determined using the Folin-Ciocalteu method, and antioxidant activity via DPPH assay. Antibacterial activity against *E. coli* and *S. aureus* was assessed using the Kirby-Bauer disk diffusion method with varying fraction concentrations (30, 60, and 90% v/v). Chloramphenicol served as a positive control, and DMSO as a negative control. PNF exhibited the highest total phenolic content (146.29 ± 0.91 µg GAE/g) and highest antioxidant activity (IC_{50} 1.73 ± 0.09 µg/g), but the lowest antibacterial activity. Conversely, PEF demonstrated the strongest antibacterial activity against both bacteria, despite not having the highest phenolic content (68.83 ± 2.63 µg GAE/g) or antioxidant activity (IC_{50} 7.59 ± 0.42 µg/g). These results suggest that *Parijoto*'s antibacterial activity is not solely attributable to phenolic compounds. Other unidentified compounds may contribute to its antibacterial effects, highlighting the need for further biomolecular research to elucidate the underlying mechanisms.

1. Introduction

The microbiota balance in the human digestive system is influenced by diet, lifestyle and food hygiene(Wibawanti et al., 2021). When digestive problems arise, some people rely on microbiota, such as yogurt, which has beneficial medical effects (Pratama et al., 2018a). The continual use of antibiotics as a common

medication raises concerns about bacterial antibiotic resistance. *Escherichia coli* and *Staphylococcus aureus* are two bacterial species with some resistant strains because of the unwise use of antibiotics. *Escherichia coli* multidrug resistance has already been detected in Indian children (Feliatra et al., 2022). On the other hand, the first observed antibiotic resistance *in S. aureus* is penicillin-resistant *S. aureus* (PRSA) in the 1940s when the infection quickly emerged in hospitals (Craft et al., 2019). The rise of bacterial resistance takes the Indonesia government's attention because antibiotics are used widely as health therapy for humans, livestock, and cultivated fishes (Feliatra et al., 2022). The strategic solution is highly required to finalize the bacterial resistance in the interest of human health.

In recent years, people have started to follow the "back to nature" campaign by reducing chemical consumption. Researchers seek natural resources to be developed as herbal medicines. Several natural products as herbal medicines contain antimicrobial, anti-inflammatory, and immunomodulatory (Sarecka-Hujar & Szulc-Musioł, 2022). Natural products with various bioactive compounds are now commonly used as an alternative for health maintenance due to their minimum side effects compared to synthetic compounds in chemical drugs (Nurdyansyah & Widyastuti, 2019). The success of treatment with natural products is associated with its phytochemical constituents, such as phenolics, alkaloids, saponins, tannins, etc (Milanda et al., 2021). Phenolic compounds, including flavonoids, have a positive correlation to antioxidant and antibacterial activities (Al-Rajhi et al., 2022).

One of the local plants in Indonesia with flavonoid content is *parijoto* (*M. speciosa*). *Parijoto* is an endemic plant grown on the Mount Muria slope in Kudus, Central Java, Indonesia (Hanum et al., 2017). It has purplish red fruits with high anthocyanin, a water-soluble natural pigment that belongs to the flavonoid groups (Sa'adah et al., 2020). Flavonoids play a role as antioxidants to combat free radicals, whereas the tannin in *parijoto* shows antimicrobial activities through enzyme inhibition mechanisms and the formation of complexes with metal ions. This tannin improves the lipid profile and increases antioxidant activities (Hanum et al., 2017).

Some previous studies have shown that *parijoto* has antibacterial activity. The n-hexane, ethyl acetate, and methanolic extract of *parijoto* showed antibacterial activities against *E. coli*, *S. aureus*, *B. subtilis*, and *P. aeruginosa* (Milanda et al., 2021). However, the antibacterial activities of *parijoto* fraction with various solvents have not been reported. The fractionation with various polar to non-polar solvents is required to optimize the effect of specific bioactive compounds in natural products. So, this study aims to obtain the antibacterial activity of various fractions of *parijoto* methanolic extract to *E. coli* and *S. aureus*. The solvents used for fractionation are n-hexane, ethyl acetate, and methanol, respectively, representing non-polar, semi-polar, and polar solvents. This study provides new insights into the antibacterial activity of different solvent fractions of *parijoto* fruit, optimizing the extraction of bioactive compounds for targeted applications. Identifying the most effective fraction against *E. coli* and *S. aureus* supports the development of natural antibacterial agents for food and pharmaceutical use.

2. Materials and methods

2.1. Materials

2.1.1 Plant material and sample preparation

The *parijoto*'s fruit was obtained from the slopes of Mount Muria in Colo, Kudus, Central Java-Indonesia. The fruits collected from the *parijoto* plant grow naturally. The selected fruits, which are mature enough and marked with purplish red skin, were then extracted and fractionated in the Laboratory of Food Technology, Universitas PGRI Semarang, Central Java-Indonesia.

2.1.2 Chemical and reagents

Methanol, n-hexane, Ethyl Acetate, Folin-Ciocalteu Reagent, and Sodium Carbonate were purchased from Merck (Germany). Gallic acid and DPPH were purchased from Sigma Aldrich (Germany). Chloramphenicol was purchased

from Oxoid (UK). DMSO (dimethyl sulfoxide) and Nutrient Agar were purchased from Merck (Germany)

2.2. Methods

2.2.1. Extraction of parijoto's fruits

The extraction method was referred to Widyastuti & Nurdyansyah (2023) with some modifications. The *parijoto*'s fruits were separated from their branches, washed, and cut into small pieces. The fruits were then dried in dryer cabinet at 50°C for 48 hours. The dried fruits were mashed and sieved with 60 60-mesh sifter, and then the powder was extracted. A 100 g of powdered fruit was macerated in 1000 mL methanol (Merck, Germany) for 24 hours with twice re-maceration with the same solvent ratio. The macerates were collected and concentrated with a rotary vacuum evaporator (DLAB Scientific, China) at 40°C and 50 rpm. The crude *parijoto*'s methanolic extract (CPME) was ready for fractionation.

2.2.2. Fractionation of crude parijoto's methanolic extract

The fractionation procedure referred to Egua et al. (2014) with modifications. The CPME residue was dissolved in 500 mL aquadest and then fractionated by liquid-liquid fractionation with 500 mL n-hexane (Merck, Germany), ethyl acetate (Merck, Germany), and methanol (Merck, Germany). The solution was then evaporated with a rotary vacuum evaporator at 40°C. The fraction obtained, n-hexane (PNF), ethyl acetate (PEF), and methanol (PMF), were tested to evaluate the antibacterial activity of *parijoto*'s fruits to *E. coli* and *S. aureus*.

2.2.3. Measurement of total phenolic content

Total phenolic content was measured using the Folin-Ciocalteu method according to the procedure described by Ghafoor et al. (2020) with modifications. The 500 µL of each PNF, PEF, and PMF were mixed with 400 µL of Folin-Ciocalteu reagent (Merck, Germany). The mixture was then incubated for 5 min at room temperature. After the incubation, 4 mL of 7% sodium carbonate (Merck, Germany) was added, and then distilled water was also added to the 10 mL final volume. The final mixture was incubated for 30 min at room temperature. The absorbances were measured at 730 nm with a UV-Vis spectrophotometer (Hitachi UH5300, Japan). Gallic acid (Sigma Aldrich, Germany) (25-150 µg/mL) was used as the standard for the calibration curve, so the total phenolic contents were expressed as gallic acid equivalents (µg GAE/mL).

2.2.4. Measurement of DPPH radical scavenging activity

The radical scavenging activity was analyzed with 1,1-diphenyl-2-picrylhydrazyl (DPPH) following the method from Ghafoor et al. (2020) with modifications. Series of each fraction were prepared at 50, 100, 150, 200, and 250 µg/mL, then 4 mL of DPPH (Sigma Aldrich, Germany) was added, and the final volumes were made up to 5 mL. The mixtures were shaken gently or vortexed for 5 sec, then incubated for 30 min at room temperature in the dark. The absorbances were measured at 517 nm using a UV-Vis spectrophotometer (Hitachi UH5300, Japan). The DPPH radical scavenging activity was measured following the equation below. Then the IC_{50} was measured with the regression formula y = ax + b from the values of DPPH radical scavenging activities.

$$DPPH\ radical\ scavenging\ (\%) = \frac{[(Absorbance\ of\ control - Absorbance\ of\ sample)x\ 100]}{Absorbance\ of\ control}$$

2.2.5. Bacterial culture

The *E. coli* and *S. aureus* were obtained from Food and Nutrition Culture Collection (FNCC), Center for Food and Nutrition Studies, Universitas Gadjah Mada, Indonesia. The Preparation of bacterial suspensions was referred to Milanda et al. (2021) with modifications. The *E. coli* FNCC 0091 and *S. aureus* FNCC 0047 were sub-cultured in nutrient agar and incubated at 37°C for 18 to 24

hours. The bacterial suspension was diluted to reach 10^6 CFU/mL cell density. Both 10^6 CFU/mL *E. coli* FNCC 0091 and *S. aureus* FNCC 0047 were inoculated to nutrient broth at 37°C for 24 hours. The cultures were ready for the antibacterial activity test.

2.2.6. Antibacterial activity test

The test was performed in a completely randomized design to derive the optimal concentration of PNF, PEF, and PMF to inhibit the growth of *E. coli* and *S. aureus* following the Kirby-Bauer disk diffusion method. The variables for each fraction were 5% chloramphenicol (Oxoid, United Kingdom) as positive control, 0.5% DMSO (dimethyl sulfoxide) (Merck, Germany) as negative control, 30%, 60%, and 90% (v/v) of each fraction as treatments. The Kirby-Bauer method.

2.3. Data analysis

The data were replicated and presented as mean ± SD. The data was statistically analyzed with SPSS version 17 to perform one-way ANOVA analysis. Significant differences among means were determined by Duncan's multiple-range test. If the *p*-value was less than 0.05, it was considered as statistically significant.

3. Results and discussions

3.1. Drying Loss and Yield Extract

The amount of compound lost from *parijoto* fruit when it was heated for several hours at 105 °C was shown by the drying loss value (Hikmawanti et al., 2021). The drying process of *parijoto*'s fruits generates 85.49% drying loss. It can be known from the dry weight of the fruits, which is 322 g obtained from 2220 g of fresh fruits (Mona et al., 2022). The herbs, any plant parts for flavoring, medicine, food, or perfume, were mostly processed by drying to get shelf-stable products. The drying method preserves the quality of herbs by reducing moisture content, which leads to the inhibition of microbial growth and alteration of chemicals during storage (Thamkaew et al., 2021). The drying process in herbs, *parijoto*'s fruits can also generate a positive impact on its materials' quality. During the drying process, the water content was removed, but it can generate several value-added compounds in dried samples (Calín-Sánchez et al., 2020; Pratama et al., 2018b). The dried *parijoto*'s fruits were assumed to be more durable during the research.

The dried *parijoto*'s fruits were macerated with methanol as one of the universal solvents which have the capability to bind and dissolve chemical compounds from natural materials, including polar, semi-polar, or non-polar compounds (Nurdyansyah & Widyastuti, 2019). The extraction process of dried *parijoto*'s fruits generates 67,45% yields (Mona et al., 2022), then followed by liquid-liquid fractionation with n-hexan (PNF), ethyl acetate (PEF), and methanol (PMF). The fractionation yields of PNF, PEF, and PMF were 13.8%, 22.8%, and 45.4%, respectively (Mona et al., 2022). The yield of PMF was the highest among others, indicating that in this fraction may contain higher chemical compounds than the other fractions due to its ability to bind polar to non-polar compounds. The lowest yield was possessed by PNF which prefers to bond with non-polar compounds. The ethyl acetate, considered a polar solvent due to the presence of polar carbon-oxygen bonds, however, still could dissolve non-polar compounds since it also has alkyl groups which are non-polar in nature. So, PEF generates a higher yield than PNF but is still lower than PMF.

3.2. Total Phenolic Content (TPC) value

Phenolic compounds are among the valuable bioactive metabolites in plants (Elshahawy et al., 2022) that have many biological activities, related to antioxidant properties to free radicals neutralization, inhibition of pro-oxidant enzymes activity (cyclooxygenase or lipoxygenase), disruption of auto-oxidation chain reactions, and chelation of transition metal ions (Złotek et al., 2019). They are generated through photosynthesis in the plant as potential secondary metabolites. Their -OH (hydroxyl) groups are characteristically bound to proteins and other various compounds, and have the ability to exhibit several bioactivities, such as antioxidant and anticancer (Nam et al., 2017).

Wijayanti & Ardigurnita (2018) reported that *parijoto*'s leaves extract possessed 3.95% of total polyphenols. These bioactive compounds provide effective antioxidant properties to counteract free radicals from lipid oxidations. Polyphenols have a protective ability to prevent oxidative stress that leads to organ damage and various degenerative diseases. Phytochemical screening of *parijoto*'s fruit fraction showed that *parijoto*'s n-hexane, ethyl acetate, and methanol fractions have polyphenolic compounds after the positive reaction of the sample's fraction with 1% $FeCl_3$. The *parijoto*'s fruits are also known to have flavonoids, saponins, and tannins based on phytochemical screenings (Syifaul Qulub et al., 2022).

The present study showed that the PNF has significantly highest total phenolic content ($p<0.05$) among the three fractions (**Table 1**). The lowest total phenolic content is possessed by PEF. The Total phenolic content of PMF is significantly higher than that of PEF but also significantly lower than that of PNF. This result indicates that the phenolic compounds of *parijoto*'s fruits are mainly non-polar because they were extracted to n-hexane as a non-polar solvent. The non-polar solvents are well known to be useful in the extraction and fractionation of polyphenols, flavonoids, terpenoids, fats, and oils (Abubakar & Haque, 2020).

Table 1. Total phenolic content of *parijoto*'s n-hexane (PNF), ethyl acetate (PEF), and methanol fraction (PMF) with gallic acids as standard

Samples	TPC (µg GAE/g)
PNF	146.29 ± 0.91^{c}
PEF	38.75 ± 1.70^{b}
PMF	68.83 ± 2.63^{a}

Note: different letters within column indicate a significant differences ($p < 0.05$)

The most polar solvent in this research is methanol. It is one of the universal solvents commonly used to extract bioactive natural products from plants. Methanol was expected to be the best solvent to extract both polar and non-polar compounds (El Houda Lezoul et al., 2020). The result showed that the most non-polar solvents obtained higher total phenolic compounds from *parijoto*'s fruits compared to ethyl acetate and methanol, which are more polar. Ethyl acetate with 0.228 polarities only obtained a few polyphenols from *parijoto*'s fruits, still lower than methanol, which is more polar with 0.762 polarities (Abubakar & Haque, 2020). These results indicate that parijoto fruit contains a high phenolic content, which may be linked to its strong antioxidant and antibacterial activities, as phenolic compounds are known for their antibacterial, antifungal, and antioxidant properties (Behiry et al., 2019).

3.3. DPPH radical Scavenging Activity

The Plant species have many antioxidant substances that are produced by different mechanisms. Several methods can be used to measure the antioxidant activity in the plant's extracts. One of the most common use methods is DPPH radical scavenging activity (Nam et al., 2017). The DPPH radical scavenging activity is based on the reduction of one-electron that reflects the free radical reducing activity of antioxidants. The antioxidant activities are highly correlated with the total flavonoid and phenolic content of the plant extract (Johari & Khong, 2019). The DPPH radical scavenging activity is commonly used for the measurement of the free radical scavenging potential of antioxidant molecules. This method is considered as one of the easy and standard colourimetric methods for the evaluation of antioxidant activities. The principle of the DPPH method is based on accepting a hydrogen atom from the scavenger molecules (antioxidant), resulting in a reduction of DPPH to DPPH2, and the purple colour changes into yellow colour. The colour change is monitored by a spectrophotometer and used for the determination of antioxidant properties (Mishra

et al., 2012). The IC_{50} or 50% inhibitory concentration values indicate the ability of the PNF, PEF, and PMF to inhibit or reduce free radicals by 50% (Nurdyansyah & Widyastuti, 2019).

The PNF exhibited the highest scavenging activity, as indicated by its lowest IC_{50} value of 1.73 µg/g which is required to inhibit 50% of free radicals. The PEF and PMF have IC_{50} at 4.13 and 7.59 µg/g, respectively (**Table 2**). PEF has significantly higher IC_{50} than PNF and lower than PMF. It indicates that PEF has scavenging activity lower than PNF but higher than PMF, based on its IC_{50}. The high radical scavenging activity possessed by PNF is due to its high total phenolic content, so it assumes that there is a correlation between total phenolic content and DPPH radical scavenging activity at PNF. Phenolic compounds as one of the secondary plant metabolites are synthesized by plant cells to act as antioxidant agents. These compounds could protect plants from the dangerous influences of oxidations (Elshahawy et al., 2022).

Table 2. The IC_{50} of DPPH radical scavenging activity of *parijoto*'s n-hexane (PNF), ethyl acetate (PEF), and methanol fraction (PMF) with gallic acids as standard

Samples	IC_{50} (µg/g)
PNF	1.73 ± 0.09^{c}
PEF	4.13 ± 2.01^{b}
PMF	7.59 ± 0.42^{a}

Note: different letters within column indicate a significant differences ($p < 0.05$)

The PEF has higher DPPH scavenging activity than PMF shown by their $IC_{50\ value}$. From this result, it is known that the DPPH scavenging activity of the non-polar fraction is higher than the polar fraction. The PNF as the most non-polar fraction, has the highest scavenging activity and the PMS as the most polar fraction has the lowest scavenging activity. The bioactive compounds that are responsible as antioxidants might be more bonded to non-polar solvents than polar solvents. So, the non-polar fraction provides stronger antioxidant activities than the polar fraction.

3.4. Antibacterial activity against *E. coli*

The correlation between phenolic compounds and the antibacterial activity of plant extract is still being discussed among researchers (Belhaoues et al., 2020). However, antibacterial activity may not be solely attributed to phenolic compounds, as other bioactive compounds, such as flavonoids, alkaloids, and terpenoids, could interact synergistically to enhance the antibacterial effects of the fractions or extracts (Mohammed et al., 2021; Villa et al., 2013). In this study, all three fractions have tighter inhibition zones than positive control and there are significant differences ($p<0.05$) between positive control and all different fractions.

Table 3 shows that PEF has the highest antibacterial activity against *E. coli* due to its wide inhibition zone. *Escherichia coli* in this study was known to be more sensitive to PEF, than PMF, and the last to PNF seen from the inhibition zones. The PNF with the highest total phenolic content and radical scavenging activity turns out to have the lowest antibacterial effect to *E. coli*. It is suggested that maybe there are some other bioactive interactions that are responsible for the antibacterial activity of *Parijoto*'s fractions. The antibacterial activity of *Parijoto*'s fractions is affected not only by its phenolic and antioxidant compounds but also by other compounds, which will have to be studied in the next studies.

The highest concentration of Parijoto fruit extract fraction exhibited the widest inhibition zone, showing a significant ($p<0.05$) antibacterial effect compared to lower concentrations. However, its inhibition zone is still significantly tighter than that of the positive control, which used chloramphenicol as an antibiotic. This result indicates that some non-polar compounds in *Parijoto*'s fruit, which are extracted by ethyl acetate, are more responsible

for its antibacterial activity compared to more non-polar compounds in PNF or more polar compounds in PMF. As the most non-polar fraction, PNF has the lowest antibacterial activity against *E. coli* and PMF, as the most polar fraction, has higher antibacterial activity than PNF but it is still lower than PEF. So, the PEF is the most potent fraction of *Parijoto*'s fruit to hamper *E. coli*'s growth and the most potent concentration is in 90% with 11.16 mm of inhibition zone's diameter.

Table 3. The inhibition zone diameters of *Parijoto*'s n-hexane (PNF), ethyl acetate (PEF), and methanol fraction (PMF) against *E. coli* FNCC 0091

Group of Treatment	Inhibition Zone (mm)		
	PNF	PEF	PMF
Chloramphenicol (Positive control)	27.06 ± 0.97^{e}	26.78 ± 1.02^{e}	26.66 ± 0.49^{e}
DMSO 0.5% (Negative control)	0 ± 0.00^{a}	0 ± 0.00^{a}	0 ± 0.00^{a}
T1 (30% of *Parijoto*'s fraction)	1.3 ± 0.32^{b}	7.18 ± 0.24^{b}	6.40 ± 0.01^{b}
T2 (60% of *Parijoto*'s fraction)	3.22 ± 0.30^{c}	10.13 ± 0.25^{c}	7.91 ± 0.57^{cd}
T3 (90% of *Parijoto*'s fraction)	4.63 ± 0.65^{d}	11.16 ± 0.77^{d}	8.27 ± 0.21^{d}

Note: different letters within column indicate a significant differences ($p < 0.05$)

The inhibition zones at *E. coli* cultures in positive and negative control, as well as also PNF, PEF, and PMF treatment are shown in **Figure 1**. It shows that DMSO 0.5% as a negative control did not inhibit the growth of *E. coli*, but chloramphenicol did as a positive control. It also shows that 90% *Parijoto*'s fractions inhibit the growth of *E. coli* better than the 30 and 60% fractions, which can be known from the diameter of inhibition zones.

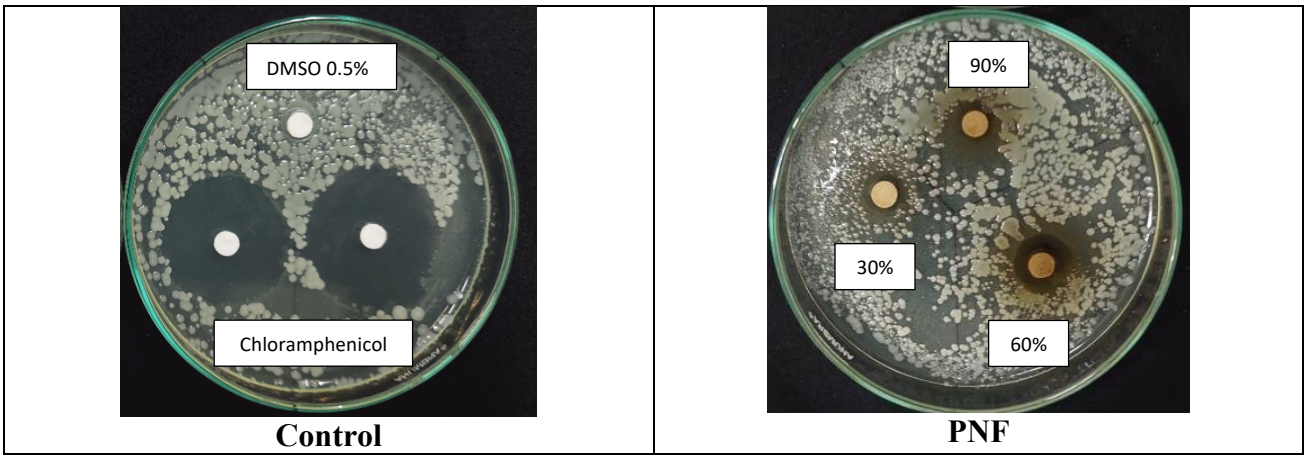

Control **PNF**

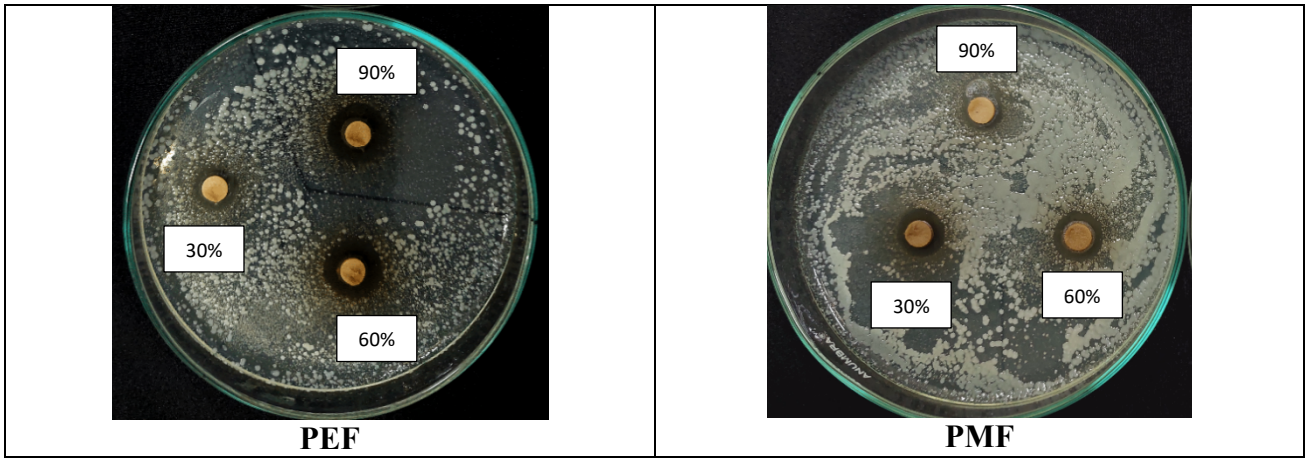

Figure 1. The inhibition zone of *E. coli* with *Parijoto*'s n-hexane fraction (PNF), ethyl acetate fraction (PEF), methanol fraction (PMF), chloramphenicol as positive control, and DMSO 0.5% as negative control.

3.5. Antibacterial activity against *S. aureus*

Staphylococcus aureus is a Gram-positive bacteria that is responsible for some major infectious diseases. It has evolved to resistant strain to some antibiotics, like methicillin and others, forming methicillin-resistant *S. aureus* (MRSA). The resistant strain of *S. aureus* is 10-fold more infectious than all multi-drug-resistant Gram-negative bacteria (Craft et al., 2019). However, some researchers suggested that Gram-positive bacteria, like *S. aureus,* are more sensitive to the presence of bioactive compounds in plant extracts (Jurić et al., 2021).

In this study, for PNF and PMF, the inhibition zones are wider than the inhibition zones which form in the *E. coli* cultures. However, for PEF, the inhibition zones are tighter than in *E. coli* cultures. These results assume that *S. aureus* is more susceptible than *E. coli* in the treatment of PNF and PMF, but it is not in the treatment of PEF. There are no differences in the order of sensitivity to Parijoto fruit extract fraction from *E. coli* cultures. *Staphylococcus aureus* is most sensitive to PEF with the widest inhibition diameter of 9.81 mm at 90% PEF concentration and most potent to PNF with a range of inhibition diameter 3.8 to 4.95 mm. The higher concentration of Parijoto fruit extract fractions inhibited the growth of *S. aureus* more than the lower concentrations (Table 4).

Table 4. The inhibition zone diameters of *Parijoto*'s n-hexane (PNF), ethyl acetate (PEF), and methanol fraction (PMF) against *Staphylococcus aureus* FNCC 0047

Group of Treatment	Inhibition Zone (mm)		
	PNF	PEF	PMF
Chloramphenicol (Positive control)	$21.83 \pm 2{,}75^{d}$	20.6 ± 2.15^{e}	22.9 ± 4.55^{e}
DMSO 0.5% (Negative control)	0 ± 0.00^{a}	0 ± 0.00^{a}	0 ± 0.00^{a}
T1 (30% of *Parijoto*'s fraction)	3.8 ± 0.37^{b}	7.1 ± 0.27^{b}	6.4 ± 0.23^{b}
T2 (60% of *Parijoto*'s fraction)	4.21 ± 0.78^{bc}	8.28 ± 0.24^{c}	8.28 ± 0.51^{c}
T3 (90% of *Parijoto*'s fraction)	4.95 ± 0.45^{c}	9.81 ± 0.78^{d}	9.24 ± 0.69^{cd}

Note: different letters within column indicate a significant differences ($p < 0.05$)

All three concentrations of Parijoto's fraction, 30, 60, and 90%, significantly ($p<0.05$) inhibit the growth of *S. aureus* compared to negative control. But the inhibition zones which are formed after the treatment were still significantly tighter than chloramphenicol as positive control. The PEF showed the strongest inhibition activity than PNF and PMF. It assumed that ethyl acetate as solvent succeeds to bind the compounds which are responsible for *Parijoto* fruit's antibacterial activities. However, the diameter of inhibition zones at PMF treatment are slightly similar to PEF, which at 60% concentration, both showed the same diameter of inhibition zone that is 8.28 mm. This result suggested that PEF and PMF may have similar antibacterial activity against *S. aureus,* so the non-polar and polar compounds which bond to ethyl acetate and methanol are more effective in inhibiting the growth of *S. aureus* than compounds which bond to n-hexan with a tighter range of diameters at 3.8 to 4.96 mm.

The inhibition zones at *S. aureus* cultures in positive and negative control, also PNF, PEF, and PMF treatment (**Figure 2**). The negative control showed no inhibition of *S. aureus* growth, while chloramphenicol, used as the positive control, exhibited the strongest antibacterial effect, as indicated by the widest inhibition zones. It is also seen that the 90% Parijoto fruit extract fraction showed more inhibition of growth of *S. aureus* than 30% and 60% fractions concentrations which can be known from the diameter of inhibition zones.

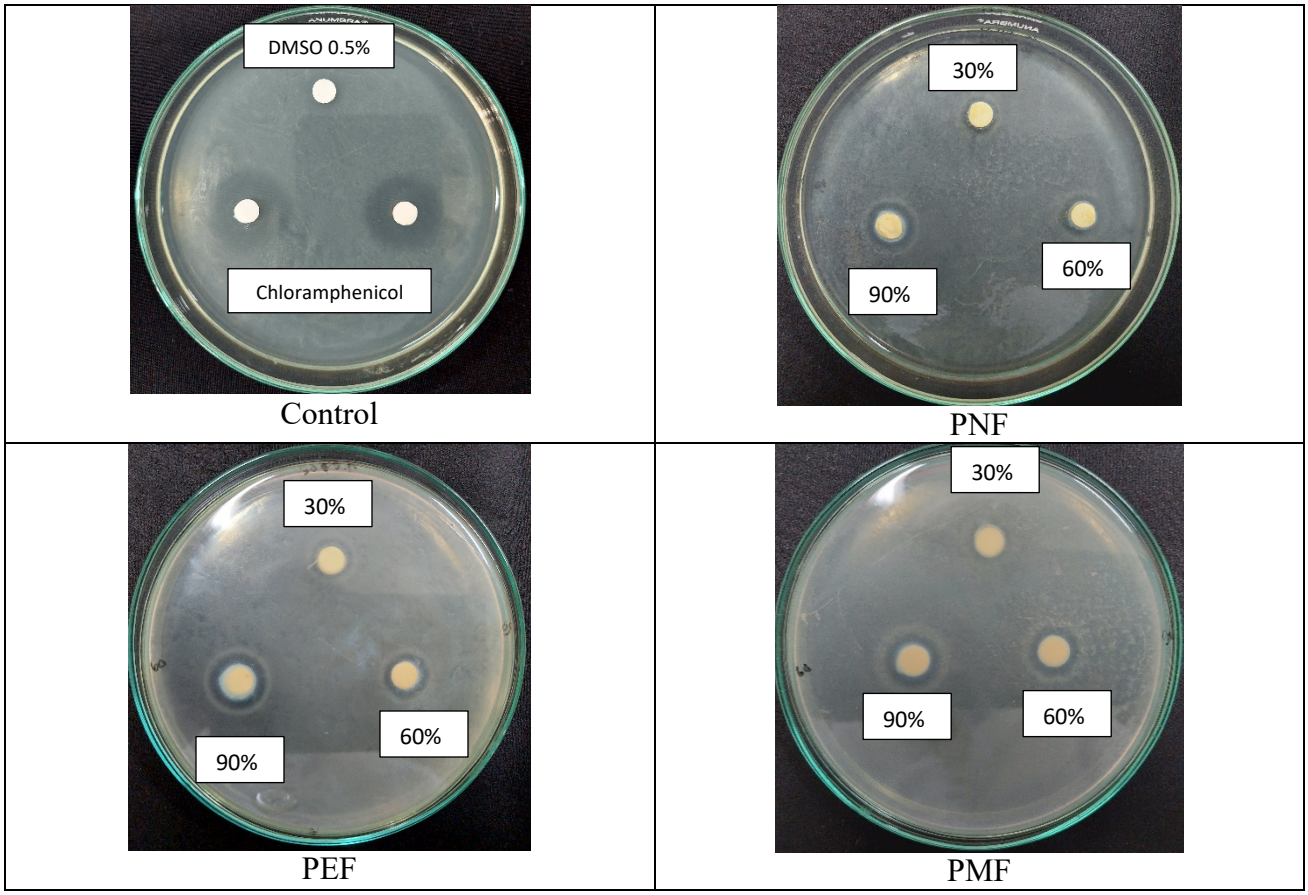

Figure 2. The inhibition zone of *S. aureus* with *Parijoto*'s n-hexane fraction (PNF), ethyl acetate fraction (PEF), methanol fraction (PMF), chloramphenicol as positive control, and DMSO 0.5% as negative control.

This study indicated that the Parijoto fruit extract fractionation was one of the techniques to determine the potency of Parijoto as a local plant in Central Java to combat the bacterial activities like *E. coli* and *S. aureus* which have pathogenicity effect to human. Antibacterial activity is mostly assumed to be correlated with total phenolic content and antioxidant activities in most plant extracts and fractions.

However, in this study, PNF with highest total phenolic content and radical-scavenging activity turns out as the lowest antibacterial activity against both *E. coli* and *S. aureus*. This indicated that the antibacterial activity of Parijoto fruit extract fractions not only correlated to phenolic compounds which leads to antioxidant activities but there might be many other interactions of Parijoto's bioactive compounds to positively induce its antibacterial activity. It needs some research to follow up the reasons why the Parijoto fruit extract fractions with high phenolic content and radical-scavenging activity turns out as the weakest one to inhibit *E. coli* and *S. aureus*. It may require advance molecular analysis to study about biomolecular interactions of Parijoto fruit extract fractions to know the right pathway which leads to its antibacterial activity

4. Conclusions

This study indicated that the Parijoto's fruit extract fractionation was one of the techniques to determine the potency of Parijoto as a local plant in Central Java to combat the bacterial activities like E. coli and S. aureus which have pathogenicity effect to human. The antibacterial activity was mostly assumed to be correlated with total phenolic content and antioxidant activities in most plant extracts and fractions. The present study showed that the n-hexane fraction (PNF) possesses highest total phenolic content and DPPH radical-scavenging activity turns out as the lowest antibacterial activity against both E. coli and S. aureus. This indicated that the antibacterial activity in Parijoto's fruit extract may be correlated not only with total phenolic content but also correlated with other factors and metabolic pathways.

5. References

Abubakar, A. R., & Haque, M. (2020). Preparation of medicinal plants: Basic extraction and fractionation procedures for experimental purposes. In *Journal of Pharmacy and Bioallied Sciences* (Vol. 12, Issue 1, pp. 1–10). Wolters Kluwer Medknow Publications. https://doi.org/10.4103/jpbs.JPBS_175_19

Al-Rajhi, A. M. H., Qanash, H., Almuhayawi, M. S., Al Jaouni, S. K., Bakri, M. M., Ganash, M., Salama, H. M., Selim, S., & Abdelghany, T. M. (2022). Molecular Interaction Studies and Phytochemical Characterization of Mentha pulegium L. Constituents with Multiple Biological Utilities as Antioxidant, Antimicrobial, Anticancer and Anti-Hemolytic Agents. *Molecules*, *27*(15). https://doi.org/10.3390/molecules27154824

Behiry, S. I., Okla, M. K., Alamri, S. A., EL-Hefny, M., Salem, M. Z. M., Alaraidh, I. A., Ali, H. M., Al-Ghtani, S. M., Monroy, J. C., & Salem, A. Z. M. (2019). Antifungal and antibacterial activities of Musa paradisiaca L. peel extract: HPLC analysis of phenolic and flavonoid contents. *Processes*, *7*(4). https://doi.org/10.3390/pr7040215

Belhaoues, S., Amri, S., & Bensouilah, M. (2020). Major phenolic compounds, antioxidant and antibacterial activities of Anthemis praecox Link aerial parts. *South African Journal of Botany*, *131*, 200–205. https://doi.org/10.1016/j.sajb.2020.02.018

Calín-Sánchez, Á., Lipan, L., Cano-Lamadrid, M., Kharaghani, A., Masztalerz, K., Carbonell-Barrachina, Á. A., & Figiel, A. (2020). Comparison of traditional and novel drying techniques and its effect on quality of fruits, vegetables and aromatic herbs. In *Foods* (Vol. 9, Issue 9). MDPI AG. https://doi.org/10.3390/foods9091261

Craft, K. M., Nguyen, J. M., Berg, L. J., & Townsend, S. D. (2019). Methicillin-resistant: Staphylococcus aureus (MRSA): Antibiotic-resistance and the biofilm phenotype. In *MedChemComm* (Vol. 10, Issue 8, pp. 1231–1241). Royal Society of

Chemistry. https://doi.org/10.1039/c9md00044e

Egua, M. O., Etuk, E. U., Bello, S. O., & Hassan, S. W. (2014). Antidiabetic potential of liquid-liquid partition fractions of ethanolic seed extract of Corchorus olitorious. *Journal of Pharmacognosy and Phytotherapy*, *6*(1), 4–9. https://doi.org/10.5897/JPP2013.0294

El Houda Lezoul, N., Belkadi, M., Habibi, F., & Guillén, F. (2020). Extraction processes with several solvents on total bioactive compounds in different organs of three medicinal plants. *Molecules*, *25*(20). https://doi.org/10.3390/molecules25204672

Elshahawy, O. A. M., Zeawail, M. E. F., Hamza, M. A., Elateeq, A. A., & Omar, M. A. (2022). Improving the Production of Total Phenolics and Flavonoids and the Antioxidant Capacity of Echinacea purpurea Callus through Biotic Elicitation. *Egyptian Journal of Chemistry*, *65*(12), 137–149. https://doi.org/10.21608/EJCHEM.2022.145210.6328

Feliatra, F., Mardalisa, M., Effendi, I., Adelina, A., & Feliatra, V. A. (2022). Biodiversity of Escherichia coli bacterial resistance to multidrug isolated on the Dumai coast of Indonesia. *Biodiversitas*, *23*(1), 10–16. https://doi.org/10.13057/biodiv/d230102

Ghafoor, K., Al Juhaimi, F., Özcan, M. M., Uslu, N., Babiker, E. E., & Mohamed Ahmed, I. A. (2020). Total phenolics, total carotenoids, individual phenolics and antioxidant activity of ginger (Zingiber officinale) rhizome as affected by drying methods. *Lwt*, *126*(March). https://doi.org/10.1016/j.lwt.2020.109354

Hanum, A. S., Prihastanti, E., & Jumari. (2017). Ethnobotany of utilization, role, and philosopical meaning of parijoto (Medinilla, spp) on Mount Muria in Kudus Regency, Central Java. *AIP Conference Proceedings*, *1868*. https://doi.org/10.1063/1.4995210

Hikmawanti, N. P. E., Fatmawati, S., & Asri, A. W. (2021). The effect of ethanol concentrations as the extraction solvent on antioxidant activity of Katuk (Sauropus androgynus (L.) Merr.) leaves extracts. *IOP Conference Series: Earth and Environmental Science*, *755*(1). https://doi.org/10.1088/1755-1315/755/1/012060

Johari, M. A., & Khong, H. Y. (2019). Total Phenolic Content and Antioxidant and Antibacterial Activities of Pereskia bleo. *Advances in Pharmacological Sciences*, *2019*. https://doi.org/10.1155/2019/7428593

Jurić, T., Mićić, N., Potkonjak, A., Milanov, D., Dodić, J., Trivunović, Z., & Popović, B. M. (2021). The evaluation of phenolic content, in vitro antioxidant and antibacterial activity of Mentha piperita extracts obtained by natural deep eutectic solvents. *Food Chemistry*, *362*. https://doi.org/10.1016/j.foodchem.2021.130226

Milanda, T., Lestari, K., & Tarina, N. T. I. (2021). Antibacterial Activity of Parijoto (Medinilla speciosa Blume) Fruit Against Serratia marcescens and Staphylococcus aureus Aktivitas Antibakteri Buah Parijoto (Medinilla speciosa Blume) terhadap Serratia marcescens dan Staphylococcus aureus. *Indonesian Journal of Pharmaceutical Science and Technology*, *8*(2), 76–85.

Mishra, K., Ojha, H., & Chaudhury, N. K. (2012). Estimation of antiradical properties of antioxidants using DPPH- assay: A critical review and results. *Food Chemistry*, *130*(4), 1036–1043. https://doi.org/10.1016/j.foodchem.2011.07.127

Mohammed, M. J., Anand, U., Altemimi, A. B., Tripathi, V., Guo, Y., & Pratap-Singh, A. (2021). Phenolic composition, antioxidant capacity and antibacterial activity of white wormwood (Artemisia herba-alba). *Plants*, *10*(1), 1–14. https://doi.org/10.3390/plants10010164

Mona, N., Widyastuti, D. A., Nurwahyunani, A., Nurdyansyah, F., Studi, P., & Biologi, P. (2022). Florea: Jurnal Biologi dan Pembelajarannya Fraksinasi Ekstrak Metanol Buah Parijoto (Medinilla speciosa Blume) dengan Pelarut Metanol, Etil Asetat, dan N-Heksana. *Florea*, *9*(2), 102–109.

https://doi.org/10.25273/florea.v%vi%i.13883

Nam, J. S., Park, S. Y., Jang, H. L., & Rhee, Y. H. (2017). Phenolic compounds in different parts of young Annona muricata cultivated in Korea and their antioxidant activity. *Applied Biological Chemistry*, *60*(5), 535–543. https://doi.org/10.1007/s13765-017-0309-5

Nurdyansyah, F., & Widyastuti, D. A. (2019). Comparison of Antioxidant Activity of Ethanolic, Methanolic, n- Hexan, and Aqueous Extract of Parkia speciosa Peel based on Half -Maximal Inhibitory Concentration Through Free Radical Inhibition. *Advance Sustainable Science, Engineering, and Technology*, *2*(2), 0200207–01. https://doi.org/10.30537/sjet.v2i2

Pratama, Y., Abduh, S. B. M., Legowo, A. M., Pramono, Y. B., & Albaarri, A. N. (2018a). Optimum carrageenan concentration improved the physical properties of cabinet-dried yoghurt powder. *IOP Conference Series: Earth and Environmental Science*, *102*(1). https://doi.org/10.1088/1755-1315/102/1/012023

Pratama, Y., Abduh, S. B. M., Legowo, A. M., Pramono, Y. B., & Albaarri, A. N. (2018b). Optimum carrageenan concentration improved the physical properties of cabinet-dried yoghurt powder. *IOP Conference Series: Earth and Environmental Science*, *102*(1). https://doi.org/10.1088/1755-1315/102/1/012023

Sa'adah, N. N., Indiani, A. M., Nurhayati, A. P. D., & Ashuri, N. M. (2020). Bioprospecting of parijoto fruit extract (medinilla speciosa) as antioxidant and immunostimulant: Phagocytosis activity of macrophage cells. *AIP Conference Proceedings*, *2260*. https://doi.org/10.1063/5.0016435

Sarecka-Hujar, B., & Szulc-Musioł, B. (2022). Herbal Medicines—Are They Effective and Safe during Pregnancy? In *Pharmaceutics* (Vol. 14, Issue 1). MDPI. https://doi.org/10.3390/pharmaceutics14010171

Syifaul Qulub, A., Nurdyansyah, F., Muliani Dwi Ujianti, R., Khoiron Ferdiansyah, M., Ayu Widyastuti, D., Rossita Dewi, L., & Rahayu, P. (2022). *Penapisan Fitokimia Ekstrak Buah Parijoto (Medinilla Speciosa Blume) Berdasarkan Perbedaan Fraksi*. *1*(1), 134–139.

Thamkaew, G., Sjöholm, I., & Galindo, F. G. (2021). A review of drying methods for improving the quality of dried herbs. In *Critical Reviews in Food Science and Nutrition* (Vol. 61, Issue 11, pp. 1763–1786). Bellwether Publishing, Ltd. https://doi.org/10.1080/10408398.2020.1765309

Villa, V. Y., Legowo, A. M., Bintoro, V. P., & Al-Baarri, A. N. (2013). Quality of Fresh Bovine Milk after Addition of Hypothiocyanite-rich-solution from Lactoperoxidase System. *International Journal of Dairy Science*, *9*(1), 24–31. https://doi.org/10.3923/ijds.2014.24.31

Wibawanti, J. M. W., Mulyani, S., Legowo, A. M., Hartanto, R., Al-Baarri, A., & Pramono, Y. B. (2021). Characteristics of inulin from mangrove apple (Soneratia caseolaris) with different extraction temperatures. *Food Research*, *5*(4), 99–106. https://doi.org/10.26656/fr.2017.5(4).662

Widyastuti, D. A., & Nurdyansyah, F. (2023). Ethanolic Extract of Parkia speciosa Peel: Its Effect on Alkaline Phosphatase and Catalase Level of Wistar Rats with "Jelantah" Exposed. *AIP Conference Proceedings*, *2606*. https://doi.org/10.1063/5.0118399

Wijayanti, D., & Ardigurnita, F. (2018). Potential of Parijoto (Medinilla speciosa) Fruits and Leaves in Male fertility. *Animal Production*, *20*(2), 81–86.

Złotek, U., Szymanowska, U., Pecio, U., Kozachok, S., & Jakubczyk, A. (2019). Antioxidative and Potentially Anti-inflammatory Activity of Phenolics from Lovage Leaves Levisticum officinale Koch Elicited with Jasmonic Acid and Yeast Extract. *Molecules*, *24*(7). https://doi.org/10.3390/molecules24071441

Acknowledgments

We would like to say thanks a lot to the Institution of research and community services of Universitas PGRI Semarang for financial assistance in this research. We also thank to all laboratory members of Department of Food Technology, Universitas PGRI Semarang for all the helpful hands during the research. This research is partially supported by Food Safety Scientific Consortium through the Research Implementation Agreement Contract No. 369/UN7.A/HK/X/2024.

CARPATHIAN JOURNAL OF FOOD SCIENCE AND TECHNOLOGY

journal homepage: **http://chimie-biologie.ubm.ro/carpathian_journal/index.html**

Research article

CHARACTERISTICS OF AMYLUM, AMYLOGRAPH, AND SWELLING POWER OF YELLOW PUMPKIN FLOUR WITH DIFFERENT FERMENTATION TIMES

Anisa Rachma Sari[1]✉, Aldia Sagitaning Putri[1], Antonia Nani Cahyanti[1], Soraya Kusuma Putri[2], Lutfi Purwitasari[3], Siti Susanti[3]

[1]Department of Agricultural Product Technology, Faculty of Agricultural Technology, Semarang University, Semarang, Indonesia

[2]Department of Food Technology, Faculty of Agricultural, Tidar University, Magelang, Indonesia

[3]Department of Food Technology, Faculty of Animal and Agricultural Sciences, Diponegoro University, Semarang, Indonesia

✉Corresponding author: Anisa Rachma Sari, Department of Agricultural Product Technology, Faculty of Agricultural Technology, Semarang University,

✉anisa_ftp@usm.ac.id

https://orcid.org/0009-0003-9887-9550

https://doi.org/10.34302/2025.17.3.6

Article history:
Received:
March 6th, 2025
Accepted:
Novembre 10th , 2025

Keywords:
Gelatinization;
Yellow pumpkin;
Retrogradation;
Fermentation time.

Abstract

Yellow pumpkin flour has disadvantages, including reduced fluffiness and a strong water-binding capacity. This study aimed to analyze the effects of fermentation duration on the amylum characteristics, amylograph properties, and swelling power of yellow pumpkin flour to determine the optimal fermentation time. A randomized experimental design with one factor—fermentation duration—was used, consisting of six treatments (0 to 5 days of fermentation), with each treatment repeated four times. The parameters measured included amylum, amylose, amylopectin, amylograph, swelling power, pH, solubility, and moisture content. The results indicated that fermentation time significantly affected most parameters except gelatinization time. Extended fermentation improved amylograph properties by enhancing gelatinization and retrogradation, although paste stability during heating decreased. However, prolonged fermentation did not enhance the flour's ability to expand, but it did increase water-binding capacity. The study concluded that one-day fermentation was optimal, as it improved gelatinization, retrogradation, and solubility while maintaining a high swelling power in yellow pumpkin flour. This fermentation period produced flour with improved functional properties, making it more suitable for various food applications. Future research should explore further modifications to enhance expansion properties while maintaining the benefits of fermentation on yellow pumpkin flour's quality.

1. Introduction

Yellow pumpkin flour has advantages including its long shelf life, ease of use in food formulations (e.g., bread products, cakes, instant noodles, flakes, rice, pasta, and composite flour), and its role as a natural coloring agent (Budianto et al., 2019; Husna et al., 2020; Pramono et al., 2021; Zhavira & Rizqiati, 2020). Additionally, yellow pumpkin flour is a convenient source of β-carotene supplementation in food products. It enhances color, taste, and moisture of bread product (Pereira et al., 2020). However, it also has some less desirable characteristics, such as being prone to clumping, limited ability to expand, and a slight tendency to bind water (Yanuwardana et al., 2013). Efforts to improve the properties of yellow pumpkin flour have focused on modifying its functional properties to achieve better characteristics (Triyani et al., 2013). Methods of flour modification include the use of acids and enzymes, such as those employed in the production of porous starch (Purwitasari et al., 2023; Witasari et al., 2024). While enzyme-based modification is relatively safer, it is often costly (Budiarti et al., 2020; Rasbawati et al., 2014; Villa et al., 2013). On the other hand, acid-based modification has drawbacks, including being less environmentally friendly and potentially toxic when accumulated in the body (Sulastri et al., 2016; Rasbawati et al., 2014).

Fermentation is an alternative method for modifying starch, as it can alter macromolecular structures and improve the functional properties of pumpkin flour (Kumari et al., 2021). It enhances the surface of starch granules and disrupts their ordered structures, leading to better functionality (Yuliana et al., 2023). Fermentation-induced changes in flour characteristics include increased viscosity, improved gelatinization ability, higher rehydration and solubility, and enhanced resistance to damage (Putri, 2019; Siletty et al., 2022). Lactic acid bacteria and yeast are commonly used as fermentation starters. Lactic acid fermentation has been shown to improve the physical properties and texture of corn flour noodles by altering the amorphous regions of starch granules and the chemical components of starch (Yuan et al., 2008). In yellow pumpkin fermentation, the starch content is reduced due to the amylolytic activity of microbes like *Lactobacillus plantarum* (Tedom et al., 2019).

In this study, *Saccharomyces cerevisiae* was used as the fermentation starter for producing fermented pumpkin flour. Previous studies demonstrated that *S. cerevisiae* exhibited higher amylum degradation ability than *Lactobacillus* sp., with fermented flour containing 48.83% amylum content compared to 49.11% in flour fermented with *Lactobacillu*s sp. (Nainggolan et al., 2019). The duration of the fermentation process is a critical factor affecting the quality of fermented flour. Longer fermentation time increases microbial activity, resulting in greater starch degradation, viscosity, and solubility (Anggraeni & Sudarminto Setyo, 2014). Research by (Hidayat et al., 2018) showed that extended fermentation liberated starch granules from the fiber matrix, leading to more intense granule breakdown and an increase in the water solubility index in *S. cerevisiae* fermented rice flour. To date, there is limited research on the effect of fermentation time using *S. cerevisiae* on the characteristics of yellow pumpkin flour. Therefore, this study was conducted to investigate the impact of *S. cerevisiae* fermentation time on the characteristics of amylum, amylograph, and swelling power of yellow pumpkin flour and to determine the optimal fermentation curation for its production.

2. Materials and methods

2.1. Materials

2.1.1. Materials

The materials used in the study included yellow pumpkin varieties of Bokor obtained from Pati, Central Java, instant dry yeast *S. cerevisiae* (Fermipan), aquades, aluminum foil, HCL, NaOH, anthrone reagents, glucose, amylose, ethanol, acetic acid, and I-KI solution.

2.1.2. Tools

The tools used in the study included biosafety cabinet, beaker glasses, glass jars, Erlenmeyer flasks, pots, measuring flasks, measuring pipettes, test tubes, petri dishes,

cooking utensils, incubators, slicers, autoclaves, counting chambers, cabinet dryers, choppers, 60-mesh sieves, cuvettes, ovens, desiccators, analytical scales, vortex mixers, water baths, digital thermometers, centrifuge tubes, micropipettes, centrifuges, UV-Vis spectrophotometers, digital pH meters, and rapid visco analyzers (RVA).

2.2. Research Design

The study used a randomized design with one factor, namely the length of fermentation time. There were six treatments, and each treatment was repeated 4 times. The treatments chosen were as follows: P1 (without fermentation as a control), P2 (1-day fermentation), P3 (2-day fermentation), P4 (3-day fermentation), P5 (4-day fermentation), P6 (5-day fermentation).

2.3. Methods

2.3.1. Starter Preparation

The starter of *S. cerevisiae* was prepared using the counting chamber method. A total of 5 g of instant dry yeast was mixed with 1,000 g of yellow pumpkin that had been pasteurized at 75°C for 3 minutes in a beaker glass. Aquades (in a 3:2 ratio to the yellow pumpkin) was added, stirred until evenly distributed, and covered with aluminum foil (Yani & Akbar, 2018). The mixture was then incubated at 30°C for 12 hours until a microorganism cell density of 106 CFU/ml was obtained (Tandrianto et al., 2014).

2.3.2. Yellow Pumpkin Fermentation

The yellow pumpkin was fermented using the method of (Sari et al., 2024) with modification. The pasteurized yellow pumpkin was placed in a sterilized glass jar. Fermentation was carried out by inoculating 3% of the starter by the weight of the yellow pumpkin, followed by the addition of aquades in a 3:2 ratio to the weight of the pumpkin. The mixture was stirred until evenly mixed. The fermentation process was conducted in an incubator at 30°C for 1, 2, 3, 4, and 5 days.

2.3.3. Fermented Yellow Pumpkin Flour Preparation

The fermentation results were filtered to separate the yellow pumpkin from the water. The yellow pumpkin was dried using a food dehydrator at 60°C for 24 hours (Herlina et al., 2021). After drying, the pumpkin was mashed using a chopper and sieved through a 60-mesh sieve (Triyani et al., 2013).

2.3.4. Analysis of Fermented Yellow Pumpkin Flour

The parameters tested in this study included the following: water content measured using thermogravimetry and amylum content determined following established methods (Joy et al., 2021); amylose levels and amylograph properties measured based on (Pasca et al., 2022); amylopectin levels were calculated as the difference between amylum and amylose levels; swelling power were determined using the Leach method as described by (Budiarti et al., 2020); pH measurement conducted using a pH meter (Putri, 2019); and solubility measured using the method described by (Winarti et al., 2022).

2.4. Data analysis

The software used for data analysis was SPSS. The data obtained were analyzed to determine whether the treatments had a significant effect using one-way ANOVA with a significance level of 5%. If a significant effect was found, the analysis was followed by the Duncan Multiple Range Test (DMRT) test at a significance level of 5%.

3. Results and discussions

The results of this study are presented in Figures 1, Table 1, and Table 2.

3.1. Composition Characteristics of Starch

The characteristics of amylum, amylose, and amylopectin in fermented yellow pumpkin flour are summarized in Figure 1. The duration of fermentation had a significant effect ($P<0.05$) on the amylum, amylose, and amylopectin levels of yellow pumpkin flour. The Duncan test results indicated that fermentation treatments were significantly different from the control (unfermented flour), and the length of fermentation also resulted in significant differences. Fermentation decreased the levels of amylum and amylopectin but increased the amylose content in yellow pumpkin flour.

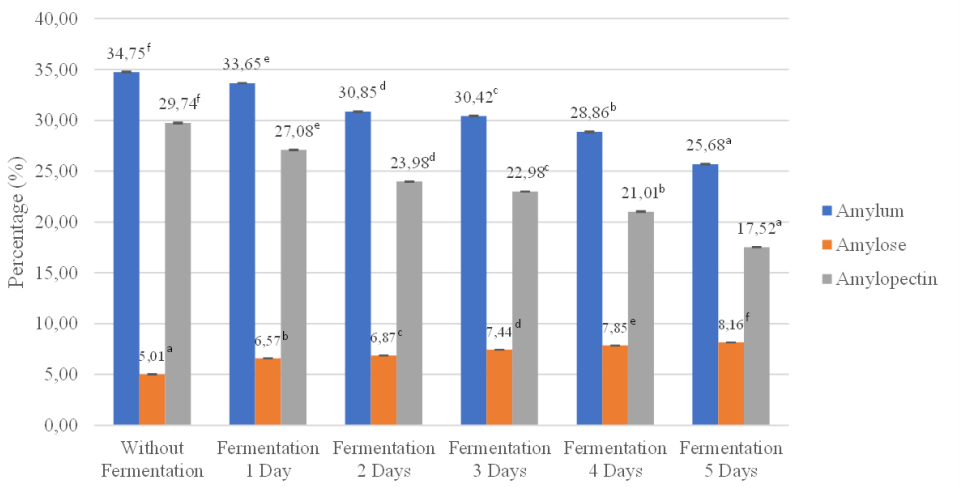

Figure 1. The characteristics of amylum, amylose, and amylopectin of fermented yellow pumpkin flour

The decrease in amylum levels was attributed to the increased production of amylase and diastase enzymes by *S. cerevisiae* during prolonged fermentation. These enzymes hydrolyzed maltose into glucose, reducing the amylum content in the flour (Yani & Akbar, 2018; Wibawanti et al., 2021). The amylum content of fermented yellow pumpkin flour (*S. cerevisiae*, 33.65%) was lower than the findings of (Fiqtinovri, 2020) for fermented elephant cassava mocaf flour (*Saccharomyces* sp., 84.44%) but higher than (Hervelly et al., 2019) for fermented sweet potato flour (*Bacillus subtilis*, 26.79%).

The increase in amylose levels was caused by the breakdown of amylum during fermentation due to amylase and pullulanase activity. These enzymes hydrolyzed specific bonds in starch converting amylopectin into short-chain amylose (Pasca et al., 2022). The breakdown of α-1,6-glycosidic bonds in amylopectin's branch chains resulted in a straight chain amylose, thereby increasing its levels (Winarti et al., 2022). Pullulanase also hydrolyzed branching α-1,6 glycosidic bonds, which contributed to the decrease in amylopectin levels (Setiarto & Widhyastuti, 2016). In this study, prolonged fermentation increased the amylose content. According to (Sumardiono et al., 2019), higher amylose content reduces the swelling capacity of starch. This finding aligns with the results shown in Table 1.

3.2. Pasting and Gelatinization Properties

The starch paste viscosity in flour served as a predictive indicator for determining the quality of the flour. According to (Setiarto & Widhyastuti, 2016), good amylograph characteristics of flour include stability, heat resistance, and strong setback viscosity, which are essential for forming the gel structure of gelatinized starch paste. The amylograph characteristics of fermented yellow pumpkin flour are presented in Table 1. The fermentation time significantly affected ($P<0.05$) the amylograph parameters, including gelatinization temperature, peak viscosity, trough viscosity, breakdown viscosity, setback viscosity, and final viscosity of yellow pumpkin flour. However, it did not significantly influence the gelatinization time ($P>0.05$).

Duncan test at a 5% significance level As the fermentation time increased, the peak, trough, setback, and final viscosity values increased, while the breakdown viscosity and gelatinization temperature decreased. According to (Wahjuningsih et al., 2024), breakdown viscosity is defined as the stability of starch under thermal conditions, where lower values indicate greater stability. Viscosity, on the other hand, refers to a liquid's resistance to flow, which is measured by the rate at which the liquid

travels through a glass tube (Wijayanti et al., 2024). These findings demonstrated improvements in the amylograph properties of fermented yellow pumpkin flour.

The modification in the microstructure of starch granules by Saccharomyces cerevisiae contributed to these changes. Structural alternations in the granules, caused by acid and enzymatic actions during the fermentation, resulted in enhanced granule erosion and chain length shortening of starch molecules (Yuliana et al., 2023).

Unlike the gelatinization temperature of breadfruit, which remained unchanged after fermentation with *L. plantarum* (Wayantika et al., 2019), the reduction in gelatinization temperature in fermented yellow pumpkin flour was likely caused by the weakening of starch granule structures during the soaking phase of fermentation. This aligns with (Aini et al., 2010), who noted that gelatinization begins with the breakdown of the amorphous region of starch granules as hydrogen bonds are disrupted, resulting in leaching and lower gelatinization temperatures.

Table 1. Pasting and Gelatinization Properties

Sample	Gelatinization Temperature	Gelatinization Time (Minutes)	Peak Viscosity (BU/cP)	Trought Viscosity (BU/cP)	Breakdown viscosity *(BU/Cp)*	Setback Viscosity (BU/cP)	Final Viscosity (BU/cP)
Control	87.55±0.632^{c}	13,00±1,414^{a}	1207,00±8,641^{a}	1205,00±4,203^{a}	2.00±0.136^{a}	843,00±8,524^{a}	2048,00±6,683^{a}
1 Day	74.60±0.441^{a}	13,00±2,160^{a}	4410.00±8,602^{b}	4426,00±5,100^{b}	-15,00±3,742^{b}	2303,00±2,450^{b}	6729,00±7,483^{b}
2 Days	75.40±0.078^{b}	13,00±1,633^{a}	4598,00±14,306^{c}	5220,00±7,483^{d}	-13,00±2,160^{bc}	3563,00±3,560^{c}	8783,00±4,082^{d}
3 Days	74.60±0.136^{a}	13.00±0.817^{a}	5207,00±2,944^{d}	5392,00±5,100^{f}	-10.00±0.817^{c}	3839,00±11,576^{d}	8447,00±4,967^{c}
4 Days	75,70±0,220^{b}	13,00±1,633^{a}	5377,00±8,165^{f}	5319,00±5,888^{e}	-15,00±1,633^{b}	4007,00±4,320^{e}	9399,00±8,602^{e}
5 Days	75.40±0.078^{b}	13,00±2,828^{a}	5296,00±6,481^{e}	4608,00±5,100^{c}	-23,00±3,560^{a}	4265,00±7,483^{f}	9584,00±5,010^{f}

Data were expressed as means ± SD, in which different superscripts in the same line significantly differ ($p<0.05$) among the various proportions.

The ease of gelatinization in fermented flour was supported by (Fiqtinovri, 2020), who explained that a lower gelatinization temperature corresponds to more efficient water absorption and starch gelatinization at lower temperatures. Additionally, the decrease in gelatinization temperature was supported by changes in amylose and amylopectin levels (Table 1), as the fermentation process increased their concentration. Increased amylose levels and altered amylopectin content contributed to lowering the gelatinization temperature (Rahman et al., 2018).

The increase in peak viscosity observed in fermented yellow pumpkin flour may have resulted from the reduction in particle size due to starch degradation by *S. cerevisiae*. Smaller particles with larger surface areas absorbed water more effectively, leading to higher peak viscosity. (Anggraeni & Sudarminto Setyo, 2014) stated that the viscosity of fermented sweet potato flour increased with fermentation duration. During gelatinization, the amylose structure of starch diffused as hydrogen bonds between amylose and amylopectin broke, resulting in a rise in viscosity. This increase continued until the peak viscosity was reached, after which the starch granule structure broke down, forming a starch paste when heated to 93℃ (Setiarto & Widhyastuti, 2016) However, after fermentation periods exceeding four days, a decrease in the peak viscosity of yellow pumpkin flour was observed. This decrease was suspected to be due to increased amylose levels in the flour, which inhibited viscosity. During gelatinization, amylose molecules exited the starch granules and formed amylose-fat inclusion complexes. The formation of these complexes reduced the amylose's ability to bond, form gels, and retrograde, thereby

inhibiting the rate of viscosity increase during heating. Additionally, the reduction in the peak viscosity was attributed to the lower pH of the flour during extended fermentation, as supported by the pH data in Table 3, which indicated a consistent decline in pH with increasing fermentation time (Nadhira & Cahyana, 2023).

Fermentation also reduced the breakdown viscosity of yellow pumpkin flour. Lower breakdown viscosity indicated greater stability of the starch under hot conditions. However, extremely low breakdown viscosity suggested a high level of starch granules destruction, which reduced the paste's stability during heating and cooking (Agustin, 2011; Aini et al., 2016). As shown in Table 2., the breakdown viscosity of fermented yellow pumpkin flour was very low, implying significant destruction of amylum granules. This result aligned with (Setiarto & Widhyastuti, 2016), who reported that fermentation decreased the heat resistance properties of gadung starch.

Setback viscosity increased with longer fermentation times, indicating an enhanced retrogradation in yellow pumpkin flour. The fermented yellow pumpkin flour exhibited a higher tendency to retrograde as fermentation duration increased. This was likely due to the higher amylose content in the flour, as noted in the study findings. Amylose was more prone to retrogradation because it recrystallizes easily when exposed to water. Increased amylose levels were one of the primary factors contributing to the high setback viscosity observed in the study. Lastly, fermentation increased the final viscosity of yellow pumpkin flour. Starch with higher final viscosity demonstrated a better ability to form a gel resistant to shear forces, making it more stable during the stirring and cooking processes (Pasca et al., 2022).

Table 2. Swelling Power, pH, Solubility & Moisture Content Characteristics

Treatment	Swelling Power (%)	pH	Solubility (%)	Moisture Content (%)
Control	24,20±0,058^{f}	5.13±0.118^{d}	3.81±0.048^{a}	14.01±2.413^{c}
Fermentation 1 Day	18,13±0,100^{e}	4.07±0.029^{c}	5.35±0.092^{b}	9.06±0.499^{b}
Fermentation 2 Days	16.42±0.113^{d}	4.08±0.013^{c}	5.45±0.096^{b}	8.44±0.846^{ab}
Fermentation 3 Days	15.20±0.113^{c}	3.98±0.005^{b}	6.50±0.116^{c}	8.43±0.453^{ab}
Fermentation 4 Days	14.93±0.083^{b}	3.86±0.019^{a}	6.79±0.068^{d}	7.83±1,264^{ab}
Fermentation 5 Days	12.47±0.061^{a}	3.83±0.005^{a}	7.32±0.051^{e}	6.61±0.554^{a}

Data were expressed as means ± SD, in which different superscripts in the same line significantly differ ($p<0.05$) among the various proportions.

3.3. Physicochemical characteristics

Swelling power was an important characteristic affecting flour quality, as it reflected the ability of starch to expand and indicated the strength of the association force within starch granules, correlating with the composition of amylum. Table 2 showed that the swelling power of yellow pumpkin flour ranged from 12.47 to 24.20%. The results indicated that the fermentation time had a significant effect ($P<0.05$) on the swelling power of yellow pumpkin flour. Duncan's further test at a 5% significance level revealed that fermented samples differed significantly from unfermented ones, and the length of fermentation time also caused significant differences in swelling. Longer fermentation times resulted in a decrease in the swelling power of yellow pumpkin flour. Kumari et al. (2021) explained that the reduction in starch content, particularly amylopectin, played a key role in lowering swelling power. Factors such as amylose to amylopectin ratio, chain length, and molecular weight distribution also influenced swelling power. Higher heating temperature increased crystal formation, enhancing granule stability and reducing swelling capacity (Sarifah et al., 2021). This could also be attributed to amylose forming complexes with lipids and the linear chains of amylopectin, which limits amylose release and decreases starch granule swelling (Kumoro et al., 2019).

Fermentation's ability to reduce swelling power in yellow pumpkin flour was found to be less pronounced than the effect of chemical modification using acetic acid. The addition of acetic acid was reported to increase swelling power by weakening hydrogen bonds in starch, allowing water to penetrate the starch granules more easily, leading to greater expansion (Triyani et al., 2013). Conversely, fermentation with lactic acid soaking demonstrated a decrease in swelling power as fermentation duration increased. The lower pH caused by lactic acid was associated with the formation of carbonyl and carboxyl groups, which accelerated amylose degradation and reduced swelling power (Yanuwardana et al., 2013; Villa et al., 2013). Table 3 supported this, showing that longer fermentation times corresponded to lower pH levels in yellow pumpkin flour. Moreover, prolonged fermentation decreases nutritional content and reduces bacterial activity in breaking down starch into amylose, which significantly affects the swelling power (Rahma et al., 2017).

Solubility referred to the ability of solids to dissolve in water and was influenced by the sugar content of the flour. Table 1 indicated that the solubility of yellow pumpkin flour ranged from 3.81 to 7.32%. The results showed that fermentation time significantly affected ($P<0.05$) the solubility of yellow pumpkin flour. Duncan's test at a 5% significance level demonstrated significant differences between fermented and unfermented samples, as well as between different fermentation durations. Longer fermentation times increased the solubility of yellow pumpkin flour. This increase was attributed to the release of simple sugars (Al-Baarri et al., 2018) from the hydrolysis of amylum by microorganisms. Higher sugar content in the flour enhanced water binding, thereby increasing solubility (Fauzi et al., 2023). Additionally, higher temperatures caused increased solubility by damaging starch granules, transforming crystalline regions into amorphous ones and allowing more amylose to leach out (Sarifah et al., 2021). Higher solubility was considered beneficial as it indicated better water-binding capacity (Purwanto et al., 2013). Furthermore, higher solubility is associated with improved digestibility (Retnowati et al., 2018).

The decrease in the pH of fermented yellow pumpkin flour with longer fermentation time was attributed to increased total acidity. This aligns with the findings of (Al-Baarri et al., 2024), who explained that microbial activity levels and the number of microbes increase with fermentation time, leading to the production of acid metabolites as a result of microbial metabolism. Longer fermentation durations enhanced yeast activity, leading to the breakdown of glucose into alcohol and organic acids, which reduced pH (Yani & Akbar, 2018). Hydrolysis of starch granules by *S. cerevisiae* also produced organic acids, particularly lactic acid, which further decreased pH levels (Anggraeni & Sudarminto Setyo, 2014). The fermentation process in flour typically leads to a decrease in pH, making the flour more acidic. For instance, during the fermentation process in making MOCAF, the acidity is primarily due to the production of lactic acid by lactic acid bacteria (LAB), which is a byproduct of starch hydrolysis (Endrina et al., 2018; Swastawati et al., 2019).

The moisture content of unfermented yellow pumpkin flour (Table 1) was 14%, whereas fermented samples had lower moisture content, ranging from 9.06% to 6.61%. These values were within acceptable limits compared to SNI 3751-2018 standard, which set maximum moisture content for wheat flour at 14.5%, cassava flour at 12%, rice flour at 13%, and corn flour at 10% (Purwanto et al., 2013). Low moisture content also indicates a high bulk density (Rachma et al., 2018). Moisture content plays a crucial role in starch quality. When the moisture content exceeds 13%, it becomes undesirable, as it increases the risk of microbial spoilage, which can negatively impact storage safety and stability (Nuswantari, 2022). The results showed that fermentation time had a significant effect ($P<0.05$) on the moisture content of yellow pumpkin flour. Duncan's further test indicated that fermentation treatments were significantly different from unfermented samples, and fermentation duration also caused significant difference in moisture

content. Longer fermentation times resulted on lower moistire content. This reduction was attributed to the degradation of starch by microorganisms, which decreased the material's water retention capacity. The moisture content of fermented yellow pumpkin flour is relatively lower compared to gadung flour fermented with *M. racemosus* and *L. plantarum*, which has a moisture content of approximately 12% (Kumoro et al., 2020). Prolonged enzymatic activity during fermentation released more bound water, softening and increasing porosity in the material. These structural changes facilitated water evaporation during drying, further reducing moisture content (Anggraeni & Sudarminto Setyo, 2014).

4. Conclusions

This study concluded that longer fermentation times decreased the levels of amylum and amylopectin while increasing the amylose content in yellow pumpkin flour. The amylograph properties of yellow pumpkin flour improved with longer fermentation, as evidenced by increases in peak, trough, breakdown, setback, and final viscosity, while the gelatinization temperature decreased. Prolonged fermentation also resulted in reductions in swelling power, pH, and moisture content, whereas solubility increased. One-day fermentation was chosen because it improved gelatinization, retrogradation, and solubility, while maintaining a high swelling power in yellow pumpkin flour.

5. References

Agustin, T. I. (2011). Modifikasi Oksidasi Pati Singkong dan Aplikasinya Sebagai Filling Agent pada Bakso Ikan. *Jurnal Kelautan*, *17*(1), 44–59.

Aini, N., Hariyadi, P., Muchtadi, T. R., & Nuri, A. (2010). Hubungan Antara Waktu Fermentasi Grits Jagung dengan Sifat Gelatinisasi Tepung Jagung Putih yang Dipengaruhi Ukuran Partikel. *Jurnal Teknologi Dan Industri Pangan*, *XXI*(1), 18–24.

Aini, N., Wijonarko, G., & Sustriawan, B. (2016). Sifat Fisik, Kimia, dan FungsionalTepung Jagung yang Diproses Melalui Fermentasi. *AGRITECH*, *36*(2), 160–169.

Al-Baarri, A. N., Dwiloka, B., Mulyani, S., Pramono, Y. B., Setiani, B. E., Rahmawati, A. A., Jordan, A., & Nababan, P. U. B. L. (2024). Protein fraction profile and physicochemical quality of Blacksoyghurt drink. *Food Research*, *8*(2), 435–442. https://doi.org/10.26656/fr.2017.8(2).143

Al-Baarri, A. N., Legowo, A. M., & Widayat. (2018). The browning value changes and spectral analysis on the Maillard reaction product from glucose and methionine model system. *IOP Conference Series: Earth and Environmental Science*, *102*(1). https://doi.org/10.1088/1755-1315/102/1/012003

Anggraeni, Y. P., & Sudarminto Setyo, Y. (2014). Pengaruh Fermentasi Alami pada Chips Ubi Jalar (Ipomoea batatas) Terhadap Sifat Fisik Tepung Ubi Jalar Terfermentasi. *Jurnal Pangan Dan Agroindustri*, *2*(2), 59–69.

Budianto, A., Karimah, I., & Mislan. (2019). Pengaruh Umur Panen dan Metode Pengeringan Terhadap Karakteristik Fisikokimia Tepung Labu Kuning (Cucurbita moschata L.) Varietas Kusuma di Banyuwangi Tahun 2016. *Jurnal Teknologi Pangan Dan Ilmu Pertanian*, *1*(1), 10–19.

Budiarti, G. I., Wulandari, A., Mutmaina, S., & Sulistiawati, E. (2020). Modified Pumpkin Flour Using Hydrogen Rich Water with a Microwave Dryer. *CHEMICA: Jurnal Teknik Kimia*, *7*(1), 19. https://doi.org/10.26555/chemica.v7i1.16230

Endrina, I., Nurwantoro, & Pramono, Y. B. (2018). Karakteristik Kimia dan Mutu Hedonik Selai Kolang Kaling dengan Variasi Konsentrasi Modified Cassava Flour (MOCAF) Sebagai Alternatif Pengganti Pektin. *Jurnal Teknologi Pangan*, *2*(2), 113–119. https://doi.org/https://doi.org/10.14710/jtp.2018.20655

Fauzi, M., Herlina, H., & Sholeha, I. M. (2023). Karakteristik Fisik dan Fungsional Tepung

Labu Kuning LA3 Desa Tegalrejo, Kecamatan Tegalsari, Kabupaten Banyuwangi. *AGRITEKNO: Jurnal Teknologi Pertanian*, *12*(2), 106–114. https://doi.org/10.30598/jagritekno.2023.12.2.106

Fiqtinovri, S. M. (2020). Karakteristik Kimia dan Amilografi Mocaf (Modified Cassava Flour) Singkong Gajah (Manihot Utilissima). *Jurnal Agroindustri Halal*, *6*(1), 49–56.

Herlina, H., Adzim, S., Nafi, A., & Nita, K. (2021). Karakteristik Tiwul Instan Subtitusi Ubi Jalar Kuning (Ipomoea batatas L.) Sebagai Sumber β-Karoten. *AgriTECH*, *41*(2), 184–194. https://doi.org/10.22146//agritech.43676

Hervelly, Rohima, E. I., & FauziahSyifa. (2019). Karakteristik Tepung Ubi Jalar (Lpomoea batatas L) Termodifikasi Secara Fermentasi Menggunakan Koji Bacillus subtilis dan Aplikasinya pada Pengolahan Pangan. *Pasundan Food Technology Journal*, *6*(2), 8–17.

Hidayat, B., Muslihudin, M., & Syamsu, A. (2018). Perubahan Karakteristik Fisikokimia Tepung Onggok Selama Proses Fermentasi Semi Padat Menggunakan Saccharomyces cerevisiae. *Jurnal Penelitian Pertanian Terapan*, *18*(3), 146–152. https://doi.org/10.25181/jppt.v18i3.1370

Husna, S. S., Hintono, A., & Rizqiati, H. (2020). Texture, Water Absorption, aw and Hedonic Quality Flakes White Millet (Panicum miliaceum) with Addition of Pumpkin Flour (Cucurbita moschata). *Journal of Applied Food Technology*, *7*(2), 29–32. https://doi.org/10.17728/jaft.7685

Joy, E.-E., Chidinma, V.-U. E., & Akusu, M. O. (2021). Physicochemical and Functional Properties of Pumpkin (Cucurbita Pepo) Pulp Flour and Acceptability of its Inclusion in Cake. *Asian Food Science Journal*, *20*(7), 57–71. https://doi.org/10.9734/afsj/2021/v20i730321

Kumari, N., C. Sindhu, S., Rani, V., Kumari, A., & Varsha, K. (2021). Effect of Fermentation on Nutrient Composition of Pumpkin Seed Flour. *Annals of Agri-Bio Research*, *26*(2), 234–237. https://www.researchgate.net/publication/357887794

Kumoro, A. C., Retnowati, D. S., Ratnawati, R., & Widiyanti, M. (2019). Effect of Temperature and Reaction Time on the Swelling Power and Solubility of Gadung (*Dioscorea hispida* Dennst) Tuber Starch during Heat Moisture Treatment Process. *Journal of Physics: Conference Series*, *1295*, 012062. https://doi.org/10.1088/1742-6596/1295/1/012062

Kumoro, A. C., Widiyanti, M., Ratnawati, R., & Retnowati, D. S. (2020). Nutritional and functional properties changes during facultative submerged fermentation of gadung (Dioscorea hispida Dennst) tuber flour using Lactobacillus plantarum. *Heliyon*, *6*(3), e03631. https://doi.org/10.1016/j.heliyon.2020.e03631

Nadhira, R., & Cahyana, Y. (2023). Kajian Sifat Fungsional dan Amilografi Pati dengan Penambahan Senyawa Fenolik: Kajian Pustaka. *Jurnal Penelitian Pangan (Indonesian Journal of Food Research)*, *3*(1), 14–19. https://doi.org/10.24198/jp2.2023.vol1.1.03

Nainggolan, E. A., Yudianto, D., & Sayekti, A. (2019). Effect of Fermentation on Physicochemical Properties of Fermented Cassava Flour. *Journal of Physics: Conference Series*, *1367*(1). https://doi.org/10.1088/1742-6596/1367/1/012083

Nuswantari, S. R. (2022). Effect of Chemical Modification By Oxidation and Esterification Process On Properties of Starch: A Review. *Eduvest - Journal of Universal Studies*, *2*(12), 2885–2896. https://doi.org/10.59188/eduvest.v2i12.709

Pasca, B. D., Muhandri, T., Hunaefi, D., & Nurtama, B. (2022). Karakteristik Fisikokimia Tepung Singkong dengan Beberapa Metode Modifikasi. *Jurnal Mutu Pangan : Indonesian Journal of Food Quality*, *8*(2), 97–104. https://doi.org/10.29244/jmpi.2021.8.2.97

Pereira, A. M., Krumreich, F. D., Ramos, A. H., Krolow, A. C. R., Santos, R. B., & Gularte, M. A. (2020). Physicochemical Characterization, Carotenoid Content and Protein Digestibility of Pumpkin Access Flours for Food Application. *Food Science and Technology (Brazil)*, *40*, 691–698. https://doi.org/10.1590/fst.38819

Pramono, Y. B., Nurwantoro, Handayani, D., Mulyani, S., & Hari Wibowo, C. (2021). Physical, chemical, stickiness and organoleptic characteristics of analog white sweet potato rice with the addition of pumpkin flours. *IOP Conference Series: Earth and Environmental Science*, *803*(1), 012039. https://doi.org/10.1088/1755-1315/803/1/012039

Purwanto, C. C., Ishartani, D., & D. Rahardian. (2013). Kajian Sifat Fisik dan Kimia Tepung Labu Kuning (Cucurbita maxima) dengan Perlakuan Blanching dan Perendaman Natrium Metabisulfit. *Jurnal Teknosains Pangan*, *2*(2), 121–130. www.ilmupangan.fp.uns.ac.id

Purwitasari, L., Wulanjati, M. P., Pranoto, Y., & Witasari, L. D. (2023). Characterization of porous starch from edible canna (Canna edulis Kerr.) produced by enzymatic hydrolysis using thermostable α-amylase. *Food Chemistry Advances*, *2*, 100152. https://doi.org/10.1016/j.focha.2022.100152

Putri, S. (2019). Pengembangan Hybrid Tepung Ubi Jalar Kaya Antioksidan. *Jurnal Kesehatan*, *10*(2), 153–162. http://ejurnal.poltekkes-tjk.ac.id/index.php/JK

Rachma, Y. A., Anggraeni, D. Y., Surja, L. L., Susanti, S., & Pratama, Y. (2018). Karakteristik Fisik dan Kimia Tepung Malt Gabah Beras Merah dan Malt Beras Merah dengan Perlakuan Malting pada Lama Germinasi yang Berbeda. *Jurnal Aplikasi Teknologi Pangan*, *7*(3). https://doi.org/10.17728/jatp.2707

Rahma, I. N., Pratama, R. H., Alfiyanti, Alwi, D. R., Astuti, W. I. S. T., & Wardhani, D. H. (2017). Swelling power and solubility of modified breadfruit flour using *Lactobacillus plantarum*. *Journal of Physics: Conference Series*, *909*, 012087. https://doi.org/10.1088/1742-6596/909/1/012087

Rahman, S., Bakar Tawali, A., & Mahendradatta, M. (2018). Artikel Penelitian Pasta Pati Biji Palado (Aglaia sp) Termodifikasi Metode Pra-gelatinisasi, Ikatan Silang, dan Asetilase Pasta Starch Gelatinization Profile Palado (Aglaia sp) Modified Seeds Pra-gelatinization Method, Crosslinking, and Asetilase. *Jurnal Aplikasi Teknologi Pangan*, *6*(4), 2017. https://doi.org/10.17728/jatp.150

Rasbawati, Dwiloka, B., Al-Baarri, A. N., M. Legowo, A., & Bintoro, V. P. (2014). Total Bacteria and pH of Dangke Preserved Using Natural Antimicrobial Lactoferrin and Lactoperoxidase from Bovine Whey. *International Journal of Dairy Science*, *9*(4), 116–123. https://doi.org/10.3923/ijds.2014.116.123

Retnowati, D. S., Kumoro, A. C., & Ratnawati, R. (2018). Physical, thermal and functional properties of flour derived from Ubi Gembili (Dioscorea esculenta L.) tubers grown in Indonesia. *Potravinarstvo Slovak Journal of Food Sciences*, *12*(1), 539–545. https://doi.org/10.5219/937

Sarifah, S., Riwayati, I., & F. Maharani. (2021). Modifikasi Tepung Labu Kuning (Cucurbita moschata) Menggunakan Metode Heat Moisture Treatment (HMT) dengan Variasi Suhu dan Lama Pengeringan. *Inovasi Teknik Kimia*, *6*(1), 42–45.

Setiarto, R. H. B., & Widhyastuti, N. (2016). Pengaruh Fermentasi Bakteri Asam Laktat Lactobacillus plantarum B307 Terhadap Kadar Proksimat dan Amilografi Tepung Taka Modifikasi (Tacca leontopetaloides) leontopetaloides)). *Jurnal Ilmu Pertanian Indonesia (JIPI)*, *21*(1), 7–12. https://doi.org/10.18343/jipi.21.1.7

Siletty, L., Polnaya, F. J., & Moniharapon, E. (2022). Karakteristik Kimia Tepung Umbi Talas (Colocasia esculenta) Kultivar Tanimbar dengan Lama Fermentasi. *AGRITEKNO: Jurnal Teknologi Pertanian*, *11*(1), 48–53.

https://doi.org/10.30598/jagritekno.2022.11.1.48

Sulastri, Y., Ihromi, S., & Nurhayati, D. (2016). Modifikasi Tepung Labu Kuning (Cucurbita Flour) dengan Hidrolisis Secara Enzimatis [. *Jurnal Ilmu Dan Teknologi Pangan*, *2*(1). http://profood.unram.ac.id/index.php/profood

Sumardiono, S., Putri, A. W. Z., Jos, B., & Pudjihastuti, I. (2019). Effect of Modification Processes on Cassava Starch: Physichochemical Properties and Expansion Ability of Coated Penute. *Journal of Physics: Conference Series*, *1295*(1), 012078. https://doi.org/10.1088/1742-6596/1295/1/012078

Swastawati, F., Al-Baari, A. N. matullah, Susanto, E., & Purnamayati, L. (2019). The effect of antioxidant and antibacterial liquid smoke nanocapsules on catfish fillet (pangasius sp.) during storage at room temperature and cold temperature. *Carpathian Journal of Food Science and Technology*, *11*(4), 165–175. https://doi.org/10.34302/2019.11.4.16

Tandrianto, J., Mintoko, D. K., & Gunawan, S. (2014). Pengaruh Fermentasi pada Pembuatan Mocaf (Modified Cassava Flour) dengan Menggunakan Lactobacillus plantarumm Terhadap Kandungan Protein. *Jurnal Teknik Pomits*, *3*(2), 1–3.

Tedom, W. D., Fombang, E. N., Ngaha, W. D., & Ejoh, R. A. (2019). Optimal Conditions for Production of Fermented Flour from Pumpkin (Cucurbita pepo L.) for Infant Foods. *European Journal of Nutrition & Food Safety*, 125–136. https://doi.org/10.9734/ejnfs/2019/v10i230105

Triyani, A., Ishartani, D., & Dimas, R. A. M. (2013). Kajian Karakteristik Fisikokimia Tepung Labu Kuning (Cucurbita moschata) Termodifikasi dengan Variasi Lama Perendaman dan Konsentrasi Asam Asetat. *Jurnal Teknosains Pangan29*, *2*(2), 29–38. www.ilmupangan.fp.uns.ac.id

Villa, V. Y., Legowo, A. M., Bintoro, V. P., & Al-Baarri, A. N. (2013). Quality of Fresh Bovine Milk after Addition of Hypothiocyanite-rich-solution from Lactoperoxidase System. *International Journal of Dairy Science*, *9*(1), 24–31. https://doi.org/10.3923/ijds.2014.24.31

Wahjuningsih, S. B., Azkia, M. N., Siqhny, Z. D., Purwitasari, L., Oktaviani, R. I., & Nazir, N. (2024). Formulation and Quality Study of Mocaf Substitute Noodles with the Addition of Multigrain. *International Journal on Advanced Science, Engineering and Information Technology*, *14*(3), 967–975. https://doi.org/10.18517/ijaseit.14.3.19599

Wayantika, T., Ishartani, D., Nursiwi, A., & Zaman, M. Z. (2019). Effect of fermentation time by Lactobacillus plantarum FNCC 0027 on chemical, physical and physico-chemical properties of modified breadfruit flour. *IOP Conference Series: Materials Science and Engineering*, *633*(1), 012002. https://doi.org/10.1088/1757-899X/633/1/012002

Wibawanti, J. M. W., Mulyani, S., Legowo, A. M., Hartanto, R., Al-Baarri, A., & Pramono, Y. B. (2021). Characteristics of inulin from mangrove apple (Soneratia caseolaris) with different extraction temperatures. *Food Research*, *5*(4), 99–106. https://doi.org/10.26656/fr.2017.5(4).662

Wijayanti, L., Muniroh, M., Al-Baarri, A. N., Fitranti, D. Y., Mahati, E., & Afifah, D. N. (2024). Modification of the GLITEROS diabetes-specific hospital enteral formula based on jicama flour and tempeh flour with the addition of sunflower seed flour. *Food Research*, *8*(2), 443–452. https://doi.org/10.26656/fr.2017.8(2).150

Winarti, S., Rosida, D. F., & Febriana, M. R. (2022). Karakteristik Fisiko-Kimia Tepung Jagung Termodifikasi Secara Fermentasi Menggunakan Lactobacillus plantarum FNCC-0027. *Jurnal Ilmu Pangan Dan Hasil Pertanian*, *6*(2), 216–229. https://doi.org/10.26877/jiphp.v6.vi2i.14389

Witasari, L. D., Heryadi, A. A., Yani, A. I. T., Nisrina, S., Purwitasari, L., & Pranoto, Y. (2024). Characterization of porous starch produced from edible canna (Canna edulis

Kerr.) via enzymatic hydrolysis using thermostable α-amylase and glucoamylase. *Biocatalysis and Agricultural Biotechnology*, *55*, 102990. https://doi.org/10.1016/j.bcab.2023.102990

Yani, A. V., & Akbar, M. (2018). Pembuatan Tepung Mocaf (Modified Cassava Flour) dengan Berbagai Varietas Ubi Kayu dan Lama Fermentasi. *EDIBLE*, *7*(1), 40–48.

Yanuwardana, Basito, & Dimas, R. A. M. (2013). Kajian Karakteristik Fisikokimia Tepung Labu Kuning (Cucurbita moschata) Termodifikasi dengan Variasi Lama Perendaman dan Konsentrasi Asam Laktat. *Jurnal Teknosains Pangan75*, *2*(2), 72–83. www.ilmupangan.fp.uns.ac.id

Yuan, M.-L., Lu, Z.-H., Cheng, Y.-Q., & Li, L.-T. (2008). Effect of spontaneous fermentation on the physical properties of corn starch and rheological characteristics of corn starch noodle. *Journal of Food Engineering*, *85*(1), 12–17. https://doi.org/10.1016/j.jfoodeng.2007.06.019

Yuliana, N., Nurdjanah, S., Setyani, S., & Novianti, D. (2023). The benefits of fermentation in improving the pasting properties of composite sweet potato flour and its application in composite white salted noodles. *Food Research*, *7*(1), 120–127. https://doi.org/10.26656/fr.2017.7(1).712

Zhavira, H., & Rizqiati, H. (2020). Effect of Yellow Pumpkin (Cucurbita moschata) Flour Addition on Proximate Levels and Calories of White Millet (Panicum miliaceum) Flakes. *Journal of Applied Food Technology*, *7*(2), 33–37. https://doi.org/10.17728/jaft.7268

Acknowledgments

The author expresses sincere gratitude to the Institute for Research and Community Service (LPPM) at the University of Semarang for funding this research through the Research Implementation Agreement Contract No. 021/USM.H7.LPPM/L/2024. Special appreciation is extended to Prof. Dr. Ir. Haslina, M.Si., and Dr. Iswoyo, S.Pt., M.P., for their invaluable insights and constructive reviews. The author also acknowledges the lecturers and laboratory staff of the Faculty of Agricultural Technology, University of Semarang, for their support in conducting this research, as well as the dedicated staff of LPPM for their assistance. Furthermore, this research was partially supported by the Food Safety Scientific Consortium through the Research Implementation Agreement Contract No. 369/UN7.A/HK/X/2024.

CARPATHIAN JOURNAL OF FOOD SCIENCE AND TECHNOLOGY

journal homepage: **http://chimie-biologie.ubm.ro/carpathian_journal/index.html**

Research article

RESEARCH ON THE NITRATES AND NITRITES CONTENT IN SOME VEGETABLE SPECIES, CLUJ COUNTY, ROMANIA AND ANTWERPEN, BELGIUM

Silvia Burcă[1], **Cerasella Indolean**[1]✉

[1]*Babeş-Bolyai University, Faculty of Chemistry and Chemical Engineering, Department of Chemical Engineering, 11 Arany Janos str., RO-400028, Cluj-Napoca, Romania*

✉*liliana.indolean@ ubbcluj.ro*

https://doi.org/10.34302/2025.17.3.7

Article history:
Received
August 5th, 2025
Accepted
September 30th, 2025

Keywords:
Field;
Vegetable;
Nitrites;
Nitrates.

ABSTRACT

The study presents the monitoring of nitrate and nitrite levels from some vegetable samples (lettuce - *Lactuca sativa*, carrot - *Daucus carota*, parsley root - *Petroselinum hortense*, kohlrabi - *Brasica oleracea* variety *gongyloyides*, spinach - *Spinacea oleracea*, celery - *Apium graveolens*, cabbage - *Brasica oleracea* and beetroot - *Beta vulgaris*) purchased from a local market in Cluj-Napoca, Romania, and a supermarket in Antwerp, Belgium. The analyses were performed using a laboratory molecular adsorption spectrophotometer. Based on the t-test for method evaluation, it was determined that the method is not affected by systematic errors. The nitrite concentrations recorded ranged from 8.6 µg/g for kohlrabi from Romania to 557.3 µg/g for red beet samples from Belgium.

Comparing the results from all vegetable samples, the main conclusion was that nitrates were below the maximum level, while nitrites were significantly above the maximum permitted limit according to European legislation (for lettuce and beetroot).

1.Introduction

The authors argue that the defining characteristic of this study lies in its contextual relevance to Romania's integration into the Schengen area. This process is anticipated to reduce, and ultimately eliminate, the disparities between Romania and other European Union member states across diverse spheres of activity and daily life. In this context, Romanian researchers are encouraged to prioritize comparative investigations that evaluate the extent to which conditions for vegetable and fruit cultivation align with European legislative standards, which are considerably more stringent—particularly with respect to permissible concentrations of nitrates and nitrites (Serra et al., 2024). Accordingly, the present study aims to assess and compare the nitrate and nitrite content of selected vegetables available on the markets of Cluj (Romania) and Antwerp (Belgium).

Nitrogen is the most abundant chemical element, about 80% of the Earth's atmosphere is made up of nitrogen. Nitrogen is a key element for some essential biomolecules: vitamins, amino acids, hormones, enzymes, nucleotides (Pham *et. al*., 2008; Kristin *et. al*., 2010).

Nitrates (NO_3^-) and nitrites (NO_2^-) are natural chemical compounds found in the soil, water, plants and even the human body.

Nitrite and nitrate levels in vegetables are a matter of concern due to their toxicity at high levels and nitrate high accumulation. Moreover, there is a lack of knowledge about their levels in some types of widely consumed vegetables such as lettuce, spinach, or cabbage.

Nitrates, the most oxidized form of nitrogen, have been known for half a millennium BC, before isolating them from the air, for preserving animal foods (E.F.S.A., 2008). Nitrates are natural components and important components in plants due to their potential for accumulation, they form naturally in living or decaying plants and animals, including the human body (Mensinga *et. al*., 2003; Lundberg *et. al*., 2004; Weitzberg *et. al*., 2004; Lundberg *et. al*., 2008; Lundberg *et. al*., 2006).

In Europe there is a tendency for plant nitrate concentrations to be higher in northern latitudes, especially in winter, due to low light intensity, on days with little light (McKnight *et. al*., 1999).

Genetic factors determine the accumulation of nitrates in vegetable matrices, leafy legumes and vegetables in which the consumable part is the root (beets, carrots, radishes) are plant species characterized by the highest content of nitrates. The differences in nitrate accumulation are due to low amounts of reductases (e.g. vegetables from the family *Chenopodiaceae*, family *Cruciferae*, family *Umbeliferae*, family *Compositae*), the deficiency in trace elements involved in the activity of reducing enzymes can lead to large accumulations of nitrate due to inhibition of the reaction discount. Nitrates can also accumulate if the carbohydrate content is low (Camargo *et. al*., 2006; Bryan *et.al*., 2005; Baty *et.al*., 2007).

The type of soil and the mineral content can affect the accumulation of nitrates, nitrates circulate from the soil to the root surface more frequently by convection than by diffusion, so the lack of water in the soil will restrict the intake of nitrates (Greenwood *et. al*., 1986).

Nitrate and nitrite levels in natural farming practices can be influenced by: duration and storage conditions (room temperature, cold, frozen) and food processing (washing, cleaning, bleaching or boiling). From literature data it is know that nitrite concentrations are about one hundred time lower than those of nitrate, while its toxicity is about the same order of magnitude higher (LD_{50} was 85 mg/kg for nitrite, and 3236 mg/kg for nitrate (rat oral)) (Liu et al., 2023; Tsikas, 2023) Nitrate levels in raw vegetables kept at ambient temperature may decrease during storage, but nitrite levels may increase through storage and wilting in close connection with endogenous activity specific to nitro reductase (Van Eysinga, 1984; Weightman *et. al*., 2006; AFSSA, 2007; Kanaan, 1992; Premuzic *et.al*., 2002; Filer *et. al*., 1970; Sánchez-Echaniz *et. al*., 2001; Jakszyn *et.al*., 2004).

After ingestion, the metabolic conversion of nitrate to nitrite will depend on biological factors (bacteria) and chemical factors (pH), which can react with secondary amines to produce nitrosamines (Calderón *et al*., 2025).

Numerous studies have shown that nitrate accumulation in vegetables is not determined just by plant species, but is also affected by several other important factors, such as soil type, texture, pH and organic metters from soil, fertilization regime (especially nitrogen dose, form of nitrogen – nitrates lead to more direct accumulation compared to ammonium or urea, etc), irrigation frequency and amount, climatic conditions (like light intensity, temperature, precipitations and humidity), as well as cultivation methods (e.g., open field vs. greenhouse, conventional vs. organic systems, hydroponic vs. soil, etc.). (Dodocioiu *et al*., 2025; Dezhangah *et al.*, 2022; Dung et al., 2024, Nguyen *et al.*, 2025).

The European Commission has established the maximum permitted doses for nitrates in lettuce and spinach; these maximum limits being

permanently verified. The effects of nitrates on the food safety of other vegetables are uncertain. The presence of significant amounts of nitrates in potatoes has often been found in arugula, while potatoes often contain insignificant levels of nitrates, but they are consumed more frequently and thus potatoes can be more dangerous (Pate, 1973; Andrews, 1986; Wallace, 1986).

The symbiotic fixation reaction of atmospheric molecular nitrogen is performed by bacteria of the genus *Rhizobium*, which form symbioses with the roots of leguminous plants (Phillips, 1968; Ezeagu *et. al*., 1995; Ezeagu, 1996; Chung *et. al*., 2004; Sánchez-Echaniz *et.al.*, 2001; Phillips, 1968).

The main sources of nitrogen used by plants are minerals, nitrates and ammonium can be adsorbed passively and actively (Schuster *et. al*., 1987; Bucur *et. al*., 2010; Lupea *et. al*., 2001; Cumpătă *et. al*., 2005).

Naturally, a balance is established between nitrates and nitrites in soil, water and plants, which can be broken by the intensive use in agriculture of natural organic fertilizers and especially synthetic nitrogen fertilizers. Their degradation products enrich the soil and can accumulate in cultivated plants to levels harmful to consumers (Ceaușescu, 1978; Mănescu *et.al*., 1994; Bibicu, 1994; Calancea, 2002; Banu *et. al*., 1982).

Nitrate is preferentially adsorbed by plants, the process being selective in relation to the species, metabolic processes, age, environmental factors. Nitrate adsorbed by plant root is reduced in the presence of the enzyme nitrate reductase and NADPH-H $^{+}$ to nitrites, which in turn are reduced to ammoniacal nitrogen in the presence of nitrite reductase and reduced ferredoxin. Nitrogen oxide is also enzymatically transformed into hydroxylamine, amides and amino acids (Hura, 2005).

The maximum quantity of nitrates accumulates in those parts of plants closer to the root, the nitrate content of leafy vegetables species is much higher in stems and petiole, as these organs conduct nitrate ion to the leaf tissues where the process of reducing nitric nitrogen, nitrates being transformed into organic compounds with nitrogen in the process of photosynthesis.

According to literature, vegetables contribute only 2 to 6% to the daily ratio of nitrite exposure, this proportion being exceeded by the endogenous transformation of nitrates from vegetables consumed into nitrites (Cumpătă *et. al*., 2005);

In conditions of refrigeration and freezing of vegetables, insignificant changes were found in terms of nitrate and nitrite content (Banu *et. al*., 1982).

Human exposure to nitrates is mainly exogenous through the consumption of vegetables, water from groundwater sources (Choudhary, 2025) and other foods, they are formed in a small endogenous proportion, exposure to nitrites is instead endogenous through the metabolism of nitrates. The dominant source of dietary nitrate is vegetables, as they contribute to 60–80 % of the total nitrate intake. (Vogiatzi, 2024). Some of the nitrites are consumed as a consequence of their use as food preservatives and to a lesser extent by their presence in vegetables. Nitrates and nitrites are added as preservatives to prevent the growth of bacteria *Clostridium botulinum* or as promoters of some food colors. (Parvizishad et al., 2017). Nitrate as such is non-toxic, but its metabolites remove nitrates from the category of regulated compounds as beneficial because of their potential to have undesirable effects on the body (Filer *et.al*., 1970; Sánchez-Echaniz *et. al*., 2001; Jakszyn *et. al*., 2004).

High concentrations of nitrates in plants, especially vegetables (up to 10 g in a single dose) pose a danger to the human and animal body for two reasons: the possibility of methemoglobin in children by converting nitrates to nitrites in saliva and the formation of carcinogenic nitrosamines under the influence intestinal microflora in the intestinal tract, through its reactions with amines or amides (Chung *et. al*., 2004; Sánchez-Echaniz *et. al*., 2001).

On the other hand, nitrite is a versatile chemical agent which has found numerous

applications ranging from dye manufacture to food preservation, so, the chanse of reaching human body is very high.

2. Materials and Methods

2.1. Sampling of Biological Material

The biological material analyzed in this study consisted of vegetables cultivated both in greenhouses and in open fields. Samples were sourced from specialized agricultural units with produce available for sale in local markets in Cluj (Romania) and from a store in Antwerp (Belgium), covering a range of origins and cultivation methods.

The vegetables collected from local markets included:

- Lettuce (*Lactuca sativa*), L
- Beetroot (*Beta vulgaris*), B
- Carrot (*Daucus carota*), C
- Parsley root (*Petroselinum hortense*), P
- Kohlrabi (*Brassica oleracea var. gongylodes*), K
- Spinach (*Spinacia oleracea*), S
- Celery (*Apium graveolens*), Ce
- Cabbage (*Brassica oleracea*), Cab

The Romanian samples were primarily obtained from private producers located in the vicinity of Cluj-Napoca, while the Belgian samples were collected from a retail outlet in Antwerp.

Upon collection, the vegetable samples were thoroughly cleaned to remove soil residues and stored at low temperatures appropriate for preserving vegetable freshness. 10 grams of each sample were weighed and homogenized using a mortar and pestle. The homogenized material was transferred to a 50 mL volumetric flask. For stabilization and preparation, 25 mL of saturated borax solution was added to each flask containing the ground plant sample. The saturated solution was prepared by dissolving 50 g of $Na_2B_4O_7 \cdot 10H_2O$ in 500 mL of hot distilled water, adding the solid until no further dissolution occurred. The flasks with the added solution were then placed in a boiling water bath and heated for 15 minutes. After cooling, 1 mL of potassium ferrocyanide solution and zinc acetate was added to each sample. The mixtures were then left to stand for 30 minutes. Finally, the samples were brought to volume with distilled water, labeled accordingly, and filtered for further analysis.

2.2. Determination of Nitrate and Nitrite Ion Content in Vegetables

The concentrations of nitrate and nitrite ions in the prepared vegetable samples were determined using molecular absorption spectrometry. The analysis was performed at a wavelength of 520 nm using the Griess reagent for nitrites and the Cd-Griess method for nitrates, in accordance with the Romanian standard STAS 11581-83.

A SHIMADZU UV-Visible spectrophotometer (Model No: UV-2550) equipped with 1 cm path length quartz cuvettes was employed for absorbance measurements.

All analyses were carried out between March and November 2024.

2.3. Analyses

2.3.1. FTIR

Fourier Transform Infrared (FTIR) spectroscopy is a valuable analytical technique for characterizing the chemical composition of vegetables. It identifies molecular vibrations, providing insights into compounds like polysaccharides, proteins, lipids, and secondary metabolites.

FTIR results can be complemented by microscopy methods, which can visualize structural aspects of leafy vegetables contributing to nitrate accumulation. Through this technique, various species of vegetables can be evaluated and, eventually, the presence of nitrate groups accumulated in the plant cells of the samples can be identified.

The FT-IR absorption spectra were recorded with a Jasco 6000 spectrometer, at room temperature, in the range 400 ‑ 4000 cm^{-1}, with a spectral resolution of 4 cm^{-1} and using the well-known KBr pellet technique.

2.3.2 Microscopy analyses

Optical microscopy techniques are invaluable for analyzing the structural and compositional aspects of vegetables.

In general, optical microscopy methods enhance the researcher's abilities to analyze and ensure the quality and safety of vegetables in both research and industry settings.

Optical microscope Motic BA310Pol was used to obtain images of analysed vegetables surfaces.

Optical Microscopy in vegetables analysis is utilized to identify histological elements such as epidermis with stomata and trichomes, thin cuticles, large vacuolated cells, cortex rich in chromoplasts (carotenoid or chlorophyl pigments, for example), parenchyma cells containing essential oils, etc.

It provides parameters to assess inadequate conditions and practices during food production.

2.4. Statistical parameters used to evaluate the analytical performance of the nitrite analysis method, ANOVA (one-way) test

For an analysis method to be used for trace level quantification, it must present a series of analytical performance characteristics, among which the absence of systematic errors, accuracy, precision, LOD and LOQ, the response range occupies a central place.

Even if the analysis method has already been validated, the analytical performance characteristics must be checked because they may differ depending on the conditions (apparatus, reagents) in the laboratory where the experiments are carried out.

The verification is carried out using synthetic samples of known rice concentration (as close as possible to the matrix characteristics of the real samples), or certified reference materials and are expressed by means of some statistical variables (Thoma *et. al.,* 2012; Habib, 2011, Hsu, *et. al*., 2009; Gemperline, 2006; International Standard ISO 6635-1984).

The test consists of the following: prepare at least 10 samples of analytical same concentration, measure a property of the analyte or one of these compounds, determine the concentration based on the calibration curve.

The average of the determinations (where n is number of determination), absolute error (e) and standard deviation ($s_{\bar{C}}$) of the selection mean were calculated with the following relations:

$$\bar{C} = \frac{\sum_{1}^{10} C_i}{10} \quad (1)$$

$$e = \left| C_A - \bar{C} \right| \quad (2)$$

$$s_{\bar{C}} = \sqrt{\frac{\sum_{1}^{n} \left(\bar{C} - C_i \right)^2}{n(n-1)}} \quad (3)$$

The value of the variable t is calculated with the relation *(4)* (Gemperline, 2006):

$$t = \frac{\left| C_A - \bar{C} \right|}{s_{\bar{C}}} \quad (4)$$

If the calculated t is less than t tabulated for the same number of degrees of freedom (k = n-1) and a chosen probability, it is concluded that the method is not affected by systematic errors, it is accurate. The accuracy of the method reflects the deviation of the average of the determined values from the value considered true and is expressed by error (module of the difference between the value considered true and the average of the determinations) or the relative error expressed by the relationship *(5)*:

$$e\% = \frac{\left| C_A - \bar{C} \right|}{C_A} \times 100 \quad (5)$$

Precision is a characteristic of performance that reflects the extent to which the method provides repeatable results.

From a statistical point of view, the precision is expressed by the standard selection deviation (s), the standard deviation of the selection mean, $s_{\bar{C}}$, or the relative standard deviation (RSD). For the calculation of variables, either the results of measurements made on the same day

(repeatability) or the results of measurements carried out in successive days (reproducibility) can be used. The relative standard deviation is expressed by the relation (Gemperline, 2006):

$$RSD = \frac{s_1}{\bar{C}} \times 100 \quad (6)$$

LOD and LOQ are two parameters of analytical performance that express the detection and determination characteristics of an analysis method. For the evaluation of LOD and LOQ, the literature describes several variants of which most often the variant of repeated measurements on blank samples is used. In the case of spectrophotometric methods, the minimum signal is calculated using the absorbances measured for blank samples with the following relation (Gemperline, 2006):

$$A_{LOD} = \bar{A}_{blanc} + 3 \times s \quad (7)$$

$$A_{LOQ} = \bar{A}_{blanc} + 10 \times s \quad (8)$$

where:

$\bar{A}_{blanc}$ - the average of the absorbances A_i measured for the blank samples;

s - standard deviation selection of the measured absorbances for the blank samples.

The Anova test (one-way) is usually used to compare the averages of more than two sets of values. If n is the number of data series and m is the total number of values, the test consists of the following: it is calculated: variance of each data series (SSW – sum of squares within the group), variance between data series (SSB- sum of squares between the groups) variance of all values in the considered series (TSS- total sum of squares).

$$R_1 = \frac{SSB}{n-1} \quad (9) \qquad R_2 = \frac{SSW}{m-n} \quad (10)$$

$$F_{calc.(n-1;m-n)} = \frac{R_1}{R_2} \quad (11)$$

F_{calc} is compared. with F_{tab}. (n-1, m-n), $p<0.05$. If $F_{calc}<F_{tab}$ the null hypothesis is admitted, i.e. between the averages of the data series there is no statistically significant difference.

The research carried out aimed to establish the accumulation of nitrate ions and nitrite ions in the organs of greenhouse and field vegetables species in Romania and Belgium, comparing the determined content with the limits imposed by the Romanian legislation in force.

3. Results and discussion

3.1. Fourier Transform Infrared (FTIR) spectroscopy is a useful tool for analyzing nitrate (NO_3^-) and nitrite (NO_2^-) contents in vegetables.

An FTIR study was performed on seven of the eight Romanian plant samples (see Figure 1a-g) in order to identify the functional groups present in plant cell structures that may be involved in the accumulation of nitrates and nitrites. The beet sample was excluded, as its intense red pigmentation interfered with the acquisition of a reliable spectrum.

The scientific literature shows that the characteristic absorption bands for nitrate group is one strong absorption around 1380 – 1410 cm^{-1} (asymmetric stretching of NO_3^-) and for nitrite groups (NO_2^-) are characteristic the peaks around 1260–1320 cm^{-1} (asymmetric stretching) and 820–860 cm^{-1} (bending vibration) (Shao et al., 2017, Ma et al, 2021)

Figure 1(a–g) presents the FTIR images of the vegetable surfaces for lettuce (a), carrot (b), parsley root (c), kohlrabi (d), spinach (e), celery (f), and cabbage (g).

In the case of present work, the characteristic nitrate absorption, observed in the range of 1500–1200 cm^{-1}, is evident in all the samples, with prominent peaks appearing around 1401 cm^{-1} and 1350 cm^{-1}.

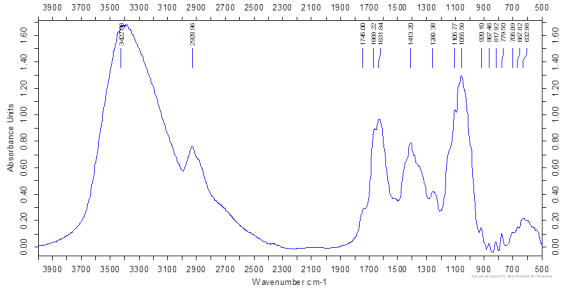

(a)

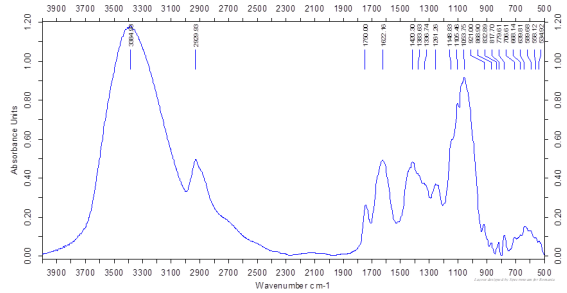

(b)

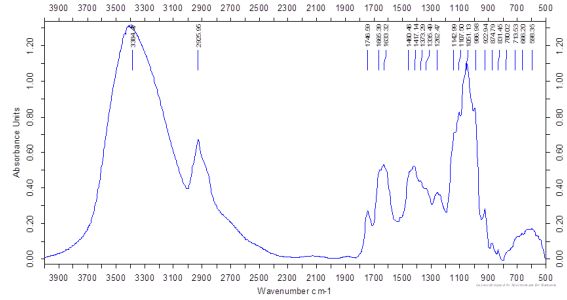

(c)

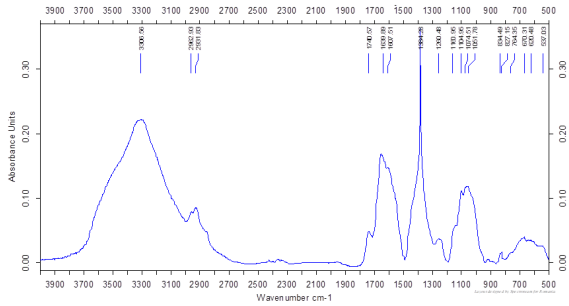

(d)

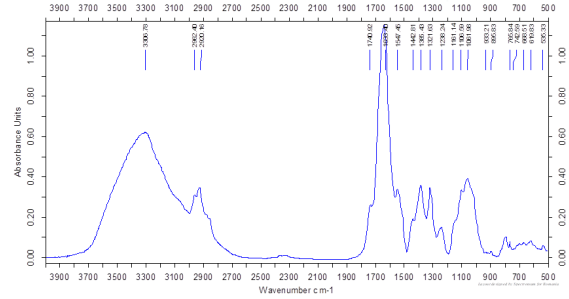

(e)

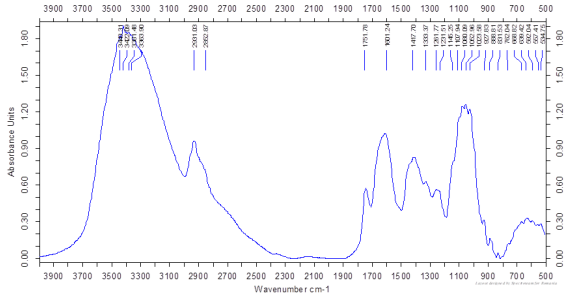

(f)

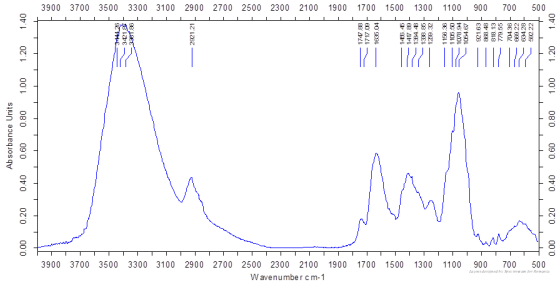

(g)

Figure 1(a–g). The FTIR images of the vegetable surfaces for lettuce (a), carrot (b), parsley root (c), kohlrabi (d), spinach (e), celery (f), and cabbage (g).

These absorption bands correspond to the asymmetric stretching mode of the N–O bond (ν_3), which results from the splitting of the ν_3 mode into two bands, designated as ν_3-high and ν_3-low (Shaviv et al, 2003).

Additionally, a peak at 1245 cm^{-1} is associated with nitrite (NO_2^-) absorption.

The peak near 1460 cm^{-1} corresponds to N=O vibrations, while the peaks at 1375 cm^{-1} and 1363 cm^{-1} are attributed to N=O and N–O vibrations, respectively. A band at approximately 1300 cm^{-1} is also assigned to N–O stretching and are in good agreement with literature data (Shao et al, 2017, Shaviv et al., 2003).

3.2. Optical Microscopy Investigations

For the same seven plant samples (out of the eight Romanian ones), an optical microscopy study was also carried out to visualize their structural features. And, in this case, the beet sample was excluded from the optical microscopy study because the intense red pigmentation of the biological material completely covered the surface of the vegetable, thus preventing image acquisition through microscopy.

Figure 2a-g shows that the vegetable tissues samples have roughness structures, with large vacuoles, where nitrates can be easily stored.

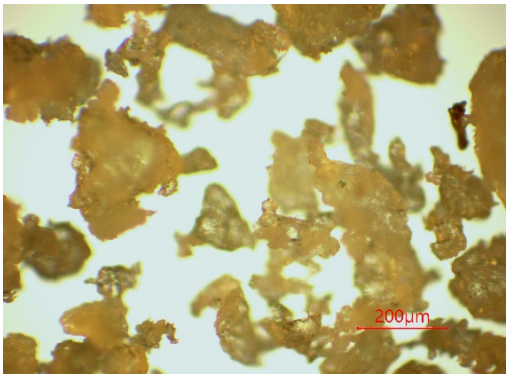

(a)

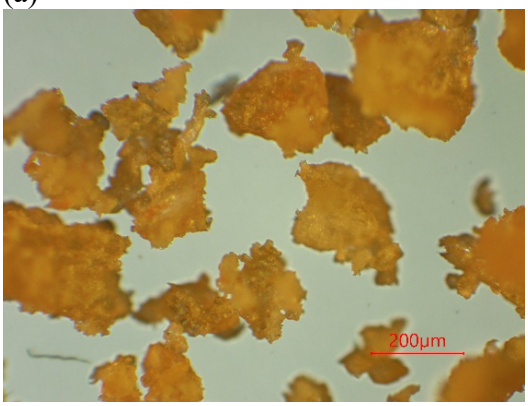

(b)

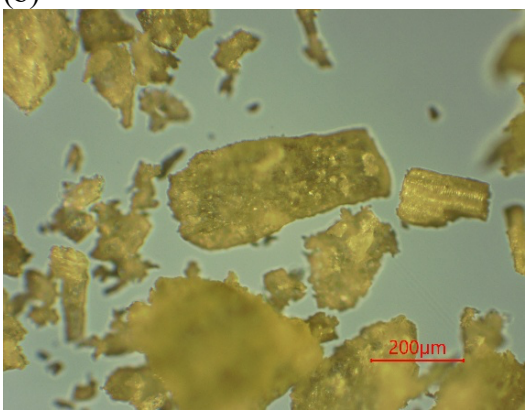

(c)

(d)

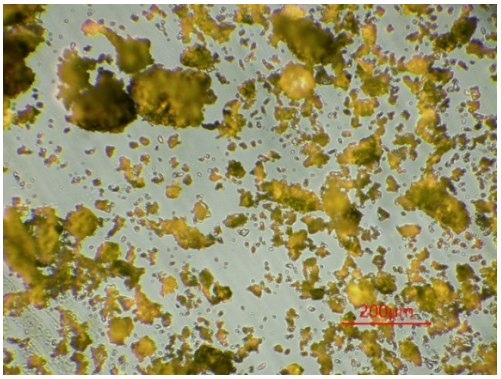

(e)

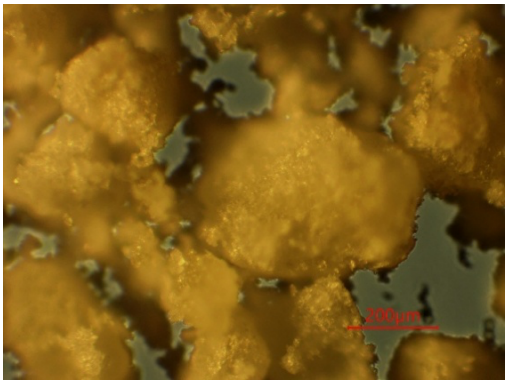

(f)

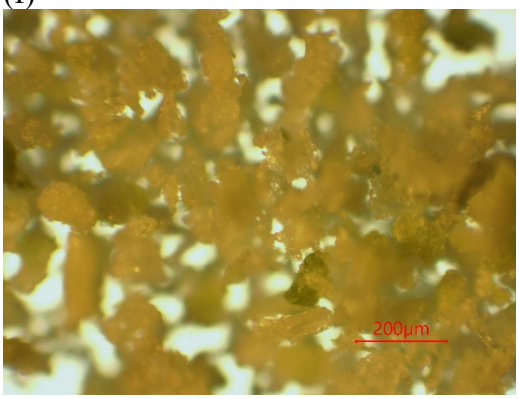

(g)

Figure 2. Optical microscope images of the vegeatables surfaces of lettuce (*Lactuca sativa*) (a), carrot (*Daucus carota*) (b), parsley root (*Petroselinum hortense*) (c), kohlrabi (*Brasica oleracea* variety *gongyloyides*) (d), spinach (*Spinacea oleracea*) (e), celery (*Apium graveolens*) (f), and cabbage (*Brasica oleracea*) (g)

As is well known, nitrates are primarily stored in the vacuoles of parenchyma cells, particularly within the leaves and roots of plants. Although optical microscopy does not allow for

the direct detection of nitrate or nitrite ions, it remains a valuable tool for examining the anatomical compartments where these ions are most likely to accumulate.

Certain vegetables are especially prone to nitrate accumulation due to their physiology and cultivation conditions.

Lettuce *(Lactuca sativa)* is well known for its high nitrate content, especially under conditions of low light intensity or excessive nitrogen fertilization.

Parsley root *(Petroselinum hortense)* may also accumulate significant nitrate levels, depending on fertilization practices and soil characteristics.

In the case of spinach *(Spinacia oleracea)*, nitrate accumulation is often extremely high, particularly within the spongy mesophyll parenchyma. In some instances, nitrate concentrations in spinach can exceed 2,500 mg/kg fresh weight.

3.1. Evaluation of Optimal Quantification Conditions and Performance Characteristics of the Nitrite Analysis Method

The maximum sensitivity of the spectrophotometric method is achieved when measurements are carried out at the optimal wavelength corresponding to the highest molar absorptivity. Under these conditions, the extinction coefficient reaches its maximum value, and the slope of the calibration curve is maximized, ensuring improved analytical sensitivity.

Based on the absorption spectrum obtained using the Griess reagent, the optimal wavelength for nitrite determination was established at 525 nm.

A calibration curve was constructed in the concentration range of 0–0.3 mg/L, using standard nitrite solutions. The spectrophotometer software was used to automatically plot the calibration curve through its "Quantitative" option, facilitating subsequent concentration determinations.

The resulting calibration line is presented in Figure 3, and its linearity confirms the reliability of the method within this range.

The equation of the calibration line is:

$$A=0.91C+0.1 \qquad (12)$$

The calibration curve demonstrates a linear relationship between absorbance and nitrite concentration within the investigated range (0–0.3 mg/L).

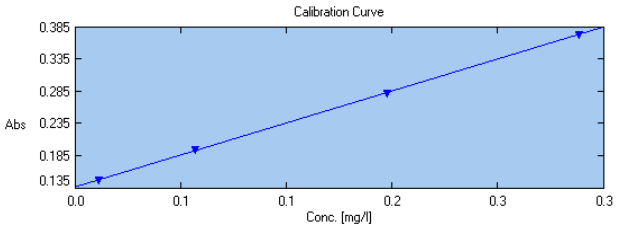

Figure 3. Calibration curve for the determination of nitrite ion concentration using the Griess spectrophotometric method (λ = 525 nm, concentration range: 0–0.3 mg/L).

The coefficient of determination (R^2 = 1.000) indicates perfect linearity, confirming that 100% of the variation in absorbance is attributable to changes in concentration.

This result also suggests a high degree of precision and the absence of systematic errors in the measurement process.

A summary of the statistical analysis of the calibration data is presented in Table 1.

Since the calculated value of the *t*-statistic is lower than the critical (tabulated) value at the chosen confidence level and number of replicates, it can be concluded that the method is not affected by systematic errors and is therefore accurate.

The accuracy of the method, evaluated in terms of relative error, was found to be 2%, which demonstrates that the measured values are in close agreement with the reference value and confirms the reliability of the procedure for real sample analysis.

The standard deviation was calculated as $s = 7.03\times10^{-3}$, and the corresponding relative standard deviation (RSD) of 3.44% reflects a satisfactory level of precision, indicating that replicate measurements are consistent and free

from significant variability. Taken together, these findings confirm that the method not only produces accurate results but also ensures reproducibility within the generally accepted limits for spectrophotometric quantification at this concentration level. This combination of accuracy and precision highlights the robustness of the method and supports its suitability for routine analytical applications

The limits of detection (LOD) and quantification (LOQ) were evaluated, and the results are summarized in Table 2.

The determined LOD and LOQ values are well below the expected nitrite concentrations in real vegetable samples, thereby confirming the method's suitability for the analysis of nitrite ions in actual biological matrices.

Table 1. Data obtained in the determination of variable t.

C_i (µg NO_2^- / mL)	$\bar{C}$ (µg NO_2^- / mL)	C_A (µg NO_2^- / mL)	$s_{\bar{C}}$	e	$t_{calc(9.99\%)}$	$t_{tab(9.99\%)}$
0.208						
0.201						
0.195						
0.208						
0.197	0.204	0.200	2.22×10^{-3}	4×10^{-3}	1.80	2.82
0.206						
0.210						
0.208						
0.208						
0.201						

Table 2. Results obtained in the determination of LOD and LOQ.

A_i	$\bar{A}$	s	A_{LOD}	A_{LOQ}	LOD (µg NO_2^- / mL)	LOQ (µg NO_2^- / mL)
0.108						
0.106						
0.101						
0.101						
0.098	0.101	3.57×10^{-3}	0.112	0.137	0.011	0.039
0.099						
0.101						
0.099						
0.101						
0.097						

Table 3. Results obtained when determining nitrite ion concentration in Romanian cabbage.

Sample type	Sample weight (g)	Concetration (µg NO_2^-/g)	$\bar{C} \pm t\times s_{\bar{C}}$, (µg NO_2^-/g)	$t_{(3.99\%)}$
(a)	10.8721	2.03		
	10.5585	1.98	**1.99±0.06**	
	10.5645	1.97		
	10.8791	2.01		
(b)	10.3988	1.95		
	10.1689	1.92		

	10.1893	1.89	**1.91±0.06**	4.54
	10.3241	1.91		
(c)	10.5035	1.83		
	10.1486	1.84	**1.86±0.06**	
	10.4123	1.89		
	10.1233	1.86		

Table 4 ANOVA test results (nitrite ion concentration in Romanian cabbage).

SSW	SSB	TSS	$F_{tab.(3.44)}$,p<0.05	$F_{calc.(3.44)}$,p<0.05
0.0097	0.0375	0.0472	4.26	17.39

Table 5. Results obtained when determining nitrite ion concentration in Belgium cabbage.

Sample type	Sample weight (g)	Concetration (µg NO_2^-/g)	$\bar{C} \pm t \times s_{\bar{C}}$, (µg NO_2^-/g)	$t_{(3.99\%)}$
(a)	10.7721	1.83		
	10.5535	1.78	**1.81±0.09**	
	10.5145	1.77		
	10.8791	1.85		
(b)	10.6221	1.82		
	10.5689	1.81	**1.80±0.05**	
	10.6893	1.77		4.54
	10.3471	1.79		
(c)	10.4129	1.76		
	10.0842	1.75	**1.78±0.07**	
	10.5123	1.78		
	10.5439	1.82		

Table 6. ANOVA test results (nitrite ion concentration in Belgium cabbage).

SSW	SSB	TSS	$F_{tab.(3.44)}$,p<0,05	$F_{calc.(3.44)}$,p<0,05
0.0089	0.0020	0.0109	4.26	1.01

3.2. Determination of Nitrite Ion Concentration in Cabbage Samples

The nitrite ion concentrations measured in Romanian cabbage are summarized in Table 3.

To assess the statistical significance of the differences among mean values, a one-way ANOVA test was performed. The results of the ANOVA analysis are presented in Table 4.

Since the calculated F-value exceeds the critical (tabulated) value, it can be concluded that the differences between the means are statistically significant. This suggests that removal of the outer leaves before consumption may lead to a reduction in nitrite intake, potentially improving the safety of the vegetable for human consumption.

The results for cabbage samples obtained from a Belgian source (Antwerp) are presented in Table 5, and the corresponding ANOVA outcomes are summarized in Table 6. In this case, the calculated F-value is lower than the critical value, indicating no statistically significant differences between the means.

These findings imply that the nitrite ion concentrations in cabbage from the Belgian and Romanian producers are comparable, and no significant variation is observed between different parts of the cabbage from the Belgian source.

On the other hand, the result of the ANOVA test for the Belgian sample suggests that, for this source, the outer leaf layer should not be

removed prior to preparation, as its removal does not significantly influence the nitrite ion concentration.

3.3. Determination of Nitrate and Nitrite Content in Root and Leafy Vegetables

Samples of carrots (C), parsley (P), beetroot (B), celery (Ce), kohlrabi (K), lettuce (L), spinach (S) and cabbage (Cab) purchased from markets in Romania and Belgium were analyzed.

Each vegetable was cut into pieces, weighed (approximately 10 g), and ground according to the procedure described in the experimental section.

As shown in Table 7, the nitrite concentrations obtained after analysis were generally within the maximum permitted limit of 200 µg/g, as specified in Order No. 84/91/2002 issued by the Ministry of Health and Family (MSF) and the Ministry of Agriculture, Food and Forestry (MAPM). However, the nitrite concentrations recorded for beetroot and spinach samples exceeded the maximum allowed limit by approximately eight times (see Table 7 and Figure 4).

As shown in Table 7, carrot samples from Belgium contain higher levels of nitrates 88.09 µg NO_3-/g comparred to 68.5 µg NO_3-/g (samples from Romania) whereas the nitrite content is nearly identical across samples (42.0 µg NO_2-/g, in the case of Belgian samples and 40.3 µg NO_2-/g, for Romanian samples).

Regarding the Belgian samples of parsley roots, the nitrate content value is 28.3 µg NO_3-/g, compared with 26.4 µg NO_3-/g for Romanian parsley. The nitrite content is also quite close (83.8 µg NO_2-/g, for Romanian samples compared to 81.2 µg NO_2-/g).

The Romanian beetroot samples accumulates smaller amount of nitrates than the samples of Belgian beet (137.4 µg NO_3-/g comparred to 187.5 µg NO_3-/g, Table 7).

The root of Romanian celery shows a slightly higher amount of nitrates than samples of Belgian celery. (17.6 µg NO_3-/g comparred to 17.0 µg NO_3-/g) just like the nitrite content (49.8 µg NO_3-/g at Romanian samples comparred to 47.9 µg NO_3-/g for Belgian samples).

Romanian Kohlrabi accumulates a larger amount of nitrates compared to the Belgian one (38.2 µg NO_3-/g comparred to 23.8 µg NO_3-/g) , as is the case with the nitrite content in the Kohlrabi root.

Similar observations can be made regarding the nitrate content in lettuce, spinach, and cabbage, both for the Romanian and Belgian vegetable samples (see Table 7).

Spinach leaves are known to accumulate high levels of nitrates, which is why spinach receives particular regulatory attention from the European Community.

Overall, the nitrite concentrations measured across the analyzed vegetable samples showed considerable variation, with several values exceeding legal limits.

Recorded concentrations ranged from 8.6 µg/g for kohlrabi from Romania to 557.3 µg/g for red beet samples from Belgium.

The differences are, however, quite small, which indicates that the types of soil in which the studied vegetables were grown are similar and probably comparable amounts of nitrogen fertilizers were used in both types of samples (Romanian and Belgian).

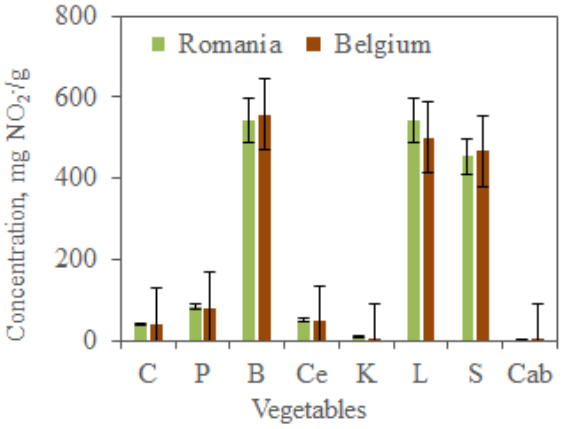

Figure 4. Nitrite content of root vegetables analyzed: carrot, parsley, beet, celery, kohlrabi, lettuce, spinach and cabbage (from Romania and Belgium).

Table 7. Results obtained (average of three determinations) in the nitrate and nitrite vegetable content determination.

Species	The analyzed organ	Nitrates (µg NO_3-/g)	Nitrites (µg NO_2-/g)
Carrots Romania (*Daucus carota*)	central cylinder	68.5	40.3
Carrots Belgium *(Daucus carota*)	central cylinder	88.09	42.0
Parsley root Romania (*Petroselinum crispum*)	central cylinder	26.4	83.8
Parsley root Belgium (*Petroselinum crispum*)	central cylinder	28.3	81.2
Beetroot Romania (*Beta vulgaris*)	pulp	137.4	542.8
Beetroot Belgium (*Beta vulgaris*)	pulp	187.5	557.3
Celery Romania (*Apium graveolens*)	pulp	17.6	49.8
Celery Belgium (*Apium graveolens*)	pulp	17.0	47.9
Kohlrabi Romania (*Brassica oleracea,-gongyloides*)	petiol	38.2	8.60
Kohlrabi Belgium (*Brassica oleracea-gongyloides*)	petiol	23.8	2.56
Lettuce Romania (*Lactuca sativa*) grown greenhouse	middle leaves	98.3	543.9
Lettuce Belgium (*Lactuca sativa*) grown greenhouse	middle leaves	94.9	500.08
Spinach Romania (*Spinacia oleracea*)	leves	198.4	453
Spinach Belgium (*Spinacia oleracea*)	leves	193.4	468
Cabbage Romania (*Brassica oleracea*)	leves	30.5	1.99
CabbageBelgium (*Brassica oleracea*)	leves	29.6	1.81

4. Conclusions

The Regulation (EU) 2023/915 has established maximum levels for nitrates in vegetables, in particular green leafy vegetables such as spinach (2000–3500 mg/kg), lettuce (2000–5000 mg/kg) and rucola (6000–7000 mg/kg). This Regulation has also a limit of 200 mg/kg for nitrates in baby food and processed cereal-based food for infants and young children [Commission Regulation (EU) 2023] (Vogiatzi et al., 2024)

Comparing these data — endorsed by EU-accredited bodies — with the analyses presented in this article shows that nitrate levels in Romanian vegetables, as in Belgian ones, comply with the applicable nitrate/nitrite regulatory limits.

The work aimed to carry out a monitoring study on the concentration levels of nitrates and nitrites in eight vegetable species commonly found in a market in Cluj Napoca, Romania, and four vegetable species purchased from a supermarket in Antwerp, Belgium.

This comparative approach represents a strong point of the current research, with the observation that the chosen analytical methods (FTIR spectroscopy and Optical microscopy) can be enriched with others, such as SEM, high-pressure liquid chromatography (HPLC),

Following the analysis of the experimental data, a relatively high concentration of nitrate ions was found in root vegetables, especially in red beet from Romania with a concentration of 542.8 µg NO_3^-/g and red beet from Belgium, for which a concentration of nitrate ions of 557.3 µg NO_3^-/g was recorded.

The leafy legumes also showed significant nitrate concentrations, so for the Romanian

spinach a concentration of 198.4 µg NO_3^-/g was registered and for the Romanian salad, produced in the greenhouse, a nitrate ion concentration of 98.3 µg NO_3^-/g was determined.

The differences between the concentrations of nitrate ions recorded for the same species, but in different locations - Romania and Belgium - are due to differences in temperature in the growing areas, light intensity, cultivation methods, chemical, physical, and geological characteristics of the soil, as well as varying amounts of soil moisture, etc.

On the other hand, the nitrite content in all samples was low - below the permissible values in the two European states and, therefore, is unlikely to pose any health threat. However, to maximize the health benefits of vegetable consumption, measures must be taken to reduce exposure to nitrates and nitrites, while maintaining the recommended intake of vegetables for the general population.

Our study presents a series of limitations due to the lack of cultivation data, among which the most important is that we did not evaluate with certainty how much seasonality affects nitrate levels in vegetables. Therefore, research could be continued by statistically analyzing summer and winter crops.

In conclusion, in order to increase the health benefits through the consumption of vegetables and fruits, it is imperative to take measures for intake reduction of nitrates and nitrites, maintaining the recommended green vegetables consume, for the good health of modern humans.

5. References

AFSSA (Agence Française de Sécurité Sanitaire des Alimentes) (2007) Estimation du niveau d'exposition aux nitrates et aux nitrites de la population française. Réponse à la demande d'appui scientifique et technique de la DGCCRF réf. 2007-SA-0070 du 8/01/2007.

Andrews, M., (1986). The partitioning of nitrate assimilation between root and shoot of higher plants: mini-review*, Plant Cell Environonment*, 9, 511-519.

Banu, C., Preda, N., Vasu, S.S., (1982) Produsele alimentare și inocuitatea lor. Editura Tehnică, București, 2-16.

Baty, J.J., Hwang, H., Ding, Z. (2007). The effect of a carbohydrate and protein supplement on resistance exercise performance, hormonal response, and muscle damage. *The Research Journal of the NSCA,* 21(2), 321-9.

Bibicu, M., (1994). Cercetări metodologice privind determinarea nitraţilor şi nitriţilor din ţesuturi vegetale şi nivelul de acumulare în produsele horticole. București, 5-6.

Bryan, N.S., Fernandez, B.O., Bauer, S.M., Garcia-Saura, M.F, Milsom, A.B., Rassaf, T., Maloney, R.E., Bharti, A., Rodriguez, J., Feelisch, M. (2005). Nitrite is a signaling molecule and regulator of gene expression in mammalian tissues Nature Chemical Biology, 1**,** 290 - 297.

Bucur, G.D., Dumitru, M., Creangă, I., Simota, C., Calciu, I., (2010). Monitorizarea poluării cu nitrați și nitriți în Jud.Argeș. Ed. Sitech, Craiova.

Calancea, L., (2002). Nitrați, nitriți și nitrosamine. Protecția mediului și sănătatea. Ed.Casa Cărții de Știință, Cluj-Napoca, 178-200.

Calderón, R., Albornoz, F., Jara, C., Palma, P., Arancibia-Miranda, N., Manquián-Cerda, K., Herrera, C., Urrutia, J., Gamboa, C. , Karthikraj, R., Muñiz-Valencia, R., Aguilar, B.R., (2025). Exploring the uptake, accumulation, and distribution of nitrate in Swiss chard and spinach and their impact on food safety and human health. Food Chemistry, 467(1), 142345- 142360.

Camargo, J.A., Alonso, A. (2006). Ecological and toxicological effects of inorganic nitrogen pollution in aquatic ecosystems: A global assessment. *Environment International*, 32, 831 - 849.

Ceaușescu, D., (1978). Analiza chimică a apei: metode simple și rapide în condiții de teren. Editura Facla,.63-64.

Chaudhary, I.J., Chauhan, R., Kale, S.S., Gosavi, S., Rathore, D., Dwivedi, V., Singh, S., Yadav, V.K.. (2025). Groundwater

Nitrate Contamination and its Effect on Human Health: A Review. *Water Conservation Science and Engineering***,** 10, 33-55.

Chung, J.C., Chou, S.S., Hwang, D.F., (2004). Changes in nitrate and nitrite content of four vegetables during storage at refrigerated and ambient temperatures, *Food Additives & Contaminants*, 21, 317–322.

Cumpătă, S.D., Beceanu, D., (2005). Nitrați și nitriți, surse de poluare a alimentelor de origine vegetală. Lucrări științifice, Seria Horticultura, USAMV Iași, 519-524.

Dezhangah, S. Nazarib, F. Kamalic, K. Hosseinid, M.-J.; Mehrasbi, M.R. (2022). A survey on nitrate level in vegetables to assess the potential health risks in Iran. *International Journal of Food Properties*, 25, 1958–1973.

Dodocioiu, A.M., Buzatu, G.-D., Botu, M. (2025). Nitrates and Nitrites in Vegetables and the Health Risk. Foods, 14, 3037-3070.

Dung,T.T.T.; Nhan, D.T.; Chau, T.B. (2024). The level of nitrate and nitrite in some fruits available in the local markets in District 7, Ho Chi Minh City, Vietnam. IOP Conf. Ser. Earth Environ. Sci., 1349, 012013-012024.

E.F.S.A. (2008). Opinion of the Scientific Panel on Contaminants in the Food chain on a request from the European Commission to perform a scientific risk assessment on nitrate in vegetables. EFSA J., 689, 1-25.

Ezeagu, I.E., Fafunso, M.A., (1995). Effect of wilting and processing on the nitrate and nitrite contents of some Nigerian leaf vegetables. *Nutrition and Health*, 10, 269-275.

Ezeagu, I. E. (1996). Nitrate and nitrite contents in ogi and the changes occurring during storage, *Food Chemistry*, 56, 77–79.

Filer, L.J., Lowe, C.U., Barness, L.A., Goldbloom, R.B., Heald, F.P., Holliday, M.A., Miller, R.W., O'Brien, D., Owen, G.M., Pearson, H.A., Scriver, C.R., Weil, W.B., Kine, O.L., Craviato, J., Whitten, C. (1970). Infant methemoglobinemia: The role of dietary nitrate. *Pediatrics,* 46*,* 475-478.

Greenwood, D.J., Hunt, J. (1986). Effect of nitrogen fertilizer on the nitrate contents of field vegetables grown in Britain. *Journal of the Science of Food and Agriculture*, **37**, 373-383.

Hura C., (2005). Contaminarea chimică a alimentelor în România, Ed.Cermi, Iași, 19.

Hudson P, Schwarz J, Baltrusaitis J, Gibson E, Grassian V (2007). A spectroscopic study of atmospherically relevant concentrated aqueous nitrate solutions. The Journal of Physical Chemistry A, 111, 544–548.

Jakszyn, P., Ibáñez, R., Pera, G., Agudo, A., García-Closas, R., Amiano, P. and González, C.A. (2004). Food content of potential carcinogens. Nitrates, nitrites, nitrosamines, heterocyclic amines and polycyclic aromatic hydrocarbons, EPIC-Spain. Catalan Institute of Oncolgy. Barcelona.

Kanaan, S.S., Economakis, C.D. (1992). Effect of climatic conditions and time of harvest on growth and tissue nitrate content of lettuce in nutrient film culture. Acta Horticulturae (ISHS), 323, 75-80.

Kristin, D., Morgan, L., Fangny, D., Sara, R., Caleb, W., Mallory, M., Andrew-White, L. W. T., Colin, D. W. (2010). Acute glycemic and blood lipid response to the ingestion of a candy bar-like protein supplement compared to its candy bar counterpart. *Journal of the International Society of Sports Nutrition*, 7(1),1.

Liu, G., Guo, H., Zhao, W., Yan, H., Zhang, E., Gao, L. (2023). Advancements in Preprocessing and Analysis of Nitrite and Nitrate since 2010 in Biological Samples: A Review. Molecules, 28(20), 7122-7149.Lundberg, J.O., Weitzberg, E., Cole, J. A., Benjamin, N. (2004). Nitrate, bacteria and human health. *Nature Reviews Microbiology.*, 2, 593 - 602.

Lundberg, O., Weitzberg, E., Gladwin, M.T. (2008). The nitrate-nitrite-nitric oxide pathway in physiology and therapeutics. *Nature Reviews Drug Discovery*, 7, 156 - 167.

Lundberg, J.O., Feelisch, M., Bjorne, H., Jansson, E.A., Weitzberg, E. (2006). Cardioprotective effects of vegetables: is nitrate the answer? *British Journal of Nutrition*,15, 359 - 362.

Lupea, A.X., Ardelean, D., Pădure, M., (2001). Chimia şi controlul alimentelor de origine animală. Editura Politehnica, Timişoara.

Ma, F., Du, C., Zheng, S., Du, Y. (2021). In Situ Monitoring of Nitrate Content in Leafy Vegetables Using Attenuated Total Reflectance − Fourier-Transform Mid-infrared Spectroscopy Coupled with Machine Learning Algorithm. *Food Anal. Meth.*, 14, 2237–2248.

Manescu, S., Cucu, S., Diaconescu, M.L., (1994). Chimia sanitară a mediului. Ed. Medicală, București, 147-149.

McKnight, G. M., Duncan, C.W., Leifert, C., Golden, M.H. (1999). Dietary nitrate in man: friend or foe? *British Journal of Nutrition*, 81, 349 - 358.

Mensinga, T. T., Speijers, G. J., Meulenbelt, J. (2003). Health implications of exposure to environmental nitrogenous compounds. *Toxicological Reviews*, 22, 41-51.

Nguyen, N.T.T., Nguyen, B.X., Habibi, N., Dabirimirhosseinloo, M.; Oliveira, L.d.A.; Terada, N.; Sanada, A.; Kamata, A.; Koshio, K. (2025). Effect of organic and synthetic fertilizers on nitrate, nitrite, and vitamin C levels in leafy vegetables and herbs. *Plants*, 14, 917-932.

Parvizishad, M., Dalvand, A., Mahvi, A.H., Goodarzi, F. (2017). A Review of Adverse Effects and Benefits of Nitrate and Nitrite in Drinking Water and Food on Human Health. Health Scope, 6(3), e14164-e14173.

Pate, J.S., (1973). Uptake, assimilation and transport of nitrogen compounds by plants, Soil Biology and Biochemistry, 5, 109-119.

Pham, H.N., Benitez, A., Hommet, F., Bombe, D., Schoefs, O., Pauss, A. (2008). A new quantitative and low-cost determination method of nitrate in vegetables, based on deconvolution of UV spectra. *Talanta Elsevier Journal*, 76, 936 - 937.

Phillips, W. E. J.,(1968). Changes in the nitrate and nitrite contents of fresh and processed spinach during storage, *Journal of Agricultural and Food Chemistry*, **16**, 88–91.

Premuzic, Z., Gárate, A., Bomilla, I. (2002). Yield and quality of greenhouse lettuce as affected by form of N fertiliser and light. Development in plant and soil sciences, 92, Springer Netherlands.

Sánchez-Echaniz, J., Benito-Fernández, J. (2001). Methaemoglobinemia and consumption of vegetables in infants. *Pediatrics*, 107, 1024-1028.

Schuster, B.E., Lee, K., (1987). Nitrate and nitrite methods of analysis and levels in raw carrots, processed carrots and in selected vegetables and grain products, *Journal of Food Science*, 52, 1632-1636.

Serra J, Marques-dos-Santos C, Marinheiro J et al (2024). Assessing nitrate groundwater hotspots in Europe reveals an inadequate designation of nitrate vulnerable zones. *Chemosphere***,** 355, 141830-141845.

Shao, Y.Q., Du, C.W., Shen, Y.Z., Ma, F., Zhou, J.M. (2017). Evaluation of net nitrification rates in paddy soil using mid-infrared attenuated total reflectance spectroscopy. *Food Anal. Meth.,* **9**, 748–755.

Shaviv, A., Kenny, A., Shmulevitch, I., Singher, L., Raichlin, Y., Katzir, A. (2003). Direct monitoring of soil and water nitrate by FTIR Based FEWS or membrane systems. *Environmental Science & Technology*, 37, 2807–2812.

Tsikas, D. (2023). GC-MS Studies on Nitric Oxide Autoxidation and S-Nitrosothiol Hydrolysis to Nitrite in pH-Neutral Aqueous Buffers: Definite Results Using ^{15}N and ^{18}O Isotopes. *Molecules*, 28, 4281-4293.

Weightman, R.M., Dyer, C., Buxton, J., Farrington, D.S. (2006). Effects of light level, time of harvest and position within field on the variability of tissue nitrate concentration in commercial crops of lettuce (*Lactuca sativa*) and endive (*Cichorium endiva*). Food Additives & Contaminants, 23, 462-469.

Wallace, W., (1986). Distribution of nitrate assimilation between the root and shoot of legumes and a comparison with wheat, *Physio Plantarum*, 66, 630 – 636.

Van Eysinga, R. (1984). Nitrate and glasshouse vegetables. *Fertilizer Research*, 5, 149-156.

Vogiatzi, G., Liontos, M., Kostakis, M.Maragou, N., Thomaidis, N.S. (2024). An updated review on nitrate exposure from drinking water and dietary sources and effect on human health. Global NEST Journal, 27(2), 06467-06480.

CARPATHIAN JOURNAL OF FOOD SCIENCE AND TECHNOLOGY

journal homepage: **http://chimie-biologie.ubm.ro/carpathian_journal/index.html**

Research article

CATALYTIC PERFORMANCE OF ACTIVATED MGO IN THE GLYCEROLYSIS OF PALM KERNEL OIL FOR TAG CONVERSION

Azza Diniari[1], Arief Rakhman Affandi[1]✉, Umar Hafidz Asyari Hasbullah[1], Sirly Eka Nur Intan[2], Ahmad Ni'matullah Al-Baarri[2], Mohamad Djaeni[3], Ching Lik Hii[4]

[1]Department of Food Technology, Faculty of Engineering and Informatics, Universitas PGRI Semarang, Semarang, Indonesia
[2]Department of Food Technology, Faculty of Animal and Agricultural Sciences, Universitas Diponegoro, Semarang, Indonesia
[3]Department of Chemical Engineering, Faculty of Engineering, Universitas Diponegoro, Semarang, Indonesia
[4]Department of Chemical and Environment Engineering, Faculty of Science and Engineering, The University of Nottingham Malaysia Campus, Selangor Darul Ehsan, Malaysia
✉ *ariefraffandi@upgris.ac.id*
https://orcid.org/0000-0003-2600-9997

https://doi.org/10.34302/2025.17.3.8

Article history:
Received
August 5th, 2025
Accepted
September 30th, 2025

Keywords:
MgO;
Coconut oil;
Monoacylglycerol;
Glycerolysis;
TAG conversion.

Abstract

The use of heterogeneous catalysts in synthesizing mono- and diacylglycerols has increased significantly, with metal oxides favoured for their thermal stability, large surface area, and easy purification. Activation is crucial for enhancing their reactivity and optimizing catalytic performance. This study aimed to evaluate the effect of the catalyst activation method in the glycerolysis reaction. Mono- and diacylglycerol (MDAG) products were synthesized via glycerolysis of coconut oil. The process used glycerol as the substrate, with a molar ratio of 1:2.3 and 2% magnesium oxide (MgO) as a catalyst. The optimal product was achieved at a reaction temperature of 175°C using water-impregnated MgO. This resulted in a triacylglycerol (TAG) conversion of 68.73%, a monoacylglycerol (MAG) content of 4.81%, a diacylglycerol (DAG) content of 26.46%, a slip melting point range of 22.8–24.7°C, and a free fatty acid (FFA) level of 0.78%.

1. Introduction

Coconut oil is a promising raw material for glycerolysis due to its high content of medium-chain fatty acids, particularly lauric acid, and its favorable physical and chemical properties (Swastawati et al., 2019). Its significant triglyceride content makes it an ideal candidate for conversion into mono- and diacylglycerols (MAGs and DAGs), valuable intermediates for food and pharmaceutical applications (Zha et al., 2014). Additionally, coconut oil offers potential health benefits, including antimicrobial properties and positive metabolic effects (Ngatirah et al., 2022). Glycerolysis of coconut oil produces products with desirable emulsifying and thickening properties,

enhancing the functionality and nutritional value of food formulations, particularly in applications like ice cream and confectionery, thus improving texture and mouthfeel.

The glycerolysis reaction process is influenced by several factors, including the reaction temperature, the type and concentration of the catalyst, the molar ratio of glycerol and oil, the mixing intensity, and the reaction time (Kombe et al., 2013). The glycerolysis reaction can run fast in the presence of a catalyst. Catalysts that can be used are enzyme catalysts, base catalysts, and acid catalysts. Enzyme catalysts have the drawback that they cannot operate at high temperatures and are also costly (Al-Baarri et al., 2018; Wibawanti et al., 2021). The weakness of acid catalysts is the slow reaction rate, the catalyst is difficult to separate from the reaction, washing the catalyst causes contamination of the reaction products (Mazubert et al., 2013). Alkaline catalysts have advantages such as fast glycerolysis reaction rates, low prices, and easy to separate catalysts. In this study using heterogeneous base catalyst. Heterogeneous base catalysts are more advantageous because they are easily separated from the reaction products and can be used several times with almost the same efficiency (Faba et al., 2012).

Triana (2014) investigated MDAG synthesis via glycerolysis using FHPKO substrates with glycerol (mole ratios of 1:1.5 and 1:2.3) and a 1% NaOH catalyst, yielding MAGs of 47.72% and 47.02%. The 1:1.5 mole ratio substrate showed a 3.70% increase in MAG, while the 1:2.3 ratio showed a larger increase of 23.09%. Hapsari (2020) further optimized MDAG synthesis by using a blend of FHPKO and coconut oil, achieving the best results with a 1:2.3 mole ratio of FHPKO to glycerol and a 1.97% NaOH catalyst, which maximized MAG and DAG production, with no detectable TAG fraction. Ngatirah et al. (2022) studied MDAG synthesis from palm kernel olein and stearin using a 1:4 glycerol ratio, 40°C, and a 10% Lypozime RM IM as catalyst, yielding a final product with an HLB value of 5.92, and a melting point of 35.56°C.

Magnesium oxide (MgO) has emerged as a promising heterogeneous catalyst for glycerolysis due to its unique physicochemical properties and ability to facilitate transesterification (Belelli et al., 2015). As a solid base catalyst, MgO offers advantages such as high stability, ease of recovery, and reusability, making it attractive for industrial applications. Its high surface area and basicity enhance catalytic activity, promoting the efficient glycerolysis of triglycerides into valuable mono- and diacylglycerols (MAGs and DAGs) (Díez et al., 2011). Additionally, the solid-state nature of MgO allows for easy separation from the reaction mixture, enabling catalyst recovery and reuse in subsequent cycles. Moreover, the versatility of MgO as a catalyst can be enhanced through modification or activation methods, such as doping with other metal oxides or combining it with alkaline solutions (Manríquez-Ramírez et al., 2013a). Consequently, MgO is suitable for various glycerolysis applications, including biodiesel production and the synthesis of food emulsifiers and functional ingredients (Anggoro et al., 2019a; Rafati et al., 2019). This study aims to examine the effect of reaction temperature and different activated MgO catalysts on the conversion rate of TAG into MAG and DAG. In addition, this study also evaluated the effect of these factors on the FFA value and slip melting point.

2. Materials and methods

2.1. Materials

Magnesium oxide (MgO) was obtained from Merck KGaA (Darmstadt, Germany). Coconut oil was purchased from PT. Barco (Jakarta, Indonesia). Glycerol (technical grade) was obtained from P&G Chemicals (Kuala Lumpur, Malaysia). Hexane, ethyl acetate, KOH, benzoic acid, ethanol, and commasie brilliant blue (CBB) were obtained from Merck KGaA (Darmstadt, Germany). All these chemical materials were of analytical grade.

2.2. Methods

2.2.1. MgO Catalyst Preparation

The root powder (2 g) was extracted with the assistance of pectinase. Extraction of phenolic compounds was tested at different material/solvent ratios (1/5, 1/7, 1/9, 1/11 and 1/13, w/v), pectinase concentrations (0.1, 0.2, 0.3, 0.4 and 0.5%, v/w), extraction times (40, 60, 80, 100 and 120 minutes), pH (3.5, 4, 4.5, 5 and 5.5) and extraction temperatures (30, 40, 50, 60 and 70C). The mixture was filtered through Whatman No.4 filter paper in vacuum and TPC and AC were then analyzed. The glycerolysis process used three catalyst types: non-activated MgO, water-impregnated MgO (MgO-H_2O), and KOH-impregnated MgO (MgO-KOH). Catalyst activation involved suspending 10 g of MgO in 50 mL of distilled water for water impregnation, or in 50 mL of 2M KOH solution for KOH impregnation. Each mixture was heated and stirred at 80°C for 2 hours using a magnetic stirrer, and it was then filtered. The filtered catalysts were dried in an oven for 6 hours and subsequently calcined at 500°C for 4 hours (Manríquez-Ramírez et al., 2013b).

2.2.2. Coconut Oil Glycerolysis with Heterogeneous Catalysts

The glycerolysis reactions were carried out in a stirred tank reactor (STR). A substrate mixture of 100 g, containing coconut oil (CNO) and glycerol in a molar ratio of 1:2.3, was introduced into the STR and heated to 165°C and 175°C. Catalysts at 2% w/w of the oil weight were then added. The reaction was carried out for 6 hours at a stirring speed of 300 rpm using a magnetic bar. Samples were taken every 60 minutes to analyze the concentrations of monoacylglycerols (MAG), diacylglycerols (DAG), and triacylglycerols (TAG) throughout the reaction. Subsequently, the reaction product was cooled to 70°C. The product mixture was separated from glycerol and the catalyst via centrifugation at 2000 rpm for 10 minutes.

2.2.3. Characterization of Heterogeneous Catalysts

The functional groups of the catalyst granules were analyzed using Fourier Transform Infrared (FTIR) spectroscopy with a Perkin Elmer UATR (USA). X-ray diffraction (XRD) analysis was conducted using a Shimadzu XRD 7000 S/L (Japan) with Cu radiation at 30 kV and 30 mA, scanning samples in the range of 2θ = 10–90° at a rate of 4°/min (Malyani, 2015). The analysis of catalyst basicity was conducted following the method of Rahul et al. (2011). A 1-gram sample of the catalyst was added to 10 mL of distilled water and stirred for 1 hour at 125 rpm using a magnetic stirrer. The catalyst was then filtered, and the resulting solution was mixed with a drop of phenolphthalein (PP) indicator until a pink color developed. Titration was performed using 0.01 M benzoic acid until the solution became colorless, and the titration volume was subsequently calculated.

2.2.4. Acylglycerol Concentration Analysis

The concentrations of MAG, DAG, and TAG in the product were analyzed using thin-layer chromatography (TLC) on G60 F254 plates. A developer solution mixture of hexane, ethyl acetate, and acetic acid in a ratio of 9:1:0.1 (v/v/v) was used. The TLC plate was activated by heating at 100°C for 1 hour, and then 1 µL of the sample was applied with a micropipette, ensuring a spot distance of 15 mm. The plate was placed in the TLC chamber until the developer reached the marked line, then air-dried at room temperature. Coomassie blue (0.02% w/v), dissolved in a mixture of acetic acid, methanol, and distilled water (1:3:6), was used for staining. The plate was scanned using a Camag Automatic TLC Scanner with WinCATS software at a wavelength of 629 nm, and MAG and DAG concentrations were quantified based on the peak area in the chromatogram.

2.2.5 Free Fatty Acid Analysis and Slip Melting Point

Free fatty acid analysis was performed according to AOCS Official Method Ca 5a-40 (2003), by calculating the percentage based on the dominant fatty acid in the sample (i.e. lauric acid). Slip melting point analysis using AOCS Cc 3-25 (AOCS, 2003) by inserting the sample into a capillary tube and kept in a freezer for 16 hours, then heated gradually (approximately 1°C per minute) until the sample melts completely.

3. Results and discussions

3.1. Characteristics of catalyst functional groups

FTIR spectroscopy was employed to characterize the functional groups present in the MgO catalysts. The spectral range analyzed spanned from 450 cm^{-1} to 4000 cm^{-1}, as illustrated in Figure 1. The FTIR analysis revealed absorption peaks at 3699 cm^{-1}, corresponding to O-H groups (indicative of hydrogen bonding). These O-H groups are associated with various functional groups, including alcohols, carboxylic acids, esters, and ethers (Jeevanandam et al., 2018). The stretching of the O-H bonds occurs within a highly polarized hydrogen bond network. This O-H stretching is attributed to water that is physically adsorbed onto the catalyst (Nayebzadeh et al., 2017). The absorption peak at 1428 cm^{-1} shows the bending vibration of the OH bond (Moorthy et al., 2015). the peak at 450 cm^{-1} absorption region characterises the strain vibrations derived from Mg-O (Sutapa et al., 2018). The absorption peak of 671 cm^{-1} and 879 cm^{-1} indicates the presence of Mg-O and Mg-O-Mg vibrations, respectively (Kandiban et al., 2015).

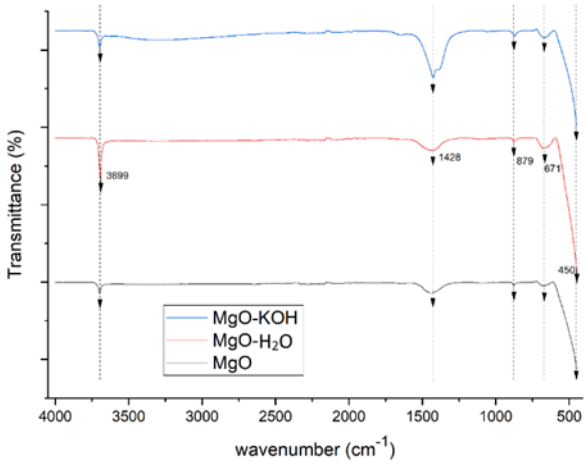

Figure 1. FTIR spectrum of activated MgO

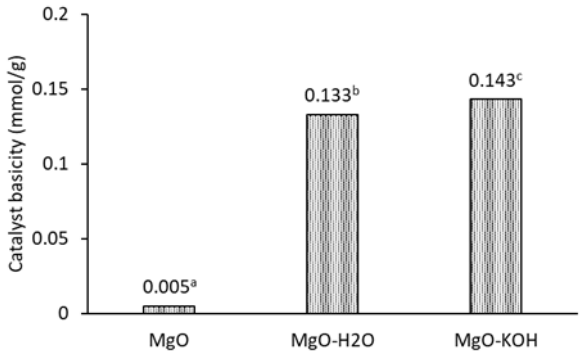

Figure 2. Basicity value of non-activated and activated MgO catalyst

Taslim et al. (2019) identified a peak at 887.26 cm^{-1} as potassium due to KOH impregnation in natural zeolite, indicating potassium oxide presence. Similarly, the KOH-impregnated catalyst in this study likely shows a comparable peak. Munandar et al. (2014) associated the 770–803 cm^{-1} range with K-O functional groups. The MgO-KOH catalyst displays a deeper spectral indentation than MgO and MgO-H_2O at 1428 cm^{-1}, likely due to an OH group, caused by hydroxyl group decomposition and adsorbed water. Strong hydrogen bonding by the OH and its presence suggests that MgO-

KOH is more basic than the other catalysts (Roni & Legiso, 2021).

3.2. Catalyst basicity

Catalyst alkalinity plays a crucial role in determining catalytic activity and can be enhanced through impregnation techniques. Figure 2 illustrates the basicity values for the activated MgO catalyst and their corresponding standards. These findings align with studies by Anggoro et al. (2019b), which reported that increasing the active metal content during impregnation, as well as optimizing calcination conditions, significantly enhances catalyst basicity and, consequently, its performance in catalytic reactions.

The incorporation of KOH into MgO increases the basicity of the catalyst. MgO-KOH exhibits a basicity of 0.143 mmol/g, higher than that of MgO-H_2O at 0.133 mmol/g and MgO alone at 0.005 mmol/g. Basic cations increase the electron density within the oxygen framework, thereby promoting its basic properties (Sahu et al., 2015). The basicity of the catalyst can be increased by impregnation, with KOH infiltration into the pores of the MgO catalyst increasing the alkalinity (Oko & Feri, 2019). Furthermore, catalyst basicity increases proportionally with the concentration of KOH applied during the impregnation process (Buchori et al., 2018).

Research by Anggoro et al. (2018) found that the addition of 2% Ca to MgO catalysts increased the basicity to 0.095 mmol/g, while a 3% Ca concentration resulted in a decrease in alkalinity to 0.035 mmol/g. This decrease in basicity at higher Ca concentrations may be due to oversaturation, where smaller Ca ions replace Mg ions within the crystal lattice. Lintang (2020) reported that MgO has a limited total basicity of 0.39 mmol/g, whereas MgO synthesised with H_2O has a higher total basicity of 2.05 mmol/g. At calcination temperatures below 900ºC, the OH group on the MgO surface remains partially intact, likely contributing to the weak base sites on the MgO-H_2O catalyst (Puriwat et al., 2010). This weak base site effect may explain the lower alkalinity of the MgO-H_2O catalyst compared to KOH.

3.3. Effect of using activated MgO catalyst on TAG conversion

The difference in TAG conversion values in the glycerolysis reaction using activated MgO catalyst and different reaction temperatures can be seen in Figure 3. During the glycerolysis process, TAG is converted to MAG and DAG. Triacylglycerol acts as a limiting reactant which will react with excess amounts of glycerol (Arwani, 2017). TAG conversion analysis that has been carried out produces a significant difference between the two temperature treatments ($P<0.05$). A temperature of 175ºC produces a higher triglyceride conversion than a temperature of 165ºC. A higher reaction temperature can decompose more TAGs (Mostafa et al., 2013). Elevated reaction temperatures increase the molecular transformation rate by providing atoms and molecules with greater kinetic energy. This energy boost leads to more frequent intermolecular collisions, making it easier for intermolecular bonds to break (Okullo & Temu, 2015). Excessive use of glycerol will maximize the conversion of TAG to MAG and DAG.

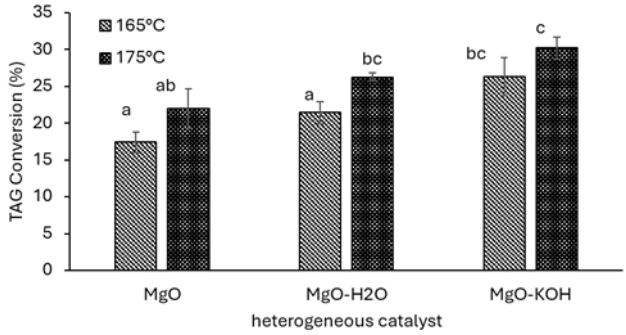

Figure 3. TAG conversion in glycerolysis reaction using different types of activated MgO catalysts (different letters indicated significantly different values ($p < 0.05$))

Figure 3 demonstrates that the use of MgO-KOH resulted in the highest TAG conversion of 30.21% at 175°C, demonstrating its superior catalytic performance compared to MgO and MgO- H_2O. These findings indicate that the alkaline properties of the catalyst significantly enhance the rate of the glycerolysis reaction (Knothe et al., 2015). Under alkaline conditions, the catalyst can attracts H^+ ions from glycerol, forming glycerolate anions, which actively catalyze the glycerolysis reaction. This observation aligns with previous studies by Buchori et al. (2019), which highlighted the effectiveness of optimized heterogeneous catalysts like KF/CaO-MgO in achieving high yields of monoglycerides through controlled reaction conditions.

3.4. Acylglycerol concentration

The results of the analysis of MAG content from the glycerolysis reaction can be seen in Figure 4. Elevating the reaction temperature facilitates the interaction between TAG molecules and glycerol, enhancing the diffusion of reactants with the catalyst's active surface. Azis et al. (2013) demonstrated that higher temperatures increase intermolecular motion, resulting in a higher kinetic energy of reacting molecules. This increased kinetic energy leads to more frequent collisions between reactant molecules, thereby increasing the reaction conversion rate. According to Moquin et al. (2006), MAG molecules can form through multiple reaction pathways, including reactions between TAG and glycerol, DAG and glycerol, as well as between glycerol and free fatty acids. Wangi et al. (2023) also mentioned that the glycerolysis reaction occurs in 6 stages (equation 1-6).

$$\text{TAG + glycerol} \rightleftharpoons \text{MAG + DAG + } 3H_2O \quad (1)$$
$$\text{DAG + glycerol} \rightleftharpoons 2\text{MAG + } 3H_2O \quad (2)$$
$$\text{TAG + MAG} \rightleftharpoons 2\text{DAG} \quad (3)$$
$$\text{TAG + } H_2O \rightleftharpoons \text{DAG + FFA} \quad (4)$$
$$\text{DAG + } H_2O \rightleftharpoons \text{MAG + FFA} \quad (5)$$
$$\text{MAG + } H_2O \rightleftharpoons \text{glycerol + FFA} \quad (6)$$

Different activation methods of MgO catalysts also have a significant effect on MAG content ($p<0.05$). Catalysts with higher basicity values can enhance MAG production, as they facilitate more effective interactions between glycerol and other molecules, providing a favorable environment for MAG formation. The MgO-KOH catalyst yielded a higher MAG fraction than other catalysts, reaching 4.31%.

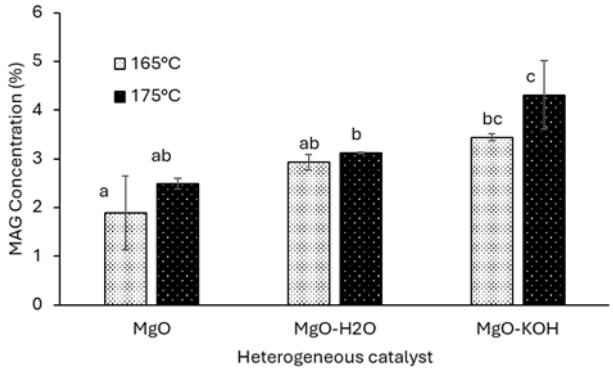

Figure 4. MAG concentration in glycerolysis reaction with different reaction temperatures and activated MgO catalysts (different letters indicated significantly different values ($p < 0.05$))

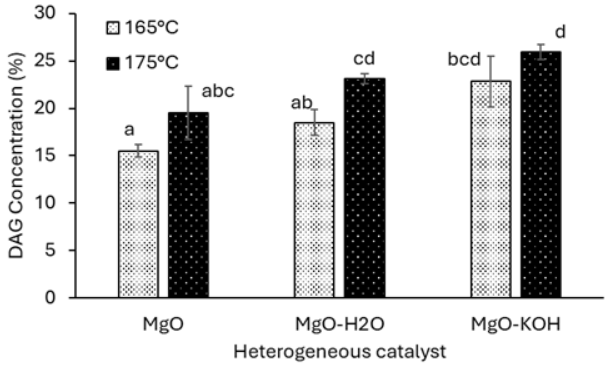

Figure 5. DAG concentration in glycerolysis reaction with different reaction temperatures and activated MgO catalysts (different letters indicated significantly different values ($p < 0.05$))

The DAG fraction had the same results as the MAG fraction where the treatment temperatures of 165ºC and 175ºC were significantly different (Figure 5). The temperature treatment of 175ºC produces a higher value than the temperature of 165ºC. The higher the reaction temperature, the greater the kinetic energy possessed by the reacting molecules. So that it has an impact on more collisions between reactant molecules so that the reaction conversion increases (Azis et al., 2013). Statistical analysis revealed that the application of MgO, MgO-H_2O, and MgO-KOH catalysts had a significant impact on the glycerolysis reaction using coconut oil as the substrate ($p<0.05$). This study found that a reaction temperature of 175°C with the MgO-KOH catalyst produced the highest diacylglycerol (DAG) fraction at 25.9%, attributed to the increased rate constant of the glycerolysis reaction at elevated temperatures (Wangi et al., 2023). These findings align with previous studies where the use of KF/CaO-MgO catalysts resulted in significant increases in monoglyceride yields under optimized reaction conditions. The combination of high surface area and strong basicity of the catalyst enhances reaction efficiency (Buchori et al., 2020).

In comparing MAG and DAG fractions, the DAG fraction was higher than MAG due to the elevated temperature and molar ratio used. During glycerolysis, hydroxyl groups interact with fatty acids, increasing DAG content (Dijkstra, 2020). A short reaction time can limit fatty acid binding to MAG, resulting in lower MAG yields. Both MAG and DAG increase during glycerolysis but eventually decrease after reaching a peak, influenced by temperature (Affandi et al., 2017). Excess FFAs in solution promote DAG formation from MAG and FFA reactions. TAG undergoes partial hydrolysis, and MAG esterifies to form DAG, which the catalyst can further convert to MAG until equilibrium is reached. Lower temperatures affect glycerol solubility, and continued glycerolysis may lead to reverse reactions, reducing MAG and raising TAG in MDAG products (Chetpattananondh & Tongurai, 2008).

3.5. Effect on free fatty acid (FFA) val

Figure 6 shows the value of FFA contained in the MDAG product produced at different reaction temperatures and activated MgO catalysts. The MDAG produced at 175°C exhibited higher free fatty acid (FFA) levels than at 165°C. This increase may occur during glycerolysis, where water formation leads to the hydrolysis of TAG, DAG, and MAG. Melwita et al. (2015) found that water in the reaction promotes hydrolysis, causing oil to form FFAs and glycerol, thus raising FFA levels that would otherwise be reduced. The increase in free fatty acid (FFA) content can also result from product degradation, influenced by oxidation or reverse reactions during glycerolysis (Zhang et al., 2015). High temperatures lower solution viscosity (Pratama et al., 2018), enhancing diffusivity between reactants, leading to increased molecular collisions and product formation, thereby reducing FFA levels in the emulsifier. However, reaction temperature has an optimal point; beyond this, collisions

between FFA and glycerol decrease, reducing reaction efficiency and causing FFA levels to rise again (Melwita et al., 2015). Elevated FFAs may further trigger saponification if the fatty acids react with the catalyst, forming soap and water. The lowest FFA content, 0.42%, was observed in the MDAG product produced at 165°C using the MgO-KOH catalyst. This low FFA level is likely due to FFA molecules formed during the reaction promptly interacting with glycerol to produce MAG and DAG.

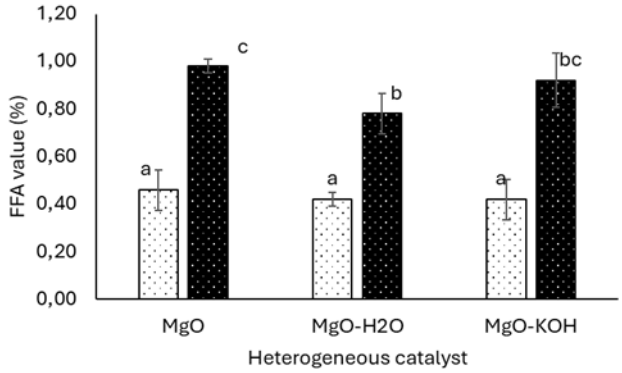

Figure 6. FFA Value of MDAG product (different letters indicated significantly different values ($p < 0.05$))

3.6 Slip melting point of MDAG prod uct

The results of the melting point of MDAG products can be seen in Table 1. Based on the analysis results, the coconut oil used in this study has a slip melting point in the range of 23.6-24.1. Products with high MAG and DAG content exhibit higher SMP values compared to those with low MDAG content. This is evidenced by the MDAG product generated in the glycerolysis reaction at a temperature of 175°C using the MgO-KOH catalyst, which resulted in SMP values ranging from 24.3 to 25.9. The melting point of the MDAG product is influenced by several factors, namely the length of the fatty acid chain, the unsaturation ratio, the position of the fatty acid in the glycerol group (Karabulut et al., 2004).

Generally, MDAG products exhibit a higher SMP value than oil due to their increased hydroxyl groups, which enable the formation of hydrogen bonds among MDAG molecules. However, some SMP values of MDAG products in this study were lower than those of the oil, likely due to the influence of glycerol present in the mixture. The high content of free glycerol in the product lowers the melting point, as glycerol has a melting point of 17.8°C, further reducing the liquid point of the product.

Table 1. Slip melting point (SMP) of MDAG product

Temperature	Catalyst	SMP (°C)
165°C	MgO	22.5-22.8
	MgO-H_2O	22.2-23.4
	MgO-KOH	21.9-22.1
175°C	MgO	22.8-24.7
	MgO-H_2O	22.8-24.7
	MgO-KOH	24.3-25.9

4. Conclusions

The MDAG product can be synthesized through a glycerolysis process using coconut oil and glycerol as substrates at a mole ratio of 1:2.3, with the addition of 2% catalyst. A reaction temperature of 175°C resulted in higher fractions of MAG, DAG, and TAG compared to 165°C, as the basicity of the catalyst enhances

the rate constant of glycerolysis. The use of the MgO-KOH catalyst yielded the highest conversion rates: 30.21% for TAG, 25.9% for DAG, and 4.31% for MAG, with a melting point range of 22.8–24.7°C and free fatty acid content of 0.7812%. The optimal product was obtained using a treatment temperature of 175°C and the MgO-KOH catalyst activation method. Therefore, activating the MgO catalyst with a KOH solution effectively produces coconut oil-based MDAG products. These products have potential applications in various food products, including ice cream and confectionery.

5. References

Affandi, A. R., Andarwulan, N., & Hariyadi, P. (2017). Pengaruh Waktu dan Suhu Gliserolisis terhadap Sifat Kimia Mono-Diasilgliserol pada Skala Pilot Plant. Journal of Food Technology & Industry/Jurnal Teknologi & Industri Pangan, 28(2).

Al-Baarri, A. N., Legowo, A. M., & Widayat. (2018). The browning value changes and spectral analysis on the Maillard reaction product from glucose and methionine model system. IOP Conference Series: Earth and Environmental Science, 102(1). https://doi.org/10.1088/1755-1315/102/1/012003

Anggoro, D. D., Buchori, L., Sasongko, S. B., & Mahmed Vincent, A. A. F. F. (2018). Synthesis of Ca/MgO catalyst using sol gel method for monoglycerides production. AIP Conference Proceedings, 1977. https://doi.org/10.1063/1.5042932

Anggoro, D. D., Buchori, L., Sasongko, S. B., & Oktavianty, H. (2019a). Basicity Optimization of KF/Ca-MgO Catalyst using Impregnation Method. Bulletin of Chemical Reaction Engineering &Amp; Catalysis, 14(3), 678–682. https://doi.org/10.9767/bcrec.14.3.4248.678-682

Anggoro, D. D., Buchori, L., Sasongko, S. B., & Oktavianty, H. (2019b). Basicity Optimization of KF/Ca-MgO Catalyst using Impregnation Method. Bulletin of Chemical Reaction Engineering & Catalysis, 14(3), 678–682. https://doi.org/10.9767/bcrec.14.3.4248.678-682

AOCS, C. (2003). 5a-40, Free fatty acids. Official Methods and Recommended Practices of the AOCS, 5th Ed., Champaign, Illinois, USA.

Arwani, A. (2017). Sintesis Mono-Diasilgliserol (MDAG) dari Stearin Minyak Aawit dengan Metode Gliserolisis Skala Laboratorium. Skripsi, 5–19.

Azis, M. M., Härelind, H., & Creaser, D. (2013). Microkinetic modeling of H2-assisted NO oxidation over Ag–Al2O3. Chemical Engineering Journal, 221, 382–397. https://doi.org/10.1016/j.cej.2013.01.107

Belelli, PG. G., Ferretti, CA. A., Apesteguía, CR. R., Ferullo, RM. M., & Di Cosimo, JI. I. (2015). Glycerolysis of methyl oleate on MgO: Experimental and theoretical study of the reaction selectivity. Journal of Catalysis, 323, 132–144. https://doi.org/10.1016/j.jcat.2015.01.001

Buchori, L., Anggoro, D. D., Sumantri, I., & Putra, R. R. (2019). Optimization of Monoglycerides Production Using KF/CaO-MgO Heterogeneous Catalysis. Bulletin of Chemical Reaction Engineering & Catalysis, 14(3), 689–696. https://doi.org/10.9767/bcrec.14.3.4251.689-696

Buchori, L., Djaeni, M., Ratnawati, R., Retnowati, D. S., Hadiyanto, H., & Anggoro, D. D. (2020). Glycerolysis using KF/CaO-MgO Catalyst: Optimisation and Reaction Kinetics. Jurnal Teknologi, 82(5). https://doi.org/10.11113/jt.v82.14585

Buchori, L., Istadi, I., Purwanto, P., Marpaung, L. C., & Safitri, R. L. (2018). Roles of K2O on the CaO-ZnO Catalyst and Its Influence on Catalyst Basicity for Biodiesel Production. E3S Web of Conferences, 31(3), 0–3. https://doi.org/10.1051/e3sconf/20183102009

Chetpattananondh, P., & Tongurai, C. (2008). Synthesis of high purity monoglycerides from crude glycerol n and palm stearin. Songklanakarin Journal of Science and Technology, 30(4), 515–521.

Díez, V. K., Ferretti, C. A., Torresi, P. A., Apesteguía, C. R., & Di Cosimo, J. I. (2011). Effect of MgO activation conditions on its catalytic properties for base-catalyzed reactions. Catalysis Today, 173(1), 21–27. https://doi.org/10.1016/j.cattod.2011.02.060

Dijkstra, A. J. (2020). Some Thoughts on the Mechanism of Ester Interchange Reactions Involving Acylglycerols. European Journal of Lipid Science and Technology, 122(10), 2000188. https://doi.org/10.1002/ejlt.202000188

Faba, L., Díaz, E., & Ordóñez, S. (2012). Aqueous-phase furfural-acetone aldol condensation over basic mixed oxides. Applied Catalysis B: Environmental, 113–114, 201–211. https://doi.org/10.1016/j.apcatb.2011.11.039

Hapsari, R. I. (2020). Optimasi Reaksi Gliserolisis pada Pembuatan MDAG (Mono-Diasilgliserol) dari Minyak FHPKO (Fully Hydrogenated Palm Kernel Oil) dan Minyak Kelapa. Universitas PGRI Semarang.

Jeevanandam, J., Chan, Y. S., & Ku, Y. H. (2018). Aqueous Eucalyptus globulus leaf extract-mediated biosynthesis of MgO nanorods. Applied Biological Chemistry, 61(2), 197–208. https://doi.org/10.1007/s13765-018-0347-7

Kandiban, M., Vigneshwaran, P., & Potheher*, V. I. (2015). Synthesis and Characterization of Mgo Nanoparticles for Photocatalytic. Conference, December, 1–5.

Karabulut, I., Turan, S., & Ergin, G. (2004). Effect of chemical interesterification on solid fat content and slip melting point of fat /oil blends. European Food Research and Technology, 218, 224–229. https://doi.org/10.1007/s00217-003-0847-4

Knothe, G., Krahl, J., & Van Gerpen, J. (2015). The biodiesel handbook. Elsevier.

Kombe, G. G., Temu, A. K., Rajabu, H. M., Mrema, G. D., & Lee, K. T. (2013). Low temperature glycerolysis as a high FFA pre-treatment method for biodiesel production. Advances in Chemical Engineering and Science, 2013.

Lintang, H. P. (2020). Studi Pengaruh Pelarut pada Sintesis Magnesium Oksida dengan Metode Kopresipitasi sebagai Katalis Basa Padat. Universitas Riau.

Malyani, A. S. (2015). Preparasi Nanopartikel Fe3O4 (MAGNETIT) serta Aplikasinya sebagai Adsorben Ion Logam Kadmium. Indonesian Journal of Chemical Science, 5(2).

Manríquez-Ramírez, M., Gómez, R., Hernández-Cortez, J. G., Zúñiga-Moreno, A., Reza-San Germán, C. M., & Flores-Valle, S. O. (2013a). Advances in the transesterification of triglycerides to biodiesel using MgO–NaOH, MgO–KOH and MgO–CeO2 as solid basic catalysts. Catalysis Today, 212, 23–30. https://doi.org/10.1016/j.cattod.2012.11.005

Manríquez-Ramírez, M., Gómez, R., Hernández-Cortez, J. G., Zúñiga-Moreno, A., Reza-San Germán, C. M., & Flores-Valle, S. O. (2013b). Advances in the transesterification of triglycerides to biodiesel using MgO-NaOH, MgO-KOH and MgO-CeO2 as solid basic catalysts. Catalysis Today, 212, 23–30. https://doi.org/10.1016/j.cattod.2012.11.005

Mazubert, A., Poux, M., & Aubin, J. (2013). Intensified processes for FAME production from waste cooking oil: A technological review. Chemical Engineering Journal, 233, 201–223. https://doi.org/10.1016/j.cej.2013.07.063

Melwita, E., Ayu, M., & Rahmi, P. (2015). Reaksi gliserolisis palm fatty acid distillate (PFAD) menggunakan co-solvent etanol untuk pembuatan emulsifier. Jurnal Teknik Kimia, 21(2), 15–23.

Moorthy, S. K., Ashok, C. H., Rao, K. V., & Viswanathan, C. (2015). Synthesis and Characterization of Mgo Nanoparticles by Neem Leaves through Green Method. Materials Today: Proceedings, 2(9), 4360–4368. https://doi.org/10.1016/j.matpr.2015.10.027

Moquin, P. H. L., Temelli, F., Sovová, H., & Saldaña, M. D. A. (2006). Kinetic modeling of glycerolysis-hydrolysis of canola oil in supercritical carbon dioxide media using equilibrium data. Journal of Supercritical Fluids, 37(3), 417–424. https://doi.org/10.1016/j.supflu.2006.01.009

Mostafa, N. A., Maher, A., & Abdelmoez, W. (2013). Production of mono-, di-, and triglycerides from waste fatty acids through esterification with glycerol. Advances in Bioscience and Biotechnology, 4(09), 900.

Munandar, A., Krisdiyanto, D., & Khamidinal, A. P. (2014). Adsorpsi Logam Pb dan Fe dengan Zeolit Alam Teraktivasi Asam Sulfat. Seminar Nasional Kimia Dan Pendidikan Kimia, 6, 138–146.

Nayebzadeh, H., Saghatoleslami, N., Haghighi, M., & Tabasizadeh, M. (2017). Influence of fuel type on microwave-enhanced fabrication of KOH/Ca12Al14O33 nanocatalyst for biodiesel production via microwave heating. Journal of the Taiwan Institute of Chemical Engineers, 75, 148–155. https://doi.org/10.1016/j.jtice.2017.03.018

Ngatirah, N., Hidayat, C., Rahayu, E. S., & Utami, T. (2022). Enzymatic Glycerolysis of Palm Kernel Olein-Stearin Blend for Monolaurin Synthesis as an Emulsifier and Antibacterial. Foods, 11(16). https://doi.org/10.3390/foods11162412

Oko, S., & Feri, M. (2019). Pengembangan Katalis CaO dari Cangkang Telur Ayam dengan Impregnasi KOH dan Aplikasinya Terhadap Pembuatan Biodiesel dari Minyak Jarak. Jurnal Teknologi Universitas Muhammadiyah Jakarta, 11(2), 103–110.

Okullo, A. A., & Temu, A. K. (2015). Modelling the Kinetics of Jatropha Oil Transesterification. Energy and Power Engineering, 07(04), 135–143. https://doi.org/10.4236/epe.2015.74013

Pratama, Y., Abduh, S. B. M., Legowo, A. M., Pramono, Y. B., & Albaarri, A. N. (2018). Optimum carrageenan concentration improved the physical properties of cabinet-dried yoghurt powder. IOP Conference Series: Earth and Environmental Science, 102(1). https://doi.org/10.1088/1755-1315/102/1/012023

Puriwat, J., Chaitree, W., Suriye, K., Dokjampa, S., Praserthdam, P., & Panpranot, J. (2010). Elucidation of the basicity dependence of 1-butene isomerization on MgO/Mg(OH)2 catalysts. Catalysis Communications, 12(2), 80–85. https://doi.org/10.1016/j.catcom.2010.08.015

Rafati, A., Tahvildari, K., & Nozari, M. (2019). Production of biodiesel by electrolysis method from waste cooking oil using heterogeneous MgO-NaOH nano catalyst. Energy Sources, Part A: Recovery, Utilization and Environmental Effects, 41(9), 1062–1074. https://doi.org/10.1080/15567036.2018.1539139

Rahul, R., Satyarthi, J. K., & Srinivas, D. (2011). Lanthanum and zinc incorporated hydrotalcites as solid base catalysts for biodiesel and biolubricants production. In Indian Journal of Chemistry (Vol. 50).

Roni, K. A., & Legiso. (2021). Kimia Organik. In NoerFiKri (1st ed.).

Sahu, P. K., Sahu, P. K., & Agarwal, D. D. (2015). Role of basicity and the catalytic activity of KOH loaded MgO and hydrotalcite as catalysts for the efficient synthesis of 1-[(2-benzothiazolylamino)arylmethyl]-2-naphthalenols. RSC Advances, 5(85), 69143–69151. https://doi.org/10.1039/c5ra11857c

Swastawati, F., Al-Baari, A. N. matullah, Susanto, E., & Purnamayati, L. (2019). The effect of antioxidant and antibacterial liquid smoke nanocapsules on catfish fillet (pangasius sp.) during storage at room temperature and cold temperature. Carpathian Journal of Food Science and Technology, 11(4), 165–175. https://doi.org/10.34302/2019.11.4.16

Sutapa, I. W., Wahab, A. W., Taba, P., & Nafie, N. La. (2018). Synthesis and structural profile analysis of the MgO nanoparticles produced through the sol-gel method

followed by annealing process. Oriental Journal of Chemistry, 34(2), 1016–1025. https://doi.org/10.13005/ojc/340252

Taslim, Bani, O., Parinduri, S., Ningsih, P., & Taruna, N. (2019). Preparation, Characterization and Application of Natural Zeolite from Tapanuli Indonesia Modified with KOH as Catalyst Support for Transesterification of Rice Bran Oil. In International Journal of Engineering Research and Technology (Vol. 12, Issue 9). http://www.irphouse.com

Triana, N. R. (2014). Aplikasi Mono-Diasilgliserol dari Fully Hydrogenated Palm Kernel Oil Sebagai Emulsifier untuk Margarin. Mutu Pangan, 1(2), 137–144.

Wangi, I. P., Supriyanto, Sulistyo, H., & Hidayat, C. (2023). Glycerolysis–interesterification in high-shear reactor using sodium silicate catalyst: effect of mixing rate on reaction kinetics. Reaction Kinetics, Mechanisms and Catalysis, 136, 881–899. https://doi.org/10.1007/s11144-023-02383-2

Wibawanti, J. M. W., Mulyani, S., Legowo, A. M., Hartanto, R., Al-Baarri, A., & Pramono, Y. B. (2021). Characteristics of inulin from mangrove apple (Soneratia caseolaris) with different extraction temperatures. Food Research, 5(4), 99–106. https://doi.org/10.26656/fr.2017.5(4).662

Zha, B., Chen, Z., Wang, L., Wang, R., Chen, Z., & Zheng, L. (2014). Production of glycerol monolaurate-enriched monoacylglycerols by lipase-catalyzed glycerolysis from coconut oil. European Journal of Lipid Science and Technology, 116(3), 328–335. https://doi.org/10.1002/ejlt.201300243

Zhang, Z., Wang, Y., Ma, X., Wang, E., Liu, M., & Yan, R. (2015). Characterisation and oxidation stability of monoacylglycerols from partially hydrogenated corn oil. Food Chemistry, 173, 70–79. https://doi.org/10.1016/j.foodchem.2014.09.155

Acknowledgments

This research is partially supported by Food Safety Scientific Consortium through the Research Implementation Agreement Contract No. 369/UN7.A/HK/X/2024.

CARPATHIAN JOURNAL OF FOOD SCIENCE AND TECHNOLOGY

journal homepage: **http://chimie-biologie.ubm.ro/carpathian_journal/index.html**

Research Article

SMART IOT-ENABLED IR-ASSISTED REFRACTANCE WINDOW DRYING KINETICS OF GUAVA PULP AND QUALITY ANALYSIS

Prachita Sharma[1], Penumala Indu[1], Harsh Dadhaneeya[1], Prabhat K. Nema[1,✉]

[1]Department of Food Engineering, National Institute of Food Technology Entrepreneurship Management-Kundli, Sonipat, India

✉drpknema.niftem@gmail.com

ORCID - 0000-0001-6419-4973

https://doi.org/10.34302/2025.17.3.9

Article history:
Received
August 26th , 2025
Accepted
September 30th, 2025

Keywords
Tray drying;
Vacuum drying;
Refractance window drying;
IoT-enabled IR-assisted;
Refractance window drying;
Total Phenolic content;
Total flavonoid content.

Abstract

This study evaluates the effect of Smart IoT-Enabled IR-Assisted Refractance Window Drying (IR-RWD) on drying kinetics as well as physicochemical and thermal characteristics of peeled and unpeeled guava pulp samples, with respect to other three drying techniques which are tray drying (TD), vacuum drying (VD), and refractance window drying (RWD). The drying experiments conducted at 60°C across four different drying techniques and revealed significant variations in drying time. The average drying times recorded for the peeled sample were 420, 420, 390, and 300 minutes for TD, VD, RWD, and IR-RWD, respectively, whereas the unpeeled guava sample exhibited drying times of 510, 450, 420, and 300 minutes. Moreover, this study highlighted that the RWD and IR-RWD dried sample displayed notably higher levels of total phenolic content (TPC) and total flavonoid content (TFC) as compared with TD and VD sample. Specifically, the TPC was observed 205.1 mg GAE/100g, and the TFC was 645.4 mg QE/100g in IR-RWU samples. An SEM analysis reveals that the peeled samples display smoother and more uniform textures than their unpeeled equivalents. Among the different drying techniques, the IR-RWD method was the most efficient, retaining the highest levels of nutrients while requiring the shortest drying time. This suggests that the IR-RWD technique could be a superior method for drying guava pulp, preserving its nutritional and antioxidant properties more effectively than the traditional TD and VD methods.

1. Introduction

RWD system is an innovative technique used to enhance the quality of liquid alimentary substances and various biomaterials through their conversion into powdered, flaked, or sheet forms. The RW drying technique has garnered significant attention within the food sector due to its ability to produce high-quality dried products and its cost-effectiveness (Abul-Fadl & Ghanem, 2011). Indirect contact drying is achieved by transferring heat from hot water to wet materials through a mylar membrane in the RW drier. The window facilitates the penetration of infrared energy into a wet sample through the mylar membrane (Dadhaneeya et al., 2023a).

Internet of Things (IoT) represents an emergent paradigm that fosters communication among electronic devices and sensors via the internet, thereby enhancing the quality of human life (Kumar, Tiwari, & Zymbler, 2019). The IoT engenders a novel landscape of opportunities for food enterprises that integrate IoT technology within the food sector to recognize and rectify supply chain challenges, uphold superior manufacturing standards, ameliorate inefficiencies, comply with and exceed food safety regulations, and provide their clientele with enhanced access (Dadhaneeya et al., 2023c). IoT integration in RW dryers offers precision, efficiency, and data-driven decision-making, contributing to higher-quality dried products, reduced energy consumption, and improved operational reliability. The IoT-enabled IR-assisted RW dryer combines RWD technologies with infrared techniques, which are further integrated with the intelligence of the IoT, bringing us one step closer to the fourth generation of the industrial revolution (Dadhaneeya et al., 2024).

Guava, scientifically referred to as *Psidium guajava*, belongs to the extensive Myrtle family (Jain, Jain, & Nema, 2011). Owing to its high nutritional value, ease of cultivation, and desirability in processed goods, guava plays a substantial role in the domestic economies of over 50 tropical nations and in international trade (Nagy S. and Shaw E. P., 1985). It is extensively grown in tropical and subtropical areas of the world. India is the world's largest producer of guava. The world's largest producer of guava is India. Guava is renowned for its exceptional nutritional value and is rich in vitamins C and A, fiber, potassium, and antioxidants. Guava is an excellent source of pectin, a crucial dietary fiber (Naseer, Hussain, Naeem, Pervaiz, & Rahman, 2018). Compared with oranges, guavas contains four times the amount of vitamin C (Flores, Wu, Negrin, & Kennelly, 2015). The high concentration of ascorbic acid found in guava renders it a potent agent for counteracting oxidation and free radicals, which are recognized as significant contributors to degenerative diseases. The antioxidant properties of guavas are believed to reduce the likelihood of developing pancreatic, stomach, esophageal, laryngeal, and oral cancer. Guava drying prolongs the longevity of the fruit, enabling it to be stored for prolonged periods without deterioration. Dried guava undergoes flavor concentration, leading to heightened sweetness and an intensified taste.

In this study guava pulp was dried using tray drying (TD), vacuum drying (VD), refractance window drying (RWD), and Infrared assisted refractance window drying (IR-RWD) techniques. This study also compared the effects of various selected drying techniques for peeled and unpeeled guava samples on their quality attributes. It is imperative to employ a drying procedure that not only yields a higher quality of the final product but also demonstrates commercial viability.

2. Materials and Methods

2.1. Sample Preparation

This study used completely ripened guava purchased from the marketplace near to NIFTEM-K. Firstly, fresh guava was cleaned with tap water and removed the top and bottom portions of the guava sample by using knife. Samples were evenly segregated into two categories, that is with and without peels. In the case of the peeled guavas, the outer layer was removed by employing a peeler. Both the samples were grinded and then the resulting mixture underwent the deseeding process through a sieve featuring a pore diameter of 2mm.

2.2. Experimental setup

There are several researchers (i.e Kheto et al., 2021) who have suggested that 60 ^{o}C is a suitable temperature for drying food-related materials, so the same was selected as drying temperature in this study. While spreading sample thickness was taken near to 5 mm. Which was selected based on preliminary trials. A laboratory scale of tray dryer (TC 303, Bajaj Process Pack Machinery Private Limited) was employed to produce tray-dried samples. The laboratory scale vacuum oven (Shel Lab) was employed to prepare vacuum-dried samples. An IoT-enabled IR-assisted RW dryer was used for preparing RW-dried and IR-

assisted RW-dried samples. The IoT-enabled IR-assisted RW dryer installed in NIFTEM-K.

2.3. Physical Properties

2.3.1. Color Analysis

A portable colorimeter was employed to quantify the chromatic attributes of the specimen in terms of L* (lightness), a* (redness), and b* (yellowness) on Petri plate (Kardile, Nema, Kaur, & Thakre, 2020).The total color difference (ΔE), Chroma (C^*), hue (h) and browning index (BI) were derived through the application of Eq. (1), (2), (3) and (4) respectively.

$$\Delta E = \sqrt{(L^* - L)^2 + (a^* - a)^2 + (b^2 - b)^2} \quad (1)$$

$$C^* = \sqrt{(a^*)^2 + (b^*)^2} \quad (2)$$

$$\mathrm{h} = \tan^{-1}\frac{b^*}{a^*} \quad (3)$$

$$\mathrm{BI} = \frac{[100(\mathrm{x} - 0.31)]}{0.172} \quad (4)$$

$$x = \frac{\mathrm{a}^* + 1.75\mathrm{L}^*}{5.645\mathrm{L}^* + \mathrm{a}^* - 3.012\mathrm{b}^*} \quad (5)$$

Where L, a and b are the color coordinates values of fresh pulp spreading at 5 mm thickness.

2.3.2. Texture Analysis

The texture analysis was performed by following the procedure as outline in Dadhaneeya, et al. (2023b).

2.3.3. Moisture Analysis

The moisture content of the samples was quantified utilizing a moisture analyzer (HE73, Mettler Toledo, Switzerland).

2.3.4. Water Activity

A water activity meter (Model-Aquala3 4TE, Decagen) was employed to measure the water activity of the samples (Kardile, Nema, Kaur, & Thakre, 2019).

2.3.5. Bulk Density

The bulk density was determined by calculating the ratio of mass of the powder to the volume of the occupied cylinder (Baeghbali et al., 2016).

2.3.6. Rehydration Ratio

The rehydration ratio was measured following the methodology outlined byZhou et al. (2022).

2.4. Chemical Properties

2.4.1. Ascorbic Acid Analysis

The ascorbic acid test was performed according to AOAC (1968) standard procedure. The process entails homogenizing about 0.25 g of samples with 25 ml of an HPO_3 - CH_3COOH solution. The resultant mixture is filtered using filter paper. Subsequently, resulting solution (2 ml) was incorporated into HPO3 - CH_3COOH solution (5 ml). Titration of the resultant solution was performed using 2,6-dichlorophenol indophenol (DCPIP) indicator solution (Dadhaneeya et al., 2025).

2.4.2. Total Phenolic Content (TPC)

The procedure for extracting bioactive compounds was performed in accordance with Carvalho Gualberto et al. (2021). The Folin-Ciocalteu spectroscopic method, as outlined by Sharanagat et al. (2019), was employed to determine the TPC.

2.4.3. Total flavonoid content (TFC)

Flavonoid levels of the sample extracts were assessed utilizing the aluminum chloride colorimetric approach as outlined by Dhua et al. (2021).

2.4.4. Antioxidant activity

The evaluation of antioxidant activity of the control and dried samples was conducted employing the DPPH (1,1-diphenyl-2-picrylhydrazyl) assay, as reported byDesai et al. (2023).

2.4.5. FTIR Analysis

A Bruker Alpha spectrometer was utilized to conduct Fourier Transform Infrared (FTIR) spectroscopy, enabling the identification of functional groups within the samples.

2.5. Thermal Analysis

Analysis of the dried guava powder samples was performed utilizing a differential scanning calorimeter (DSC 1, STAR^e System) and STAR^e Evaluation software.

2.6. SEM-EDS

A small quantity of guava powder samples was mounted on aluminum plates and subsequently coated with gold to enhance image quality. Structural analysis was performed utilizing a Thermo Scientific Axia Scanning

Electron Microscope, operating at an accelerating voltage of 5 kV and a magnification of 350. The mounted samples underwent Energy Dispersive X-ray Spectroscopy (EDS) analysis to ascertain their elemental composition.

2.7. Statistical analysis

The experimental procedures were replicated three times, with the outcomes reported as average value ± the standard deviation. Statistical analysis was conducted employing OriginPro 2021, software produced by OriginLab Corporation. To determine significant differences ($p < 0.05$) among mean values, a one-way ANOVA was employed, followed by Tukey's test for multiple comparisons. Additionally, Principal Component Analysis (PCA) was applied to the mean values.

3. Results and discussions

3.1. Drying characteristics

The variation of moisture content over drying time is illustrated in Figure 1 (a & b). The moisture loss in the IR-RWD sample occurred rapidly due to the dual-sided heating mechanism intrinsic to this method. The upper surface of the sample was exposed to IR radiation, which facilitated direct heat transmission to the material via electromagnetic waves. The bottom surface of the sample was synchronously heated using RWD. The cumulative impact of these heating processes created a uniform temperature gradient throughout the sample, allowing rapid moisture evaporation from both sides. Figure 1 (a) illustrates the relationship between moisture content and drying time for peeled samples, subsequently Figure 1 (b) illustrates the unpeeled sample. The time taken for drying peeled samples was observed TP (420 min), VP (420 min), RWP (390 min) and IR-RWP (300 min). The drying times recorded for the unpeeled samples were TU (510 minutes), VU (450 minutes), RWU (420 minutes), and IR-RWU (300 minutes). Nevertheless, the TU sample had the longest drying duration, while presenting a steep gradient. Similar graph of moisture content over drying time was also observed by Dadhaneeya et al. (2023b).

Figure 1 (c & d) **(a)** depicts the correlation between the drying rate (DR) and time across various drying methods. Figure 1 (c & d) illustrates that the drying rate curve attains its peak value within 60 minutes for all samples. The drying rate curve at first exhibited an increase in drying rate until reaching a peak. This may be ascribed to the presence of free unbound water in the pore space of the samples, which might be rapidly eliminated. The drying rate escalated till it reached its peak point. Upon reaching the apex, all the unbound water had evaporated. Subsequent reaching the peak, the drying rate saw a decline owing to the need for more energy to vaporize the bound water present in the pore space Dadhaneeya et al. (2023b). For the peeled sample the highest peak values were observed for vacuum drying, while for the unpeeled sample highest peak values were observed for IR-RW drying. Similar graph of drying rate vs drying time was also reported by Mella et al. (2022).

a)

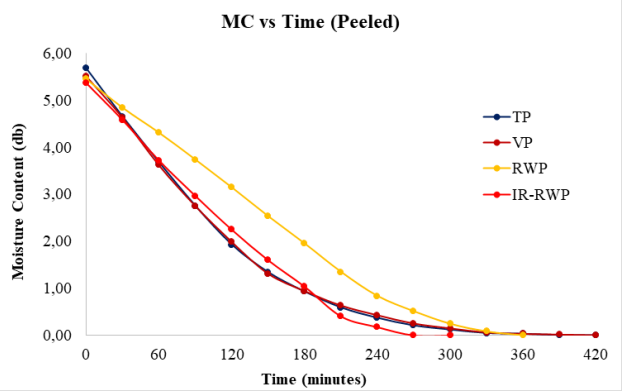

b)

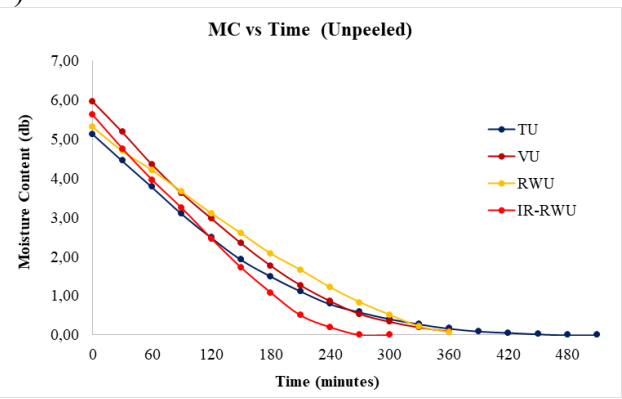

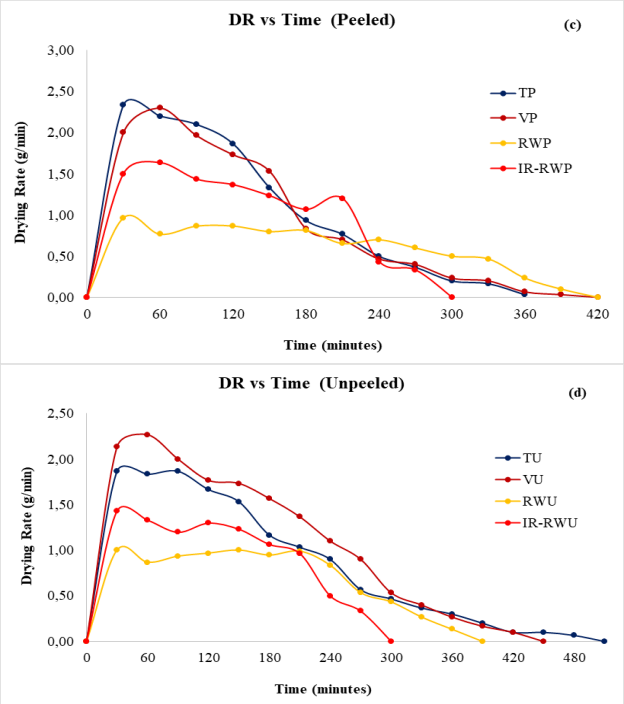

Figure 1. Drying kinetics of graphs of: **(a)**moisture content of peeled sample**(b)** moisture content of unpeeled sample **(c)** drying rate vs time of peeled sample**(d)** drying rate vs time unpeeled sample

3.2. Moisture Analysis and Water Activity

The moisture content of the dried guava powders is given in Table 1. The fresh peeled pulp had a moisture content of 85.1%. While fresh unpeeled pulp contained a moisture content of 86.13%. The dried powder samples exhibited moisture levels ranging from 3.67% (IR-RWU) to 7% (TP). The IR-RWU sample showed the lowest moisture content, whereas the TP sample had the highest. All powder samples were secured in zip-lock pouches and stored in a desiccator. However, some might have the chance to absorb atmospheric moisture.

Water activity was observed highest in the TP sample and lowest in the IR-RWU sample. While fresh guava pulp had a water activity of 0.98. RWP and RWU samples also had low water activity. A significant difference in water activity was noted between IR-RWP and TU samples, potentially due to more effective drying in the IR-RW dryer. As shown in Table 1, all water activity values fell within the range of 0.33-0.49, which is considered safe for storage (a_w< 0.6) (Dissa et al. 2008).

3.3. Color properties

Color differences, denoted by ΔE, of samples subjected to different drying techniques were analyzed to determine its effect on visual quality, which also serves as an essential indicator of product acceptance.Among the treatments, IR-RWU had the lowest ΔE value, indicating minimal color change and excellent preservation of the original appearance. There was no significant difference between RWP and IR-RWP color change values. Samples TU and VU exhibited intermediate color changes with values of 32.38 and 33.12, respectively. Analysis of the color change values of peeled and unpeeled samples indicates significant differences between both. Similar lower color differences in RW dried product was also reported by Baeghbali et al. (2016) and Nemzer et al. (2018). **Chroma values** of the dried samples have been evaluated to determine the intensity and vivacity of their color, which is essential in influencing customer attraction and product quality. The measured chroma values varied from 28.48 in the IR-RWU sample to 36.32 in the RWP sample. A higher chroma rating, shown by the RWP sample at 36.32, denotes a more vivid and intense color. **Hue** of the dried samples was observed within the range of 0.08 to 0.22, with RWP and RWU samples recording the lowest hue value of 0.08 and the IR-RWU sample exhibiting the highest value of 0.22. **Browning index** is a crucial metric that indicates the degree of non-enzymatic browning occurring throughout the drying process. The IR-RWP sample had the greatest browning index at 69.65, indicating considerable browning resulting from strong heat exposure during the IR-assisted RWD process. Numerous researchers have used anti-browning agents to minimize the browning effects that arise during the drying process, as noted byDadhaneeya et al. (2023b) in their study. In the current study, there was no anti-browning agent used to mitigate browning effects. This decision was motivated by the rising consumer appetite for natural food items free from chemical additives. The focus on preserving the quality of products without the use of chemical additives aligns with the overarching movement towards clean-label goods, which emphasize natural food.

Table. 1 Physical properties of dried guava with different drying techniques

(TP: Tray dried peel guava sample; **TU:** Tray dried unpeeled guava sample; **VP:** Vacuum dried peel guava sample; **VU:** Vacuum driedunpeeled guava sample; **RWP**:

Physical Properties	**TP**	**TU**	**VP**	**VU**	**RWP**	**RWU**	**IR-RWP**	**IR-RWU**
Water Activity	0.48 ± 0.005^{a}	0.45 ± 0.005^{a}	0.41 ± 0.1^{b}	0.39 ± 0.02^{b}	0.38 ± 0.1^{bc}	0.35 ± 0.02^{cd}	0.35 ± 0.01^{cd}	0.33 ± 0.02^{d}
Bulk Density (g/cm³)	640 ± 10^{a}	620 ± 5^{ab}	640 ± 10^{a}	610 ± 5^{b}	430 ± 5^{d}	430 ± 10^{d}	510 ± 5^{c}	510 ± 10^{c}
Moisture Content	7.01 ± 0.17^{a}	6.32 ± 0.57^{a}	5.18 ± 0.15^{b}	5.16 ± 0.1^{b}	5.11 ± 0.4^{b}	4.48 ± 0.33^{bc}	4.52 ± 0.15^{b}	3.67 ± 0.15^{c}
Rehydration Ratio (RR)	1.96 ± 0.05^{c}	1.97 ± 0.05^{c}	2.39 ± 0.11^{bc}	2.62 ± 0.18^{bc}	2.94 ± 0.58^{ab}	3.41 ± 0.38^{a}	2.7 ± 0.17^{abc}	2.89 ± 0.15^{ab}
Δ E	35.17 ± 0.51^{b}	32.38 ± 2.31^{c}	38.28 ± 0.76^{a}	33.12 ± 0.14^{bc}	39.19 ± 0.15^{a}	34.58 ± 0.32^{bc}	34.65 ± 0.25^{bc}	27.08 ± 0.87^{d}
Chroma	31.87 ± 0.59^{bc}	29.83 ± 1.31^{cd}	35.51 ± 0.64^{a}	30.97 ± 1.31^{bc}	36.32 ± 0.11^{a}	32.51 ± 0.25^{b}	34.99 ± 0.11^{a}	28.48 ± 0.31^{d}
Hue	0.09 ± 0.001^{c}	0.11 ± 0.006^{c}	0.11 ± 0.003^{c}	0.09 ± 0.01^{c}	0.08 ± 0.003^{c}	0.08 ± 0.004^{c}	0.16 ± 0.01^{b}	0.22 ± 0.02^{a}
Browning Index (BI)	53.63 ± 1.18^{cd}	51.44 ± 1.41^{d}	61.7 ± 1.18^{b}	54.05 ± 5.07^{cd}	61.26 ± 0.35^{b}	56.39 ± 0.38^{bcd}	69.65 ± 1.49^{a}	59.27 ± 1.85^{bc}
Chemical Properties								
TPC (mg GAE/100g)	147.59 ± 6.71^{e}	152.86 ± 4.75^{e}	162.2 ± 4.30^{de}	171.56 ± 2.12^{cd}	172.73 ± 4.5^{cd}	195.56 ± 5.09^{ab}	184.66 ± 7.63^{bc}	205.1 ± 12.26^{a}
TFC (mg QE/100g)	496.5 ± 5.76^{d}	501.4 ± 9.61^{d}	511.4 ± 5.12^{cd}	521.3 ± 7.51^{c}	620.6 ± 7.51^{b}	625.6 ± 6.65^{ab}	638.6 ± 4.16^{ab}	645.4 ± 8.33^{a}
DPPH (%)	89.58 ± 1.08^{e}	93.53 ± 0.85^{cd}	92.41 ± 0.38^{d}	93.31 ± 0.66^{cd}	95.12 ± 0.53^{bc}	96.37 ± 0.55^{ab}	96.05 ± 0.62^{b}	98.24 ± 0.41^{a}
Ascorbic Acid (mg/100g)	67.5 ± 0.5^{b}	72.5 ± 4.1^{b}	84.2 ± 4.95^{a}	85.43 ± 5.94^{a}	91.37 ± 3.16^{a}	92.37 ± 4.9^{a}	86.83 ± 3.01^{a}	92.17 ± 2.53^{a}

Refractance window dried peel guava sample; **RWU:** Refractance window dried unpeeled guava sample; **IR-RWP:** IR-assisted Refractance window dried peel guava sample; **IR-RWU:** IR-assisted Refractance window dried unpeeled guava sample

3.4. Texture Analysis

The textural characteristics of the dried samples were laid out in Figure 2, revealing significant differences in mechanical and structural characteristics across various drying techniques. **The hardness** values of the dried samples varied from 3906.81 g in the IR-RWP sample to 8246.41 g in the TU sample. The reduced hardness value in IR-RWP samples indicates a comparatively softer texture, possibly resulting from uniform heat distribution with controlled drying that maintains cellular structures. **The adhesiveness** of the dried samples, defined as the amount of force needed to counteract the attractive forces between the sample and its contact surface, exhibited considerable variation. The range encompassed -0.172 g·sec in RWU samples to -5.76 g·sec in TU samples. **Springiness** is a measure of the ability of a sample to return to its original shape after deformation. For this sample springiness ranges were observed from 0.044 in VP-dried samples to 0.145 in IR-RWP samples. **Cohesiveness,** representing the internal bonding strength of a material, varied from 0.03 in VP samples to 0.166 in IR-RWP samples. **Gumminess,** which combines cohesiveness and stickiness, was observed in the range of 161.10 g for VP samples to 527.44 g for RWP samples. **Chewiness,** a derived property combining hardness, cohesiveness, and flexibility, indicates the effort required to masticate the sample to a swallowable state. The values ranged from 10.28 g in VP samples to 46.41 g in RWP samples. Lastly, **resilience,** a measure of the sample's energy recovery capacity after compression, ranged from 0.014 in VP-dried samples to 0.05 in IR-RWP samples.

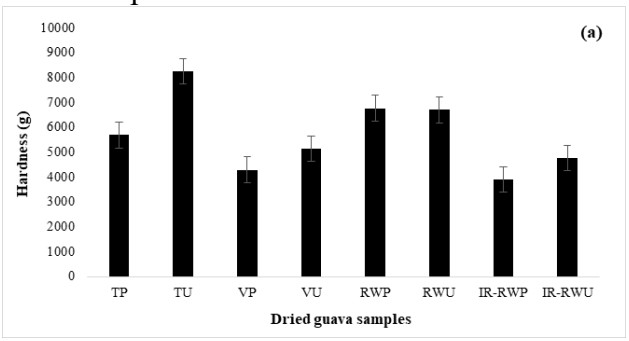

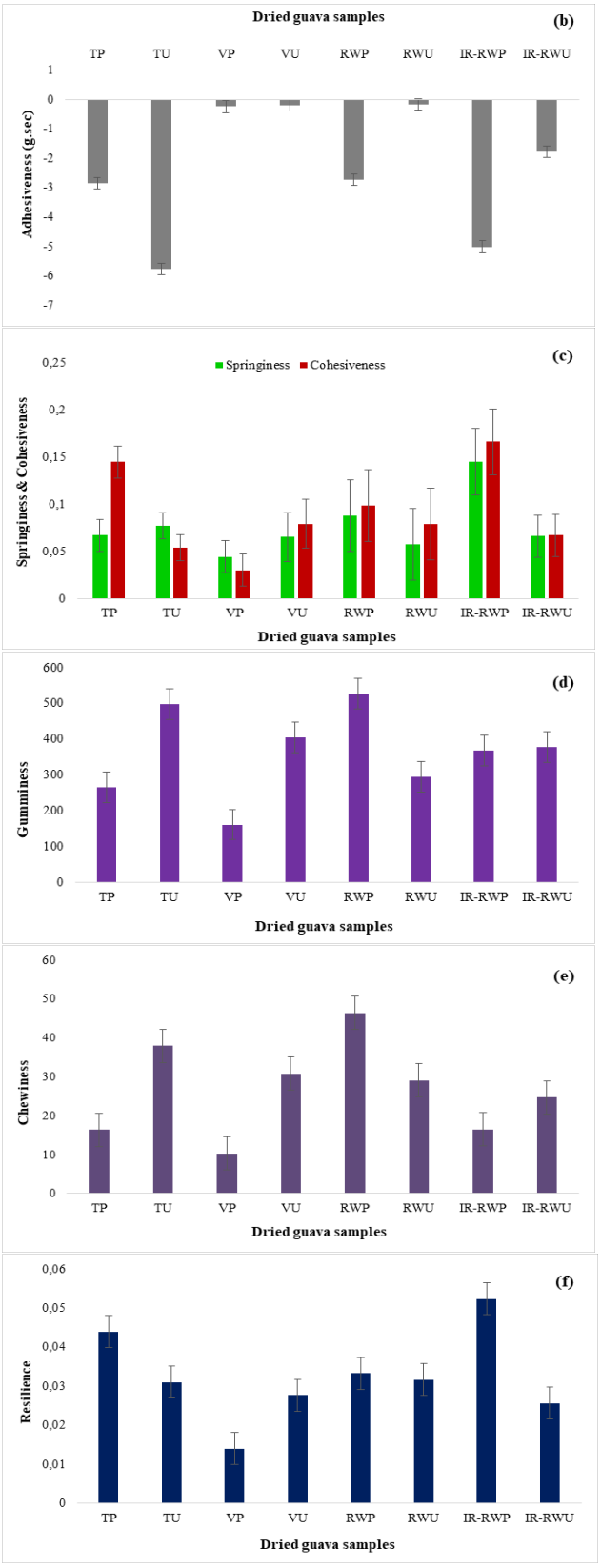

Figure 2. Textural parameter values of peeled and unpeeled dried guava obtained by various dehydration techniques **(a)** hardness **(b)**adhesiveness **(c)** Springiness&cohesiveness **(d)** gumminess **(e)** chewiness **(f)** resilience

3.5. Bulk density and Rehydration ratio (RR)

Table 1 provides detailed bulk density values for different samples. The bulk density of the dried samples indicated substantial differences across drying techniques and sample categories. TP and VP samples had the greatest bulk density values of 640 g/cm³, which were statistically comparable to the TU sample. TU samples had a somewhat reduced bulk density of 620 g/cm³ in comparison to TP and VP. The lowest bulk density values were recorded in the RWU and RWP samples, which was 430 g/cm³. The reduced bulk density in RWP, RWU, IR-RWU, and IR-RWP is primarily due to the gentle drying processes that maintain porosity and cellular integrity, hence decreasing the compactness of the final product.

The RR measures the capacity of dried samples to absorb water and recover their original structure, revealing the integrity and porosity of the dry matrix. The higher RR measured in RWU and RWP (3.41 and 2.94, respectively) indicate improved water absorption capacity, presumably due to better porosity and structural integrity throughout the drying process. In contrast, the lowest RR was observed in TP and TU, with values of 1.96 and 1.97, respectively. This is due to the denser structure and lower porosity of samples that undergo tray drying, which restricts access to water during rehydration.

3.6. Ascorbic Acid

Among the dried guava samples, the total ascorbic acid level varied between 67.5 mg/100g and 92.3 mg/100g as shown in Table 1. The RWU sample had the greatest ascorbic acid content. TP sample showed the lowest concentration of ascorbic acid of 67.5 mg/100g. It was also determined that the TU sample had 72.5 mg/100g of ascorbic acid. The ascorbic acid content is extremely responsive to light, oxygen, pH, heat, and other specific environmental factors (Horuz, Bozkurt, Karataş, & Maskan, 2017). The substantial decrease in ascorbic acid concentration in TP and TU samples can be attributed to the direct contact of heat medium and extended periods of drying. Analysis revealed that the VP and VU samples contained 84.2 mg/100g and 85.4 mg/100g of ascorbic acid, respectively. The RWP sample had 91.3 mg/100g of ascorbic acid. The concentrations of 86.8 mg/100g and 92.1 mg/100g were observed in the IR-RWP and IR-RWU samples, respectively. The slightly lower values of ascorbic acid in IR samples might be due the IR radiation. Analysis revealed that the unpeeled samples had a higher concentration of ascorbic acid in comparison to the peeled samples. The elevated levels of AA in the guava peel may account for this observation (Contreras-Calderón et al. 2011). Very closed values of ascorbic acid content in guava sample was also reported by Lim et al. (2007) and Leiton-Ramírez et al. (2020).

3.7. TPC

The IR-RWU dried guava was found to have the highest concentration of TPC of 205.1 mg GAE/100g as shown in Table 1. TPC was observed lowest in the TP sample, with 147.5 mg GAE/100g. While the TU sample had TPC values of 152.8 mg GAE/100g. In the IR-RWP sample, the GAE content was 184.6 mg/100g. The RWP and RWU samples had 172.7 mg of GAE per 100g and 195.5 mg of GAE per 100g, respectively. Higher retention of TPC in RW-dried guava than in tray and vacuum-dried samples could be attributed to the liberation of phenolics bound to the cellular structure of the dehydrated sample as a result of rapid heating and lower drying time (Rajoriya, Bhavya, & Hebbar, 2023). The presence of significant quantities of phenolic chemicals in guava peels may explain the elevated levels of TPC observed in unpeeled sample (Marina, Z; Noriham, 2014).

3.8. TFC

The range of values observed was 496.5 mg QE/100g (TP) to 645.4 mg QE/100g (IR-RWU), as depicted Table 1. The analysis showed that the TU and IR-RWP samples had 501.4 mg QE/100g and 638.6 mg QE/100g of TFC, respectively. The values of VP (511.4 mg QE/100g) and VU (521.3 mg QE/100g) were determined to be moderate, and no significant difference was observed. Zhang et al. (2024) observed similar trends for the jamun pulp. RW drying is a relatively gentle drying technique with less drying time thus

retaining high TFC.Liu et al. (2018) observed that guava peel contained significant flavonoid content. Higher readings of TFC in unpeeled samples may be attributed to this reason.

3.9. Antioxidant activity

The antioxidant activity of the dehydrated samples was assessed through DPPH radical scavenging activity. The % inhibition was observed to vary between 89.58% (TP) to 98.24% (IR-RWU) shown in Table 1. The IR-RWU sample was found to have the highest antioxidant capacity due to it having high amounts of TPC and TFC. TP sample had the lowest antioxidant activity because of having low amounts of TPC and TFC. The elevated temperature of 60°C in a tray, vacuum, RW, and IR-RW dryers may have induced the degradation of cell components (Dadhaneeya et al., 2023b). In addition, the thermal inactivation of oxidative enzymes could have may have impeded the breakdown of antioxidant constituents, resulting in increased retention (Liang et al., 2018). Additionally, both enzymatic and non-enzymatic browning may have contributed to higher retention (Liang et al., 2018; Jogihalli et al., 2017).

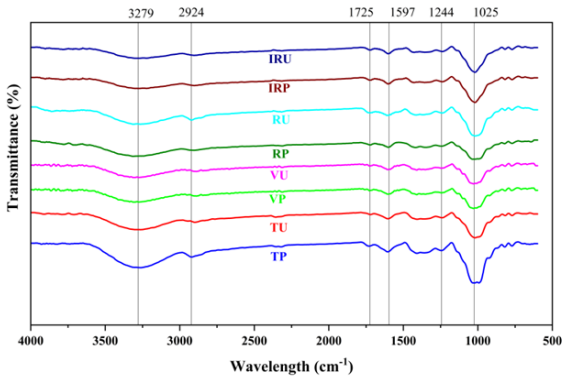

a)

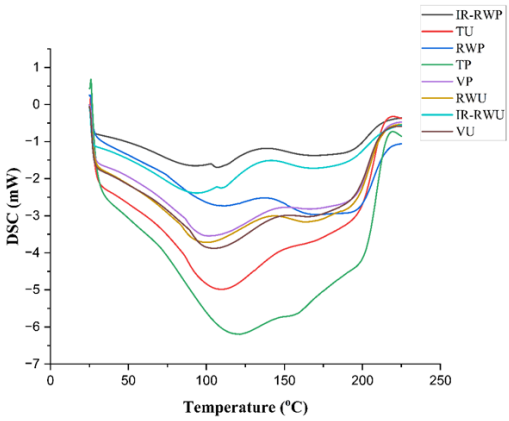

b)

Figure 3. (a) FTIR graph of dried guava samples **(b)** DSC curves of guava powders

3.10. FTIR

FTIR spectra of peeled and unpeeled guava powder obtained by varying drying methods are displayed in Figure 3(a). using Fourier transform infrared spectroscopy (FTIR). The powders exhibited six notable absorbance peaks. These peaks were observed at 3279 cm^{-1} (a strong peak) and within the range of 3280-3297 cm^{-1}, respectively. These peaks are indicative of OH bonds and are attributable to the presence of carbohydrates, proteins, alcohols, and phenolic chemicals. At this point deeper peak means stronger absorption was observed in TP and TU sample. Due to longer hot-air exposure can promote polymerization, crosslinking or condensation reactions (e.g., Maillard-type products, caramelization) that produce new hydroxyl-rich polymeric species with strong OH absorptions (Han et al. 2017). Elongated C-O bonds were detected at 1025 cm^{-1} in the 1025-1231 cm^{-1} range, which is a distinctive band associated with lignin, anhydride or alcohol, and phenols. A peak at 1725 cm^{-1} exhibited C = O stretches. The peak at 2924 cm^{-1} exhibited CH_2 asymmetrical stretching bands 2856-2928 cm^{-1}, indicating the presence of lipids, proteins, carbohydrates, and nucleic acids. The peak observed at 1244 cm^{-1} corresponds to the C = O stretching vibration within the bands 1237-1745 cm^{-1}. These bands are indicative of the presence of phospholipid, cholesterol ester, hemicellulose, pectin and lignin. The peak at 1597 cm^{-1} may be attributed to C = C and N-H bonds, indicating the existence of amide II structures, primarily in

proteins.Athmaselvi et al. (2014) reported similar peaks in the FTIR study of freeze-dried guava.

3.1.1. Thermal Analysis

The DSC curves (Figure 3b) exhibit a broad endothermic peak for all the dried powders. The peaks were obtained at 121.04℃, 109.52℃, 101.50℃, 104.46℃, 111.40℃, 99.98℃, 92.85℃ and 93.78℃ for TP, TU, VP, VU, RWP, RWU, IR-RWP and IR-RWU samples respectively. Comparable findings were reported by Osorio et al. (2011) for hot air-dried and lyophilized guava powder. The complex endothermic peaks encompass the volatilization of water, the melting of pectin found in guava, and potential demethylation, dihydroxylation, and decarboxylation of pectin and other polysaccharides (Athmaselvi et al., 2014). The TP sample shows an intense peak, causing a larger heat flow leading to a lower thermal stability of the sample. By contrast, IR-RW sample showed the lowest peak temperatures, suggesting earlier onset of structural transitions. The intermediate peak values of the vacuum-dried and refractance window-dried samples indicate moderate thermal resistance. These findings align with earlier observations in fruit polysaccharide systems, where different drying techniques significantly shifted DSC peak temperatures, reflecting altered molecular interactions and stability (Zhang et al., 2024).

3.12. Microstructure and Energy Dispersive Spectroscopy

Figure 4 exhibits Scanning Electron Microscopy (SEM) pictures of dried guava samples subjected to various drying techniques and conditions, offering a comprehensive view of their microstructures. The SEM images of the TP sample exhibit relatively smooth and compact structures, which indicate less presence of irregularities. The TU sample exhibits greater irregularity than the TP sample, showing visible cracks and larger particle aggregation. The peel is likely to contribute to heterogeneity in the drying process. The VP sample structure exhibits a flaky texture characterized by low porosity. The VD conditions appear to maintain structural integrity while minimizing shrinkage effects. The VU sample displays more pronounced fibrous structures, suggesting the peel's impact on the drying process. The RWP surface exhibits a rough texture with few cracks present. The RWD technique produces a denser texture relative to tray drying, while maintaining surface smoothness. The microstructure of RWU exhibits improved fibrous networks characterized by greater irregularities in comparison to RWP. This indicates that the peel substantially influences the structural configuration during this drying process. The surface morphology of IR-RWP is predominantly smooth, exhibiting minimal porous regions. The incorporation of infrared heat in RWD enhances moisture removal while preserving surface integrity. Shende & Datta (Shende & Datta, 2019) reported similar results of microstructure of mango powder. Infrared-assisted drying improves moisture removal, resulting in more pronounced textural features in unpeeled samples. Peeled samples demonstrate smoother and more uniform textures relative to their unpeeled counterparts, as the presence of the peel results in heightened surface irregularities.

Table 2 displays the weight % of carbon (C), oxygen (O), aluminum (Al), and potassium (K) in several dried guava samples examined by Scanning Electron Microscopy with Energy Dispersive Spectroscopy (SEM-EDS). The carbon content in all samples is mostly uniform, with minor increases seen in unpeeled samples (e.g., RWU and IR-RWU). The oxygen % increases in TD and RWD samples, with minor decreases seen in VD and IR- RWD samples. Aluminum concentration is negligible, with the maximum amount (0.5%) seen in VP and RWU. The potassium level exhibits fluctuation, with the greatest percentage recorded in IR-RWU (2.9%) and the lowest in TU and RWP (1.8%) sample. These data could influence the selection of drying techniques for maximum nutrient retention in guava processing.

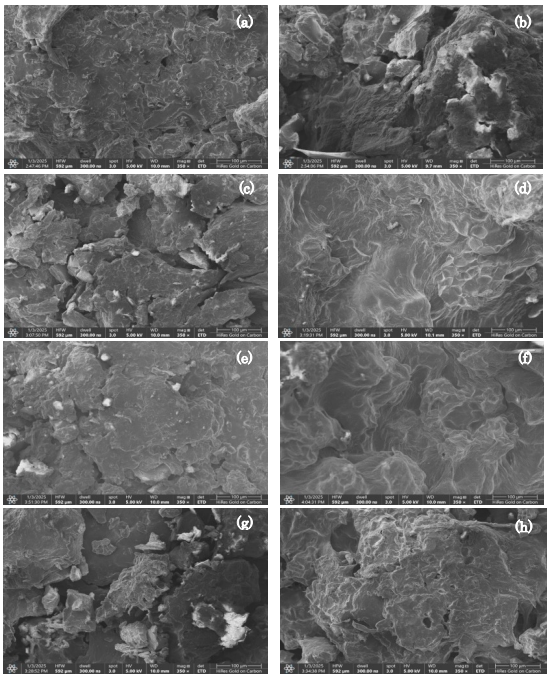

Figure 4 SEM images of Guava sample **(a)** TP **(b)** TU **(c)** VP **(d)** VU **(e)** RWP **(f)** RWU **(g)** IR-RWP **(h)** IR-RWU sample

Table 2. Elemental Composition of Dried Guava Samples through Energy Dispersive Spectroscopy

	Weight in percentage			
	C	**O**	**Al**	**K**
TP	33.7	63.6	0.3	2.1
TU	33	63.6	0.1	1.8
VP	33.3	58.4	0.5	2.4
VU	33.9	61.4	0.3	2.5
RWP	33.2	63.9	0.2	1.8
RWU	35.1	61.4	0.5	2.2
IR-RWP	33.5	63.1	0.3	2.6
IR-RWU	34.1	61.5	0.3	2.9

3.13. Analytic of quantitative data using multivariate analysis techniques

PCA is a statistical method that decreases the dimensionality of a dataset while retaining the most significant details (Subrahmanyam et al., 2024). The resulting biplot can be displayed in Figure 5. The PCA biplot presented separate groupings of samples in each of the four quadrants clearly and concisely, which indicates significant differences between entities. The biplot reveals that RWP, RWU, and IR-RWP are situated in the upper right quadrant of the plots, with chroma, BI, Ascorbic Acid, and TFC. This indicates that these attributes are more strongly preserved in those specified treatments. TP and TU were closely positioned alongside pH and bulk density on the contrary side, exhibiting higher values in the aforementioned samples. Although the VU sample was also located in the same quadrant. However, it is far from the pH and bulk density characteristics. The close proximity of the RWU samples to RR, Ascorbic Acid, and TFC indicates that these particular treatments have the highest retention of physicochemical attributes. The RWP sample exhibits a strong correlation with the chroma characteristic, indicating a substantial amount of this property in the RWP sample. IR-RWU is located in the bottom right quadrants alongside the TSS, AA, TPC, and Hue, which is the precise reason for the better preservation of these attributes in the IR-RWU sample. The results of the PCA analysis align with the theoretical analysis offered in the present article.

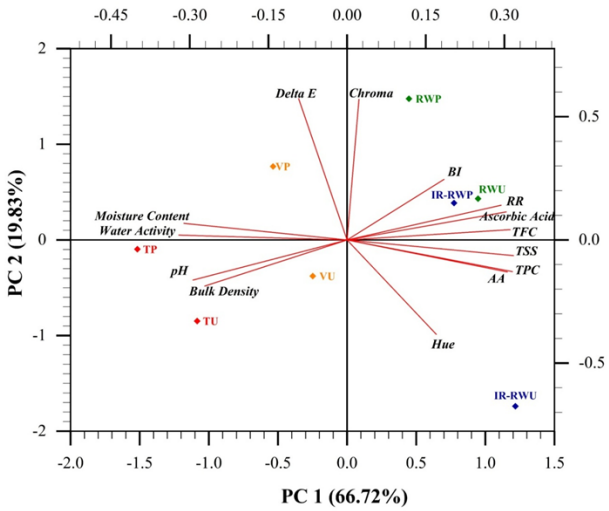

Figure 5. Biplot for multivariate analysis

4. Conclusions

Infrared refractance window drying is a novel and potentially advantageous technique for drying guava. In the current study we observed that among various drying techniques, the IR-

RW method has emerged as a superior method, offering a significantly reduced drying time of just 300 minutes. Experimental results demonstrated that the IR-RWD technique not only reduced the drying time but also excelled in preserving the physicochemical properties of guava. The TPC was observed 205.1 mg GAE/100g, TFC was observed 645.4 mg QE/100g, and ascorbic acid was 92.17 mg/100g in the IR-RW dried samples. The IR-RWD samples exhibited approximately 15% higher TPC, 20% higher TFC, 4% higher Antioxidant Activity, and 25% higher Ascorbic Acid content compared to the traditional drying techniques, such as tray drying and vacuum drying. An SEM analysis reveals the microstructural differences resulting from various drying techniques and peeling conditions, concluding that the peeled samples display smoother and more uniform textures than their unpeeled equivalents. The study concluded that IR-RWD technique ensures better retention of nutrients and antioxidants, better structural integrity, superior color, texture, and overall physical properties of the dried guava sample. This makes IR-RWD a highly effective method for making guava powder. These findings can act as a guide for selecting the best drying technology for guava powder.

5.References

Abul-Fadl, M. M., & Ghanem, T. H. (2011). Effect of Refractance-window (RW) drying method on quality criteria of produced tomato powder as compared to the convection drying method. *World Applied Sciences Journal*, *15*(7), 953–965.

AOAC. (1968). *AOAC Method-Ascorbic-Ac 967 21*.

Athmaselvi, K. A., Kumar, C., Balasubramanian, M., & Roy, I. (2014). Thermal, Structural, and Physical Properties of Freeze Dried Tropical Fruit Powder. *Journal of Food Processing*, *2014*, 1–10. https://doi.org/10.1155/2014/524705

Baeghbali, V., Niakousari, M., & Farahnaky, A. (2016a). Refractance Window drying of pomegranate juice: Quality retention and energy efficiency. *LWT - Food Science and Technology* *66*, 34–40. https://doi.org/10.1016/j.lwt.2015.10.017

Baeghbali, V., Niakousari, M., & Farahnaky, A. (2016b). Refractance Window drying of pomegranate juice: Quality retention and energy efficiency. *LWT - Food Science and Technology*, *66*, 34–40. https://doi.org/10.1016/j.lwt.2015.10.017

Carvalho Gualberto, N., Santos de Oliveira, C., Pedreira Nogueira, J., Silva de Jesus, M., Caroline Santos Araujo, H., Rajan, M., … Narain, N. (2021). Bioactive compounds and antioxidant activities in the agro-industrial residues of acerola (Malpighia emarginata L.), guava (Psidium guajava L.), genipap (Genipa americana L.) and umbu (Spondias tuberosa L.) fruits assisted by ultrasonic or shaker extracti. *Food Research International*, *147*(March). https://doi.org/10.1016/j.foodres.2021.110538

Contreras-Calderón, J., Calderón-Jaimes, L., Guerra-Hernández, E., & García-Villanova, B. (2011). Antioxidant capacity, phenolic content and vitamin C in pulp, peel and seed from 24 exotic fruits from Colombia. *Food Research International*, *44*(7), 2047–2053. https://doi.org/10.1016/j.foodres.2010.11.003

Dadhaneeya, H., Kesavan, R. K., Inbaraj, B. S., Sharma, M., Kamma, S., Nayak, P. K., & Sridhar, K. (2023a). Impact of Different Drying Methods on the Phenolic Composition , In Vitro Antioxidant Activity , and Quality Attributes of Dragon Fruit Slices and Pulp. *MDPI Foodsfoods*, *12*, 1387. https://doi.org/10.3390/foods12071387

Dadhaneeya, H., Kumar, P., Saikia, D., Kondareddy, R., & Ray, S. (2023b). The impact of refractance window drying on the physicochemical properties and bioactive compounds of malbhog banana slice and pulp. *Applied Food Research*, *3*, 100279. https://doi.org/10.1016/j.afres.2023.100279

Dadhaneeya, H., Nema, P. K., & Arora, V. K. (2023c). Internet of Things in food processing and its potential in Industry 4 . 0 era : A review. *Trends in Food Science &*

Technology, *139*(July), 1–14. https://doi.org/10.1016/j.tifs.2023.07.006

Dadhaneeya, H., Nema, P. K., Arora, V. K., Balasaheb, S., & Pawar, K. R. (2024). Smart next-gen drying solution: A study of design, development and performance evaluation of IoT- enabled IR-assisted refractance window dryer. *Drying Technology*, *42*(15), 2212–2231. https://doi.org/10.1080/07373937.2024.2415422

Dadhaneeya, H., Nema, P. K., & Warepam, S. C. (2025). Advanced Modeling Approaches for Quality Assessment of Papaya Leather Dried in IoT- - Enabled IR- - Assisted Refractance Window Dryer. *Journal of Food Process Engineering*, *48*(2), e70059. https://doi.org/10.1111/jfpe.70059

Desai, S., Upadhyay, S., Sharanagat, V. S., & Nema, P. K. (2023). Physico-functional and quality attributes of microwave-roasted black pepper (Piper nigrum L.). *International Journal of Food Engineering* , *19*(11), 561–572. https://doi.org/10.1515/ijfe-2023-0207

Dhua, S., Kheto, A., Singh Sharanagat, V., Singh, L., Kumar, K., & Nema, P. K. (2021). Quality characteristics of sand, pan and microwave roasted pigmented wheat (Triticum aestivum). *Food Chemistry*, *365*(June), 130372. https://doi.org/10.1016/j.foodchem.2021.130372

Dissa, A. O., Desmorieux, H., Bathiebo, J., & Koulidiati, J. (2008). Convective drying characteristics of Amelie mango (Mangifera Indica L. cv. 'Amelie') with correction for shrinkage. *Journal of Food Engineering*, *88*(4), 429–437. https://doi.org/10.1016/j.jfoodeng.2008.03.008

Flores, G., Wu, S. B., Negrin, A., & Kennelly, E. J. (2015). Chemical composition and antioxidant activity of seven cultivars of guava (Psidium guajava) fruits. *Food Chemistry*, *170*, 327–335. https://doi.org/10.1016/j.foodchem.2014.08.076

Han, M. M., Yi, Y., Wang, H. X., & Huang, F. (2017). Investigation of the Maillard reaction between polysaccharides and proteins from longan pulp and the improvement in activities. *Molecules*, *22*(6),5–8. https://doi.org/10.3390/molecules22060938

Hasan, M. M., El-Badry, N., Ghanem, T. H., & Nasr, A. (2024). Quality attributes of dried guava pulp using refractance window Vs. hot air drying. Journal of Agricultural Research V, 49(2), 34–49.

Horuz, E., Bozkurt, H., Karataş, H., & Maskan, M. (2017). Effects of hybrid (microwave-convectional) and convectional drying on drying kinetics, total phenolics, antioxidant capacity, vitamin C, color and rehydration capacity of sour cherries. *Food Chemistry*, *230*, 295–305. https://doi.org/10.1016/j.foodchem.2017.03.046

Jain, P. K., Jain, P., & Nema, P. K. (2011). Quality of guava and papaya fruit pulp as influenced by blending ratio and storage period. *American Journal of Food Technology*, *6*, 507–512.

Jogihalli, P., Singh, L., & Sharanagat, V. S. (2017). Effect of microwave roasting parameters on functional and antioxidant properties of chickpea (Cicer arietinum). *Lwt*, *79*, 223–233. https://doi.org/10.1016/j.lwt.2017.01.047

Kardile, N. B., Nema, P. K., Kaur, B. P., & Thakre, S. M. (2019). A Comparative Study of Suitability of Low-Density Polyethylene and Coextruded Laminate Pouches for Storage Stability and Shelf Life Prediction of Instant Puran Powder. *Journal of Packaging Technology and Research*, *3*(3), 223–233. https://doi.org/10.1007/s41783-019-00071-y

Kardile, N. B., Nema, P. K., Kaur, B. P., & Thakre, S. M. (2020). Comparative semi-empirical modeling and physico-functional analysis of hot-air and vacuum dried puran powder. *Journal of Food Process Engineering*, *43*(1), 1–11. https://doi.org/10.1111/jfpe.13137

Kheto, A., Dhua, S., Nema, P. K., & Sharanagat, V. S. (2021). Influence of drying temperature on quality attributes of bell pepper (Capsicum annuum L.): Drying kinetics and modeling, rehydration, color, and antioxidant analysis. *Journal of Food Process Engineering,* e13880. https://doi.org/10.1111/jfpe.13880

Kumar, S., Tiwari, P., & Zymbler, M. (2019). Internet of Things is a revolutionary approach for future technology enhancement: a review. *Journal of Big Data*, *6*(1). https://doi.org/10.1186/s40537-019-0268-2

Leiton-Ramírez, Y. M., Ayala-Aponte, A., & Ochoa-Martínez, C. I. (2020). Physicochemical properties of guava snacks as affected by drying technology. *Processes*, *8*(1), 1–12. https://doi.org/10.3390/pr8010106

Liang, L. C., Zzaman, W., Yang, T. A., & Easa, A. M. (2018). Effect of conventional and superheated steam roasting on the total phenolic content, total flavonoid content and DPPH radical scavenging activities of black cumin seeds. *Pertanika Journal of Tropical Agricultural Science*, *41*(2), 663–676.

Lim, Y. Y., Lim, T. T., & Tee, J. J. (2007). Antioxidant properties of several tropical fruits: A comparative study. *Food Chemistry*, *103*(3), 1003–1008.
https://doi.org/10.1016/j.foodchem.2006.08.038

Liu, X., Yan, X., Bi, J., Liu, J., Zhou, M., Wu, X., & Chen, Q. (2018). Determination of phenolic compounds and antioxidant activities from peel, flesh, seed of guava (Psidium guajava L.). *Electrophoresis*, *39*(13), 1654–1662. https://doi.org/10.1002/elps.201700479

Marina, Z; Noriham, A. (2014). Quantification of total phenolic compound and in vitro antioxidant potential of fruit peel extracts. *International Food Research Journal*, *21*(5), 1925–1929.

Mella, C., Vega-Gálvez, A., Uribe, E., Pasten, A., Mejias, N., & Quispe-Fuentes, I. (2022). Impact of vacuum drying on drying characteristics and functional properties of beetroot (Beta vulgaris). *Applied Food Research*, *2*(1), 100120. https://doi.org/10.1016/j.afres.2022.100120

Nagy S. and Shaw E. P. (1985). Guava : An exotic fruit with potential in Queensland. *Queensland Agricultural Journal*, (January 1985), 93–98.

Naseer, S., Hussain, S., Naeem, N., Pervaiz, M., & Rahman, M. (2018). The phytochemistry and medicinal value of Psidium guajava (guava). *Clinical Phytoscience*, *4*(1). https://doi.org/10.1186/s40816-018-0093-8

Nemzer, B., Vargas, L., Xia, X., Sintara, M., & Feng, H. (2018). Phytochemical and physical properties of blueberries, tart cherries, strawberries, and cranberries as affected by different drying methods. *Food Chemistry*, *262,* (April), 242–250.
https://doi.org/10.1016/j.foodchem.2018.04.047

Osorio, C., Carriazo, J. G., & Barbosa, H. (2011). Thermal and structural study of guava (Psidium Guajava L) powders obtained by two dehydration methods. *Quimica Nova*, *34*(4), 636–640. https://doi.org/10.1590/S0100-40422011000400016

Rajoriya, D., Bhavya, M. L., & Hebbar, H. U. (2023). Far infrared assisted refractance window drying : Influence on drying characteristics and quality of banana leather. *Drying Technology*, *41*(13), 2143–2155. https://doi.org/10.1080/07373937.2023.2220777

Sharanagat, V. S., Suhag, R., Anand, P., Deswal, G., Kumar, R., Chaudhary, A., … Nema, P. K. (2019). Physico-functional, thermo-pasting and antioxidant properties of microwave roasted sorghum [Sorghum bicolor (L.) Moench]. *Journal of Cereal Science*, *85*(July 2018), 111–119. https://doi.org/10.1016/j.jcs.2018.11.013

Shende, D., & Datta, A. K. (2019). Optimization study for refractance window drying process of Langra variety mango. *Journal of Food Science and Technology*. https://doi.org/10.1007/s13197-019-04101-0

Subrahmanyam, K., Gul, K., Paridala, S., Sehrawat, R., More, K. S., Dwivedi, M., & Jaddu, S. (2024). Effect of cold plasma pretreatment on drying kinetics and quality

attributes of apple slices in Refractance window drying. *Innovative Food Science and Emerging Technologies*, *92* (December 2023), 103594. https://doi.org/10.1016/j.ifset.2024.103594

Zhang, Q., Pertin, O., Kamdi, H. S., Durgawati, Xiao, H. W., & Sutar, P. P. (2024). Modified refractance window drying of jamun pulp (Syzygium cumini) based on innovative infrared and microwave radiation techniques . *Drying Technology*, *42*(5), 1–20. https://doi.org/10.1080/07373937.2024.2317739

Zhou, Y. H., Pei, Y. P., Sutar, P. P., Liu, D. H., Deng, L. Z., Duan, X., … Xiao, H. W. (2022). Pulsed vacuum drying of banana: Effects of ripeness on drying kinetics and physicochemical properties and related mechanism. *LWT - Food Science and Technology*, *161*(March), 113362. https://doi.org/10.1016/j.lwt.2022.113362

Acknowledgments.

The authors are thankful to the National Institute of Food Technology Entrepreneurship and Management, Sonipat, Haryana (NIFTEM-K), for their support and for providing a laboratory facility to carry out this research (NIFTEM communication reference number NIFTEM-P-2025-010). The authors also acknowledge UGC-DAE CSR, Indore for carrying out measurements of DSC, SEM and SEM-EDS.

CARPATHIAN JOURNAL OF FOOD SCIENCE AND TECHNOLOGY

journal homepage: **http://chimie-biologie.ubm.ro/carpathian_journal/index.html**

Research article

ENHANCEMENT OF ANTIOXIDANT ACTIVITY, NUTRITIONAL COMPOSITION, AND CRUDE FIBER CONTENT IN MILKFISH SAUSAGE (*Chanos chanos*) THROUGH ADDITION OF MORINGA LEAF POWDER AND FRESH MORINGA LEAVES

Dyah Ilminingtyas Wahyu Handayani[1], Laurentinus Laki[1], Fatma Puji Lestari[1]✉, Selma Mutiarahma[1], Ahmad Ni'matullah Al-Baarri[2], Lutfi Purwitasari[2]

[1] *Faculty of Agricultural Technology, University of 17 Agustus 1945 Semarang, Central Java, Indonesia*
[2] *Department of Food Technology, Faculty of Animal and Agricultural Sciences, Diponegoro University, Semarang, Central Java, Indonesia*
✉ *fatma-pujilestari@untagsmg.ac.id*
https://orcid.org/0000-0002-6368-2024

https://doi.org/10.34302/2025.17.3.10

Article history:
Received
June 16th , 2025
Accepted
October 25th, 2025

Keywords
Moringa leaves;
Milkfish sausage;
Antioxidant activity;
Nutritional composition;
Functional food.

Abstract
This study investigates the impact of Moringa leaf powder and fresh Moringa leaves (*Moringa oleifera* L.) on the antioxidant activity, chemical composition, and crude fiber content of milkfish (*Chanos chanos*) sausage. Milkfish is valued for its high protein and omega-3 content but poses challenges in processing due to its numerous fine bones. Sausage production offers an effective way to debone and transform milkfish into a convenient and versatile food product. Incorporating Moringa leaves enhances its nutritional profile, as Moringa is rich in essential vitamins, minerals, protein, and antioxidants that provide various health benefits. This study employed a completely randomized design with three treatments: a control (K0), 6% Moringa leaf powder (K1), and 12% fresh Moringa leaves (K2), each replicated three times. Antioxidant activity was measured using the DPPH method, with data analyzed through one-way ANOVA followed by Duncan's Multiple Range Test at a 5% significance level. Results showed that both Moringa leaf powder and fresh leaves significantly increased antioxidant activity, with values of 0.7112% (K0), 16.8424% (K1), and 17.0608% (K2). The proximate composition and crude fiber content also improved significantly, demonstrating the potential of Moringa-fortified milkfish sausage as a functional food.

1. Introduction

Milkfish (*Chanos chanos*) is highly nutritious fish widely cultivated in aquaculture due to its rich in essential nutrition for human health. It contains a significant amount of amino acids such as leucine (8%), lysine (7,3%), phenyl alanine (6,7%) and histidine (6,1%) (Murthy et al., 2016). Additionally, milkfish is a good source of unsaturated fatty acids (50,74%) of which monounsaturated fatty acids (MUFAs)

like oleic acid, as well as polyunsaturated fatty acids (PUFAs) like palmitic acid and oleic acid (Nopiyanti et al., 2023). It also contains significant amounts of vitamins (A, B1, B12) and minerals such as calcium, magnesium, and potassium, making it a valuable dietary component (Malle et al., 2019). However, the presence of numerous fine bones in milkfish poses a challenge for direct consumption, limiting its culinary applications and consumer appeal. Processing milkfish into sausage offers an innovative solution, transforming it into a convenient, boneless product suitable for diverse culinary uses especially fulfilling consumer desires (Yusuf et al., 2018).

Sausages are versatile and boneless product, functions as an alternative product innovation to expand the application of milkfish in the development of functional foods. Enhancing milkfish sausage functional benefits could be done by incorporating with bioactive ingredients. Moringa leaves are rich in protein (25%), vitamins (A, C, E), minerals (calcium, potassium, iron), and bioactive compounds such as phenolics and flavonoids, which exhibit potent antioxidant activity (González-Burgos et al., 2021). This antioxidant can improve the shelf life by delaying lipid oxidation and enhancing the physicochemical and sensory properties of fish product (Mashau et al., 2021). Given these advantages, moringa leaf is an attractive ingredient for milkfish sausage production, providing health benefits and enhancing product stability.

Moringa leaves are widely recognized for their antioxidant properties that play a critical role in human health by neutralizing free radicals. In Indonesia, moringa leaves were often used as medicinal ingredients for conditions such as colds, improving breast milk production, reducing fever, and treating gout. Additionally, they were utilized as food ingredients in dishes such as clear vegetable soup, stir-fried dishes, and crackers (Khasanah et al., 2023). Antioxidants are essential in reducing oxidative stress, which is linked to chronic diseases such as cancer, diabetes, and cardiovascular disorders. The high levels of polyphenols, flavonoids, and other bioactive compounds in moringa leaves contribute to their strong antioxidant activity, helping to protect cells and tissues from damage caused by free radicals (Segwatibe et al., 2023). Besides that, phenolic content also can be act as an antimicrobial in food (Swastawati et al., 2019). It was reported that moringa leaves acted as antioxidants that inhibited free radicals, increased glutathione, which served as a radioprotective agent, and inhibited lipid peroxidation induced by radiation (Amalia et al., 2024; Sabrina et al., 2024). The consumption of moringa leaves containing flavonoids was also reported to help reduce worker fatigue levels by increasing glutathione peroxidase levels (Prasetio et al., 2023). Fortified fish products incorporating moringa leaf flour have shown significant improvements in nutritional quality and consumer acceptability. Research indicates that the addition of moringa leaf flour to tilapia nuggets enhances protein content by 0.5-13.18% and increases vitamin A levels (β-carotene) from 1.82 to 20.76% (Sagita et al., 2024). Studies has shown the physicochemical properties of catfish sausage fortified with moringa leaf flour also reflect enhanced nutritional profiles, with protein content reaching 18.09% (Rahayu et al., 2022).

Given the growing demand for natural antioxidants and functional foods, this study aims to evaluate the effect of Moringa leaf powder and fresh Moringa leaves on the antioxidant activity, proximate composition, and crude fiber content of milkfish sausage. By leveraging the bioactive compounds in Moringa leaves, the research seeks to develop a nutrient-dense and health-promoting functional food product that meets consumer preferences and contributes to sustainable food innovation.

2. Materials and methods

2.1. Research Design

The study employs an experimental laboratory approach using a Completely Randomized Design (CRD) to assess the impact of various concentrations and forms of Moringa leaf on milkfish sausage. This design includes three treatments: a control group (K0) without Moringa leaves, a 6% Moringa leaf powder

addition (K1), and a 12% fresh Moringa leaves addition (K2). Each treatment is replicated three times, resulting in nine experimental units. The CRD structure minimizes potential biases, allowing observed variations to be attributed directly to the effects of Moringa leaf treatments rather than to external factors, thereby supporting rigorous statistical analysis.

2.2. Methods

2.2.1. Sample Preparation

Fresh milkfish was obtained from ponds in Tugu District, Semarang, Central Java, Indonesia. Fish transportation was used styrofoam box with ice cube to maintain the freshness. The processing of milkfish begins with fish weeding where the scales and internal organs are removed and separating the meat from the bones, spines, skin and head. The filleted meat is washed using clean water to eliminate any remaining impurities, and the residual water is discarded. Milkfish fillet was grinded with ice for 10 minutes and stored in a freezer to preserve its quality and freshness.

2.2.2. Moringa Leaf Preparation

Moringa leaf powder supplied by PT. Moringan Organik Indonesia and fresh Moringa leaves sourced locally. The fresh moringa leaves were sorted and removed the stalk. The leaves were cleaned, blanched at 80°C for 3 minutes, and finely ground.

2.2.3. Milkfish Sausage Making

The milkfish paste was mixed with the Moringa leaves as treatment (K1 and K2), along with other ingredients such as tapioca flour, MSG, and spices (Table 1). Each blend was stuffed into sausage casings. The sausages were then immersed in ice water at 11-17°C for 60 minutes and hot water sequentially at 60°C for 10 minutes to solidify the texture and enhance flavor. Boiling process was carried out at 90°C for 10 minutes.

Table 1. Milkfish sausage formulation

Ingredients	Amount
Milkfish fillet	200 g
Tapioca flour	20 g
Sugar	3,6 g
Cooking oil	5 g
Monosodium glutamate	1,5 g
Salt	4 g
Garlic	3 g
Red onion	6 g
Nutmeg	0,25 g
Coriander	1 g
Pepper	1 g
Ginger	1 g
egg	1 pcs
Ice cube	60 g

2.2.4. Proximate Composition

The proximate composition of milkfish sausage was performed by using (AOAC, 1990) method. The analysis including carbohydrate, moisture, protein, fat, crude fibre and ash content, was determined using the following methods: by difference, a hot air oven (105°C), the Kjeldahl method, a Soxhlet apparatus, gravimetric and a furnace (550°C), respectively.

2.2.5. Antioxidant Analysis

The data were analyzed statistically using one-way Analysis of Variance (ANOVA) to detect significant differences between treatments at a 5% significance level. When significant differences were observed, Duncan's Multiple Range Test (DMRT) was applied to further analyses specific pairwise comparisons. The use of these statistical tests ensured that the results were robust and could reveal even subtle

effects of Moringa additions on the dependent variables.

2.3. Data analysis

Results were analyzed by one-way analysis of variance (ANOVA) method and significant differences among means from triplicate analyses at ($p<0.05$) were determined by Fisher's least significant difference (LSD) procedure using the Statgraphics software (Centurion XV).

3. Results and discussions

3.1. Antioxidant analysis

The antioxidant activity of milkfish sausage (Chanos chanos) was shown in Figure 1. The result was significantly enhanced by the addition of Moringa leaf powder (6%) and fresh Moringa leaves (12%), with average antioxidant activity values of 16.8424% (K1) and 17.0608% (K2), respectively. The control (K0) recorded significantly lower activity at 0.7112%. Statistical analysis using one-way ANOVA indicated a significant effect of Moringa leaf addition on antioxidant activity ($p < 0.05$). Duncan's Multiple Range Test (DMRT) further confirmed significant differences between all treatments.

The significant enhancement in antioxidant activity observed in milkfish sausages supplemented with Moringa leaf powder and fresh leaves can be attributed to the rich bioactive compound profile of Moringa. These compounds include phenolics, flavonoids, and vitamin C, which act as primary antioxidants by donating hydrogen atoms or electrons to neutralize free radicals like DPPH. Several antibacterial compounds contained in moringa leaves included tannins, triterpenoids, saponins, and flavonoids (Arifan et al., 2021). Moringa leaves were reported to contain several flavonoid compounds, including myricetin, rutin, quercetin, naringenin, kaempferol, and apigenin (Prasetyaningrum et al., 2022).

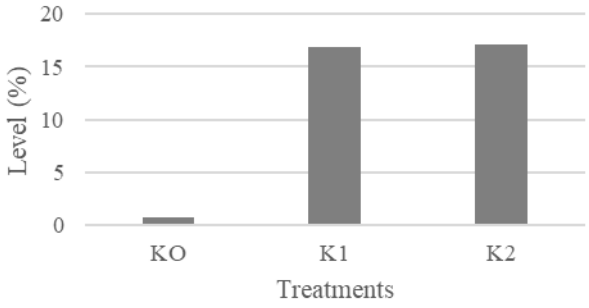

Figure 1. Antioxidant activity of milkfish sausage control (K0), fortified with 6% of Moringa leaf powder (K1), and 12% of fresh Moringa leaves (K2)

In this study, the highest antioxidant activity was recorded in sausages with 12% fresh Moringa leaves (K2), slightly exceeding the activity of sausages with 6% Moringa leaf powder (K1). These results align with prior findings where Moringa was noted for its potent free radical scavenging properties, largely due to phenolic compounds like kaempferol and quercetin (Gao et al., 2022; Swastawati et al., 2019). One potential explanation for the higher activity in K2 compared to K1 could be the preservation of phenolic and flavonoid compounds in fresh Moringa leaves. Processing into powder may cause partial degradation of these sensitive bioactive molecules due to heat and oxidation. However, the overall antioxidant activities in both Moringa-supplemented sausages were markedly superior to the control (K0), which had minimal activity. This underscores the effectiveness of Moringa leaves as a functional additive for enhancing antioxidant properties in processed foods.

Despite the increase in antioxidant activity, the results revealed that the activity in all samples remained below 50%, suggesting moderate efficacy in capturing free radicals. While higher concentrations of Moringa could potentially boost antioxidant activity further,

preliminary sensory analyses revealed diminished acceptability in terms of taste, texture, and aroma at higher Moringa levels. The study from (Trigo et al., 2023) were adding moringa powder in food product and beverage. The adding in food product like nugget can increase phenolic compound led to an increase in the lightness and reduction in the hardness, redness and chewability. on the other side, adding moringa to beverage in higher consentration caused greenish coloration, flavor degradation and imparted a bitter taste due to the presence of catechin. Therefore, the balance between functional benefits and sensory attributes must be optimized to ensure consumer acceptability (Yusuf et al., 2018). This finding highlights the need for future research into refining the incorporation methods of using Moringa extracts with concentrated bioactives to enhance antioxidant effects without compromising product quality.

3.2. Proximate analysis

The addition of Moringa leaves influenced the proximate composition of the sausages, as shown in Table 2. In general, the effect of moringa leaves fortified milkfish sausage was no significantly different in all treatment.

Table 2. Proximate analysis of milkfish sausage

Parameters	Treatments (%)		
	K0	K1	K2
Moisture	67.0801	67.2492	67.3038
Ash	0.9632	1.1801	1.1082
Fat	4.7135	3.7012	3.9789
Protein	12.0161	12.1694	12.0975
Carbohydrate	15.2272	15.7001	15.4883

The analysis indicated that the moisture content was slightly elevated in the Moringa-supplemented sausages compared to the control. Based on Indonesian National Standard (SNI) of sausage: 01-3820-1995, the result was a bit over with the maximum standard of moisture content 67%. This increase is likely due to the high moisture-retaining capability of Moringa leaves, which may enhance the texture and juiciness of the product (Haruni et al., 2024). Compared to the moisture content of sausages made from mackerel (65%), the samples in this study had higher moisture content (Afifah et al., 2023). The technique to reduce the moisture content in sausages was applied using edible coatings, as in the study by (Rofikoh et al., 2021), which reduced the water content of tilapia sausages from 68% at 0 days of storage to 64% after 21 days of storage. The ash content, indicative of mineral presence, was significantly higher in both Moringa-supplemented treatments (1.18% for K1 and 1.11% for K2) compared to the control (0.96%). This increase supports the notion that Moringa leaves are a valuable source of essential minerals such as calcium and potassium (Mashau et al., 2021). The observed ash content values were well within the SNI standard of ≤3%, demonstrating that Moringa leaves contribute positively to the nutritional profile of the sausages without compromising quality standards.

Conversely, fat content decreased in both fortified treatments (3.70% for K1 and 3.98% for K2) compared to the control (4.71%). This reduction may be attributed to the binding effect of Moringa's dietary fibers, which could reduce fat absorption during processing. Additionally, Moringa leaves have a relatively low-fat content, contributing to the overall reduction in sausage fat levels. Compared to the fat content of sausages made from other types of fish, the fat content of milkfish sausages, both with and without the addition of moringa leaves, was still lower than that of sausages made from tilapia fish, which was 5.8% (Maharani et al., 2023). The lower fat content enhances the health appeal of the product while meeting the SNI standard for fat in sausages (≤25%).

Protein content showed a slight increase in sausages supplemented with Moringa leaf

powder (12.17%) compared to the control (12.02%), while fresh Moringa leaves resulted in a similar protein level (12.10%). Compared to the protein content of fermented shrimp sausages (9-11%), milkfish sausages with the addition of moringa leaves had higher protein content (Fitriana et al., 2021). However, it was not significantly different from that of barracuda fish sausages (12.58%) (Swastawati et al., 2023). Although these increases are modest, they highlight Moringa's potential as a protein-rich ingredient that complements the fish protein base of the sausage. However, the relatively minor increase suggests that the primary protein contribution still comes from the fish component of the sausage. All treatments exceeded the SNI standard for protein content in sausages (≥13%). This occurred similarly to the study by (Swastawati et al., 2021), where nuggets made from milkfish contained protein levels of 13-15%. Boiled or steamed milkfish contained protein levels of 79-83% (Nopiyanti et al., 2023). In the study by (IZMAIL et al., 2022), several proteins detected in fish sausages derived from fish such as tilapia, mullet, and threadfin bream were identified as myosin heavy chain, alpha-actinin, paramyosin, actin, tropomyosin, and myosin light chains.

Carbohydrate content was slightly higher in Moringa-supplemented sausages (K1: 15.70%; K2: 15.49%) than in the control (K0: 15.23%). This increase could be attributed to the polysaccharides and fiber content in Moringa leaves, which are classified as carbohydrates. However, all treatments exceeded the SNI standard for carbohydrates in sausages (at least 8%), which could be a limiting factor for product certification. Despite this, the higher carbohydrate and fiber content contributes to the product's functional benefits, such as improved digestive health and reduced glycemic load, making it an attractive option for health-conscious consumers. Overall, this study confirms that incorporating Moringa leaves into milkfish sausage not only enhances its antioxidant activity but also improves its nutritional profile across several parameters while maintaining compliance with food safety standards.

3.3. Crude fiber

The addition of Moringa leaves significantly increased the crude fiber content of the sausages: 1.07% (K0), 3.10% (K1), and 3.02% (K2) shown in Figure 2.

This improvement underscores the role of Moringa leaves as a dietary fiber source, which can support digestive health and reduce risks of chronic diseases (Kustiani et al., 2024). This significant enhancement underscores the role of Moringa leaves as an excellent source of dietary fiber. Moringa fiber content, particularly insoluble fiber, contributes to its ability to bind water, improve texture, and potentially promote digestive health by enhancing bowel regularity. These findings align with previous studies that have reported high fiber content in Moringa leaf-based products, emphasizing its potential as a functional food ingredient (Mallillin et al., 2014; Rahmi et al., 2019).

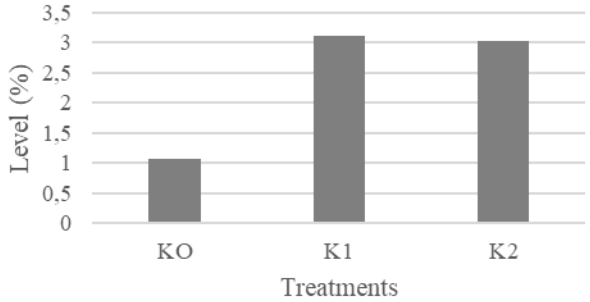

Figure 2. Crude fibre of milkfish sausage control (K0), fortified with 6% of Moringa leaf powder (K1), and 12% of fresh Moringa leaves (K2)

The higher crude fiber content in Moringa-supplemented sausages also offers significant health benefits beyond improving digestive function. Dietary fiber has been associated with reduced risks of cardiovascular diseases, improved lipid profiles, and better glycemic control. The increased fiber levels observed in this study make the Moringa-supplemented sausages a promising functional food option for addressing chronic health issues. These results highlight the potential of Moringa-supplemented milkfish sausages as a novel and nutritionally enhanced alternative to conventional meat products.

4. Conclusions

The addition of Moringa leaves, in both powdered (6%) and fresh (12%) forms, significantly enhanced the antioxidant activity, crude fiber content, and nutritional composition of milkfish sausages. The inclusion of Moringa leaves markedly increased antioxidant activity, crude fiber, protein, and ash contents, contributing to improved health benefits. However, water and carbohydrate contents exceeded SNI standards, suggesting the need for further optimization to meet regulatory requirements. Overall, Moringa-supplemented milkfish sausages offer a promising avenue for producing nutritious, antioxidant-rich food products with potential health benefits, though further research on formulation and sensory quality is recommended to maximize consumer acceptability and compliance.

5. References

Afifah, D. N., Ratna Sari, I., Prastifani, N. T., Fulyani, F., Anjani, G., Widyastuti, N., & Hastuti, V. N. (2023). Effect of Fermentation Time on Nutrition Content, Physical Properties, pH, Amino Acids, Fatty Acids Composition and Organoleptics on Fermented Mackerel Sausage (Rastrelliger kanagurta Cuvier) Characteristics. *International Journal of Food Studies*, 12(1), 57–70. https://doi.org/10.7455/ijfs/12.1.2023.a4

Agustini, T. W., Hadiyanto, H., Amalia, U., & Wijayantia, I. (2019). Potential of melanin free ink as antioxidant and its application for preserving and predicting shelf life of salted-boiled milkfish. *International Journal of Postharvest Technology and Innovation*, 6(1), 57–69. https://doi.org/10.1504/ijpti.2019.10025855

Amalia, N. I., Budisulistyo, T., Wibowo, D. A., & Sareharto, T. P. (2024). The Effect of Moringa Leaves Extracts on MDA Level in Male Mice Exposed to Electromagnetic Radiation of Mobile Phones. *Jurnal Kedokteran Diponegoro (Diponegoro Medical Journal)*, 13(4). https://doi.org/10.14710/dmj.v13i4.43905

AOAC. (1990). Official Methods of Analysis. Association of Official Analytical Chemists, 1(Volume 1), 73–80. https://doi.org/10.7591/cornell/9781501766534.003.0007

Arifan, F., Broto, R. W., Sapatra, E. F., & Pujiastuti, A. (2021). Utilization of moringa oleifera leaves for making hand sanitizers to prevent the spread of COVID-19 virus. IOP Conference Series: Earth and Environmental Science, 623(1), 012015. https://doi.org/10.1088/1755-1315/623/1/012015

Fitriana, L. Y., Maharani, N., Anjani, G., & Afifah, D. N. (2021). Nutrient content and fatty acid profile of fermented shrimp (Litopenaeus vannamei) sausage. *Food Research*, 5(S3), 76–84. https://doi.org/10.26656/fr.2017.5(S3).002

Gao, Q., Wei, Z., Liu, Y., Wang, F., Zhang, S., Serrano, C., Li, L., & Sun, B. (2022). Characterization, Large-Scale HSCCC Separation and Neuroprotective Effects of Polyphenols from Moringa oleifera Leaves. *Molecules,* 27(3). https://doi.org/10.3390/molecules27030678

González-Burgos, E., Ureña-Vacas, I., Sánchez, M., & Gómez-Serranillos, M. P. (2021). Nutritional value of moringa oleifera Lam. Leaf powder extracts and their neuroprotective effects via antioxidative and mitochondrial regulation. *Nutrients*, 13(7). https://doi.org/10.3390/nu13072203

Haruni, D. S., Nuhriawangsa, A. M. P., & Febrinasari, R. P. (2024). Acceptability and

Nutritional Value of Mackerel Fish Nugget with Additions of Moringa Leaves Flour for Stunting Children Under-Five Years in West Nias Regency . NST Proceedings : The 1st International Conference Muhammadiyah Yogyakarta – Hospital & Healthcare Management, 2024 (2023), 61–71.

Izmail, P. M., Riyadi, P. H., & Fahmi, A. S. (2022). Effect Of Different Types Of Fish On Fish Sausages With The Addition Of Transglutaminase. *Journal of Advances in Food Science & Technology*, 12–20. https://doi.org/10.56557/jafsat/2022/v9i17595

Khasanah, R., Jumari, J., & Nurchayati, Y. (2023). Etnobotani Tanaman Kelor (Moringa oleifera L.) di Kabupaten Pemalang Jawa Tengah. *Jurnal Ilmu Lingkungan*, 21(4), 870–880. https://doi.org/10.14710/jil.21.4.870-880

Kustiani, A., Adyas, A., Nurdin, S. U., & Indriani, Y. (2024). Minerals and dietary fibre source snack made from Moringa leaves enriched with ginger. *International Journal of Public Health Science (IJPHS)*, 13(2), 682.
https://doi.org/10.11591/ijphs.v13i2.22948

Maharani, D., Anggo, A. D., Suharto, S., Arifin, M. H., & Amalia, U. (2023). Characteristics and Omega-3 Content of Tilapia Sausage Subtitued with Mackerel Fish (Rastrelliger kanagurta) Oil. *Journal of Advances in Food Science & Technology*, 34–42. https://doi.org/10.56557/jafsat/2023/v10i38278

Malle, S., Tawali, A. B., Tahir, M. M., & Bilang, M. (2019). Nutrient composition of milkfish (Chanos chanos, Forskal) from Pangkep, South Sulawesi, Indonesia. Malaysian *Journal of Nutrition*, 25(1), 155–162. https://doi.org/10.31246/mjn-2018-0105

Mallillin, A. C., Trinidad, T. P., Sagum, R. S., Leon, M. P. de, Borlagdan, M. P., Baquiran, A. F. P., Alcantara, J. S., & Aviles, T. F. (2014). Mineral availability and dietary fiber characteristics of Moringa oleifera. *Food and Public Health*, 4(5), 242–246. https://doi.org/10.5923/j.fph.20140405.05

Mashau, M. E., Ramatsetse, K. E., & Ramashia, S. E. (2021). Effects of adding moringa oleifera leaves powder on the nutritional properties, lipid oxidation and microbial growth in ground beef during cold storage. *Applied Sciences* (Switzerland), 11(7). https://doi.org/10.3390/app11072944

Murthy, L., Padiyar, P., Rao, B., Asha, K., Jesmi, D., Girija, P., Prasad, M., & Ravishankar, C. (2016). Nutritional Profile and Heavy Metal Content of Cultured Milkfish (Chanos chanos). *Fishery Technology*, 53, 245–249. https://consensus.app/papers/nutritional-profile-and-heavy-metal-content-of-cultured-murthy-padiyar/c3d242b1c1955b2bbd30506fb4f5e028/

Nopiyanti, V., Fahmi, A. S., Swastawati, F., Kurniasih, R. A., & Riyadi, P. H. (2023). Product characteristics, amino acid and fatty acid profiles of milkfish (Chanos chanos) with different cooking methods. *Food Research*, 7(Supplementary 3), 86–96. https://doi.org/10.26656/fr.2017.7(S3).12

Prasetio, D. B., Setyaningsih, Y., Suhartono, & Suroto. (2023). Increased Antioxidants of Tile Factory Workers in Reducing Work Fatigue Given Moringa Leaves. E3S Web of Conferences, 448, 05014. https://doi.org/10.1051/e3sconf/202344805014

Prasetyaningrum, A., Widayat, W., Jos, B., Ratnawati, R., Riyanto, T., Prinanda, G. R., Le Monde, B. U., & Susanto, E. E. (2022). Optimization of Sequential Microwave-Ultrasonic-Assisted Extraction of Flavonoid Compounds from Moringa oleifera. *Trends in Sciences*, 20(1), 6401. https://doi.org/10.48048/tis.2023.6401

Rahayu, S. D., Dwi Ujianti, R. M., & Nurdyansyah, F. (2022). Physicochemical Characteristics of Catfish (Clarias sp) Sausage with Addition of Moringa Leaf Flour (Moringa oleifera). *Advance Sustainable Science Engineering and Technology*, 4(1), 0220107. https://doi.org/10.26877/asset.v4i1.11878

Rahmi, Y., Wani, Y. A., Kusuma, T. S., Yuliani, S. C., Rafidah, G., & Azizah, T. A. (2019). Profil Mutu Gizi, Fisik, dan Organoleptik Mie Basah dengan Tepung Daun Kelor (Moringa Oleifera). Indonesian *Journal of Human Nutrition*, 6(1), 10–21. https://doi.org/10.21776/ub.ijhn.2019.006.01.2

Rofikoh, R., Darmanto, Y. S., & Fahmi, A. S. (2021). Quality of gelatin from tilapia (Oreochromis niloticus) by-products and its effects as edible coating on fish sausage during chilled storage. IOP Conference Series: Earth and Environmental Science, 919(1), 012034. https://doi.org/10.1088/1755-1315/919/1/012034

Sabrina, H. A., Budisulistyo, T., Juniarto, A. Z., & Sareharto, T. P. (2024). The Effect of Moringa Leaves Extract on Sperm Motility in Male Mice Exposed to Electromagnetic Radiation of Mobile Phone. *Jurnal Kedokteran Diponegoro (Diponegoro Medical Journal)*, 13(3), 147–151. https://doi.org/10.14710/dmj.v13i3.43904

Sagita, D., Handayani, B. R., & Cicilia, S. (2024). Quality of Tilapia Nuggets Fortified With Moringa Leaf Flour. Jurnal Perikanan Unram, 14(2), 754–760. https://doi.org/10.29303/jp.v14i2.839

Segwatibe, M. K., Cosa, S., & Bassey, K. (2023). Antioxidant and Antimicrobial Evaluations of Moringa oleifera Lam Leaves Extract and Isolated Compounds. *Molecules*, 28(2). https://doi.org/10.3390/molecules28020899

Swastawati, F., Al-Baari, A. N. matullah, Susanto, E., & Purnamayati, L. (2019). The effect of antioxidant and antibacterial liquid smoke nanocapsules on catfish fillet (pangasius sp.) during storage at room temperature and cold temperature. *Carpathian Journal of Food Science and Technology*, *11*(4), 165–175. https://doi.org/10.34302/2019.11.4.16

Swastawati, F., Ambariyanto, A., Cahyono, B., Wijayanti, I., Chilmawati, D., Hadiyanto, H., & Al-Baarri, A. (2021). Physicochemical Changes And Sensory Quality Of Liquid Smoked Milkfish Nuggets. *African Journal of Food, Agriculture, Nutrition and Development*, 21(7), 18261–18278. https://doi.org/10.18697/ajfand.102.19440

Swastawati, F., Antami, H. A., & Purnamayati, L. (2023). Applying edible coating based on chitosan and liquid smoke on the quality and microstructure of barracuda fish sausage (Sphyraena sp.). IOP Conference Series: *Earth and Environmental Science*, 1137(1), 012030. https://doi.org/10.1088/1755-1315/1137/1/012030

Swastawati, F., Al-Baari, A. N. matullah, Susanto, E., & Purnamayati, L. (2019). The effect of antioxidant and antibacterial liquid smoke nanocapsules on catfish fillet (pangasius sp.) during storage at room temperature and cold temperature. *Carpathian Journal of Food Science and Technology*, *11*(4), 165–175. https://doi.org/10.34302/2019.11.4.16

Trigo, C., Castelló, M. L., & Ortolá, M. D. (2023). Potentiality of Moringa oleifera as a Nutritive Ingredient in Different Food Matrices. *Plant Foods for Human Nutrition*, 78(1), 25–37. https://doi.org/10.1007/s11130-022-01023-9

Yusuf, M., Legowo, A. M., Albaarri, A. N., Darmanto, Y. S., Agustini, T. W., & Setyastuti, A. I. (2018). Mapping performance of the fishery industries innovation: A survey in the North Coast of Java. *IOP Conference Series: Earth and Environmental Science*, *102*(1). https://doi.org/10.1088/1755-1315/102/1/012083

Acknowledgments

This research is partially supported by Food Safety Scientific Consortium through the Research Implementation Agreement Contract No. 369/UN7.A/HK/X/2024

CARPATHIAN JOURNAL OF FOOD SCIENCE AND TECHNOLOGY

journal homepage: **http://chimie-biologie.ubm.ro/carpathian_journal/index.html**

Research article

FIXING PLASTIC FOOD BOTTLES SYSTEM FOR ROTARY APPARATUSES

Miorița Ungureanu[1]✉, Ioana Lucia Crăciun[1], Diana Lemian[2], Teodora Ungureanu[3]

[1]*Faculty of Engineering, Technical University of Cluj-Napoca, North University Centre at Baia Mare, V. Babes St. 62A, 430083, Baia Mare, Romania*

[2]*Advanced Research Centre for Ambiental Quality and Building Physics, Technical University of Civil Engineering of Bucharest, 021414 Bucharest, Romania*

[3]*National Institute for Research and Development in Constructions, Urbanism and Sustainable Spatial Development URBAN-INCERC, 021652 Bucharest, Romania*

✉*miorita.ungureanu@imtech.utcluj.ro*

ORCID Number: 0000-0002-5427-5857

https://doi.org/10.34302/2025.17.3.11

Article history:
Received
August 11th 2025
Accepted
September 22th 2025

Keywords:
Plastic food bottles;
Conveyor;
Fixing device.

Abstract

This research analyses a novel *Fixing plastic food bottles system* for conveyors and the turntable of rotary apparatuses. At relatively high conveyor speeds, plastic food bottles tend to tip over or slide on the conveyor belt on which they are placed. To address this issue, we developed the *Fixing plastic food bottles system*, designed to preserve plastic food bottles in an upright orientation and ensure the spacing between subsequent bottles for accurate movement. An in-depth examination of the kinematic and dynamic characteristics of flexible transport systems reveals that inertia force and jerk (the derivative of acceleration) during initiation and cessation are the underlying causes of this phenomenon. We examined several modelling methodologies for the acceleration and deceleration of conveyors in these situations, based on numerical applications. Furthermore, we examined the impact of the fastening mechanism on plastic food bottles during initiation and cessation at different accelerations. Through the study presented in this paper, we have deepened important aspects of operation for the model created, the *Fixing plastic food bottles system*, with the goal of being practically made and used in the food industry for filling liquids such as milk, yogurt, juices, or water, as well as for capping operations.

1. Introduction

Currently, the plastic bottle clamping system that is widely used in the rotary plastic bottle processing devices is based on a worm drive at the bottles entrance on the turntable, the bottles are held in position on the turntable by two pairs of superposed ratchet wheels, which rotate together with the turntable, and for the transfer of bottles from the augers to the turntable, two profiled wheels are used, both at the entrance and at the exit (Shiba, 1975). Also, a device for separating bottles with a star wheel with a protective effect on the bottles was created (Preti *et al*., 2010). This paper presents a new 'System

for fixing plastic bottles in rotary tightness testing apparatuses' (Ungureanu *et al.,* 2020), which we continue to study and analyze with the aim of implementing it in industry.

Fixing the bottles and their behavior during transport will be an aspect studied. An optimal fixation requires the analysis of phenomena such as tangential contact that can leave traces of wear or can deform the bottle (Ostergaard *et al*., 2017).

The kinematics and dynamics of the conveyors (Feng et al., 2020; Zeng et al. 2020) and, respectively, of the fixing system are of interest to choose the optimal solution for driving them with electric motors (Umoren *et al.,* 2016; Yang *et al.* 2018). In the practice of driving conveyors, it has been concluded that driving by means of frequency converters (Jeftenić *et al.* 2009) is beneficial for the purpose of modelling the shock (jerk) that occurs when starting and stopping (Li et al. 2018; Doçi et al. 2023). The transient processes that occur when the conveyors are put into operation are influenced by the type of electric drive motor, by the size and character of the variation of the external forces (Guo et al. 2020; Francik *et al.* 2018), and in the case of non-uniform loads, a dynamic study is necessary during their operation (Hea *et al.* 2018). In the case of conveyors and fixing devices that are the subject of our study (Figure 1) there are no large or uneven loads, the transported plastic bottles have the same mass and are evenly distributed, therefore we will only analyze the phenomena that occur when starting and stopping. In these phases, the S-curve motion profile can be modelled according to various functions: trapezoidal, parabolic and cosinusoidal by means of the frequency driver (Crăciun *et al.* 2012; Ostergaard and Danjou 2017; Pop *et al.* 2019).

Thus, the present study is focused on two main directions:

- Analysis of three models of acceleration and deceleration variation, selecting the option that presents the minimum jerk;

- Analysis of stresses and deformations occurring in the bottle's body during startup and stopping.

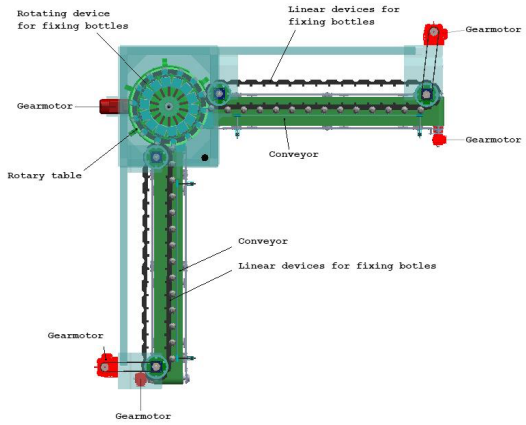

Figure 1. Plastic food bottle fixing system for rotary apparatuses

2. Description of the Proposed Plastic Food Bottle Fixing System for Rotary Devices

The system proposed by us is intended for fixing and dividing the bottles on the linear means of transport and on the turntable of the rotary devices, and according to the invention it consists of two vertical devices for fixing the bottles, one located at the entrance, and one located at the exit from the turntable. This system presents the following advantages over other systems that perform the same role (Shiba, 1975): simple construction with few moving elements; the elastomer elements ensure a flexible grip, dampening vibrations; a precise driving and transfer of the bottles; fixing devices ensure a flexible grip without deforming or damaging them due to dynamic stresses; the proposed system has a modular construction not only of the conveyors but also of the fixing devices, which allows the individual replacement of the main bottle fixing elements in case of damage or change of the processed bottles.

The aim of fixing is to keep the bottles in a vertical position on the conveyor belt, at relatively high speed, and to transfer the bottles into categories when passing from the linear route to the circular one. The main components of the system are: a rotary bottle device for

fixing and transferring bottles and two vertical devices for fixing and transferring bottles. This bottle fixing and transfer system can be used in numerous industrial applications for operations such as compliance testing of plastic food bottles; bottle filling; capping etc. The system ensures a flexible grip of plastic food bottles, thus avoiding the deformation or damage of the bottles, respectively the production of waste. The prevention of waste is an important aspect of the circular economy, a target that is considered from the concept phase.

Another advantage of the system is the fact that it ensures precise driving and transfer distribution of the bottles, which allows us to increase the productivity of the installation it serves. Increasing productivity is a key goal in the field of advanced manufacturing.

The proposed new system for securing plastic food bottles for rotary devices is shown in Figure 1 and consists of a rotating device for fixing bottles and two linear devices for fixing bottles. The linear bottle fixing devices are located above the horizontal conveyors. The conveyor together with the linear bottle fixing device ensures the entry of bottles on the rotary table, and the conveyor together with the linear device for fixing the bottles ensures the evacuation of the bottles from the rotary table. The two linear bottle fixing devices are identical and consist of two vertical drums, on which the profiled belt is mounted. On the outer side, the profiled belt is provided with grooves sized according to the shape of the bottles. The actuation of the linear device for fixing the bottles is ensured by the gearmotor. The rotary table is made up of the turntable, fixed on the vertical shaft, and the rotary device for fixing the bottles. The operation of the rotary table is carried out by the gearmotor by means of a transmission. On the shaft of the rotary table, above the turntable, the rotating device for fixing the bottles is mounted. Above the rotary table are placed the processing devices, which can be: tightness testing devices, filling devices, capping devices, etc.

The rotating device for fixing the bottles (Figure 3) consists of a metal drum on which the profiled elastomer bushing is mounted. The elastomer bushing of the drum will have the profile and pitch of the grooves identical to that of the belt of linear fixing devices, to ensure the connection between the conveyors and the rotary table, and respectively the transfer of the bottles (Figure 2). Also, in order to ensure the operation of the system, the speeds of the flexible belt conveyors, the speeds of the two linear devices and the tangential speed of the rotating device must be equal.

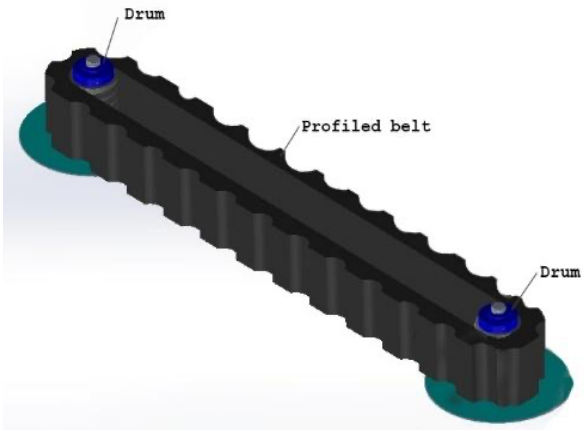

Figure 2. Linear device for fixing the bottles

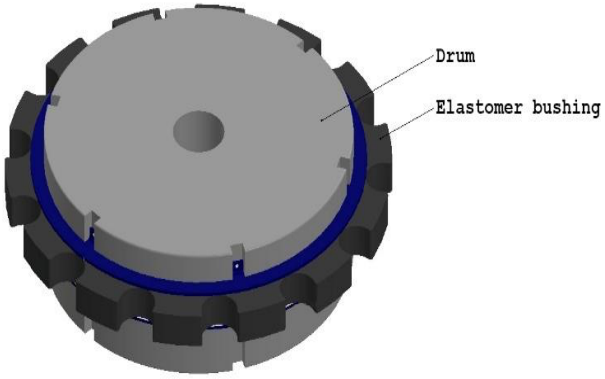

Figure 3. Rotating device for fixing the bottles

3. Materials and Methods

To develop a system that is operational for both the kinematic characteristics and the stresses encountered in extreme cases, we propose to establish an optimal control model for the electric motors driving the conveyors and the bottle securing devices. Additionally, we will conduct simulation testing of the plastic food bottle under the maximum stresses that occur due to its securing in the device.

3.1. Study of system start and stop

In the case of system start-up and stop, we are interested in its kinematic study in order to create the working model of the electric encoder. Thus, the use of speed modeling in the operation of conveyors is a problem that concerns us. The kinematic parameters that influence the positioning of the glass when switching from one means of transport to another are: the value of the regime speed; acceleration value at start-up and stop and the modelling of the speed S-curve (Bebić and Ristić; Hea *et al.* 2018).

Speed variation is currently made using frequency converters that follow mathematical curves, generally named S-curves. Studies in the field of conveyors and other mechanical systems have demonstrated that S-type designs are effective, as they substantially reduce shocks in the system (Halepoto et al. 2026; Crăciun *et al.* 2017).

The S-curves used to model start and stop speeds can be generated using different variations of speed over time, the most common being the third-degree parabola and the sine (Crăciun *et al.* 2017).

In this case, the situation of a vertical bottle-fixing device with S-curves at start and stop will be analyzed for three acceleration modelling variants during acceleration and braking periods: trapezoidal, parabolic and cosine. To make a comparison between these three acceleration modelling variants, a numerical application was performed with the following data of the vertical bottle-fixing device: speed v = 0.46 m/s, acceleration a = 0.15 m/s^2, acceleration and deceleration time $t_a = t_f = 3$ s. Symmetrical curves are generated at start-up and stop, which is why we conducted the study only for start-up. Under these conditions, we will evaluate the resulting jerk as a basis for choosing the optimal modeling variant.

The equations of motion for three acceleration modeling variants are presented below.

Notations: $v_{01}(t)$-speed; a_1- acceleration; t_1-accelerating time; j_1- jerk.

3.1.1. Triangular variation of acceleration

Jerk variation:

$$j(t) = \begin{cases} j_{01} = j_1 \\ j_{12} = 0 \\ j_{23} = -j_1 \end{cases} \quad (1)$$

Acceleration variation:

$$a(t) = \begin{cases} a_{01}(t) = j_1 \cdot t \\ a_{12}(t) = a_1 \\ a_{23}(t) = a_1 - j_1(t - t_2) \end{cases} \quad (2)$$

Speed variation:

$$v(t) = \begin{cases} v_{01}(t) = j_1 \frac{t^2}{2} \\ v_{12}(t) = v_{01}(t_1) + a_1(t - t_1) \\ v_{23}(t) = v_{12}(t_2) + a_1(t - t_2) - j_1 \frac{(t-t_2)^2}{2} \end{cases} \quad (3)$$

Displacement:

$$x_{01}(t) = \frac{j_1 \cdot t^3}{6} \quad (4)$$

$$x_{12}(t) = x_{01}(t_1) + v_{01}(t_1) \cdot (t - t_1) + \frac{a_1}{2}(t - t_1)^2 - \frac{j_1}{6}(t - t_1)^3 \quad (5)$$

Boundary values:

$a_{01}(t_1) = j_1 \cdot t_1 = a_1$; $v_{12}(t_2) = v_{01}(t_1) + a_1(t_2 - t_1) - j_2 \frac{(t_2-t_1)^2}{2}$

The variation curves of the kinematic parameters (jerk, acceleration and speed) were generated using MATLAB program, for v = 0.46 m/s and acceleration duration $t_a = 3$ s. The graphs obtained are shown in Figures 4, 5, and 6 and they represent the speed, acceleration, and jerk profiles over time for a parabolic variation of acceleration.

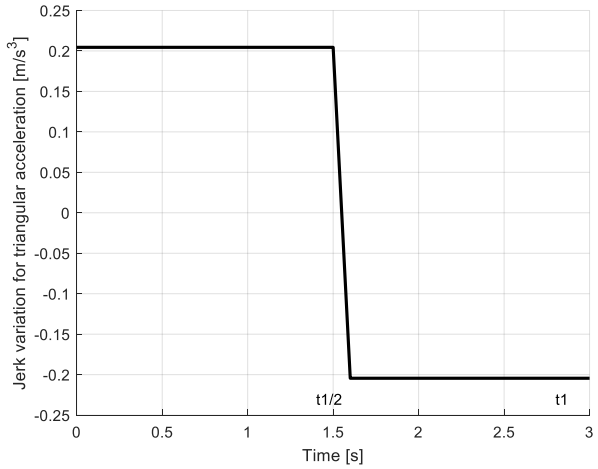

Figure 4. Jerk variation for triangular acceleration

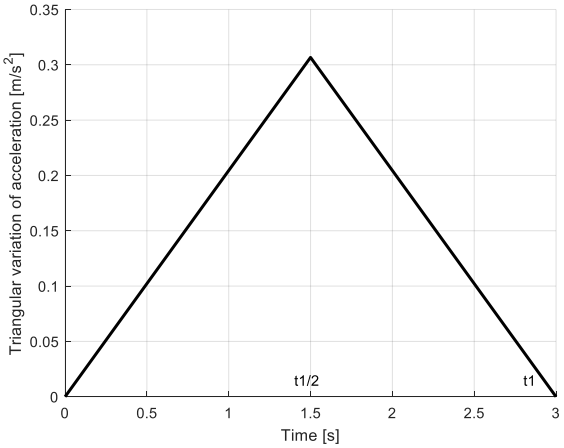

Figure 5. Triangular variation of acceleration

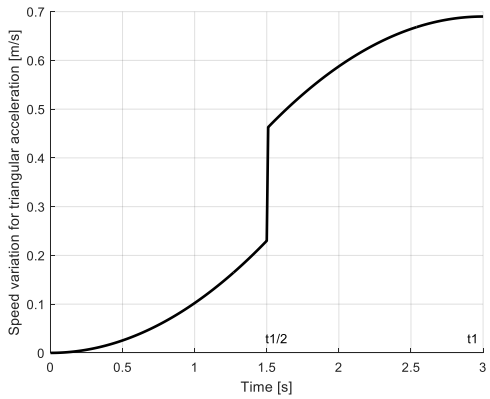

Figure 6. Speed variation for triangular acceleration

3.1.2. Parabolic variation of acceleration

Jerk variation:

$$j_{01} = j_1 - \frac{2j_1}{t_1}t \quad (6)$$

Acceleration variation:

$$a_{01} = j_1 t - \frac{j_1}{t_1}t^2 \quad (7)$$

Speed variation:

$$v_{01} = j_1 \frac{t^2}{2} - \frac{j_1}{t_1}\frac{t^3}{3} \quad (8)$$

Displacement:

$$x_{01}(t_1) = j_1 \frac{t_1^3}{6} - j_1 \frac{t_1^4}{12t_1} = j_1 \frac{t_1^3}{12} \quad (9)$$

Boundary values: $a_{01}(t_1) = 0;\ j_{01}(t_1) = -j_1\ m/s^3;\ j_{01}(t_1/2) = 0;\ a_{01}(t_1/2) = a_1\ m/s^2$.

After running the numerical simulation in MATLAB with a speed of v=0.46m/s and time parameters t_a=t_f=3s, the graphs in Figures 7, 8, and 9 were obtained. These show the speed, acceleration, and jerk profiles over time for a parabolic variation of acceleration.

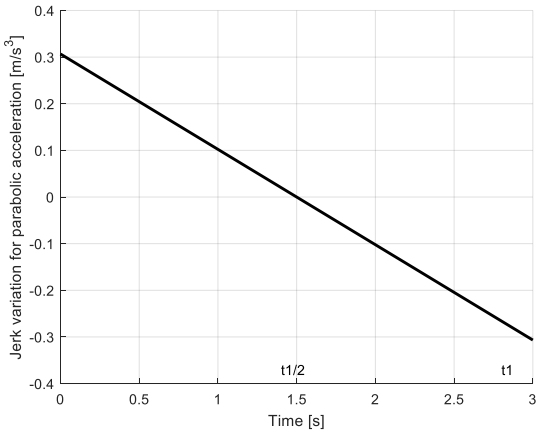

Figure 7. Jerk variation for parabolic acceleration

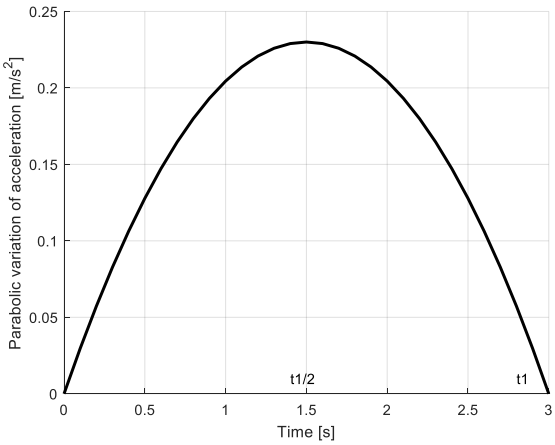

Figure 8. Parabolic variation of acceleration

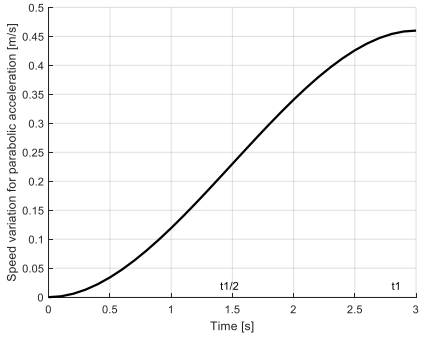

Figure 9. Speed variation for parabolic acceleration

3.1.3. Cosinusoidal variation of acceleration

Jerk variation

$$j_{01}(t) = j_1 sin\ \frac{2j_1}{a_1}\ t = j_1 sin\ \frac{2\pi}{t_1}\ t \quad (10)$$

Acceleration variation:

$$a_{01}(t) = \frac{a_1}{2}(1 - cos\ \frac{2j_1}{a_1}\ t) = \frac{a_1}{2}(1 - cos\ \frac{2\pi}{t_1}\ t) \quad (11)$$

Speed variation:

$$v_{01}(t) = \frac{a_1}{2}(t - \frac{a_1}{2j_1} sin\ \frac{2j_1}{a_1}\ t) = \frac{a_1}{2}(t - \frac{t_1}{2\pi} sin\ \frac{2\pi}{t_1}\ t) \quad (12)$$

Displacement:

$$x_{01}(t) = \frac{a_1}{2}\left(\frac{t^2}{2} + \frac{t_1^2}{4\pi^2} cos\ \frac{2\pi}{t_1}\ t - \frac{t_1^2}{4\pi^2}\right) \quad (13)$$

Boundary values: $j_{01}(t_1/4) = j_1$; $a_{01}\left(\frac{t_1}{2}\right) = a_1$; $a_{01}(t_1) = 0$; $v_{01}(t_1) = v_1$.

After running the numerical simulation in MATLAB with a speed of v=0.46m/s and time parameters t_a=t_f=3s, the graphs in Figures 10, 11, and 12 were obtained. These show the speed, acceleration, and jerk profiles over time for a parabolic variation of acceleration.

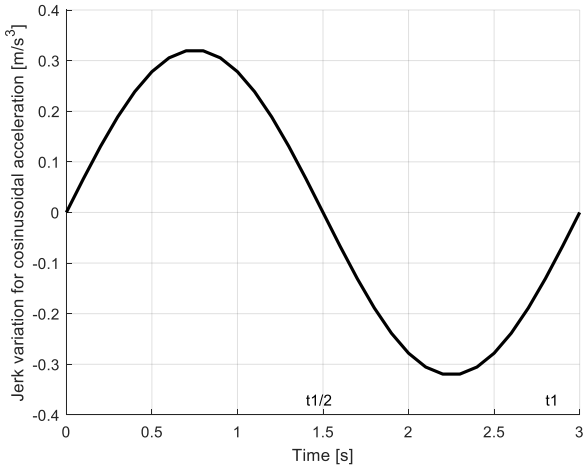

Figure 10. Jerk variation for cosinusoidal acceleration

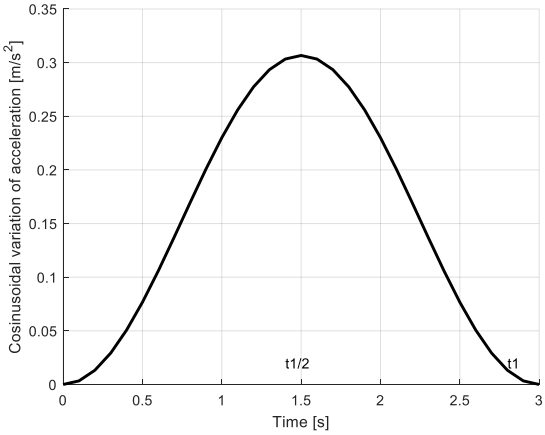

Figure 11. Cosinusoidal variation of acceleration

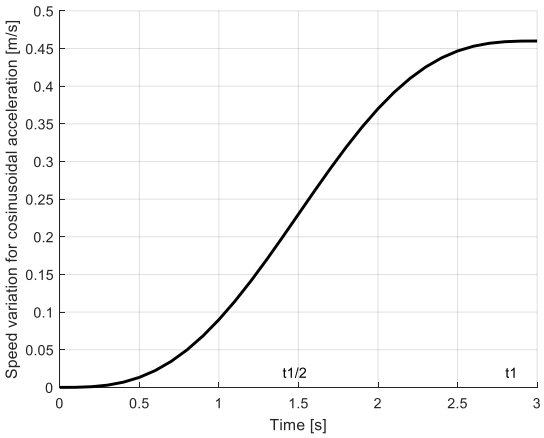

Figure 12. Speed variation for cosinusoidal acceleration

3.1.4. Data analysis

Substituting the numerical values for speed and time in equations 1-13 and performing the calculations we obtained the numerical maximum values for acceleration and jerk of the three modeling variants of the kinematic parameters as can be seen in Table 1, it resulted that the most advantageous modeling is the one with triangular, acceleration because in this case the shock induced in the system is minimal.

Table 1. Maximum values of acceleration and jerk for triangular, parabolic and cosinusoidal variation of acceleration

Acceleration/ Jerk	Triangular	Parabolic	Cosinusoidal
a_1	0.30 m/s^2	0.20 m/s^2	0.30 m/s^2
j_1	0.20 m/s^3	0.30 m/s^3	0.320 m/s^3

3.2. Finite Element Analysis of Stresses and Deformations in Food Plastic Bottles during Startup and Shutdown the Conveyors

Fixing bottles and their behavior during transportation requires analysis of phenomena such as: tangential contact, which can leave wear marks or deform the glass (Ostergaard and Danjou, 2017; Ekinci *et al.* 2022). A simulation of the stresses that occur in the glass when fixed with the help of devices allows us to predict potential deformations of the glass during startup or shutdown. Based on simulating the operating conditions in a mechanical system, the verification of its components is carried out, identifying possible shortcomings, and gaining detailed knowledge of the phenomena, which will later allow us to take constructive measures for necessary improvements (Caban *et al.* 2019; Andras at al. 2021).

Finite element analysis is a technical analysis that allows us to predict the performance of a structure or mechanism under load during service or an overload caused by extreme conditions (Monkova *et al*. 2024; Ojoa and Shittub, 2023; Keawjaroen and Suvanjumrat, 2017).

Most of them plastic bottles used in the food industry are made from polyethylene terephthalate (PET) and high-density polyethylene (HDPE) (Ekinci *et al.,* 2022; Suvanjumrat and Puttapitukporn, 2011). Polyethylene terephthalate (PET) has lower mechanical strength properties compared to high-density polyethylene (HDPE), which is why in our study we simulated the mechanical stresses on bottles made of polyethylene terephthalate (PET) (Suvanjumrat and Puttapitukporn, 2011; Benyathiar et al. 2022).

Polyethylene terephthalate, coded as PET, PETE, is a thermoplastic polymer resin of the polyesters. From a structural point of view, PET can exist both as amorphous and as semi-crystalline. Crystallinity and its physical and mechanical properties are dependent on processing conditions in the manufacture of bottles. (Demirel *et al.,* 2011).

3.2.1. Data analysis

An important issue to ensure a flexible grip of the bottle in the profiled belt is establishing the contact pressure between the profiled belt and the bottle. Related to this, we have studied the total deformation and the equivalent stress, realized in a simulation software, following the application of the force that appears as a result of the displacement of the 0.5 l bottle from PET material, on the linear device, for the speed differed speeds and for differed acceleration or deceleration to the start or to braking at the linear device. PET material, on the linear device, for the speed differed speeds and for differed acceleration or deceleration corresponding to the start or to braking at the linear device. The

values of the speeds and of the accelerations are presented in Table 1.

The calculation of mechanical stresses and deformations was performed for the moment of system startup, that is, during acceleration until a constant speed is reached. During braking, the deceleration process is symmetric, and the stresses will be the same but in the opposite direction.

The simulation was performed for the three acceleration modeling variants presented in section 3.1, namely for the triangular variation of acceleration, the parabolic variation of acceleration, and the cosine variation of acceleration. For the analysis of stresses and deformations occurring during startup and braking, the following assumptions were made: a) the surface on which the inertial force acts is considered to be half of the contact area between the profiled band and the glass; b) the deformation of the rubber was not taken into consideration.

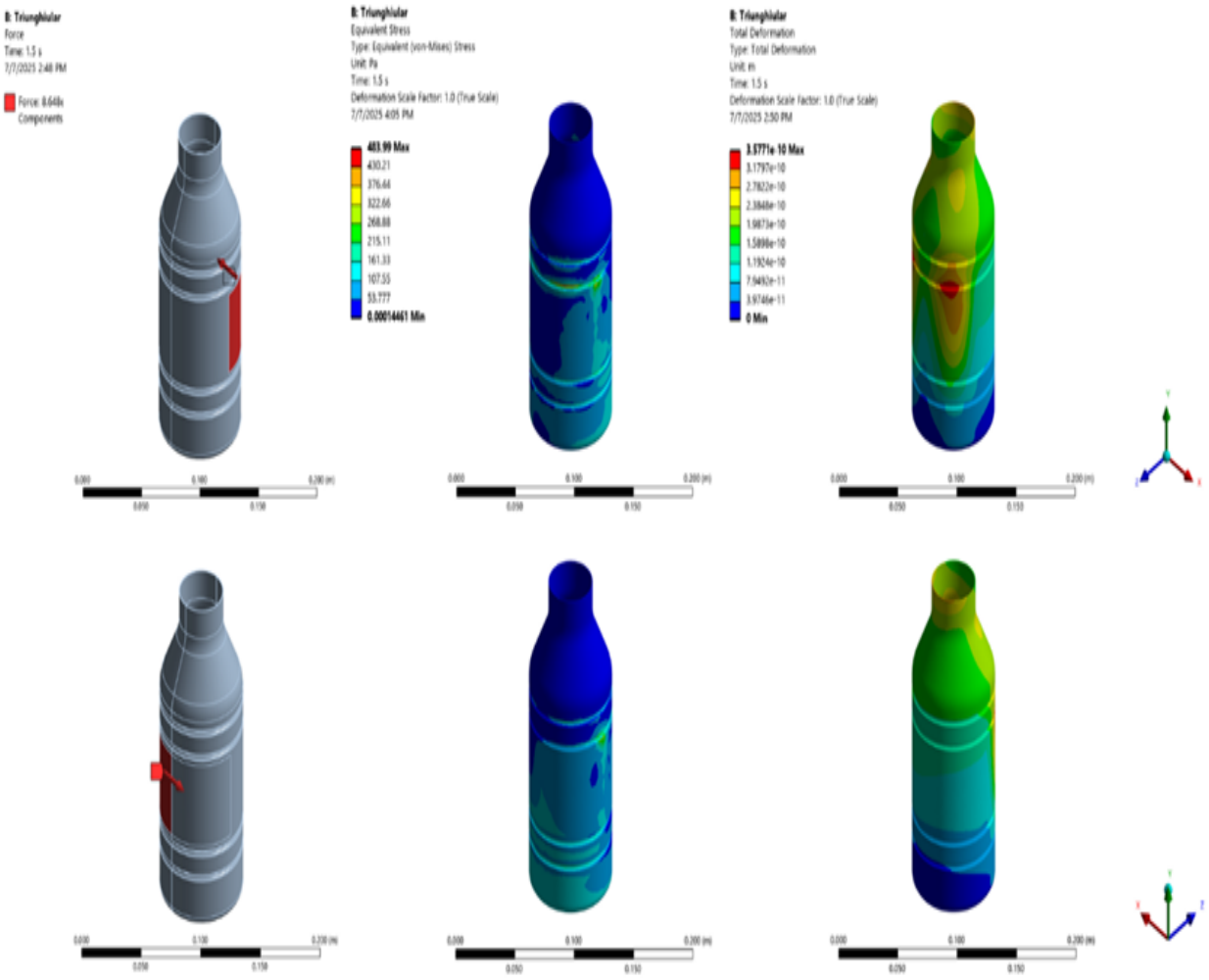

Figure 13. Stresses and deformations of PET glass for the triangular acceleration modeling

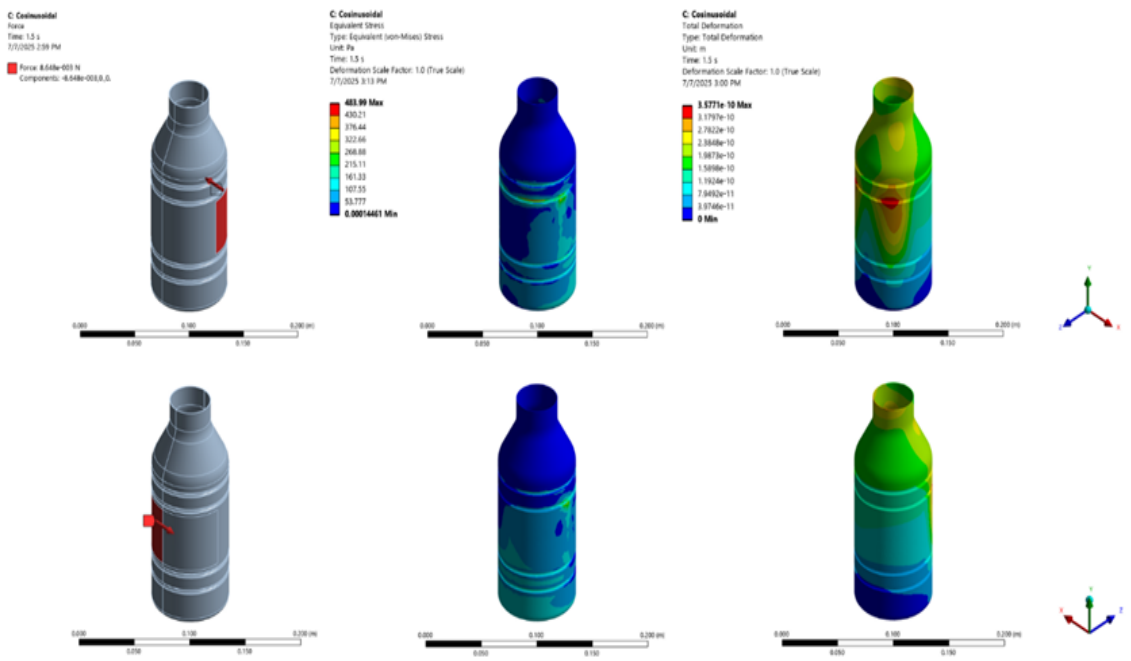

Figure 14. Stresses and deformations of PET glass for the parabolic acceleration modeling

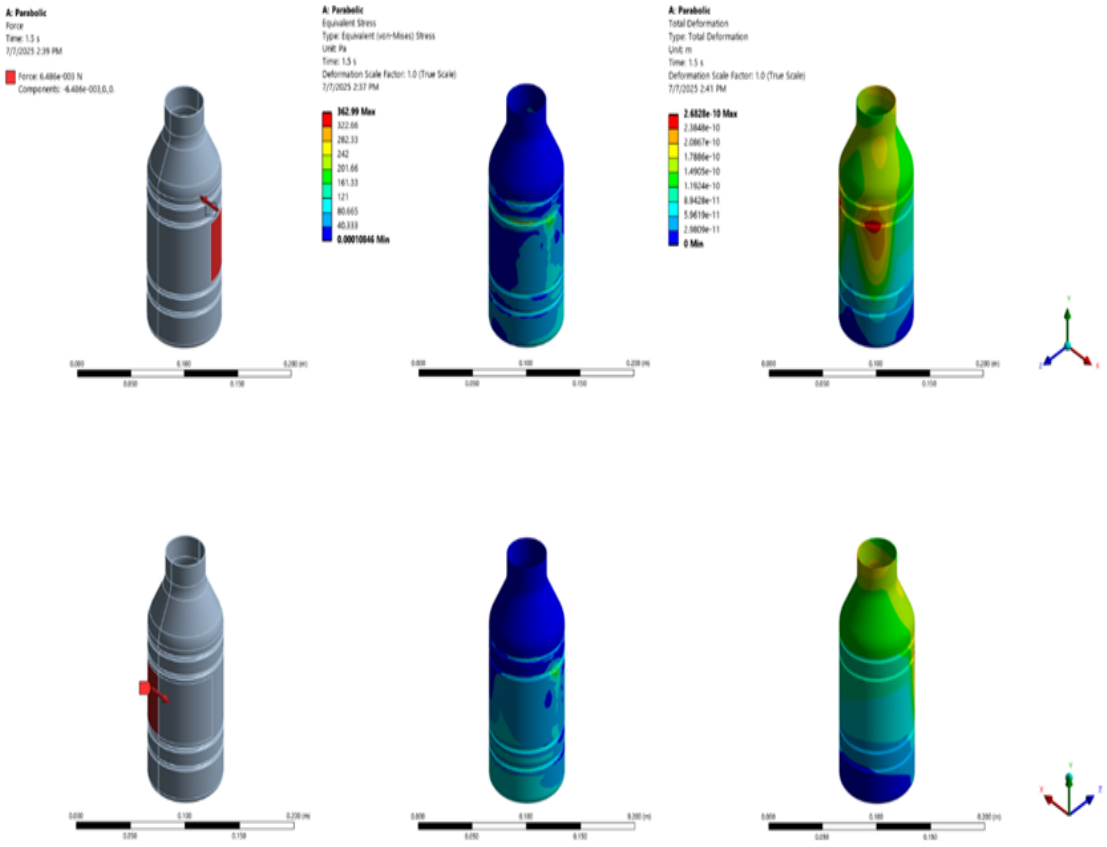

Figure 15. Stresses and deformations of PET glass for the cosine acceleration modeling

The stresses and deformations in the PET material glass for the load values occurring during startup and shutdown under the action of the fixing device were analyzed using the finite element modeling tool in the ANSYS program for all three cases of acceleration modeling (triangular, parabolic, and cosine), with imposed values for speed and time being v=0.46 m/s and time $t_a=t_f=3$s. The results of the simulation are shown in Figures 13, 14 and 15.

3.2.2. Results and discussions

The prediction of a proper fixation of the glass without it being damaged is based on the condition that the maximum yield stress of the design does not exceed the specified material property. The stresses that result in the glass for the three loading cases analyzed and presented in Figures 13-15 are below the PET material's limit. For the triangular variation of acceleration, the highest stress, the von Mises stress value of 483.99 Pa for the PET glass material, is lower than the PET material's yield limit of 55 MPa. For the parabolic variation of acceleration, the highest stress, the von Mises stress value of 362.99 Pa for the PET glass material, is lower than the PET material's yield limit of 55 MPa. For the cosine variation of acceleration, the highest stress, the von Mises stress value of 483.99 Pa for the PET glass material, is lower than the PET material's yield limit of 55 MPa. Thus, it can be concluded that the deformation of the glass due to inertial force is reversible for all three acceleration modeling cases. The deformations of the PET glass in all three simulation cases are very small. It can be observed that the smallest deformation value results from the parabolic acceleration modeling, with slightly higher values in the triangular and cosine acceleration models.

4. Conclusions

The plastic food bottle clamping system presented in this study is suitable for relatively high operational speeds and this offers several comparative advantages over other systems fulfilling the same function, such as those based on a worm drive at the bottles' entrance on the turntable (Shiba, 1975) and systems using a star-wheel bottle separator with a protective effect (Preti et al., 2010). Specifically, the system has a simpler construction with few moving elements, dampens vibrations, and ensures precise guidance and transfer of bottles. The clamping devices provide flexible gripping without deforming or damaging the bottles under dynamic loads. The modular design of the clamping devices allows individual replacement of the main clamping elements in case of damage or when processing bottles of different sizes.

To demonstrate the functionality of the newly created plastic food bottle clamping system, numerical simulation in MATLAB and using FEA analysis in ANSYS were performed in a virtual environment. After numerical analysis in MATLAB it resulted that to minimize shocks during startup and, respectively, during the shutdown of the belts, vertical clamping devices for the bottles, and the turntable, an "S" curve velocity model and a triangular acceleration and deceleration model are proposed. Moreover, for acceleration modeling scenarios, we analyzed the impact of the clamping mechanism on plastic food bottles during start-up and stop at different accelerations through finite element analysis of stresses and deformations in polyethylene terephthalate (PET) bottles. In all cases, stresses remained well below the material's allowable limits, and the resulting deformations were within acceptable values.

In conclusion a triangular acceleration and deceleration model are proposed, because, for this type of modeling, the shock induced in the system is minimal, and the glass deformation due to inertial force is reversible.

For the usual operating high speed of conveyors, according to the simulations conducted in this study, it results that the glass deformation due to inertial force is minimal and reversible, and the stresses of PET bottles are within admissible limits of the material. In conclusion, the plastic food bottle clamping system is suitable for use in the food industry, for example, in the process of filling bottles, capping, or in the process of manufacturing plastic food bottles when testing them for leakage.

5. References

Andras, A., Radu, S. M., Brînas, I., Popescu, F. D., Budilică, D. I., & Korozsi, E. B. (2021). Prediction of material failure time for a bucket wheel excavator boom using computer simulation. *Materials*, 14(24), 7897. https://doi.org/10.3390/ma14247897

Bebić, M. Z., & Ristić, L. B. (2018). Speed controlled belt conveyors: Drives and mechanical considerations. *Advances in Electrical and Computer Engineering*, 18(1). https://doi.org/10.4316/AECE.2018.01007

Benyathiar, P., Kumar, P., Carpenter, G., Brace, J., & Mishra, D. K. (2022). Polyethylene terephthalate (PET) bottle-to-bottle recycling for the beverage industry: A review. *Polymers*, 14(12), 2366. https://doi.org/10.3390/polym14122366

Caban, J., Nieoczym, A., Misztal, W., & Bart, D. (2019). Study of operating parameters of a plate conveyor used in the food industry. *IOP Conference Series: Materials Science and Engineering*, 710, 012020. https://doi.org/10.1088/1757-899X/710/1/012020

Craciun, A., & Ungureanu, M. (2012). Analysis shock to start and stop an elevator. *Transactions of the VŠB-Technical University of Ostrava, Mechanical Serie*s, 58(2), 11–15. https://doi.org/10.22223/tr.2012-2/1916

Craciun, I., Ungureanu, M., & Stoicovici, D. I. (2017). An analysis of the oscillatory movements of the suspension ropes for an elevator with parabolic speed modeling and continuous deceleration. *IOP Conference Series: Materials Science and Engineering*, 200(1). https://doi.org/10.1088/1757-899X/200/1/012016

Demirel, B., Yaraş, A., & Elçiçek, H. (2011). Crystallization behavior of PET materials. *BAÜ Fen Bil. Enst. Dergisi*, 13(1), 26–35. https://doi.org/10.14356/kona.2015016

Doçi, I., & Krasniqi, R. (2023). Design and control of automatic bottles packaging line with modular modeling and simulations. *U.P.B. Sci. Bull., Series D*, 85(1).

Ekinci, A., Öksüz, M., Ates, M., & Aydin, I. (2022). Thermal and mechanical properties of polypropylene/post-consumer poly(ethylene terephthalate) blends: Bottle-to-bottle recycling. *Journal of Polymer Research*, 29, 433. https://doi.org/10.1007/s10965-022-03229-6

Feng, N. Y., Zhang, M., Li, G., & Meng, G. (2020). Dynamic characteristic analysis and startup optimization design of an intermediate drive belt conveyor with non-uniform load. *Science Progress*, 103(1), 1–20. https://doi.org/10.1177/0036850419881089

Francik, S., Lapczynska-Kordon, B., Slomka-Polonis, K., & Knapczyk, A. (2018). Model of technological line for bottling of fruit juices. *Engineering for Rural Development*, Jelgava, 23–25 May 2018. https://doi.org/10.22616/ERDev2018.17.N428

Guo, Y., & Wang, F. (2020). Multi-body dynamic equations of belt conveyor and the reasonable starting mode. *Symmetry*, 12(9), 1489. https://doi.org/10.3390/sym12091489

Halepoto, I. A., Shaikh, M. Z., Chowdhry, B. S., & Uqaili, M. A. (2016). Design and implementation of intelligent energy efficient conveyor system model based on variable speed drive control and physical modeling. *International Journal of Control and Automation*, 9(6), 379–388. https://doi.org/10.14257/ijca.2016.9.6.36

Hea, D., Panga, Y., Lodewijksa, G., & Liu, X. (2018). Healthy speed control of belt conveyors on conveying bulk materials. *Powder Technology*, 327, 408–419. https://doi.org/10.1016/j.powtec.2018.01.002

Jeftenić, B., Ristić, L., Bebić, M., & Štatkić, S. (2009). Controlled induction motor drives supplied by frequency converters on belt conveyors – Modeling and commissioning. *IEEE*, 978-1-4244-4649-0 https://doi.org/10.1109/IEEECONF.2009.5646810

Keawjaroen, P., & Suvanjumrat, C. (2017). A master shape of bottles for design under

desirable geometry and top load test. *MATEC Web of Conferences*, 95, 02008. https://doi.org/10.1051/matecconf/201795020 08

Li, J., & Pang, X. (2018). Belt conveyor dynamic characteristics and influential factors. *Shock and Vibration*, 2018, Article ID 8106879. https://doi.org/10.1155/2018/8106879

Monkova, K., Monka, P. P., & Vodilka, A. (2024). Comparison of the bending behavior of cylindrically shaped lattice specimens with radially and orthogonally arranged cells made of ABS. *Polymers,* 16(7), 979. https://doi.org/10.3390/polym16070979

Ojoa, O. T., & Shittub, R. A. (2023). Design and finite element method-based structural analysis of a PET bottles-to-plastic flakes recycling plant. *International Journal of Industrial Engineering and Management*, 14(1), 25–40. https://doi.org/10.24867/IJIEM-2023-1-322

Ostergaard, N., & Danjou, S. (2017). On numerical simulation of the dynamics of bottles in conveyor systems. *Journal of Applied Packaging Research*, 9(3), 60–72.

Ostergaard, N., & Danjou, S. (2017). On numerical simulation of the dynamics of bottles in conveyor systems. *Journal of Applied Packaging Research*. https://repository.rit.edu/japr/vol9/iss3/4

Pop, N., Vlădăreanu, L., Migdalovici, M., Pop, A. I., & Radulescu, M. (2019). Trajectory optimization for mobile robots using model predictive control. *Periodicals of Engineering and Natural Sciences*, 7(1). https://doi.org/10.21533/pen.v7i1.376.g260

Preti, F., Barbieri, M., & Paolo, P. (2010). Star wheel. U.S. Patent No. 7,832,546 B2. U.S. *Patent and Trademark Office*. https://patents.google.com/patent/US7832546B2/en

Shiba, K. (1975, January 13). Apparatus for rotating bottles. United States Patent No. 3,957,154. Osaka, Japan.

Suvanjumrat, C., & Puttapitukporn, T. (2011). Determination of drop-impact resistance of plastic bottles using computer-aided engineering. *Kasetsart Journal (Natural Sciences)*, 45, 932–942.

Umoren, M. A., Essien, A. O., & Ekpoudom, I. I. (2016). Design and implementation of conveyor line speed synchronizer for industrial control applications: A case study of Champion's Breweries PLC, Uyo. *Nigerian Journal of Technology (NIJOTECH)*, 35(3), 618–626. https://doi.org/10.4314/njt.v35i3.21

Ungureanu, M., Marina, M., Stoicovici, D., & Ungureanu, N. (2020). Sistem de fixare a sticlelor de plastic pentru aparate rotative de testare a etanșeității. Brevet de Invenție RO nr. 133200/2020. https://osim.ro/wp-content/uploads/Publicatii-OSIM/BOPI-Inventii/2020/bopi_inv_08_2020.pdf

Yang, C., Liu, J., Li, H., & Zhou, L. (2018). Energy modeling and parameter identification of dual-motor-driven belt conveyors without speed sensor. *Energies,* 11(12), 313.https://doi.org/10.3390/en11123313

Zeng, F., Yan, C., Wu, Q., & Wang, T. (2020). Dynamic behaviour of a conveyor belt considering non-uniform bulk material distribution for speed control. *Applied Sciences*, 10(12), 4436. https://doi.org/10.3390/app10134436

Acknowledgment

Funding: This research received no external funding

CARPATHIAN JOURNAL OF FOOD SCIENCE AND TECHNOLOGY

journal homepage: **http://chimie-biologie.ubm.ro/carpathian_journal/index.html**

Research article

ENZYMATIC CAROTENOID CLEAVAGE IN YELLOW PASSION FRUIT (*Passiflora flavicarpa*) POMACE

Martina Widhi Hapsari[1]✉, Supriyadi[2], Andriati Ningrum[2], Swastika Dewi[3], Nurul Hasniah[3]

[1] *Department of Food Technology, Science and Technology Faculty, Universitas Nasional Karangturi, Semarang 50127, Indonesia*
[2] *Department of Food and Agricultural Product Technology, Faculty of Agricultural Technology, Universitas Gadjah Mada, Yogyakarta 55281, Indonesia*
[3] *Food Technology Department, Faculty of Animal and Agricultural Sciences, Universitas Diponegoro, Semarang 50275, Indonesia*
✉*martina.widhi@unkartur.ac.id*
https://orcid.org/0009-0001-2078-7029,

https://doi.org/10.34302/2025.17.3.12

Article history:
Received
June 11th 2025
Accepted
October 17th 2025

Keywords:
Carotenoid Cleavage;
Dioxygenase (CCD);
Enzymatic activity;
Molecular weight;
Volatile compounds;
Yellow passion fruit pomace.

Abstract
Carotenoid Cleavage Dioxygenase (CCD) is a type of enzyme that plays a role in forming flavor compounds from natural carotenoid sources, such as yellow passion fruit. The study aims to describe the partial purification of CCD enzymes from yellow passion fruit pomace and to identify the optimum pH and temperature performance of CCD enzymes, carotenoid compounds, and volatile compounds in yellow passion fruit pomace. The enzyme was partially purified using centrifugation, 80% ammonium sulfate precipitation, dialysis with a membrane cutoff of 12 kDa, and Sodium Dodecyl Sulfate Polyacrylamide Gel Electrophoresis. The relative activity of CCD enzymes on dialysis was 31.94%, showing that there was CCD enzyme activity that can oxidize the β-carotene substrate. The optimum temperature of CCD enzymes was 60 °C, while the optimum pH value was 7. The analysis of carotenoids using HPLC-PDA showed that yellow passion fruit pomace contains β-carotene, neoxanthin, ζ-carotene, and luteinepoxide. The dominant protein produced by dialysis had a molecular weight of 40 kDa. There were 19 volatile compounds identified in the yellow passion fruit pomace. The activity of CCD enzymes from yellow passion fruit pomace using carotenoid substrate can be used as a biocatalyst in the natural flavor industry

1. Introduction

Several exotic fruits are commonly used for juice-making in several countries. Unfortunately, after the juice production, the pomace as a by-product has not been utilized completely. The agricultural byproducts, which are widely available and rich in organic chemicals, offer both a challenge and an opportunity (Rame *et al*., 2023; Al-Baarri *et al.*, 2019). Yellow passion fruit is one of the fruits that are usually used for juice making and producing byproducts. Yellow passion fruit is

type of passion fruit that contains beneficial chemical compounds, such as citric acid, ascorbic acid, lactic acid, malonic acid, niacin, riboflavin, vitamin A and C (Ayuningtyas & Broto, 2023). The residues from passion fruit processing represent 76% of the weight of the processed fruits, of which 26% is made up of the seeds (Ferrari *et al*., 2004). Annually, these seeds amount to tons of solid residues whose disposal involves operational costs for the pulp and juice industries and represents an environmental problem (Malacrida & Jorge, 2012). Whereas by-products of exotic fruits still contain high levels of various health-enhancing substances that can be extracted from the byproducts, for example, as a raw material for nutraceutical, and nutritional, and can be used for enzyme production (Ayala-Zavala *et al*., 2011; Ruiz-Sola & Rodríguez-Concepción, 2012). The primary health benefits of carotenoids are ascribed to their antioxidant properties (Andarwulan *et al*., 2021).

Carotenoid cleavage dioxygenases (CCD) are a family of enzymes that catalyze the oxidative cleavage of carotenoids. The distinctive yellow, orange, and red colors of fruits and vegetables are caused by phytonutrients called carotenoids (Anjani *et al*., 2022). This CCD enzyme can be used as a precursor for natural flavor formation. In a previous study, thirteen carotenoids were identified and separated in passion fruit using HPLC, with z-carotene identified as the predominant compound (Mercadante *et al*., 1998). β-carotene and lycopene were also identified in passion fruit by-products (Da Silva *et al*., 2014). Yellow passion fruit contains β-ionon and other volatile compounds from the breakdown of non-volatile precursors (Janzantti *et al*., 2012; Leão *et al*., 2014). The presence of β-ionons and carotenoids indicates that in passion fruit, a CCD enzyme breaks down carotenoids into volatile compounds. The formation of or isoprenoids as aroma-impact compounds by enzymatic reaction has been identified in several plants, e.g., star-fruits, nectarines, quince, rose, osmanthus flower, seaweed, tomato, petunia flower, melon, citrus (Baldermann *et al*., 2005, 2010; Fleischmann, Lutz-Röder, *et al*., 2002; Fleischmann, Studer, *et al*., 2002; Huang *et al*., 2009; Simkin *et al*., 2004). CCD enzymes can degrade β-carotene to β-ionon which has a fruity-like aroma.

This study aimed to identify carotenoid compounds with HPLC-PDA, describe partial purification of CCD enzymes from yellow passion fruit pomace, identify the optimum pH, temperature performance, and molecular weight of CCD enzymes, and identify volatile compounds in yellow passion fruit pomace by using GC/MS.

2. Materials and methods

2.1 Materials

Yellow passion fruit *(Passiflora flavicarpa)* has been obtained from Lintang Panglipuran farm, Sleman, Yogyakarta, Indonesia. β-Carotene was purchased from Sigma-Aldrich, America. Tris–HCl, MgCl2, KCl, Tween 40, sodium dodecyl sulfate (SDS), acrylamide, and bisacrylamide were all purchased from Merck, Germany. All other reagents were at least of analytical grade.

2.2 Methods

2.2.1 Identification of carotenoid compounds

Carotenoids were isolated from pandan leaves using the method published by Ningrum *et al* (Ningrum *et al*., 2015), with some modifications. Three grams of the plant were powdered and extracted with 30 mL of hexane, acetone, and methanol (2:1:1, v/v/v), which was repeated until the extraction solvent was colorless. The extract was then saponified by adding 8 mL of 40% methanolic potassium hydroxide for 1 hour. Next, 30 mL of hexane was used to extract the carotenoids. The extract was then rinsed with distilled water until it reached neutral pH and dried with sodium sulphate. After evaporation, the residue was soaked in acetone and filtered through a 0.45 μm membrane filter for HPLC-PDA analysis.

A C18 reverse-phase analytical column was utilized with a gradient solvent system of acetone (A) and water (B). Initially, a mixture of 70% acetone and 30% water was used, with a linear increase to 95% acetone over 20 minutes, and then further increased to 100% acetone by

50 minutes. The flow rate was set to 0.5 mL/min, with wavelength scanning between 350 and 550 nm. The HPLC system (Accela, Thermo) featured a quaternary gradient and a photodiode array detector. Semi-quantitative analysis of other carotenoids was achieved by applying peak areas to a calibration curve based on β-carotene.

2.2.2. Enzyme purification

The pulp of fully ripened yellow passion fruit (1 kg) was processed to make juice. After filtration, the remaining pomace, a by-product of the juice extraction, was collected. The pomace was homogenized in a sample buffer (125 mmol/l KCl, 5 mmol/l $MgCl_2$, 50 mmol/l Tris, pH 7, 1:2 w/v) using a blender for 120 seconds. The homogenized mixture was centrifuged at 7000 g at 20 °C for 10 minutes, after which the sediment was discarded, and the supernatant underwent ammonium sulfate precipitation (80%, 24 hours, 4 °C). The resulting precipitate was dissolved in sample buffer and dialyzed using a membrane with a 12 kDa cutoff at 4 °C for 24 hours, with the buffer replaced three times. Protein concentration was determined using the Lowry assay, with bovine serum albumin as the standard.

2.2.3. Enzyme assay

The carotenoid-cleavage activity was measured following the method outlined in (Huang et al., 2009). The breakdown of the substrate, β-carotene, was analyzed using a UV/VIS spectrophotometer at 505 nm. In each enzymatic assay, a reaction mixture containing the enzyme extract, a carotenoid/Tween 40 substrate, and a buffer solution was incubated. The buffer solution consisted of 100 mM Tris-base, 125 mM KCl, and 5 mM $MgCl_2$. The carotenoid/Tween 40 substrate solution was prepared according to (Huang *et al*., 2009): 1 mg of β-carotene was dissolved in acetone, combined with 1 g of Tween 40 also dissolved in acetone, thoroughly mixed, and the solvent was evaporated. The remaining mixture was diluted with 10 mL of H_2O and filtered through a 0.45-mm filter.

Enzymatic activity was assessed by measuring the absorbance of each sample (250 mL of crude enzyme, 1675 mL of Tris buffer, and 75 mL of carotenoid substrate) and control (1925 mL of Tris buffer and 75 mL of carotenoid substrate) over 20 minutes at 505 nm, starting immediately after substrate addition. The substrate's degradation was monitored through time-course measurements for the entire 20 minutes. The change in absorbance before and after incubation was used to calculate relative enzymatic activity. Each experiment was conducted in triplicate.

2.2.4. Influence of temperature and pH on the enzymatic activity

The effect of temperature on carotenoid-cleavage activity was evaluated by incubating the enzymatic reaction mixture at several temperatures (30, 45, 60, 75, 90 °C) for 10 min. The effect of pH on carotenoid-cleavage activity was evaluated at several pH values of the Tris buffer containing 100 mm Tris-base, 125 mm KCl, and 5 mm $MgCl_2$ (pH 5-9). Then, the activity was spectrophotometrically determined, as described above. All experiments were performed in triplicate.

2.2.5. Determination of molecular weight

Denaturing polyacrylamide gel electrophoresis (SDS-PAGE) was carried out in a Mini Protein Cell (BioRad) using commercially available 30% polyacrylamide gels stained with commercially available Coomassie blue. All runs were carried out under constant voltage conditions (100 V) at room temperature for ± 2 h.

2.2.6. Volatile compounds

Ten grams of yellow passion fruit pomace was a mixture with pentane:dichlorometan (2:1 v/v). The mixture was stored in the freezer for 24 h. After that, the solution was filtered through a 0.45 μm membrane filter. Filtrate was added sodium anhydrous and evaporated. The free volatile compounds were analysed by gas chromatography-mass spectrometry (GC-MS) using the following temperature program: initial temperature 80 °C, ramped to 250 °C at 10 °C/min and held for 10 min. The mass scan range was set to m/z 50–300. Helium was used as carrier gas at a constant flow rate of 1.7 mL/min. The identification of volatile compounds was based on a comparison of the mass spectra of each component with the mass spectral library WILEY.

3. Results and discussions

3.1 Identification carotenoid compounds

Yellow passion fruit has orange pulp, which indicates carotenoids. In this study, carotenoid compounds were identified to determine the types of carotenoids contained in yellow passion fruit pomace as CCD enzyme substrates. Carotenoids in yellow passion fruit pomace extracts were identified by comparison with retention time and absorption spectrum. In this study, the identification of carotenoid compounds was performed by comparing the chromatogram of the sample with that of the standard using an overlay method. This method enables the retention times of both the sample and the standard to align in the same positions. Peaks with retention times that correspond to the standard are identified as belonging to the sample. Furthermore, carotenoid identification can also be achieved by comparing the spectrum generated by the standard with that of the sample; both spectra should correspond closely.

In Figure 1, there are four identified carotenoids, including neoxanthin, z-carotene, b-carotene, and luteinepoxide. The chromatogram shows the presence of four identified carotenoid peaks: at a retention time of 26 minutes is ζ-carotene, at 27 minutes is neoxanthin, at 28 minutes is β-carotene, and from 29 to 30 minutes is luteinepoxide In the previous studies, it was found that yellow passion fruit found thirteen types of carotenoids identified; phytoene, phytofluene, β-carotene, ζ-carotene, neurosporene, lycopene, prolicopene, monoepoxy β-carotene, β-cryptoxanthin, β-citraurin, antheraxanthin, violaxanthin and neoxanthin (Mercadante *et al*., 1998). Another study reported on yellow passion fruit containing carotenoid compounds such as; lutein, luteinepoxide, lycopene, zeaxanthin, β-carotene and β-cryptoxanthin as the dominant carotenoid compounds (Pertuzatti *et al*., 2015). The existence of differences in carotenoid compounds can be due to several factors, such as different varieties, different extraction methods, and the condition of the equipment used.

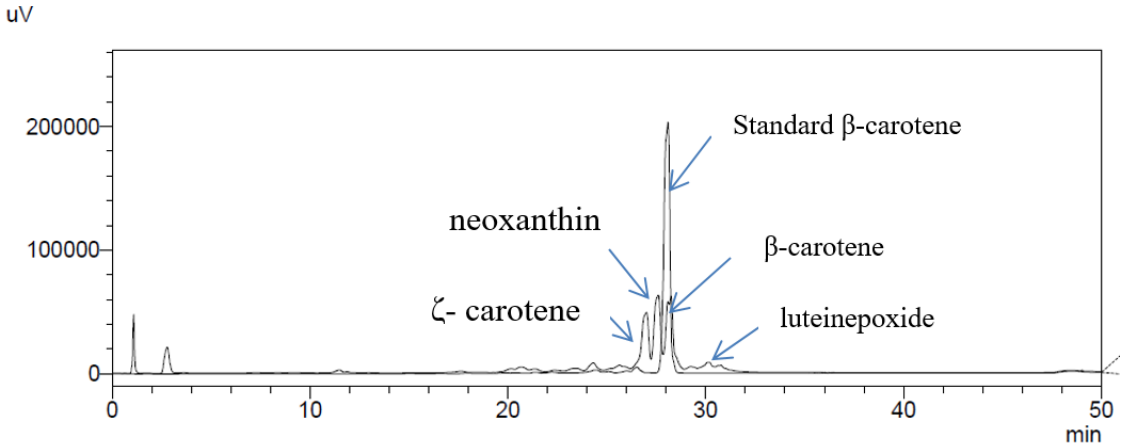

Figure 1. HPLC chromatogram of carotenoids of yellow passion fruit pomace

Table 1 shows information regarding retention time, absorption maxima, and semi-quantification of the carotenoids found in yellow passion fruit pomace. β-Carotene, neoxanthin, and lutein were found as major carotenoids in HPLC chromatogram (Figure 1). The major carotenoids content of yellow passion fruit pomace consisted of 9,51 ppm of neoxanthin, 9,41 ppm of β-carotene and 7,44 of ζ- carotene.

Table 1. Carotenoids identified in yellow passion fruit pomace by using HPLC analysis

Carotenoid	Peak	Retention time (min)	λ_{max} (nm)	Literatur (Britton *et al*., 1995)	Semi quantification (ppm)
ζ- carotene	1		380	380	7.44
	2	26.998	401	402	
	3		426	426	
Neoxanthin	1		412	416	9.51
	2	27.597	435	438	
	3		464	466	
β - carotene	1		427	-	9.41
	2	28.087	450	454	
	3		478	480	
Luteinepoxide	1		419	416	0.93
	2	29.238	441	440	
	3		467	468	

Table 1 shows several variations in the maximum wavelengths formed and indicates a shift in wavelength between the sample and the literature. This can be caused by several factors, including interactions with types of carotenoids present in the extract, the acidity level of the solution, oxidation effects, and other factors (Britton *et al*., 1995). Once the types of carotenoids in the sample are identified, the carotenoid content can be calculated semi-quantitatively by applying the obtained peak height to the β-carotene calibration. The results of this study show that carotenoids are still present in the yellow passion fruit pomace. This was also found in the study by Da Silva *et al*. (2014), which reported that by-products from several tropical fruits, such as pineapple, acerola, guava, and passion fruit in Brazil, contain higher levels of β-carotene, lycopene, flavonoids, and anthocyanins compared to their juice. In addition to serving as precursors for carotenoid-derived aroma compounds, the presence of carotenoids in yellow passion fruit pomace and juice indicates that carotenoids act as provitamin A, which plays an important role in eye health and have antioxidant activity (Murillo *et al*., 2013).

3.2.Isolation and characterization of yellow passion fruit pomace carotenoid cleavage enzyme

As can be seen in **Table 2**, each stage of CCD enzyme purification from yellow passion fruit pomace was increased. Increased activity of CCD enzymes after precipitation of ammonium sulfate and dialysis compared with crude enzymes. The relative activity of crude enzyme from yellow passion fruit pomace was 20.30 ± 0.65% which increased after precipitation to 27.28 ± 0.23% and the dialysis increased to 31.94 ± 0.31%. Protein concentration in crude enzyme was 1.12 ± 0.12 mg / mL and decreased significantly after dialysis to 0.06 ± 0.07 mg / mL. Purification by the addition of ammonium sulfate results in decreased enzyme protein content because the non-enzyme protein was precipitated.

Table 2 also shows that the purity level of CCD enzyme from pomace increased after precipitation and dialysis compared to the relative activity value of the crude enzyme. These data indicate that purification treatments can enhance the relative activity of the CCD enzyme. In the study by Baldermann *et al*. (2009), the relative activity of the CCD enzyme from tea leaves was obtained at 60% using acetone for protein precipitation. Partial purification was also performed on quince fruit (*Cydonia oblonga*) through centrifugation, 85%

acetone precipitation, ultrafiltration (300 kDa, 50 kDa), and isoelectric focusing (pH 3-10) yielding a relative activity of 75%.

Table 2 Protein Content and Relative Activity of CCD

Sample	Protein concentration (mg/mL)	Relative Activity (%)
Crude enzyme	1.12±0.12	32.45
Precipitation	0.15±0.07	40.65
Dialysis	0.07±0.52	61.54

Determination of optimum temperature and pH was carried out on CCD enzymes on dialysis results. The determination of the optimum temperature was carried out by reacting the enzyme with the substrate at different temperatures (30, 45, 60, 75, 90 °C). From the perspective of protein structure, temperature affects the looseness and density of bonds in the enzyme's protein structure (Al-Baarri et al., 2018). Meanwhile, the determination of the optimum pH was performed by reacting the CCD enzyme with the β-carotene substrate under different pH conditions (5, 6, 7, 8, 9). The results for the optimum temperature and pH of the CCD enzyme can be seen in Figure 2.

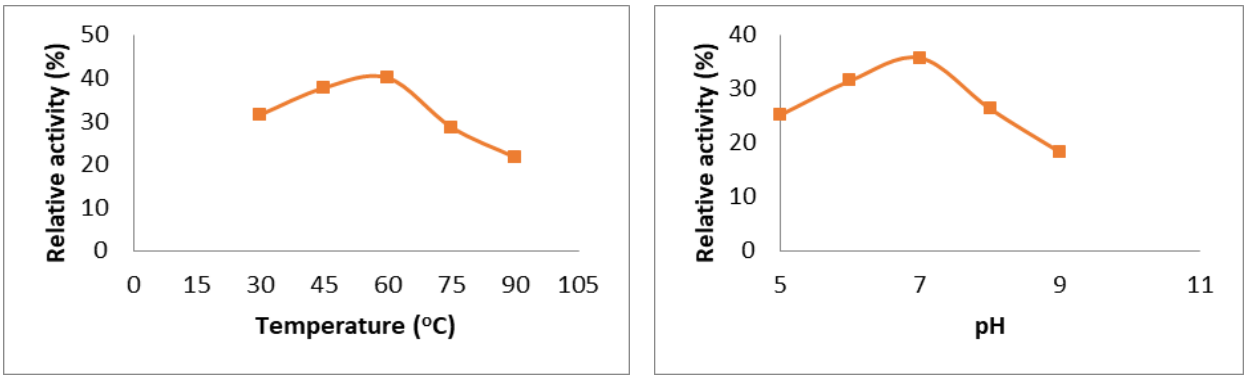

(a) (b)

Figure 2. Temperature (a) and pH (b) dependence of carotenoid-cleavage activity of dialysis enzyme

The optimum temperature of the CCD enzyme was 60 °C (Figure 2). Until the optimum temperature is reached, the enzyme activity will rise in line with the temperature (Pertiwiningrum *et al*., 2017). At the optimum temperature, the conformation of the enzyme's protein structure is ideally positioned to bind the substrate and form the product, resulting in the highest activity.

Temperature changes also affect the bonds that maintain the enzyme's molecular conformation. Conformational changes impact the enzyme's active site, as certain heat conditions can break hydrogen bonds. Breaking one hydrogen bond can lead to the more manageable disruption of subsequent hydrogen bonds within the polypeptide chain, resulting in enzyme protein denaturation. The optimum temperatures of CCD in various plants were 45 °C in nectarines and starfruit and 70 °C in tea (Baldermann *et al*., 2005, 2010; Fleischmann, Studer, *et al*., 2002). These high optimum temperatures of carotenoid cleavage activity indicate that the enzyme can be an excellent alternative for the food industry, especially for several thermal processes.

The optimum pH value of b-carotene degradation activity was found to be 7 (Figure 2), while the optimum pH values for carotenoid-cleavage activity were reported in tea leaves as 7.4, in star fruit as 8.5, and quince in the range of 6– 9 (Baldermann *et al*., 2005; Fleischmann, Lutz-Röder, *et al*., 2002). At the optimum pH, the enzyme maintains the correct three-

dimensional conformation to bind the substrate effectively (Pratama et al., 2018). Under conditions outside the optimum pH, the enzyme's conformation begins to change, causing the substrate to be misaligned with the enzyme's active site. This misalignment hinders the catalytic process from proceeding optimally, resulting in reduced enzyme activity (Al-Baarri, Legowo, Wratsongko, et al., 2019).

3.3. Determination of protein molecular weight of CCD

Proteins that moved and halted at a specific migration distance during the electrophoresis process are indicated by the presence or absence of bands at that migration distance (Al-Baarri *et al*., 2024). After SDS-PAGE and commasie blue, seven protein bands were detected in the crude enzyme, six protein bands in precipitation with ammonium sulfate, and three bands in dialysis (Figure 3).

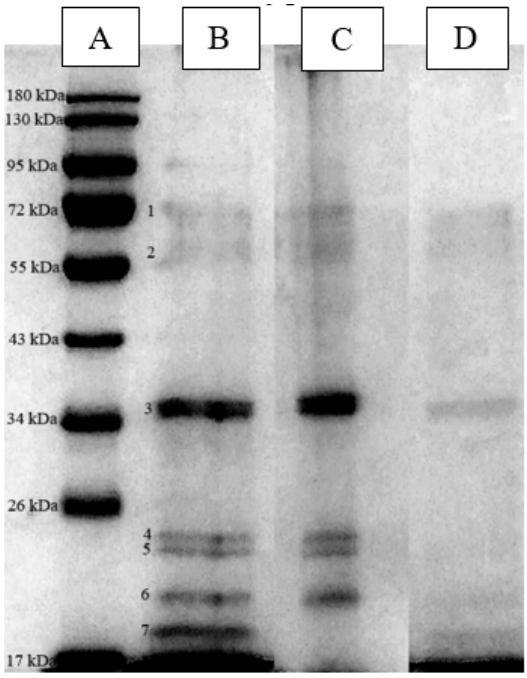

Figure 3. Polyacrylamide gel electrophoresis of the partially purified enzyme. (A) Marker (B) Crude enzyme (C) Precipited with ammonium sulfate (D) Dialysis enzyme

The molecular weight of the proteins was calculated from the calibration curve of the standard proteins (Rf value vs. mol.mass) used for the SDS PAGEs. Based on the results of colour intensity analysis using ImageJ, it can be seen that the dominant CCD enzyme band protein from the yellow passion fruit pomace is found at a molecular weight of 40 kDa. In previous studies, CCD enzymes isolated from *Arabidopsis thaliana* plants had a molecular weight of 66 kDa (Schwartz *et al*., 2004), and three bands were detected from quince fruit *(Cydonia oblonga)* which is 21.8 kDa, 23.9 kDa, and 25.9 kDa (Baldermann *et al*., 2005). The difference in molecular weight of CCD enzymes because the composition of CCD enzymes is different in each plant.

3.4 Identification of volatile compounds

From the identification results of yellow passion fruit pomace compounds using GC-MS, 18 types of volatile compounds were found with the highest number of components from terpene compounds (Table 3). Other groups of compounds are aldehydes, esters, alkene, phenol, naphthalene, and alcohol. Volatile compounds in the dominant yellow passion fruit pomace are ethyl hexanoate (15.67%) and 1-hexanol (14.07%).

Table 3 Volatile Compound in yellow passion fruit pomace

Group of Compound	Compound in yellow passion fruit pomace	% Relative Area
Aldehid	Heksanal	2.09
Terpene	α-gurjunene	6.09
	Veridiflorol	2.27
	Juniper champor	3.17
	Farnesol	6.38
	(+)-Aromadendrene	2.00
	Spathulanol	2.77
	Squalene	4.36
	Patchoulene	3.69
Alkena	Docosane	1.46
Alkohol	1-hexanol	14.07
Phenol	Phenol, 2 methoxy-3-(2 propenyl)	7.13
	3-allyl-6-methoxy phenol	1.41
Ester	ethyl hexanoate	15.67
	Butyl acetate	1.38
Naphtalene	1-naphtalenol	3.38
	1-naphtalenemethanol	1.99
Acid	Geranic acid	1.71

Ethyl hexanoate gives the aroma of sweet, floral, fruity. Hexanoate and acetate esters provide a fruity, sweet, citrus aroma. Esters, terpenes, alcohols, octanal compounds, dodecanol compounds and passion fruit scents, fruity, citric, and candy are scents detected in mature mature passion fruit (Janzantti *et al*., 2012; Janzantti & Monteiro, 2014; Leão *et al*., 2014). Terpenoid compounds are carotenoid derivatives that can give a distinctive flavour and aroma.

4. Conclusions

Carotenoid compounds identified in yellow passion fruit pomace: ζ-carotene, neoxanthin, β-carotene and luteinepoxide. The purified fraction showed carotenoid cleavage activity with β-carotene as substrate. The optimum temperature for enzymatic carotenoid-cleavage is 60 °C, whereas the optimum pH value of carotenoid cleavage activity is 7. Dominant volatile compounds in yellow passion fruit pomace are ethyl hexanoate and 1-hexanol.

5. References

Al-Baarri, A. N., Dwiloka, B., Mulyani, S., Pramono, Y. B., Setiani, B. E., Rahmawati, A. A., Jordan, A., & Nababan, P. (2024). Protein fraction profile and physicochemical quality of Blacksoyghurt drink. *Food Research*, *8*(2), 435–442.

Al-Baarri, A. N., Legowo, A. M., Hadipernata, M., Broto, W., Auliyana, E., Puspitoasih, A. D., Wratsongko, A. C. D., Izzati, L., Michael, Handoko, Y. D. P., Yusuf, M., Wahda, H. M., & Pangestika, W. (2019). Inhibitory action of hypoiodous acid (hio) against browning on apple through the analysis of lightness appearance. *IOP Conference Series: Earth and Environmental Science*, *309*(1), 2–7. https://doi.org/10.1088/1755-1315/309/1/012010

Al-Baarri, A. N., Legowo, A. M., & Widayat. (2018). The browning value changes and spectral analysis on the Maillard reaction product from glucose and methionine model system. *IOP Conference Series: Earth and Environmental Science*, *102*(1). https://doi.org/10.1088/1755-1315/102/1/012003

Al-Baarri, A. N., Legowo, A. M., Wratsongko, A. C. D., Puspitoasih, A. D., Izzati, L., Auliana, E., Michael, Pangestika, W., Hadipernata, M., & Broto, W. (2019). Effect of Hypoiodous Acid (HIO) treatment on color and pH changes in snake fruit (Salacca edulis Reinw.) during room temperature storage. *IOP Conference Series: Earth and Environmental Science*, *292*(1). https://doi.org/10.1088/1755-1315/292/1/012042

Al-Baarri, N., Cahyarani Puspita, N., Saraswati, & Średnicka-Tober, D. (2021). Antioxidants such as flavonoids and carotenoids in the diet of Bogor, Indonesia residents. *Antioxidants*, *10*(4), 587.

Anjani, G., Ayustaningwarno, F., & Eviana, R. (2022). Critical review on the immunomodulatory activities of carrot's β-carotene and other bioactive compounds. *Journal of Functional Foods*, *99*, 105303. https://doi.org/https://doi.org/10.1016/j.jff.2022.105303

Ayala-Zavala, J. F. N., Vega-Vega, V., Rosas-Domínguez, C., Palafox-Carlos, H., Villa-Rodriguez, J. A., Siddiqui, M. W., Dávila-Aviña, J. E., & González-Aguilar, G. A. (2011). Agro-industrial potential of exotic fruit byproducts as a source of food additives. *Food Research International*, *44*(7), 1866–1874.

Ayuningtyas, I. P., & Broto, W. (2023). The preparation of virgin coconut oil using acid from passion fruit extract at different temperature and incubation time. *Journal of Applied Food Technology*, *10*(1), 23–26.

Baldermann, S., Kato, M., Kurosawa, M., Kurobayashi, Y., Fujita, A., Fleischmann, P., & Watanabe, N. (2010). Functional characterization of a carotenoid cleavage dioxygenase 1 and its relation to the carotenoid accumulation and volatile emission during the floral development of Osmanthus fragrans Lour. *Journal of Experimental Botany*, *61*(11), 2967–2977.

Baldermann, S., Naim, M., & Fleischmann, P. (2005). Enzymatic carotenoid degradation and aroma formation in nectarines (Prunus persica). *Food Research International*, *38*(8–9), 833–836.

Britton, G., Liaaen-Jensen, S., & Pfander, H. (1995). *Carotenoids: Isolation and Analysis. Volume 1A*. Birkhäuser Verlag.

Da Silva, L. M. R., De Figueiredo, E. A. T., Ricardo, N. M. P. S., Vieira, I. G. P., De Figueiredo, R. W., Brasil, I. M., & Gomes, C. L. (2014). Quantification of bioactive compounds in pulps and by-products of tropical fruits from Brazil. *Food Chemistry*, *143*, 398–404.

Ferrari, R. A., Colussi, F., & Ayub, R. A. (2004). Characterization of by-products of passion fruit industrialization utilization of seeds. *Revista Brasileira de Fruticultura*, *26*, 101–102.

Fleischmann, P., Lutz-Röder, A., Winterhalter, P., & Watanabe, N. (2002). *Carotenoid cleavage enzymes in animals and plants*. ACS Publications.

Fleischmann, P., Studer, K., & Winterhalter, P. (2002). Partial purification and kinetic characterization of a carotenoid cleavage enzyme from quince fruit (Cydonia oblonga). *Journal of Agricultural and Food Chemistry*, *50*(6), 1677–1680.

Huang, F.-C., Horváth, G., Molnár, P., Turcsi, E., Deli, J., Schrader, J., Sandmann, G., Schmidt, H., & Schwab, W. (2009). Substrate promiscuity of RdCCD1, a carotenoid cleavage oxygenase from Rosa damascena. *Phytochemistry*, *70*(4), 457–464.

Janzantti, N. S., Macoris, M. S., Garruti, D. S., & Monteiro, M. (2012). Influence of the cultivation system in the aroma of the volatile compounds and total antioxidant activity of passion fruit. *LWT-Food Science and Technology*, *46*(2), 511–518.

Janzantti, N. S., & Monteiro, M. (2014). Changes in the aroma of organic passion fruit (Passiflora edulis Sims f. flavicarpa Deg.) during ripeness. *LWT-Food Science and Technology*, *59*(2), 612–620.

Leão, K. M. M., Sampaio, K. L., Pagani, A. A. C., & Da Silva, M. A. A. P. (2014). Odor potency, aroma profile and volatiles composition of cold pressed oil from industrial passion fruit residues. *Industrial*

Crops and Products, *58*, 280–286.

Malacrida, C. R., & Jorge, N. (2012). Yellow passion fruit seed oil (Passiflora edulis f. flavicarpa): physical and chemical characteristics. *Brazilian Archives of Biology and Technology*, *55*, 127–134.

Mercadante, A. Z., Britton, G., & Rodriguez-Amaya, D. B. (1998). Carotenoids from yellow passion fruit (Passiflora e dulis). *Journal of Agricultural and Food Chemistry*, *46*(10), 4102–4106.

Murillo, E., Nagy, V., Agócs, A., & Deli, J. (2013). Carotenoids with κ-end group. In M. Yamaguchi (Ed.), *Carotenoids: Food Sources, Production and Health Benefits* (pp. 49–78). Nova Science Publishers.

Ningrum, A., Minh, N. N., & Schreiner, M. (2015). Carotenoids and norisoprenoids as carotenoid degradation products in pandan leaves (Pandanus amaryllifolius Roxb.). *International Journal of Food Properties*, *18*(9), 1905–1914.

Pertiwiningrum, A., Anggraini, F. D., & Fitrianto, N. A. (2017). Isolation and identification of bacterial protease enzyme of leather waste. *Journal of the Indonesian Tropical Animal Agriculture*, *42*(1).

Pertuzatti, P. B., Sganzerla, M., Jacques, A. C., Barcia, M. T., & Zambiazi, R. C. (2015). Carotenoids, tocopherols and ascorbic acid content in yellow passion fruit (Passiflora edulis) grown under different cultivation systems. *LWT-Food Science and Technology*, *64*(1), 259–263.

Pratama, Y., Abduh, S. B. M., Legowo, A. M., Pramono, Y. B., & Albaarri, A. N. (2018). Optimum carrageenan concentration improved the physical properties of cabinet-dried yoghurt powder. *IOP Conference Series: Earth and Environmental Science*, *102*(1). https://doi.org/10.1088/1755-1315/102/1/012023

Rame, R., Purwanto, P., & Sudarno, S. (2023). Biotechnological approaches in utilizing agro-waste for biofuel production: An extensive review on techniques and challenges. *Bioresource Technology Reports*, *24*, 101662. https://doi.org/https://doi.org/10.1016/j.biteb.2023.101662

Ruiz-Sola, M. Á., & Rodríguez-Concepción, M. (2012). Carotenoid biosynthesis in Arabidopsis: a colorful pathway. *The Arabidopsis Book/American Society of Plant Biologists*, *10*, e0158. https://doi.org/10.1199/tab.0158

Schwartz, S. H., Qin, X., & Loewen, M. C. (2004). The biochemical characterization of two carotenoid cleavage enzymes from Arabidopsis indicates that a carotenoid-derived compound inhibits lateral branching. *Journal of Biological Chemistry*, *279*(45), 46940–46945.

Simkin, A. J., Underwood, B. A., Auldridge, M., Loucas, H. M., Shibuya, K., Schmelz, E., Clark, D. G., & Klee, H. J. (2004). Circadian regulation of the PhCCD1 carotenoid cleavage dioxygenase controls emission of β-ionone, a fragrance volatile of petunia flowers. *Plant Physiology*, *136*(3), 3504–3514.

Acknowledgments

This research is partially supported by Food Safety Scientific Consortium through the Research Implementation Agreement Contract No. 369/UN7.A/HK/X/2024

CARPATHIAN JOURNAL OF FOOD SCIENCE AND TECHNOLOGY

journal homepage: **http://chimie-biologie.ubm.ro/carpathian_journal/index.html**

Research article

ASSESSMENT OF COMMERCIAL HYDROCOLLOIDS, *Neolitsea cassia* LEAVES EXTRACT, AND SPIRULINA IN ENHANCING CRUMB PROPERTIES OF RICE-BASED LEAVENED FOOD PRODUCTS

Rathnayake, H. A.[1]✉, Navaratne S. B.[2], Navaratne C. M.[3]

[1]*Department of Food Technology, Faculty of Technology, Rajarata University of Sri Lanka, Mihintale, Sri Lanka*

[2]*Department of Food Science and Technology, Faculty of Applied Sciences, University of Sri Jayewardenepura, Gangodawila, Nugegoda, Sri Lanka*

[3]*Department of Agricultural Engineering, Faculty of Agriculture, University of Ruhuna, Mapalana, Kamburupitiya, Sri Lanka*

✉ *hrathnay@tec.rjt.ac.lk*

ORCID Number: 0000-0002-3086-0023

https://doi.org/10.34302/2025.17.3.13

Article history:
Received
May 29th 2025
Accepted
Septemeber 17th 2025

Keywords:
Crumb texture;
Guar gum;
Natural binding agents;
Sodium alginate;
Xanthan gum.

Abstract

Hydrocolloids are usually applied in leavened food products for the purpose of improving crumb textural and structural properties along with the storage stability. The current study was focused on assessing the effect of selected commercially available hydrocolloid materials (Xanthan gum, Guar gum, Sodium alginate), *Neolitsea cassia* leaves mucilage, and dehydrated Spirulina (*Spirulina maxima*) powder on the quality characteristics of rice-based leavened products that are fermented and gelatinized under slightly high initial air pressure conditions. Eleven rice-based (rice: wheat, 50: 50 w/w) dough samples, comprising different levels of commercial hydrocolloids (0.5%, 0.75%), *N. cassia* leaves extract (5%, 10%), and dehydrated Spirulina powder (1%, 1.5%) were prepared. Then, they were fermented and gelatinized in an enclosed chamber at 1.0 kg/cm^2 initial air pressure. Crumb volume, texture, cellular structure properties, and the storage stability of each crumb sample were evaluated and compared with a control. Results revealed the application of 0.75% Guar gum imparted to having a comparatively high crumb volume, specific volume and low bulk density, hardness, and a low crumb hardening rate during storage, despite uneven crumb cellular structure due to coalesced gas cells. Mucilaginous materials extracted from *N. cassia* leaves contributed to having a higher moisture retention capacity of the crumb during storage. The addition of dehydrated Spirulina powder also contributes resulting in a product with better volume and texture with an acceptable effect on preserving crumb characteristics during the storage.

1. Introduction

In case of developing leavened food products from composite flour, particularly comprising non-glutinous sources, hydrocolloids are frequently applied to improve the functional dough properties as well as to improve the keeping quality of the finished products (Shittu, Aminu, & Abulude, 2009). Xanthan gum, Guar gum, Alginates, Locust bean gum, Gum arabic, Carrageenan can be named as some examples of commercially available natural hydrocolloids that are commonly used in developing leavened baked products (Das, Raychaudhuri, & Chakraborty, 2015; Hager & Arendt, 2013; Salehi, 2019; Wang, Lu, Li, Zhao, & Han, 2017). Other than these hydrocolloids, various plant mucilage and algae are being utilized to enhance the texture of leavened food products.

The most common plant sources with edible grade mucilaginous materials available in Sri Lanka are, *Neolitsea cassia* (locally called Dawul kurundu) leaf extracts, *Abelmoschus esculentus* (Ladies' fingers) extract, *Durio zibethinus* (Durian) seeds extracts, and *Dillenia retusa* (locally called Goda Para) fruits extracts (Kasunmala, Navaratne, & Wickramasinghe, 2017; Navaratne, 2007). However, *A. esculentus* extract and *D. zibethinus* seeds extracts are heat stable; thus, can disturb the texture and the mouthfeel of the finished product. Mucilaginous materials in *N. cassia* leaves contain certain complex polysaccharides, which can bind with water and form a hydrocolloid solution (Wijerathne, Chandrajith, & Navaratne, 2018). *N. cassia* leaves extracts are commonly used in Sri Lanka as a texture improver and a binding agent in making a traditional sweet named "Aasmie". A previous study conducted by Navaratne (2007) has proved that the application of *N. cassia* leaves extracts (10%) can result a lower bulk density and an improved sensory profile in wheat flour bread while retarding the crumb staling by 6 to 8 hours.

Spirulina, an edible blue-green microalga belong to two genera of Spirulina and Arthrospira is rich in protein (55%-70%) with essential amino acids. Besides, Spirulina contains essential fatty acids (18%), vitamins (Vitamin B12, Vitamin E, and β-carotene), minerals (Calcium, Iron, Phosphorous, Potassium, Sodium, etc.), and pigments (Chlorophyll a, Phycocyanin, Allophycocyanin, Lutein, and Zeaxanthin) (Hosseini, Shahbazizadeh, Khosravi-Darani, & Mozafari, 2013; Massoud, Khosravi-darani, Nakhsaz, & Varga, 2016; Minh, 2014). Massoud et al. (2016) have stated that Spirulina can produce hydrocolloids, which contribute to reducing the degree of moisture loss, thereby reducing the dehydrating and hardening of crumb during storage. Moreover, the application of Spirulina can add a special color and a flavor to the finished product as well (Hosseini et al., 2013; Minh, 2014).

According to the study conducted by Rathnayake, Navaratne, and Navaratne (2019), fermentation followed by gelatinization of rice-related dough under slightly high pressurized condition (initial pressure at 1.0 kg/cm^2) contributed to having a higher leavened gas retention capacity with improved crumb cellular structure properties against a crumb sample developed under normal atmospheric conditions. Under this tell-tale, the current study was conducted by combining the two concepts of "incorporating a food hydrocolloid material" and "conducting the fermentation and gelatinization under slightly high air pressure condition" to obtain rice-related crumb samples with better crumb quality attributes, mechanical properties and storage stability.

2. Materials and methods

2.1. Materials

Paddy (BG300) was obtained from Rice Research and Development Institute, Bathalegoda, Sri Lanka. The obtained paddy was cleaned, de-hulled, and polished. The well-polished rice was soaked in an excess amount of water (25±2 ºC for 4 hours), drained off, and ground (National Grinder, MX 110PN, Japan). The obtained rice flour was dried (65±2 ºC, 3 hours) in a hot air oven (Lader, GPME350SSVISS080, UK) and passed through an 180 μm sieve (Sieve shaker, Endicotts, minor 200, UK).

Refined wheat flour, baker's dry yeast, salt, sugar, and shortening were purchased from a supermarket in Colombo, Sri Lanka.

Food grade hydrocolloids namely Xanthan gum, Guar gum, and Sodium alginate were purchased from Glorchem Enterprises, Bankshell Street, Colombo 11, Sri Lanka. Fresh *Neolitsea cassia* leaves were collected directly from growers near Colombo, Sri Lanka. The plucked *N. cassia* leaves were stored under refrigerated conditions for the subsequent use of the study. Dehydrated Spirulina (Spirulina maxima) powder (DSP) was received from a grower near Kalutara, Sri Lanka and sieved using a 90 µm sieve to obtain particles less than 90 µm.

2.2. Methods

2.2.1. Preparation of N. cassia leaves extract (NCLE)

Approximately 10.00±0.05 g (Axis analytical balance, ALN220, Poland) of partially dehydrated (under refrigerated condition) *N. cassia* leaves were hot water blanched for about 3 minutes. Thereafter, the leaves were gently rubbed in 100 ml water (25±1 ^{o}C) until the water get viscous with the mucilaginous materials of *N. cassia* leaves. Then, the extraction was filtered through several layers of muslin cloths. A similar procedure was followed to obtain the 5 % NCLE using approximately 5.00±0.05 g of partially dehydrated *N. cassia* leaves in 100 ml of water.

2.2.2. Preparation of rice-based leavened crumb samples

All the dough formulations comprised 50.00, 50.00, 1.00, 2.00, 1.60, and 2.00 grams of rice flour, wheat flour, salt, baker's dry yeast, sugar, and shortening respectively (on 100 g flour basis). Different levels of hydrocolloids, NCLE, and DSP were added to these formulations separately as illustrated in Table 1, to prepare eleven dough samples. These dough samples were subjected to fermentation (29±1 ^{o}C for 180 minutes) at 1.0 kg/cm^2 initial air pressure condition in an enclosed fermentation chamber followed by gelatinization (15 minutes) within the same chamber (15 minutes) while releasing the internal pressure with parallel to the starch gelatinization (Rathnayake et al., 2019).

Table 1 The levels of different hydrocolloids, NCLE and DSP added in to the dough formulations

Sample number	Abbreviation	Hydrocolloid/NCLE/DSP*	Level of different hydrocolloids/NCLE/DSP* incorporated into 100g of flour†
1	C	Control	No
2	XG0.5	Xanthan gum	0.5g
3	XG0.75	Xanthan gum	0.75g
4	GG0.5	Guar gum	0.5g
5	GG0.75	Guar gum	0.75g
6	SA0.5	Sodium alginate	0.5g
7	SA0.75	Sodium alginate	0.75g
8	NCLE5	5% NCLE	60ml
9	NCLE10	10% NCLE	62ml
10	DSP1	DSP	1g
11	DSP1.5	DSP	1.5g

*NCLE: *N. cassia* Leaves Extract; DSP: Dehydrated Spirulina Powder

†The level of hydrocolloid materials were selected based on literature; Xanthan gum, Guar gum, Sodium alginate (Collar et al., 1999; Das et al., 2015), NCLE (Navaratne, 2007), DSP (Massoud et al., 2016).

2.2.3. Analysis of crumb quality attributes

All the gelatinized crumbs were allowed to cool for 25 minutes (29±1 ºC, 67 % RH). Crumb volume (cm^3) was determined according to the seed displacement method as described by Aplevicz, Ogliari, and Sant'Anna (2013). Thereafter, specific volume (cm^3/g) and bulk density (g/cm^3) of the crumb samples were calculated based on the results obtained for crumb volume.

After cooling the gelatinized crumbs for 90 minutes (29±1 ºC, 67 % RH), the texture profile was analyzed using CT3 texture profile analyzer (Brookfield, M08-372-F1116, USA) considering the guidelines mentioned by Angioloni and Collar (2009) with selected adjustments. Sample height of 20±1 mm, two compression cycles, 25 mm diameter probe (TA11/1000), 50 % deformation, 5 g trigger load, 1 mm/s test speed, and 4500 g cell load. Hardness (g), Springiness (mm), Cohesiveness, Gumminess (g), and Chewiness (mJ) of the crumb samples were calculated from the compression curve of force vs. time using Brookfield TexturePro CT software.

2.2.4. Analysis of crumb cellular structure properties (Image analysis)

Cellular structure properties of scanned images (300 dpi) of the gelatinized crumbs (flatbed scanner, Canon Lide-120) (30 images per sample) were evaluated using ImageJ software following the guidelines depicted by Pérez-Nieto et al. (2010) with some adjustments. Before the image analysis, the scale of measurement was adjusted for "cm" concerning a known distance. Thereafter, a selected area of the scanned image was converted into a grayscale image (8 bit) and thresholded. Crumb porosity (%), cell density (gas cell count per unit area), average cell area (cm2), and cell circularity were assessed using the ImageJ software. Fractal dimension of scanned, grayscale, threshold images were also evaluated (box-counting method) by the same software.

2.2.5. Analysis of crumb storage stability

Gelatinized crumbs were packed in double laminated packaging material (OPP/LLDPE; Gauge 200) and stored at normal atmospheric conditions (29±2 ºC, 67 % RH) for 48 hours. Moisture content (%) (Kern and Sohn, DBS 60-3, Germany) and hardness (g) (CT3 texture profile analyzer) of the gelatinized crumb samples were evaluated at 24-hour intervals.

2.3. Data analysis

All the experiments were triplicated. Analysis of variance (ANOVA) followed by Tukey comparison was used to compare the mean values under 95 % confidence level using Minitab 17.1.0 statistical software. Graphical illustrations were performed using Microsoft Excel 2013.

3. Results and discussions

3.1. Crumb quality attributes

Crumb volume (cm^3), specific volume (cm^3/g), and bulk density (g/cm^3) are categorized as the major parameters that represent the leavened gas retention ability of a dough structure (Selmo & Salas-Mellado, 2014). Numfon (2007) has reviewed that the application of hydrocolloids can elevate the dough viscosity resulting in a higher gas retention capacity. According to the results given in Table 2, GG0.75 shows the highest crumb volume, highest crumb specific volume, and the lowest bulk density among the eleven crumbs. Moreover, almost all the crumbs prepared by incorporating different types of hydrocolloids, NCLE, and DSP have significantly high ($P<0.05$) volume, specific volume, and significantly low ($P<0.05$) bulk density compared to the control; except the crumbs containing Xanthan gum. The strong gluten–hydrocolloid interactions available with xanthan gum may cause to limit the dough extension and hence reduce the loaf volume (Zannini, Waters & Arendt 2014). Nevertheless, as per the results given in Table 2, the application of NCLE (NCLE5, NCLE10) and DSP1.5 contributed to a crumb volume, specific volume, and bulk density that do not significantly different ($P<0.05$) to GG0.75.

Selmo and Salas-Mellado (2014) have observed that with the increment of dehydrated Spirulina powder concentration (from 1 to 4%), crumb specific volume gets increased. The results of the current study also represent

significantly high (P<0.05) crumb volume, crumb specific volume, and a significantly low (P<0.05) bulk density in DSP1.5 compared to DSP1. The addition of a protein source like Spirulina supports preventing the dough system collapse during fermentation of gluten-free products. This phenomenon assists in forming a network to entrap leavened gas, thereby improving the loaf volume (Minh, 2014; Selmo & Salas-Mellado, 2014).

Table 2. Volume, Specific volume, and Bulk density of the eleven gelatinized crumbs prepared by incorporating different types of hydrocolloids, NCLE, and DSP

	Sample	Crumb volume (cm^3)	Specific volume (cm^3/g)	Bulk density (g/cm^3)
1	C	52.23 ± 0.87^{d}	1.84 ± 0.02^{de}	0.54 ± 0.01^{ab}
2	XG0.5	54.46 ± 1.70^{cd}	1.87 ± 0.05^{cde}	0.54 ± 0.01^{abc}
3	XG0.75	51.83 ± 1.47^{d}	1.78 ± 0.06^{e}	0.56 ± 0.02^{a}
4	GG0.5	60.52 ± 1.47^{ab}	2.14 ± 0.05^{a}	0.47 ± 0.01^{de}
5	GG0.75	61.63 ± 1.27^{a}	2.16 ± 0.05^{a}	0.46 ± 0.01^{e}
6	SA0.5	60.73 ± 0.78^{ab}	2.11 ± 0.02^{ab}	0.47 ± 0.01^{de}
7	SA0.75	57.51 ± 2.42^{abc}	2.02 ± 0.11^{abc}	0.50 ± 0.03^{cde}
8	NCLE5	57.45 ± 0.44^{abc}	1.20 ± 0.03^{abcd}	0.50 ± 0.01^{bcde}
9	NCLE10	57.66 ± 1.48^{abc}	1.20 ± 0.05^{abcd}	0.50 ± 0.01^{bcde}
10	DSP1	56.09 ± 1.42^{bcd}	1.96 ± 0.05^{bcd}	0.51 ± 0.01^{bcd}
11	DSP1.5	60.83 ± 2.28^{ab}	2.14 ± 0.09^{a}	0.47 ± 0.02^{de}

Results are represented as mean±SD of replicates; mean values in the same column with different superscripts are significantly different at 0.05 significant level

Table 3. Texture Profile analysis of the eleven gelatinized crumb samples prepared by incorporating different hydrocolloids, NCLE, and DSP

	Sample	Hardness (g)	Springiness (mm)	Cohesiveness	Gumminess (G)	Chewiness (mJ)
1	C	1318.30 ± 78.50^{ab}	9.72 ± 0.48^{ab}	0.54 ± 0.02^{abc}	735.90 ± 61.30^{ab}	70.36 ± 8.97^{ab}
2	XG0.5	1146.70 ± 97.00^{bc}	10.29 ± 0.65^{a}	0.57 ± 0.02^{a}	665.10 ± 47.70^{bcd}	68.42 ± 9.20^{ab}
3	XG0.75	1480.00 ± 55.70^{a}	9.88 ± 0.21^{ab}	0.56 ± 0.02^{ab}	823.40 ± 55.20^{a}	78.67 ± 4.44^{a}
4	GG0.5	1038.30 ± 62.40^{c}	9.43 ± 0.31^{ab}	0.50 ± 0.02^{abcd}	654.30 ± 62.60^{bcd}	60.53 ± 5.01^{b}
5	GG0.75	1010.00 ± 30.40^{c}	9.80 ± 0.28^{ab}	0.42 ± 0.05^{d}	465.50 ± 34.90^{e}	41.45 ± 7.43^{c}
6	SA0.5	1095.00 ± 56.80^{c}	9.85 ± 0.14^{ab}	0.52 ± 0.03^{abc}	573.50 ± 59.90^{cde}	55.31 ± 5.22^{bc}
7	SA0.75	1146.70 ± 59.70^{bc}	9.17 ± 0.02^{b}	0.48 ± 0.02^{bcd}	569.90 ± 48.50^{cde}	54.40 ± 6.69^{bc}
8	NCLE5	1141.70 ± 80.10^{bc}	9.83 ± 0.46^{ab}	0.55 ± 0.04^{abc}	539.07 ± 6.40^{de}	52.84 ± 3.11^{bc}
9	NCLE10	1198.30 ± 46.50^{bc}	9.71 ± 0.09^{ab}	0.52 ± 0.03^{abc}	474.30 ± 24.00^{e}	42.60 ± 2.53^{c}
10	DSP1	1483.30 ± 92.50^{a}	9.46 ± 0.40^{ab}	0.47 ± 0.03^{cd}	688.00 ± 6.20^{abc}	62.94 ± 4.06^{ab}
11	DSP1.5	1135.00 ± 69.00^{c}	9.29 ± 0.27^{ab}	0.54 ± 0.04^{abc}	605.00 ± 72.70^{bcde}	55.36 ± 5.33^{bc}

Results are represented as mean±SD of replicates; mean values in the same column with different superscripts are significantly different at 0.05 significant level

Texture Profile is another important quality parameter that highly depends on the crumb cellular structure properties. It resembles the aesthetic sensation within the human mouth in order to determine the consumer acceptability (Hager & Arendt, 2013; Li & Nie, 2015). The application of hydrocolloids contributes to increasing the water-binding ability of the dough to obtain moist and softer crumbs (Hager & Arendt, 2013).

The application of hydrocolloids in developing leavened baked products contributes to increase the water-binding ability and to obtain moist and softer crumbs (Hager & Arendt 2013). According to the results given in Table 3, the application of different types of hydrocolloids, NCLE, and DSP contributed to lowering the hardness of the crumbs compared to the control (except XG0.75 and DSP1). Souther (2005), Hager and Arendt (2013), and Kondakci et al. (2015) have also observed that the crumb hardness gets increased with the increment of hydrocolloid concentration, particularly with xanthan gum. The reason for this phenomenon is that the addition of higher concentrations of hydrocolloids may contribute to increasing the dough/ batter viscosity. Thus, the viscosity itself can negatively affect in increasing the crumb hardness (Numfon 2007). Besides, this may also occur as a result of the increment of the thickness of the crumb cell walls that surround the air space (Rosell, Rojas & Barber 2001; Guarda et al. 2004).

As per the results given in Table 3, DSP1.5 shows a significantly low ($P<0.05$) hardness compared to DSP1. Because, the microalgal biomass can increase the water-holding capability of the dough and, hence contributes to obtaining a softer crumb in leavened baked products (Massoud et al., 2016). However, the hardness of the crumbs that contained NCLE and DSP show higher values compared to the crumbs that contained Guar gum. When considering the gumminess and chewiness values, all the crumb samples with different hydrocolloids, except XG0.75 have lower gumminess and chewiness values compared to the control (C).

There is no significant difference ($P>0.05$) between the springiness of all the crumbs with different hydrocolloids and DSP. Hydrocolloids can withhold the thickening and gelling characteristics and have the ability to form links between the molecules in a food system. Thus, the formed network can build a three-dimensional lattice; of which, oil droplets or particles can be permanently trapped without separating. That results in having a higher springiness value (Souther, 2005). Generally, those higher springiness values represent the higher recoverability from the first deformation in texture profile analysis (Singh, Jha, Chaudhary, & Upadhyay, 2014).

3.2.Cellular structure properties (Image analysis)

Crumb cellular structural properties play a significant influence on the physical and organoleptic properties of leavened baked products (Falcone et al., 2004; Lassoued, Babin, Della Valle, Devaux, & Réguerre, 2007). Acceptable crumb cellular structure, softer texture with more elastic properties are excellent parameters that represent improved crumb cellular structure properties containing a greater number of small, uniform, and thin-walled gas cells (Tebben & Li, 2019). Higher number of gas cells per unit area (cell density) with an acceptable average cell area, higher cell circularity, and lower FD validate the fineness and the uniformity of crumb cellular structure, while a higher porosity indicates the presence of a greater number of larger gas cells (Che Pa et al., 2013). Figure 1 and Table 4 represent the scanned images and the cellular structure properties of the eleven gelatinized crumbs respectively.

According to Table 4, XG0.5 and XG0.75 have the highest cell density, lowest porosity, lowest average cell area, higher cell circularity values, and lower FD values compared to the other crumbs. This represents a finer crumb cellular structure of XG0.5 and XG0.75 (Figure 1). Even though, xanthan gum shows comparatively negative effects in crumb volume (Table 2) and texture related properties (Table 3), it contributed to developing crumb samples

with more uniform and finer cellular structure compared to the other hydrocolloids, NCLE, and DSP. During the leavening process, hydrocolloids may contribute to reinforcing the gluten network around the gas cells while increasing their stability resulting in a higher number of gas cells in a unit area (Tebben & Li, 2019). Crumbs that contained DSP (DSP1, DSP1.5) exhibit higher cell density values compared to the crumbs that contained Guar gum, Sodium alginate, and NCLE. Nevertheless, crumbs comprising DSP having higher porosity, FD, and lower cell circularity than that of the crumbs that contained Xanthan gum, Sodium alginate, and NCLE, representing the presence of more coalesced and irregular cell structure.

Despite contributing for a higher crumb volume and better texture properties, Figure 1 and Table 4 evident that Guar gum (GG0.5 and GG0.75) resulting in a crumb with more coalesced gas cells, denoting a lower cell density, higher porosity and higher average cell area.

Table 4 Cellular structure properties (Image analysis) of the eleven gelatinized crumbs prepared by incorporating different types of hydrocolloids, NCLE, and DSP

	Sample	Cell density (number of cells/cm^2)	Porosity (%)	Average cell area (cm^2)	Cell circularity	Fractal dimension (FD)
1	C	23.544±4.510^{de}	32.943±2.796^{bc}	0.015±0.003^{bc}	0.487±0.050^{ab}	1.668±0.033^{ab}
2	XG0.5	33.373±3.532^{ab}	27.001±2.563^{e}	0.008±0.001^{d}	0.503±0.033^{ab}	1.657±0.029^{b}
3	XG0.75	34.787±4.860^{a}	28.681±2.008^{de}	0.008±0.001^{d}	0.512±0.032^{a}	1.672±0.028^{ab}
4	GG0.5	19.084±3.638^{e}	36.709±4.450^{a}	0.020±0.006^{a}	0.471±0.033^{ab}	1.690±0.031^{ab}
5	GG0.75	24.032±4.290^{d}	35.929±4.480^{ab}	0.016±0.005^{b}	0.500±0.057^{ab}	1.696±0.037^{ab}
6	SA0.5	25.160±5.780^{cd}	31.195±3.161^{cd}	0.014±0.003^{bc}	0.509±0.040^{ab}	1.653±0.033^{b}
7	SA0.75	25.922±3.023^{cd}	33.516±2.764^{abc}	0.013±0.002^{bc}	0.500±0.029^{ab}	1.688±0.027^{ab}
8	NCLE5	24.897±3.771^{cd}	32.045±3.279^{cd}	0.013±0.002^{bc}	0.494±0.038^{ab}	1.679±0.050^{ab}
9	NCLE10	25.612±2.822^{cd}	32.678±1.947^{bc}	0.013±0.002^{bc}	0.495±0.043^{ab}	1.687±0.034^{ab}
10	DSP1	28.991±4.220^{bc}	32.360±2.738^{bcd}	0.011±0.002^{cd}	0.471±0.078^{ab}	1.697±0.049^{ab}
11	DSP1.5	26.354±4.250^{cd}	34.600±3.379^{abc}	0.014±0.003^{bc}	0.455±0.061^{b}	1.703±0.052^{a}

Results are represented as mean±SD of replicates; mean values in the same column with different superscripts are significantly different at 0.05 significant level.

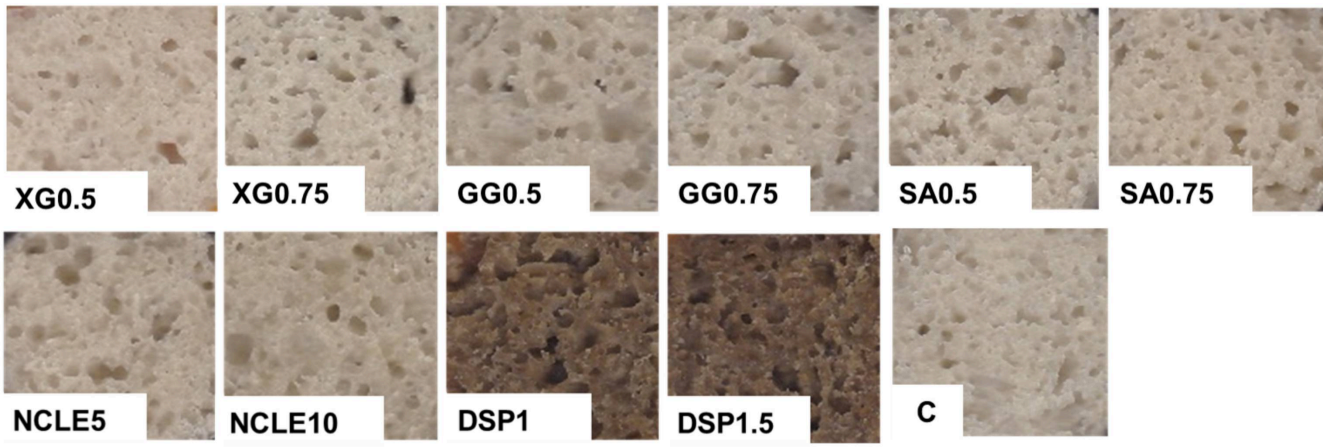

Figure 1. Scanned images (300dpi) of the eleven gelatinized crumbs prepared by incorporating different types of hydrocolloids, NCLE, and DSP

3.3. Storage stability

Usually, leavened baked products begin to undergo certain chemical and physical changes during storage which causes deterioration of the quality of the product (staling) (Angioloni & Collar, 2009; Mondal & Datta, 2008). The most common deteriorative effects of crumb staling include retrogradation of amylopectin, re-organization of polymers within the amorphous region, loss of moisture content, and moisture migration (Guarda, Rosell, Benedito, & Galotto, 2004). Thus, decrement of crumb moisture content and crumb hardening are the most prominent indications of crumb staling (Shittu et al., 2009). However, the ability of retarding the crumb staling of different hydrocolloids can vary due to the molecular structure of the hydrocolloids and the interaction of each hydrocolloid material with the starch molecules (Das et al., 2015).

According to plot "A" in Figure 2, the initial moisture contents of crumbs prepared by incorporating Xanthan gum, Guar gum, and DSP1.5 are higher than that of the control sample. Moreover, crumbs prepared by incorporating NCLE (NCLE5 and NCLE10) show the lowest moisture loss during storage. Further, according to plot "A" in Figure 2, the rate of the crumb moisture reduction within the first 24 hours is higher than the second 24 hours in all eleven crumbs. However, the rate of crumb moisture reduction within the first 24 hours is more prominent in the control crumb (C) as well as XG0.5, GG0.5, and GG0.75.

Plot "B" in Figure 2 depicts that the control crumb (C) having the highest increment in the hardness while GG0.75 having the lowest values during the storage period. The increment of hardness within the first 24 hours is more prominent in XG0.5, XG0.75, SA0.75, NCLE5, DSP1, and C in comparison to the other crumbs. Plot "B" in Figure 2 further demonstrates that, XG0.75, SA0.5, NCLE10, DSP1.5, and C exhibit a relatively higher degree of crumb hardening within the second 24 hours of storage. However, the hardness value of GG0.5 show a declined manner within the second 24 hours' period.

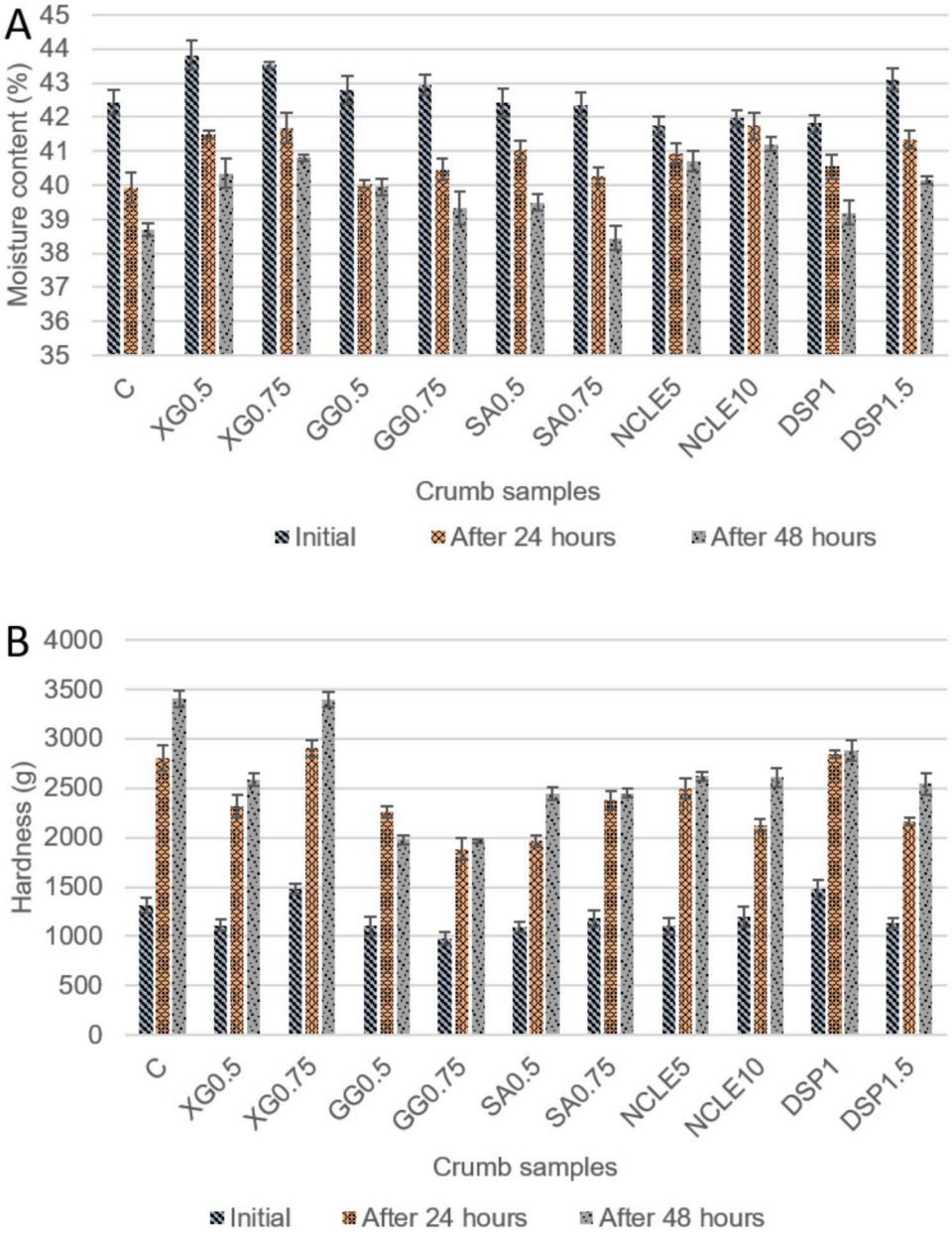

Figure 2. Storage stability of the eleven gelatinized crumbs prepared by incorporating different types of hydrocolloids, NCLE, and DSP (A) Deviation of the moisture content during the storage period, (B) Deviation of crumb hardness during the storage period. (Results are represented as mean±SD of replicates)

Since the moisture in the crumb of a leavened food product acts as a plasticizer, the moisture retention capability of the crumb shows a huge role in reducing the rate of crumb firming during storage. Otherwise, the reduction of the moisture content in a crumb during storage may lead to the formation of bonds either between starch polymers themselves or between protein and starch. This causes the increment of the hardness of the crumb (Das et al., 2015). The application of hydrocolloids causes retarding the staling process by improving the water retention capacity and also showing a potential hindering effect on amylopectin retrogradation (Guarda et al., 2004). However, the ability of retarding the crumb staling of each hydrocolloid varies due to the molecular structure of the hydrocolloids and

the interaction of each hydrocolloid material with the starch molecules (Das et al., 2015).

4. Conclusions

Type and the dosage of hydrocolloids can significantly affect the textural and structural properties of gelatinized crumbs. Despite uneven crumb cellular structure, the application of Guar gum at 0.75% has contributed to improving crumb volume and texture-related properties as well as reduce the crumb hardening rate during storage comparatively Xanthun Gum and Sodium Alginate. NCLE helped to have a higher moisture retention capacity than the other hydrocolloid materials but it did not significantly contribute to reducing the rate of crumb hardening. Moreover, the application of DSP in 1.5% also imparts a significant role in improving crumb volume and texture of leavened food products coupled with an acceptable role in reducing the staling effect similar to Guar gum and Sodium alginate.

5. References

Angioloni, A., & Collar, C. (2009). Bread crumb quality assessment: A plural physical approach. *European Food Research and Technology*, *229*(1), 21–30. https://doi.org/10.1007/s00217-009-1022-3

Aplevicz, K. S., Ogliari, P. J., & Sant'Anna, E. S. (2013). Influence of fermentation time on characteristics of sourdough bread. *Brazilian Journal of Pharmaceutical Sciences*, *49*(2), 233–239. https://doi.org/10.1590/S1984-82502013000200005

Che Pa, N. F., Chin, N. L., Yusof, Y. A., & Abdul Aziz, N. (2013). Measurement of bread crumb texture via imaging of its characteristics. *Journal of Food, Agriculture and Environment*, *11*(2), 48–55.

Collar, C., Andreu, P., Martínez, J. ., & Armero, E. (1999). Optimization of hydrocolloid addition to improve wheat bread dough functionality: a response surface methodology study. *Food Hydrocolloids*, *13*(6), 467–475. https://doi.org/10.1016/S0268-005X(99)00030-2

Das, L., Raychaudhuri, U., & Chakraborty, R. (2015). Effects of hydrocolloids as texture improver in coriander bread. *Journal of Food Science and Technology*, *52*(6), 3671–3680. https://doi.org/10.1007/s13197-014-1296-8

Falcone, P. M., Baiano, A., Zanini, F., Mancini, L., Tromba, G., Montanari, F., & Nobile, M. A. (2004). A novel approach to the study of bread porous structure: Phase-contrast X-Ray microtomography. *Journal of Food Science*, *69*(1), 38–43. https://doi.org/10.1111/j.1365-2621.2004.tb17865.x

Guarda, A., Rosell, C. M., Benedito, C., & Galotto, M. J. (2004). Different hydrocolloids as bread improvers and antistaling agents. *Food Hydrocolloids*, *18*, 241–247. https://doi.org/10.1016/S0268-005X(03)00080-8

Hager, A. S., & Arendt, E. K. (2013). Influence of Hydroxypropylmethylcellulose (HPMC), Xanthan gum and their combination on loaf specific volume, crumb hardness and crumb grain characteristics of gluten-free breads based on rice, maize, teff and buckwheat. *Food Hydrocolloids*, *32*(1), 195–203. https://doi.org/10.1016/j.foodhyd.2012.12.021

Hosseini, S., Shahbazizadeh, S., Khosravi-Darani, K., & Mozafari, M. (2013). Spirulina paltensis: Food and function. *Current Nutrition & Food Science*, *9*(3), 189–193. https://doi.org/10.2174/1573401311309030003

Kasunmala, I. G. G., Navaratne, S. B., & Wickramasinghe, I. (2017). Extraction and characterization of mucilaginous material from Dawul Kurundu Leaves (Neolitsea involucrate) and Godapara Fruits (Dillenia retusa). *International Journal of Food Science and Nutrition*, *2*(2), 16–19.

Kondakci, T, Ang, AMY & Zhou, W 2015, 'Impact of sodium alginate and xanthan gum on the quality of steamed bread made from frozen dough', Cereal Chemistry, vol. 92, no. 3, pp. 236–245. doi: 10.1094/CCHEM-03-14-0036-R.

Lassoued, N., Babin, P., Della Valle, G., Devaux, M. F., & Réguerre, A. L. (2007). Granulometry of bread crumb grain: Contributions of 2D and 3D image analysis at different scale. *Food Research International*, *40*(8), 1087–1097. https://doi.org/10.1016/j.foodres.2007.06.004

Li, J. M., & Nie, S. P. (2015). The functional and nutritional aspects of hydrocolloids in foods. *Food Hydrocolloids*, *53*, 46–61. https://doi.org/10.1016/j.foodhyd.2015.01.035

Massoud, R., Khosravi-darani, K., Nakhsaz, F., & Varga, L. (2016). Evaluation of physicochemical, microbiological and sensory properties of croissants fortified with Arthrospira platensis (Spirulina). *Czech Journal of Food Sciences*, *34*(4), 350–355. https://doi.org/10.17221/289/2015-CJFS

Minh, N. P. (2014). Effect of Saccharomyces cerevisiae, Spirulina and preservative supplementation to sweet bread quality in bakery. *International Journal of Multidisciplinary Research and Development*, *1*(4), 36–44.

Mondal, A., & Datta, A. K. (2008). Bread baking–A review. *Journal of Food Engineering*, *86*(4), 465–474. https://doi.org/10.1016/J.JFOODENG.2007.11.014

Navaratne, S. B. (2007). Exploring possibility of using Davulkurundu (Neolitsea involurate) leaf extract to improve leavening action and crumb structure of wheat bread. *Tropical Agricultural Research and Extension*, *10*, 67–73.

Numfon, R. (2007). Effects of different hydrocolloids on properties of gluten-free bread based on small broken rice berry flour. *Food Science and Technology International*, *23*(4), 310–317. https://doi.org/10.1177/1082013217690064

Pérez-Nieto, A., Chanona-Pérez, J. J., Farrera-Rebollo, R. R., Gutiérrez-López, G. F., Alamilla-Beltrán, L., & Calderón-Domínguez, G. (2010). Image analysis of structural changes in dough during baking. *LWT - Food Science and Technology*, *43*(3), 535–543. https://doi.org/10.1016/j.lwt.2009.09.023

Rathnayake, H. A., Navaratne, S., & Navaratne, C. (2019). Improving porous crumb structure of rice-related leavened food products by fermentation and gelatinization at slightly higher air pressure conditions. *Journal of Texture Studies*, *50*(6), 564–570. https://doi.org/10.1111/jtxs.12465

Salehi, F. (2019). Improvement of gluten-free bread and cake properties using natural hydrocolloids: A review. *Food Science and Nutrition*, *7*, 3391–3402. https://doi.org/10.1002/fsn3.1245

Selmo, M. S., & Salas-Mellado, M. M. (2014). Technological quality of bread from rice flour with Spirulina. *International Food Research Journal*, *21*(4), 1523–1528.

Shittu, T. A., Aminu, R. A., & Abulude, E. O. (2009). Functional effects of Xanthan gum on composite cassava-wheat dough and bread. *Food Hydrocolloids*, *23*(8), 2254–2260. https://doi.org/10.1016/j.foodhyd.2009.05.016

Singh, N., Jha, A., Chaudhary, A., & Upadhyay, A. (2014). Enhancement of the functionality of bread by incorporation of Shatavari (Asparagus racemosus). *Journal of Food Science and Technology*, *51*(9), 2038–2045. https://doi.org/10.1007/s13197-012-0731-y

Souther, B. J. (2005). *The effect of Xanthan gum and Guar gum on enhancing the quality and preventing lipid rancidity in yeast bread supplemented with flaxseed*. The Faculty of Virginia Polytechnic Institute and State University. Retrieved from https://pdfs.semanticscholar.org/3f03/315bcb5c7585320235c43d1e7889736c2a96.pdf

Tebben, L., & Li, Y. (2019). Effect of Xanthan gum on dough properties and bread qualities made from whole wheat flour. *Cereal Chemistry*, *96*(2), 263–272. https://doi.org/10.1002/cche.10118

Wang, K., Lu, F., Li, Z., Zhao, L., & Han, C. (2017). Recent developments in gluten-free bread baking approaches: A review. *Food Science and Technology*, *37*, 1–9.

https://doi.org/10.1590/1678-457X.01417

Wijerathne, P. A. K. C., Chandrajith, V. G. G., & Navaratne, S. B. (2018). Controlling of post-harvest losses of selected leafy vegetables and green chilies by coating with plant mucilages. *Agricultural Resaerch and Technology*, *16*(5), 171–177. https://doi.org/10.19080/ARTOAJ.2018.16.556005

Acknowledgments

Research Council, University of Sri Jayewardenepura, Sri Lanka [Grant number: ASP/01/RE/SCI/2019/12]. The Department of Food Science and Technology, University of Sri Jayewardenepura. Mr. R. R. L. Jayathilaka for providing dehydrated Spirulina powder.

CARPATHIAN JOURNAL OF FOOD SCIENCE AND TECHNOLOGY

journal homepage: **http://chimie-biologie.ubm.ro/carpathian_journal/index.html**

Research article

FUTURE FOODS DEVELOPMENT: EFFECT OF TEMPERATURE, FEED MOISTURE AND COCONUT ADDITION ON THE PHYSICOCHEMICAL PROPERTIES OF EXTRUDED CORN SNACKS

Uzochukwu, C. C. [1], Ikegwu, T. M. [1✉], Ezeh-Nwandu, M. C. [1], Agu, H. O.[1,3]

[1]Department of Food Science and Technology, Faculty of Agriculture, Nnamdi Azikiwe University, P.M.B 5025, Awka Anambra State, Nigeria.

[2]FOCAS Research Institute, Technological University Dublin, Camden Row, Dublin 8, Ireland.

[3]TETFund Centre of Excellence for BioMedical, Engineering and Agricultural Translational Studies (TCE-BEATS), Nnamdi Azikiwe University Awka, Anambra State, Nigeria.

✉tm.ikegwu@unizik.edu.ng

https://doi.org/10.34302/2025.17.3.14

Article history:
Received
July 3rd , 2025
Accepted
October 29th 2025

Keywords:
Extrusion,
Functional properties,
Heat treatment,
Spread ratio,
Traditional snack foods,
Product development.

Abstract

The study investigated the effect of temperature, feed moisture and coconut addition on the physicochemical properties of extruded corn snacks. The samples processed and data collected analyzed using standard methods. The results findings revealed that there were significant variations ($P<0.05$) in the proximate composition of the extruded corn-coconut snack samples. The ash, moisture, fire and fat contents ranged from 3.54-3.82%, 4.94-5.60%, 2.87-3.15% and 8.90-9.15%, respectively. The protein content of the extruded snack samples varied from 9.93 to 12.31%, while the carbohydrate content ranged from 66.36 to 69.40%. Carbohydrate content was highest in FGH (69.40%) and lowest in BCO (66.36%). The moderate fat content can aid in the absorption of fat-soluble vitamins (ADEK). Significant differences ($p<0.05$) were also observed in some of the functional properties of the extruded corn-coconut snacks with the emulsion stability ranging from 10.00 to 11.33%, while emulsion activity ranged from 9.14 to 9.91%. The oil absorption capacity, bulk density and foaming capacity ranged from 1.93-2.98%, 0.57-0.76% and 11.17-15.60%, respectively. Oil absorption capacity varied significantly, with NPO and BCO samples exhibiting the highest values (2.98 g/g), reflecting their potential for flavor retention and mouthfeel enhancement. Bulk density ranged from 0.57 to 0.76 g/cm³, where higher values (e.g., QRW and YXZ) imply denser products, potentially influencing packaging and textural properties. Foaming capacity varied between 11.17% and 15.60%, with NPO demonstrating the most pronounced ability to entrap air, which is crucial for snack lightness and volume. The colour and physical properties of the extruded snacks also varied significantly ($p<0.05$) among the samples. The results of the sensory evaluation revealed that the sample VST was ranked the highest in terms of overall acceptability, while sample SOA was ranked least.

1. Introduction

In traditional Igbo society, snacks are taken as delicacy after each days' work. Other times, they are enjoyed by the extended family when a relation or family member return from travel. Some of the traditional snack foods include eating of maize with either maize, coconut, African black pea (*ube*) or palm kernel, eating of African salad (*Abacha*) with either palm kernel coconut, eating of African black with palm kernel, among others (Eke, 2025). The knowledge of snacking in traditional Igbo society may be used for new food product development in what may be referred to as the future foods. Other authors (Ikegwu, 2023) stated that the development of a new food product involves innovation which is the key for propagating and adopting new ideas. It is important that these novel product ideas are developed to meet international standard given that most of this traditional food practices are been given attention by other cultures due to globalization. It is therefore imperative that extrusion technology could be employed.

Development of traditional snack foods through extrusion cooking recognizes the thermomechanical processes for heat and mass transfer in ensuring that products meet desired expectations (Ikegwu, 2023). It was noted that maize/corn could be eaten fresh or in dried forms in Igboland and noted that the corn, coconut and ube snacking could earn Nigeria United Nation Cultural Status (Eke, 2025). The pear, when eaten with corn, could either be roasted or cooked. The use of maize-coconut for snack food production would encourage the global acceptance of the traditional food relics through pressure changes and shear which are combined to produce effects such as cooking, sterilization, drying, melting, texturizing, conveying, puffing, mixing and kneading. Extrusion is a combined high-temperature-short-time (HTST) process in a continuous operation to push material using a piston or a screw with pressure and shear through a die with a given shaper. The homogeneity and consistency of the thermal process permit the production of high-quality final products with minimum waste (An addendum to S5.06, Environmental Agency, Bristol). The extrusion process combines pumping, mixing, kneading, heating and cutting all in one process and can result in a preferred appearance and texture. Thus, extrusion technology is widely used in the food industry in cereals, snacks, pet food, feed, confectionery products, modified starches, baby food, and instant foods (Nwadi *et al.,* 2023; Offiah *et al.,* 2018). Extrusion is also a good way of processing pulses because of its versatility and flexibility, as well as the ability to reduce and inactivate bioactive factors that are naturally present in pulses and reduce cooking time when incorporated into products (Offiah *et al.,* 2018).

The feed moisture management is the key from an economic and feed quality point of view. The amount of moisture in bound form, brought by macro ingredients like corn, in a feed formula contributes to the production efficiency. Importantly, the moisture in compounded feed can assist cooking and conditioning, providing better machine efficiency (higher throughput at lower energy consumption), pellet quality, and feeding value (enhanced nutrient value). Kinetics of heat-moisture-steam application in feed processing and quality deterioration presents a completely new dimension for cost reduction during the feed formulation process, which does not depend only on the raw material cost but on the efficient production to enhance the feeding value for better product performance (Gurbuz, 2017; Inyang *et al.,* 2018). A sufficient moisture level is important as it reduces energy usage during the pelleting process and ensures that production runs more smoothly by lowering the risk of blockages. This is important for preventing nutrient losses due to excessive heat production. Furthermore, it guarantees good product quality at an optimal moisture level to positively affect product hardness. Extrusion technology has been used for snack production in starchy foods, whereby the temperature used at a definite time affects the quality and the characteristics of the snacks (Singh *et al*., 2017). Snacking have remained a part of the human diet for time immemorial and are its growth are been influenced be population, urbanization and the

need for convenience foods with huge contribution to energy and nutrient intake (Ndife *et al.,* 2020; Ugwunyi *et al.,* 2020). The demand for snacks is attributed to the rapid population and urbanization of both developed and developing countries (Ugwuanyi *et al.,* 2020). Snacks are important to many consumers' daily nutrient and caloric intake (Ibe *et al.,* 2025; Heitman *et al.,* 2023). The most widely consumed snacks are cereal-based products, generally low in nutrient density (Rehm and Drewnowski, 2017). They are generally regarded as convenience foods and have been part of the human diet for a long time (Hess *et al.,* 2016). Snack foods are cheap, easy to eat and readily available on the streets, shops and schools (Ugwuanyi *et al.,* 2020). Snack formulation from a blend of maize and coconut stems from the array of functional effects of coconut on food products. Coconut has dietary fiber and unsaturated fatty acids, which are very important in nutrition (Hewlings, 2020). Some researches on extruded snacks from either corn or coconut flour have focused on developing nutrient-rich food products, without recourse on the combination of the two ingredients for food product development (Table 1).

Table 1. Extruded snacks from Either Corn or Coconut

S/N	Research	Author
1.	Corn-Based Extruded Snacks Supplemented with Bilberry Pomace Powder: Physical, Chemical, Functional, and Sensory Properties	Blejan *et al.,* 2025
2.	Extruded snacks from industrial by products: a review	Grasso, 2020
3.	Extruded snacks with byproducts of coconut	Sali, 2024
4.	Amylose-lipid complex formation during extrusion cooking: effect of added lipid type and amylose level on corn-based puffed snacks	Thachil *et al.*, 2014
5.	Coconut Inflorescence Sap Honey: A Promising Supplementary Food among Tribals	Vadassery *et al.,* 2023
6.	The effects of feed moisture and dried coconut meal content on the physicochemical, functional, and sensory properties of gluten-free Riceberry rice flour-based extruded snacks	Piaura and Itthivadhanapong, 2023
7.	Development of extruded Ready-To-Eat (RTE) snacks using corn, black gram, roots and tuber flour blends	Reddy *et al.,* 2014
8.	Single Screw Extrusion Processing of Enriched Snacks at Various Levels of Brewers Spent Yeast and Soybean Meal	Olumurewa and Oladele, 2020

Coconut is rich in fiber (4.22%), vitamins, and minerals (Lehman, 2022). It is believed to be a "functional food" because it provides many health benefits beyond its nutritional content (Rachael, 2020). Coconut is low in digestible carbohydrates, contains no gluten, and is loaded with health-promoting fiber and important nutrients (Hewlings, 2020). Coconut flour is a soft, flour-like product made from the pulp of a coconut. Coconut flour is extremely high in fiber, with almost double the amount found in wheat bran. It contains more calorie-free fiber than other wheat alternatives and provides a good source of protein (Samarajeewa, 2024). Coconut provides many health benefits: it can improve digestion, help regulate blood sugar, protect against diabetes, help prevent heart disease and cancer, and aid in weight loss (Lalitha, 2014). Coconut is rich in energy-yielding fat (47.2%) and minerals (mg/kg) like phosphorus (184.2 mg/ kg), potassium (224.8 mg/kg), zinc (43.5 mg/kg), iron (37.9 mg/kg), magnesium (178.1 mg/kg), and about 50.0 mg/kg manganese (Amoo, 2004). The

utilization of defatted coconut flour as a high protein and fiber ingredient in food formulations has been clearly reported (Samarajeewa, 2024; Usman *et al.,* 2015). The protein content of defatted coconut flour was in the range of 17.2–20.0% on dry weight basis (Adebowale and Komolafe, 2018; Pathirana *et al.,* 2020). Coconut protein fractions contain a substantial amount of glutamic acid, argentine, aspartic acid, and lysine, with values ranging from 17.0–24.9, 12.3–17.9, 5.6–9.3, and 3.5–4.1 g/ 100 g of protein, respectively (Pathirana *et al.,* 2020). Due to the array of nutritional benefits, coconut could be incorporated in snack foods involving corn to produce high-value food products. According to Matetal *et al.* (2022), coconut could be utilized for various commercial products ranging from desiccated coconut, oil, raw kernels, milk, to coconut water thus serving as both oilseed and a source of food for the population due to its rich content of fibre and energy.

The major chemical component of the maize is carbohydrate, which provides up to 72 to 73% of the kernel weight (Sundaresan *et al.,* 2023). Maize is used as a basic food ingredient in its original or modified form. Maize grains are a rich source of starch (72%), ash (17%), protein (10.4%), fiber (2.5%), oil (4.8%), vitamins and minerals (Farhad *et al.,* 2009). The oil and protein contents are commercially valuable and used in food product manufacturing (Małecki *et al.,* 2021; Surjirtha and Mahendran, 2015). Its grains have great nutritional value and can be processed into various products such as cornmeal, grits, starch, flour, tortillas, snacks, and breakfast cereals. The percentage moisture content of all the maize varieties studied ranged from 11.10 to 13.96%; this is higher than the result recorded by Ape *et al.* (2016) whose moisture content was 7.16% for maize bought from the Ogbete market in Enugu, Nigeria. Crude fat is an important component of maize grains. Improvement in fat content aids good human health as they act as vehicle for fat-soluble vitamins.

Sali (2024) had instigated the production of snacks from extruded coconut by-products and barnyard millets. The findings revealed that the corn grits, coconut testa concentrate, coconut testa fibre and coconut fibre could be extruded for snack products and with barnyard millet. The findings of Sali (2024) nutritional, antioxidant, antimicrobial and functional properties. Sahu (2018) studied the storability of maize-millet based soy fortified extruded snack, while Edima-Nyah *et al.* (2022) evaluated the quality of maize-coconut snack bars enriched with different levels of malted African breadfruit seed flour. These studies indicated that snacks with coconut inclusion are rich in nutrients that could posit it a functional food in nutraceutical studies.

This present study is limited to the production, physical, proximate, functional, colorimetry and sensory properties of extruded snacks from maize-coconut. Further studies may wish to investigate the product optimization as well as carry-out animal studies to investigate the best economic product and the health effect of the consumption of the snack.

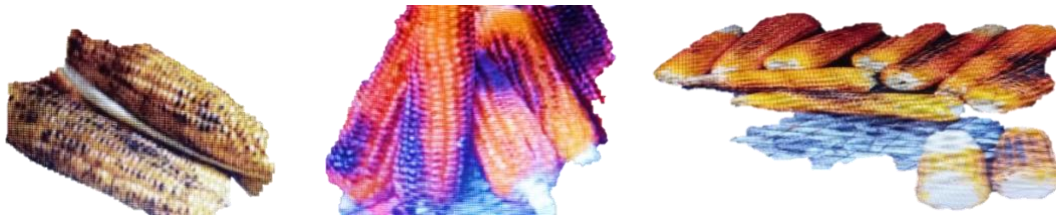

Figure 1. Corn with Maize

Figure 2. Extruded corn-coconut snacks

2. Materials and Methods

2.1. Source of Materials

Maize (dehulled) and mature coconut were purchased for extrusion at the Eke Awka local market, Awka South, Anambra State, Nigeria. All other chemicals used in this study were of reagent grade, purchased from reputable laboratory in Awka and Enugu State.

All extrudates were milled into flours using a hammer mill with a 1 mm diameter round whole perforated screen. Pre-cooked flours were composite flours combined from two extrusion runs. A pre-study was set up to determine the best blending ratio of the maize and coconut flours used in extrusion based on the protein quality.

2.2.Preparation of Raw Materials

The white corn grain and coconut were sorted to remove spoilt and defective ones as well as defective seeds to prevent the production of poor quality and unhealthy products. The grains and coconut were washed, cleaned and dried at ambient temperature to remove surface moisture. Below are the flowcharts for the preparation of the corn and coconut samples.

2.2.1.Procedure for the Preparation of Coconut Flour

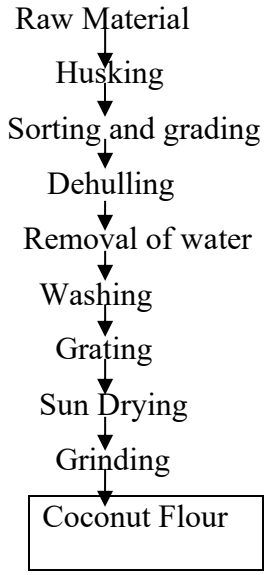

Figure 3. Flowchart for Processing of Coconut Flour

2.2.2.Procedure for The Preparation of Corn Flour

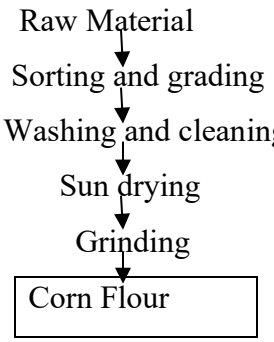

Figure 4. Flowchart for Corn Flour Processing

2.2.3. Production of extruded snacks

The washed and dried seeds and legumes were ground in industrial millers to grit sizes, packed in airtight containers and taken for extrusion. The seeds were fed into the extrusion machine with moisture and temperature, and the groundnuts varied at different levels. The extruded snacks were packed in zip-lock bags to prevent moisture absorption that could cause oxidative activities leading to rancidity.

2.2.4. Procedure for the production of corn-coconut-based extruded snacks

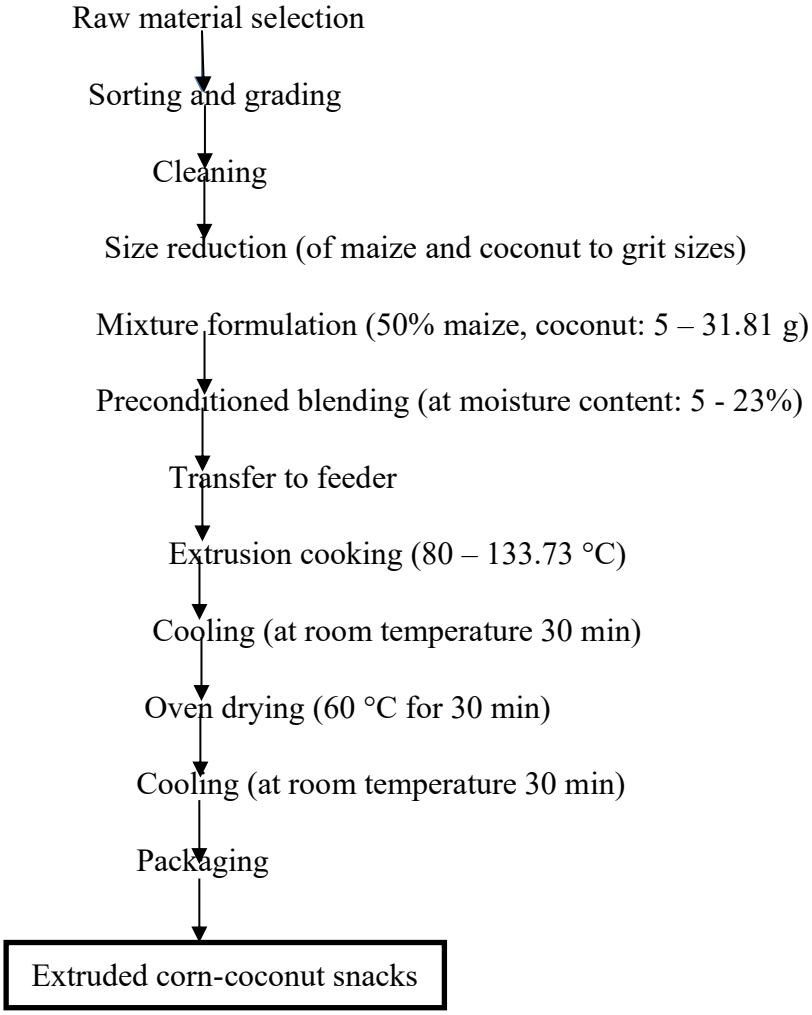

Figure 4. Extrusion of Snacks from Corn-coconut Blends

2.3.Proximate Analysis

The proximate analysis of the crude extract for moisture content and ash content was performed using the AOAC method (2021). The nitrogen content was calculated using the micro-Kjeldahl method, and the nitrogen content was multiplied by a factor of 6.60 to convert it to protein. After subtracting the total percent of other food nutrients from 100 percent, the total carbohydrate content was calculated.

2.3.1.Moisture Content (W%)

Moisture content basically implies water content. It is a commonly measured property in food products; legal and labelling requirements, cost of the product, microbial stability, food quality and food processing operations are why moisture content is essential in food products (NIMALSIRI, 2015). The moisture content will be determined by measuring the mass of food before and after the water has been removed (MOORE, 2020). Moisture content is defined through the following equation: %mixture = (M_{water}/M_{sample}) × 100.

Determination of Moisture Content

Pre-weighed empty crucible was labelled (W_1). Exactly 3 g of the crude extract was weighed into the pre-weighed empty crucible (W_2) and dried for 3 h at 105℃ in a hot drying oven. The crucible was removed and weighed after cooling in desiccators. The drying, cooling, and weighing process was repeated until the weight (W_3) was constant. The weight loss caused by moisture was measured.

$$\text{Moisture (\%)} = \frac{W_2 - W_3}{W_2 - W_1} \times 100 \quad (1)$$

Where: W_1= weight of the empty crucible

W_2= weight of empty crucible+ crude extract

W_3= weight of empty crucible + dried crude extract

2.3.2.Determination of Ash Content

The pre-weighed empty crucible was labelled (W_1). Three (3 g) grammes of the crude extract was weighed into a pre-weighed empty crucible (W_2) and heated at 550℃ for 5 h in a lenton muffle furnace. The ash was weighed after cooling in a desiccator (W_3). The difference between the pre-weighed crude extract and the ash in the crucible was used to calculate the weight of the ash. Percentage ash was calculated using the equation below:

$$\text{Ash (\%)} = \frac{W_2 - W_3}{W_2 - W_1} \times 100 \quad (2)$$

Where: W_1= weight of empty crucible

W_2= weight of empty crucible+ crude extract

W_3= weight of empty crucible + ash

2.3.3.Determination of Crude Protein

The micro-Kjedahl technique was used to determine the crude protein content of the crude extract. In a micro-Kjedahl digestion flask, the sample 2 g was weighed along with 20 cm^3 of distilled water. It was shaken and left to rest for a while. Following the addition of one selenium catalyst tablet, 20 cm^3 concentrated sulphuric acid was added. The flask was cooked at 100℃ for 4 h on the digestion block until the digestion was clear. The flask was taken off the block and set aside to cool. The contents were transferred to a 50 cm^3 volumetric flask and diluted with water to the desired concentration. An aliquot of the digest 10 $cm^3$was transferred to another micro-Kjedahl flask with 20 cm^3 of distilled water and placed in the micro-Kjedahl distillation unit's distilling outlet. Under the condenser outlet, a conical flask containing 20 cm^3 of boric acid indicator was inserted. By opening the funnel stopcock, a 40% sodium hydroxide solution 20 cm^3 was added to the contents of the Kjeldahl flask. To minimize sucking back, the distillation process was started with heat supplied and regulated. The distillation was terminated when all of the accessible distillate had been collected in 20 cm^3 of boric acid. By titrating with 0.01N H_2SO_4, the nitrogen in the distillate was determined; the end point was reached when the color of the distillate changed from green to pink. Protein content was

determined by multiplying total nitrogen content by a constant, 6.60, based on the assumption that protein contains roughly 16% nitrogen, which includes both real protein and non-protein nitrogen and does not distinguish between available and unavailable protein. The crude protein was calculated by using the equation below:

$$\text{Crude protein (\%)} = \%\ \text{Nitrogen} \times 6.60 \quad (3)$$

The nitrogen content of the sample is given by formula below:

$$\text{Nitrogen (\%)} = \frac{T_V \times Na \times 0.014 \times V_1}{G \times V_2} \times 100 \quad (4)$$

Where: T_V = titre value of the acid

Na = normality of acid

V_1 = volume of distilled water used for distillation of the digest

V_2 = volume of aliquot used for distillation

G = original of sample used

2.3.4. Determination of crude fibre:

Crude fibre was determined by the method of JAMES (2015). The processed sample (5.0 g) (W_1) was boiled in 150 mL of 1.25% H_2SO_4 solution for 30 min under reflux. The boiled sample was washed in several portions of hot water using a two-fold cloth to trap the particles. It was returned to the flask and boiled again in 150 mL of 1.25% NaOH for another 30 min under same condition. After washing in several portion of hot water, the sample was allowed to drain dry before being transferred quantitatively to a weighed crucible where it was dried in the oven at 105°C to a constant weight. It was thereafter taken to a muffle furnace where it was burnt, only ash was left of it (W_2). The weight of the fibre was determined by difference and calculated as a percentage of the weight of sample analyzed thus:

$$\text{Crude fiber (\%)} = \frac{W_1 - W_2}{W_1}\ x\ \frac{100}{1} \quad (5)$$

Where:

W_2 = Weight of crucible +sample after washing, boiling and drying

W_3 = Weight of crucible +sample of ash

2.3.5. Determination of crude fat

This was determined by solvent gravimetric extraction method described by KIRK and SAWYER (2016). Five gram of sample (W_1) was wrapped in a porous paper (whatman filter paper) and put in a thimble. The thimble was put in a soxlet reflux and mounted into a weighted extraction flask containing 200 mL of petroleum ether. The upper of the reflux flask was connected to a water condenser.

The solvent (petroleum ether) was heated, boiled vaporized and condensed into the reflux flask filled. Soon the sample in the thimble was covered with the solvent until the reflux flask filled up and siphoned over, carrying its oil extract down to the boiling flask. This process was allowed to go on repeatedly for 4 h before the defatted sample was removed, the solvent recovered and the oil extract was left in the flask. The flask (containing the oil extract) was dried in the oven at 60°C for 30 min to remove any residual solvent. It was cooled in desiccator and weighed (W_2). The weight of oil (fat) extract was determined by difference and calculated as a percentage of the weight of sample analyzed thus:

$$\text{Fat (\%)} = \frac{W_1 - W_2}{W_1}\ x\ \frac{100}{1} \quad (6)$$

Where:

W_1 = weight (g) of empty extraction flash

W_2= Weight of flash oil (fat) extract

2.3.6. Determination of Carbohydrate

The total carbohydrate proportion in the crude extract was calculated using the percentage dry method. This is done by subtracting the total percent of other food nutrients from 100%. This is done by using the equation below:

Carbohydrate (%) = 100% - (% crude protein + % ash + % moisture + % fiber + % fat) (7)

2.4. Physical Analysis

2.4.1. Determination of thickness

Thickness of biscuits was determined by measuring the diameter of four biscuit samples placed edge to edge with a digital Vernier caliper. An average of six values was taken for each set of samples. Average value for thickness was reported in millimeter.

2.4.2. Determination of diameter

The diameter was determined by placing the edge of the samples on edge and measuring it with a digital Vernier caliper. An average of six values was taken for each set of samples. The average value for diameter was reported in millimetres.

2.4.3. Determination of weight

The weight of the sample was measured as average values of six individual samples with the help of an analytical weighing balance. The average value for weight was reported in grams.

2.4.4. Determination of spread ratio

The spread ratio was calculated by dividing diameter by thickness.

2.4.5. Hardness (HD)

Hardness will be measured as the maximum force (N) applied to break the extrudates. Hardness will be measured using a TMS-2000 Texture press (Food Technology Corporation, Sterling, VA, USA) equipped with a 1,334 N load cell and thin blade shear compression cell (Model CS-2) using a transducer speed of 0.33 cm/s. Measurements will be repeated six times for each moisture temperature treatment and reported as mean ± standard deviation (n = 2).

2.4.6. Expansion ratio (ER)

The expansion ratio is the ratio between the diameter of the extrudates and the diameter of the extruder die office (3 mm). An electronic digital caliper (Model 62379-521, Traceable Products, TX, USA) will be used. Measurements will be repeated 4 times on extrudates from each moisture temperature treatment and reported as mean ± standard deviation (n = 2).

2.4.7. Bulk density (BD)

Bulk density will be determined by measuring the weight of extrudates required to fill a 1000 mL container, recorded in g/L. Extrudates are randomly added into the container and shaken a few times during filling. Measurements will be repeated 6 times for each moisture-temperature treatment and reported as mean ± standard deviation (n = 2).

2.4.8. Specific mechanical energy (SME)

Specific mechanical energy will be determined by the twin-screw extruder computer control system and recorded during extrusion. Measurements will be repeated twice for each moisture temperature treatment and reported as mean ± standard deviation (n = 2).

2.5. Determination of Functional Properties

2.5.1. Determination of Swelling Index

The swelling index (SI) was determined using the method described by TAKASHI and SIEB ((2011) with slight modification. Exactly 1 g of sample was mixed with 10 ml distilled water, and the slurry was heated at a constant temperature (60, 70, 80, and 90°C) in a water bath for 15 min, centrifuged at 3,000*g* for 10 min, and the SC was expressed as a percentage increase in sample weight.

2.5.2. Determination of Water Absorption Capacity

One gram of sample was mixed with 10 mL distilled water and allowed to stand at ambient temperature (30 ± 2 °C) for 30 min, then centrifuged for 30 min at 3,000 rpm or 2000 × g. Water absorption was examined as per cent water bound per gram sample.

2.5.3. Determination of Oil Absorption Capacity

One gram of sample was mixed with 10 mL sample oil (Sp. Gravity: 0.9092) and allowed to stand at ambient temperature (30 ± 2 °C) for 30 min, then centrifuged for 30 min at 300 rpm or 2000 × g. Water absorption was examined as percent water bound per gram sample.

2.5.4. Determination of emulsification

One (1) g sample, 10 mL distilled water and 10 mL soybean oil was prepared in a calibrated centrifuge tube. The emulsion was centrifuged at 2000 × g for 5 min. The ratio of the height of

the emulsion layer to the total height of the mixture was calculated as emulsion activity in percentage.

The emulsion stability was estimated after heating the emulsion contained in the calibrated centrifuged tube at 80 °C for 30 min in a water bath, cooling for 15 min under running tap water and centrifuging at 2000 × g for 15 min. The emulsion stability expressed as percentage was calculated as the ratio of the height of the emulsified layer to the total height of the mixture.

2.5.5. Determination of Foam Capacity

The foam capacity (FC) and Foam stability (FS) by (Narayana and Rao, 1982) were determined as described with slight modification. The 1.0 g sample sample was added to 50 mL distilled water at 30 ± 2 °C in a graduated cylinder. The suspension was mixed and shaken for 5 min to foam. The volume of foam at 30 s after whipping was expressed as foam capacity using the formula:

$$\textit{Foam capacity}\ (\%) = \textit{volume of foam} - \textit{Volume of foam volume of foam BW} \times 100 \quad (8)$$

Where, AW = after whipping, BW = before whipping

The volume of foam was recorded 1 h after whipping to determine foam stability as per percent of initial foam volume.

2.6.Samples encoding

Table 2. Samples encoding

Code	Formulation
NPO	85% maize, 15% coconut, 15% feed moisture and baked at 133.64 °C
BCO	95% maize, 5% coconut, 20% feed moisture and baked at 120 °C
COA	95% maize, 5% coconut, 10% feed moisture and baked at 80 °C
UST	85% maize, 15% coconut, 23.4% feed moisture and baked at 100 °C
YXZ	95% maize, 5% coconut, 20% feed moisture and baked at 120 °C
QRW	75% maize, 25% coconut, 10% feed moisture and baked at 120 °C
QWU	68.18% maize, 31.82% coconut, 15% feed moisture and baked at 100 °C
VST	75% maize, 25% coconut, 10% feed moisture and baked at 80 °C;
SOA	75% maize, 25% coconut, 20% feed moisture and baked at 120 °C
ABC	85% maize, 15% coconut, 6.59% feed moisture and baked at 100 °C
KSI	85% maize, 15% coconut, 15% feed moisture and baked at 100 °C
SOP	95% maize, 5% coconut, 20% feed moisture and baked at 80 °C
FGH	75% maize, 25% coconut, 20% feed moisture and baked at 80 °C

3. Results and Discussion

3.1. Proximate Composition of the Samples

The proximate composition of the samples are shown in Table 4. The moisture content of the maize-coconut snack ranged between 4.94 % and 5.60 %. This index is presumed as one of the most important determinants for the shelf-stability of food products. The result showed a significant ($p<0.05$) increase in the dependency in linear terms of blending ratio and feed moisture content. However, temperature as a linear independent variable, blending ratio, and feed moisture interactions had no significant effect in the quadratic model. The moisture content of the maize-coconut extruded snack increased with the feed moisture levels at all the studied levels. The damaged starch could be the reason for higher values in moisture content in prepared snack foods. These results agreed with Asare *et al*. (2012). Krishnasree *et al.* (2023) reported that higher moisture input in peanut extrusion also reported the high moisture content of the final product. The present results supported those previous findings, where a rise

in feed moisture increased the moisture content of the extruded product.

The protein content of all combination products of maize-coconut extruded snacks ranged from 9.93% to 12.31%. There was a significant difference ($p<0.05$) in the protein content of the samples; the result of this study was similar to Kayacier *et al*. (2014), who reported 15.5 per cent crude protein from wheat and legumes (chickpea, soy and pea) blend. Awolu *et al.* (2015) reported 15.9-24 per cent crude protein from rice, cassava, and Kersting's groundnut blends. Tiwari *et al.* (2011) reported 15.3 per cent to 18.8 per cent of crude protein from broken rice pieces and legumes by-products blend. However, the result of the present study is observed to be less than the reported value (27.7-29.2 per cent) of Wani and Kumar (2016) research on ready-to-eat snacks from rice, cassava and Kersting's groundnut composite flours.

The fat content of the extruded snacks in this study ranged from 8.90% to 9.16%. The result showed a significant ($p < 0.05$) difference in the fat content of the final product. These findings suggest that 10-20 per cent of coconut addition to the maize system would considerably raise the overall fat content.

Table 3. Proximate Composition of the Samples (%)

Samples	Ash	Moisture	Fiber	Fat	Protein	Carbohydrate
NPO	$3.82^{a}\pm0.03$	$5.60^{a}\pm0.14$	$2.87^{c}\pm0.03$	$8.90^{c}\pm0.00$	$11.13^{b}\pm0.01$	$67.69^{l}\pm0.00$
BCO	$3.79^{ab}\pm0.01$	$5.50^{ab}\pm0.14$	$3.02^{b}\pm0.01$	$9.03^{b}\pm0.04$	$12.31^{a}\pm0.28$	$66.36^{l}\pm0.00$
COA	$3.75^{b}\pm0.02$	$5.40^{abc}\pm0.14$	$3.05^{b}\pm0.01$	$9.12^{a}\pm0.01$	$10.26^{e}\pm0.20$	$68.43^{k}\pm0.01$
UST	$3.73^{b}\pm0.03$	$5.30^{bc}\pm0.14$	$3.05^{b}\pm0.02$	$9.15^{a}\pm0.01$	$10.30^{cd}\pm0.00$	$68.48^{j}\pm0.00$
YXZ	$3.73^{b}\pm0.02$	$5.20^{c}\pm0.14$	$3.05^{b}\pm0.04$	$9.16^{a}\pm0.01$	$10.30^{cd}\pm0.14$	$68.85^{f}\pm0.00$
QRW	$3.65^{c}\pm0.05$	$4.96^{d}\pm0.03$	$3.05^{b}\pm0.05$	$9.14^{b}\pm0.02$	$10.40^{cd}\pm0.14$	$68.82^{g}\pm0.00$
QWU	$3.65^{c}\pm0.04$	$4.96^{d}\pm0.01$	$3.15^{a}\pm0.05$	$9.14^{a}\pm0.03$	$10.60^{b}\pm0.14$	$68.52^{i}\pm0.00$
VST	$3.65^{c}\pm0.02$	$4.97^{d}\pm0.01$	$3.15^{a}\pm0.04$	$9.07^{b}\pm0.01$	$10.25^{de}\pm0.07$	$68.93^{e}\pm0.00$
SOA	$3.65^{c}\pm0.01$	$4.97^{d}\pm0.02$	$3.15^{a}\pm0.02$	$9.06^{b}\pm0.04$	$10.65^{c}\pm0.35$	$68.54^{h}\pm0.01$
ABC	$3.57^{d}\pm0.04$	$4.97^{d}\pm0.02$	$3.15^{a}\pm0.01$	$9.06^{b}\pm0.03$	$9.96^{e}\pm0.05$	$69.32^{d}\pm0.00$
KSJ	$3.56^{d}\pm0.03$	$4.95^{d}\pm0.03$	$3.14^{a}\pm0.01$	$9.06^{b}\pm0.01$	$9.96^{e}\pm0.04$	$69.34^{c}\pm0.00$
SOP	$3.55^{d}\pm0.03$	$4.95^{d}\pm0.04$	$3.14^{a}\pm0.03$	$9.05^{b}\pm0.01$	$9.93^{e}\pm0.03$	$69.38^{b}\pm0.00$
FGH	$3.54^{d}\pm0.03$	$4.94^{d}\pm0.04$	$3.14^{a}\pm0.04$	$9.04^{b}\pm0.02$	$9.95^{e}\pm0.04$	$69.40^{a}\pm0.00$

Values are mean ± standard deviation of triplicates. The values with the same letter down a column are not significantly different at $p< 0.05$.

The interaction of barrel temperature and feed moisture has a significant negative effect on the fat content of extruded products. The results of this study were higher, with Sharma *et al.* (2016) that reported 3.19 % crude fat in expanded snack food processed from maize, sorghum, bengal gram, rice and soya chunks. Similarly, Tumuluru *et al.* (2013) observed that 0.19 to 1.30 per cent of crude fat from rice flour and fish co-extrudates. However, the result of this study is lower (8.1-15.7 per cent) than Awolu *et al*. (2015), which prepared the ready-to-eat snack food from rice, cassava and kersting's groundnut composite flours by extrusion technique. This may be due to the differences in crop types and the processing methods employed during the flour formulation.

Crude fiber content of the prepared snack food ranged from 2.87-3.15 %. Fiber particles usually hinder the product's expansion by rupturing the cell walls before the gas bubbles expand to their full potential. Consequently, extruded products with high fiber content are usually compact, tough, non-crispy, and have undesirable textures (Liu *et al*., 2000). The fiber value of the snack food of this study was similar to the investigations of Guzmán-Ortiz *et al.* (2015); they were reported fiber content of 1.7 to 3.2 per cent in a blend of maize and lima bean snack food. However, the results of this study

were lower than Chanvrier *et al.* (2013); they were reported 5.4-16.9 per cent in processed ready-to-eat starch-based extruded cereals snack food from whole wheat, wheat flour and corn flour. Barrel temperatures and moisture contents had no significant effect on the crude fiber content of resultant snacks.

The ash content increased and ranged between 3.54 and 3.82%. The extrudates with the addition of lupine showed higher ash content, which was directly proportional to the number of lupine amounts added. The ash content in extruded snacks was significantly ($p < 0.05$) different. Barrel temperature and moisture content were not showed a significant effect on the ash content of prepared snacks. A similar result (1.5 to 3.8 per cent) was reported by Awolu *et al*. (2015) in ready-to-eat extruded snacks produced from composite flour with rice, cassava and Kersting's groundnut flours.

The carbohydrate contents in the maize-coconut extruded snacks ranged from 66.36% to 69.40 %. The highest carbohydrate content was observed in sample FGH. The least carbohydrate content was observed in sample BCD. The carbohydrate content of the extrudates was significantly ($p <0.05$) different. Processing methods like whole grain flour may increase carbohydrate content in snack food (Robin *et al.,* 2015). Similar results were reported by Oliveira *et al*. (2017), who reported 57.27-83.76 per cent of carbohydrates in extruded products from maize flour and whole grain wheat flour. Barrel temperature and moisture content had no significant effect on the total carbohydrate content of resultant snacks.

3.2. Functional Composition of the Samples

The Bulk density of the extruded product of this study ranged from 0.57 to 0.76 g/cm^3. Bulk Density was significantly ($p<0.05$) dependent linearly on the blending ratio and barrel temperature. It was also observed that elevated Bulk Density is desirable for superior ease of dispensability and decline of paste thickness in the extrusion process (Awolu *et al*., 2015). The bulk density values of the product in this study were higher than reported studies on the extrusion of different maize and legume-based products. This higher Bulk Density may be attributed to the difference in blending ratios, crop types and usage of whole-grain maize flour. In the present study, increased BD can correlate to an increased maize flour.

Table 4. Functional Properties of the Samples

Samples	ES (%)	EA (%)	OAC (g/ml)	BD (g/cm^3)	FC (%)
NPO	$11.33^{a}\pm0.02$	$10.80^{a}\pm0.14$	$2.98^{a}\pm0.01$	$0.57^{g}\pm0.01$	$15.60^{a}\pm0.14$
BCO	$11.31^{a}\pm0.01$	$9.85^{b}\pm0.04$	$2.98^{a}\pm0.01$	$0.66^{e}\pm0.0$	$14.60^{b}\pm0.28$
COA	$11.12^{b}\pm0.01$	$9.86^{b}\pm0.04$	$1.93^{b}\pm0.02$	$0.62^{f}\pm0.01$	$12.60^{c}\pm0.42$
UST	$11.07^{bc}\pm0.04$	$9.90^{b}\pm0.12$	$1.94^{b}\pm0.02$	$0.68^{d}\pm0.01$	$12.55^{c}\pm0.64$
YXZ	$11.07^{bc}\pm0.02$	$9.91^{b}\pm0.12$	$1.95^{b}\pm0.02$	$0.76^{ab}\pm0.05$	$11.17^{e}\pm0.04$
QRW	$11.07^{bc}\pm0.02$	$9.90^{b}\pm0.10$	$1.95^{b}\pm0.01$	$0.76^{a}\pm0.03$	$12.70^{c}\pm0.14$
QWU	$11.05^{cd}\pm0.01$	$9.90^{b}\pm0.08$	$1.96^{b}\pm0.01$	$0.75^{abc}\pm0.02$	$12.80^{c}\pm0.14$
VST	$11.04^{cde}\pm0.02$	$9.90^{b}\pm0.06$	$1.97^{b}\pm0.01$	$0.70^{bcd}\pm0.03$	$12.60^{c}\pm0.14$
SOA	$11.03^{cde}\pm0.02$	$9.58^{bc}\pm0.40$	$1.98^{b}\pm0.01$	$0.71^{abc}\pm0.03$	$12.75^{c}\pm0.21$
ABC	$11.00^{de}\pm0.03$	$9.54^{bcd}\pm0.47$	$1.94^{b}\pm0.01$	$0.74^{bc}\pm0.01$	$12.75^{c}\pm0.07$
KSJ	$11.01^{cde}\pm0.03$	$9.14^{d}\pm0.02$	$1.94^{b}\pm0.04$	$0.70^{cde}\pm0.02$	$11.76^{d}\pm0.02$
SOP	$10.00^{de}\pm0.04$	$9.15^{cd}\pm0.02$	$1.96^{b}\pm0.02$	$0.71^{abc}\pm0.02$	$11.73^{de}\pm0.02$
FGH	$10.99^{e}\pm0.04$	$9.15^{cd}\pm0.01$	$1.93^{b}\pm0.08$	$0.72^{abcd}\pm0.02$	$11.72^{de}\pm0.01$

Values are mean ± standard deviation of triplicates. The values with the same letter down a column are not significantly different at $p< 0.05$.

The higher concentrations of the fiber and protein may influence the starch gelatinization process and the rheological properties of the raw materials used in the extrusion process (Yagci

and Gögüs, 2008). Feed with higher moisture levels may lead to a high Bulk density of the product (Saini, 2015). This trend may be due to the temperatures used in extrusion cooking is not sufficient to cause moisture vaporization, and moisture retained in extruded products may reduce the puffing and result in high BD of the product (Asare *et al*., 2012). The heat generation in the extrusion process can convert moisture into vapour when the product exits from the die; this leads to a flash-off the moisture quickly and results in an expanded structure with large alveoli and lower BD. This process leads to crumples in cell organization, which usually disintegrates up on cooling of the product (Filli *et al.,* 2013).

The emulsion activity index indicates the ability of the proteins to induce the formation of the newly created dispersed particles in emulsions, and in this study, the values ranged from 9.14-10.80%, there was a significant difference in the emulsion activity of the extrudates, whereas Emulsion stability value reflects the ability of food protein to form an emulsion that can withstand stress and remain unchanged over a stipulated period of time, under specific conditions (Hoang, 2024). There was a significant decrease in the emulsion stability as the temperature increased. The emulsion properties depend on the type, concentration and solubility of the proteins (Achinewhu, 1983).

Foam capacity of the composite sample blends progressively ranged from 11.17 to 15.60%, and there was a significant ($p<0.05$) increase. Foam capacity is the ability of the flour to foam when water and heat are applied and is dependent on soluble proteins (Samaila *et al.,* 2017). The significant variation in the foam capacity of the composite blends could be attributed to differences in the samples solubilized protein and polar and non-polar lipids. High foam capacity in extruded snacks is undesirable; however, preparation at reduced pressure minimizes its formation (Samaila *et al.,* 2017). The values obtained for foam capacity in this study were higher than 6.67 to 10.33 % reported for wheat and cocoyam flour blends (Anon *et al*., 2021) and 8.20 - 11.28 % reported for finger millet, wheat, soybean and peanut flour blends (Okache *et al*., 2020). These variations could be attributed to differences in the composite flour blends.

Oil absorption capacity (OAC) increased from 1.93 to 2.98 g/ml. The highest oil absorption capacity recorded could be attributed to the lipid binding capacity of the hydrophobic proteins present in the flour. The values obtained were, however, lower than the range (1.61-1.79 g/g) reported by Orisa and Udofia (2020). This could be attributed to differences in the method employed and the proportion of the raw materials used. Oil absorption capacity has been attributed to the physical entrapment of oil. Samples with high oil content are an indication of high level of energy and calories. Previous researchers have shown that the frequency of some diseases associated with high-fat diets, including diabetes and obesity, is on the increase (Honerlaw *et al*., 2019).

The data obtained led to the classification of the extruded corn-coconut snacks into three groups; high, medium and low functionality (Table 5). The classification was further corroborated by the results of the principal component analysis (Fig. 1) in which the clustering of the samples within some ranges were used to classify them. Alefew *et al.* (2024) advocated the enriching of snack foods as part of a diet-based remedy for reducing malnutrition in the population. Thus, the use of coconut known for its fibre and other rich bioactive components along with maize produced extruded snacks with high functional properties.

Table 5. Classification of the samples based on the Functional Properties

Sample	Classification	Functional Characteristics
NPO	High Functionality	Excellent emulsion, oil retention, and foaming
BCO	High Functionality	High oil absorption, good emulsion properties
QRW	Medium Functionality	Dense texture, average oil and air retention
YXZ	Medium Functionality	Similar to QRW, moderately functional
KSJ, FGH	Low Functionality	Poor oil and air retention, low emulsion performance

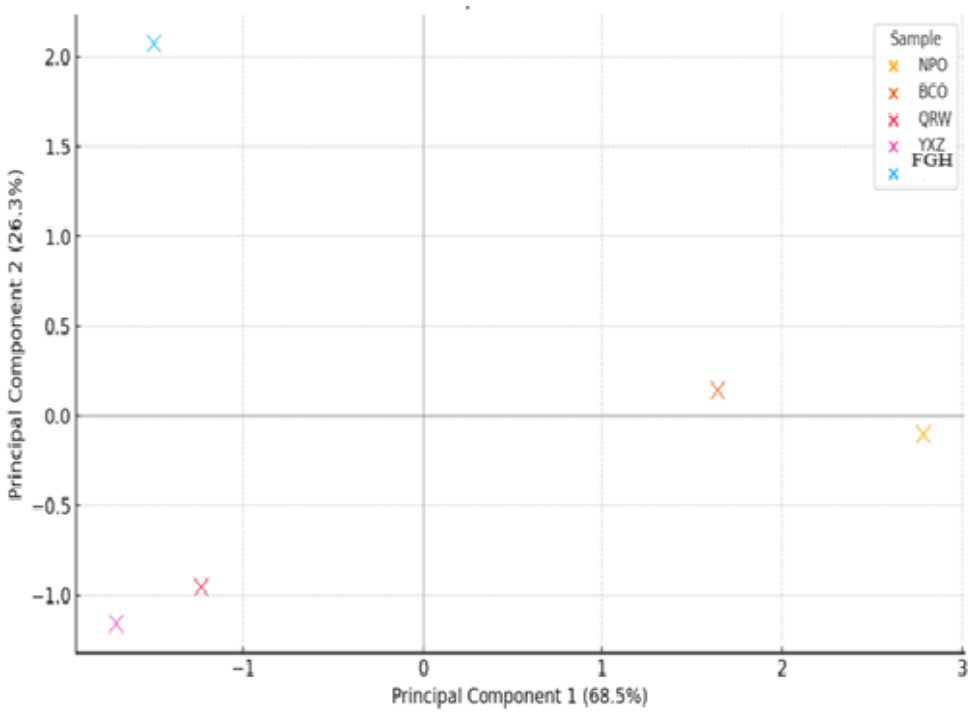

Figure 5. Principal Component Analysis (PCA) of the Functional Properties of Extruded Corn-Coconut Snack samples

The principal component analysis (PCA) showed that NPO and BCO closely clustered, indicating similar functional profiles (Fig. 5). They showed high emulsion stability, high oil absorption capacity, and strong foaming capacity. Thus, their position in the top-right quadrant reflects high scores across multiple variables, especially those positively loading on both PC1 and PC2 as a functionally rich samples ideal for light, flavourful snacks, with good fat-binding capability. It was evident that percentage contribution of coconut. The barrel temperature and feed moisture of the extruded corn-coconut snack influenced the functional properties.

The graph also showed that QRW and YXZ are at the middle to right-centre and could be classified in the medium functionality. The NPO and BCO are very close to each other but at a distant from NPO/BCO. Therefore, QRW and YXZ possessed moderate oil absorption with higher bulk density, which likely pulled them apart from the high-functionality classification. The samples appear to align more with bulkier, denser products, potentially suitable as crunchy or compact snacks rather than aerated ones.

The bottom of the graph showed a clear separation from the other samples, exhibiting least values in oil absorption, foaming capacity and emulsion stability. Since it is at the bottom of the graph, it could be described as a separate and weaker in functional profile classification which could be attributed to lower protein or fat interaction effects. The FGH sample might be best suited for formulations where minimal oil and air retention is preferred (e.g., dry snacks or flour blends).

3.1.3. Colour Composition of the Samples

The Colour composition of the samples are presented in Fig. 6. Colour is an important attribute in food acceptability, being an indicator of quality, conservation state, flavour expectation and commercial value (Fradique *et al*., 2010). The results of ΔE (Total colour change, TCC) ranged from 38.34 to 55.13. LEB 18 in the extruded snacks caused the reduction of a*, b*, C* and luminosity (L*). The results were like those obtained in other studies that evaluated the influence of the addition of coconut on the colour of foods (Fradique *et al.,* 2010; Joshi *et al.,* 2014). Colour is one of the most important characteristics of extruded products since it shows the extent of thermal treatment. Changes in colour can be used as an indicator of the extent of browning reactions for example caramelization, maillard reactions, degree of cooking plus pigment degradation that take place during extrusion cooking (Serge *et al*., 2011).

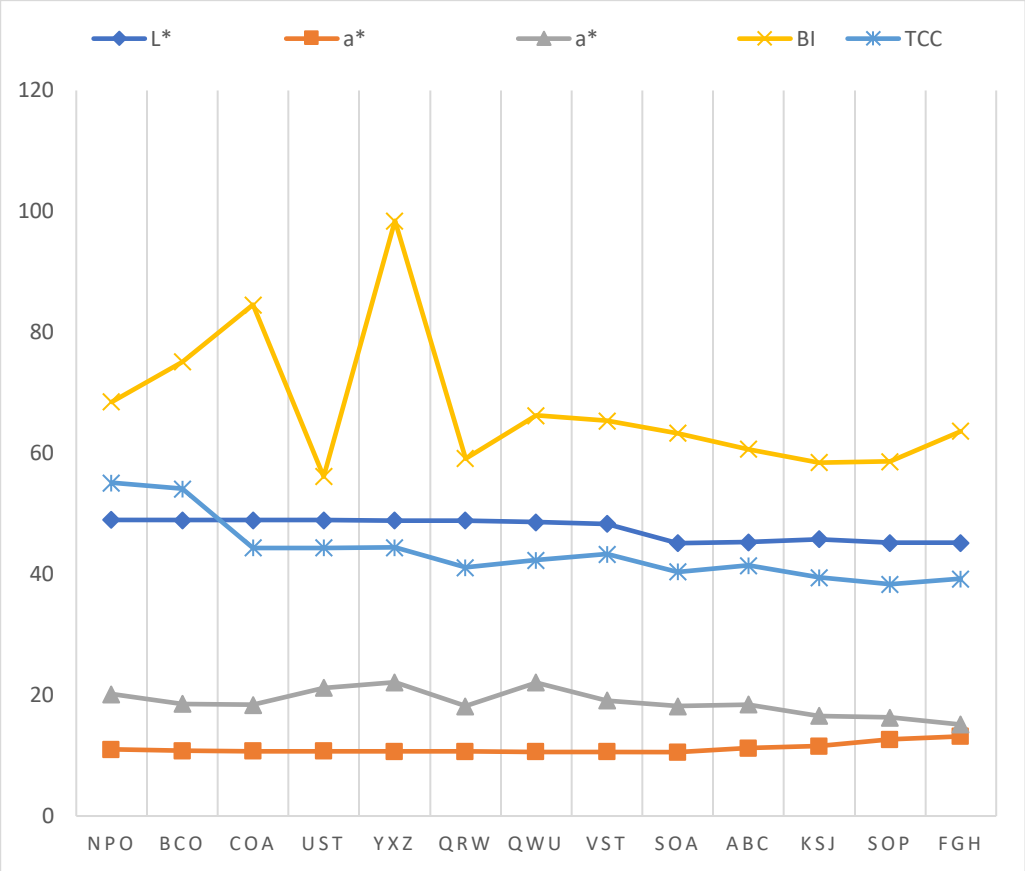

Figure 6. CIEL Colour Classification of the Snack samples

Colour parameters are important because they are used to assess changes in raw material and formulation due to boiling within the extruder barrel (Mjoun and Rosentrater, 2011); therefore, colour is important because it is the first attribute perceived by consumers, and it

determines the acceptance or rejection of a product (Rampersad *et al*., 2003). The increased ΔE could be due to the increased PSF concentration, which causes the snacks to have a darker formulation colour. To compare the values of different formulations, ΔE was observed at a temperature range of 120 to 180 °C. The extrusion process caused a significant decrease ($P < 0.05$) in ΔE. It is known that redox reactions between sugars and proteins (amino acids) in foods at high temperatures can promote non-enzymatic browning (Maillard reaction), resulting in the darkening of the final product (Nayak *et al.,* 2011). Therefore, the observed decrease in ΔE values can be attributed to the Maillard reaction as a result of the extrusion process. This effect is consistent with what has been reported by other researchers (Norfezah *et al.,* 2011).

Furthermore, pigment degradation due to extrusion temperatures could have generated products of the Maillard reaction that promoted changes in colour values, as observed in the extruded and unprocessed (raw) products. Therefore, it can be concluded that changes in the colour of the ready-to-eat snacks are due to increasing concentrations of PSF and the processing conditions.

3.4.a. Physical Properties of the Samples

The volumes of the samples were considered. Overall, there was no significant ($p<0.05$) difference in the volume. It is important to note that higher Volume is mostly obtained at lower feed moisture contents. This increase in VP could be related to dough rheology.

The minimum and maximum hardness values were 4.07 and 4.86. This may be due to the generation of shear pressure inside the barrel while increased the rate of gelatinization of dough. The hardness was also influenced by moisture content. Hardness was positively correlated with feed moisture. A similar effect was observed by Seth *et al.* (2015). Inside the extruder, the starch-based material gets plasticized due to the reduction of viscosity and dissipation of mechanical energy with increasing feed moisture; hence, extrudates become denser and harder with compressed bubbles.

Table 6a. Physical Properties of the Samples

Samples	Volume	Specific volume	Density	Hardness	Height
NPO	$1.92^{a}\pm0.03$	$0.42^{g}\pm0.00$	$2.40^{a}\pm0.00$	$4.85^{a}\pm0.07$	$1.40^{a}\pm0.14$
BCO	$1.94^{a}\pm0.01$	$0.57^{b}\pm0.01$	$2.21^{b}\pm0.01$	$4.50^{ab}\pm0.42$	$1.46^{a}\pm0.18$
COA	$1.96^{a}\pm0.02$	$0.49^{de}\pm0.00$	$2.00^{j}\pm0.00$	$4.50^{ab}\pm0.41$	$1.45^{a}\pm0.18$
UST	$1.96^{a}\pm0.04$	$0.49^{cde}\pm0.00$	$2.02^{g}\pm0.00$	$4.50^{ab}\pm0.38$	$1.44^{a}\pm0.18$
YXZ	$1.96^{a}\pm0.05$	$0.50^{cd}\pm0.00$	$2.01^{h}\pm0.00$	$4.50^{ab}\pm0.36$	$1.49^{a}\pm0.01$
QRW	$1.96^{a}\pm0.06$	$0.49^{cde}\pm0.00$	$2.01^{h}\pm0.00$	$4.49^{ab}\pm0.34$	$1.44^{a}\pm0.04$
QWU	$1.92^{a}\pm0.06$	$0.24^{h}\pm0.00$	$2.01^{h}\pm0.00$	$4.50^{ab}\pm0.34$	$1.46^{a}\pm0.05$
VST	$1.92^{a}\pm0.09$	$0.50^{c}\pm0.00$	$2.01^{h}\pm0.00$	$4.50^{ab}\pm0.33$	$1.45^{a}\pm0.06$
SOA	$1.92^{a}\pm0.12$	$0.49^{cde}\pm0.01$	$2.00^{ij}\pm0.01$	$4.12^{b}\pm0.01$	$1.31^{a}\pm0.25$
ABC	$1.90^{a}\pm0.10$	$0.49^{cde}\pm0.00$	$2.03^{f}\pm0.00$	$4.09^{b}\pm0.01$	$1.44^{a}\pm0.07$
KSJ	$1.90^{a}\pm0.08$	$0.49^{e}\pm0.00$	$2.05^{d}\pm0.00$	$4.07^{b}\pm0.03$	$1.42^{a}\pm0.06$
SOP	$1.90^{a}\pm0.10$	$2.04^{a}\pm0.00$	$2.04^{e}\pm0.00$	$4.22^{ab}\pm0.01$	$1.41^{a}\pm0.06$
FGH	$1.89^{a}\pm0.07$	$0.48^{f}\pm0.00$	$2.07^{c}\pm0.00$	$4.10^{b}\pm0.01$	$1.33^{a}\pm0.01$

Values are mean ± standard deviation of triplicates. The values with the same letter down a column are not significantly different at $p < 0.05$.

Li (2021) posited that smaller air cells in extrudates, caused by increased breaking strength, lead to higher hardness. Nur-Adibah *et al.* (2024) obtained a hardness value that ranged from 9.74 kg to 25.71 kg for a fibre-rich okara-based expanded snack which established that the hardness of snacks were inversely related to the expansion ratio (r = 68.7%). The increase in feed moisture resulted in a significant increase ($p < 0.05$) in the hardness of the extrudate.

This effect is because higher moisture content decreases the shear of the plasticized mass inside the extruder, reducing the gelatinized starch and preventing the growth of air bubbles in the snacks. This is lower than 16.2 to 43.4 N reported by Joshi *et al.* (2014) on corn extrudates added with microalga.

The specific volume of the snack products was about 0.42–2.04%. Results agree with previous findings. Fleischman et al. (2016) observed that increasing wheat bran content in wheat extrudates resulted in a less expanded and more compact structure with smaller air bubbles. Recently, including 16% common bean flour in optimized corn-based snacks gave a Vs reduction of 23% (Felix-Medina *et al.,* 2020).

The density of the snack products was about 2.00–2.40 g/cm3. Feeding temperature during extrusion had a significant inverse effect on snack density, whereas feeding moisture did not. (Ruiz-Armenta *et al*., 2018) obtained low Density (103 – 204 g /L). Ruiz-Armenta *et al.* (2018) reported the density (168 – 260 kg /m^3) of rice and beer industry waste second-generation snacks. Tovar-Jimenez *et al.* (2015) reported Density (approximately 150 –260 kg /m^3) on third-generation snacks from potato starch, corn starch, milled oranges and monoglycerides.

The height of the snack ranged between 1.33 cm and 1.49 cm, with sample FGH having the lowest value and sample YXZ the highest. There was a significant ($p<0.05$) difference in the height of the samples.

3.4.b. Physical Properties of the Samples

The results for the physical properties of the maize-coconut-based snacks are summarized in Table 4.1.4b. The diameter values ranged from 4.91 to 5.93; there was a significant ($p < 0.05$) difference. The findings indicate that the diameter of extrudates increased with an increase in temperature at all the coconut/maize mixing ratios. This may be because increasing barrel temperature could increase the degree of gelatinization and the extent of superheated steam that causes the snack to expand more (Korkerd *et al.,* 2016; SUE *et al.,* 2015). Temperature determines the vapour pressure of the moisture and, thus, the degree of puffing. This is probably due to the stretching of the molecules at higher temperatures, which causes a higher degree of gelatinization Guha And Ali (2006). Low moisture conditions and an increase in barrel temperature led to increased expansion (Leonel *et al.,* 2009).

The mean wall thickness was obtained and ranged between 0.42 to 0.54, respectively. However, some pellets had a higher expansion; significant differences ($p < 0.05$) were obtained between the different extrusion temperatures or feed moisture contents in the porosity (%) or in the mean wall thickness of the expanded products. Indicating that expanded products with higher porosity tended to have thinner walls, regardless of the conditions that were used (extrusion temperature and feed moisture content).

Weight ranged from 3.86 – 4.55 g/cm^3. Gasparre *et al*. (2020) reported weight ranging from 1.35-1.54 g/cm^3 in rice-based gluten-free extruded snacks blended with tiger nut flour. The higher weight (3.86 – 4.55 g/cm^3) obtained in this study could be attributed to feed moisture and feed blends. Weight is the constant value for matter and the mass of a food particle divided by its volume, excluding open and closed pores (Shefali And Florian, 2017).

Table 6b. Physical Properties of the Samples

Samples	Diameter	Thickness	Spread ratio	Weight
NPO	5.93^{a}±0.04	0.54^{a}±0.01	10.98^{e}±0.01	4.55^{a}±0.21
BCO	5.46^{b}±0.68	0.53^{a}±0.02	10.41^{j}±0.01	4.30^{b}±0.14
COA	5.04^{bc}±0.10	0.49^{b}±0.01	10.28^{k}±0.00	3.95^{c}±0.05
UST	5.04^{bc}±0.11	0.46^{bc}±0.01	10.96^{f}±0.00	3.95^{c}±0.03
YXZ	5.06^{bc}±0.15	0.44^{cd}±0.01	11.47^{d}±0.00	3.94^{c}±0.03
QRW	5.03^{bc}±0.13	0.48^{b}±0.00	10.43^{i}±0.00	3.94^{c}±0.01
QWU	4.95^{c}±0.06	0.48^{b}±0.00	10.26^{l}±0.00	3.87^{c}±0.04
VST	4.96^{c}±0.02	0.42^{d}±0.01	11.80^{a}±0.00	3.86^{c}±0.01
SOA	4.96^{c}±0.02	0.43^{cd}±0.01	11.52^{c}±0.00	3.86^{c}±0.02
ABC	4.97^{c}±0.02	0.44^{cd}±0.01	11.55^{b}±0.00	3.87^{c}±0.02
KSJ	4.98^{bc}±0.02	0.46^{bc}±0.02	10.93^{g}±0.00	3.89^{c}±0.08
SOP	4.91^{c}±0.08	0.47^{bc}±0.02	10.45^{h}±0.00	3.88^{c}±0.06
FGH	4.92^{c}±0.08	0.48^{b}±0.01	10.25^{m}±0.00	3.93^{c}±0.02

Values are mean ± standard deviation of triplicates. The values with the same letter down a column are not significantly different at $p< 0.05$.

The spread ratio of the snack ranged between 10.25 and 11.80, with sample FGH having the lowest value and sample VST the highest. There was a difference ($p < 0.05$) in the spread ratio of the samples.

The probability plot of the residuals of the physical properties determined against spread ratio showed that some of the data were skewed either to the left or right of the graph indicating non-normal distribution (Fig. 7).

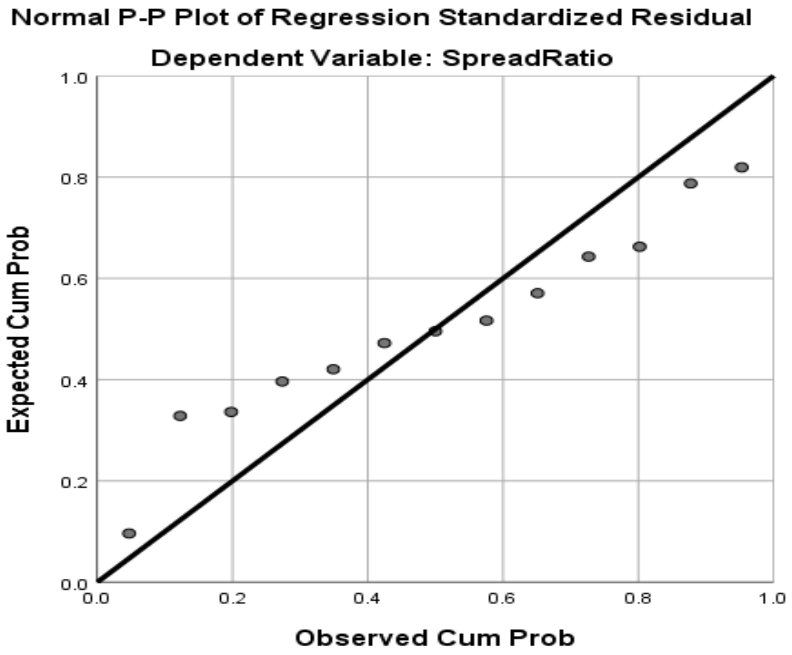

Figure 7. Normal Probability Plot of Regression Standardized Residual Vs Spread Ratio

Pearson correlation indicates that an increase in spread ratio of the samples would lead to non-significant ($p>0.05$) decrease in the volume of the extruded snacks ($r^2 = 0.003481$). The spread ratio was negatively correlated with specific volume, density, hardness, diameter, thickness and weight of the extruded snacks, but positively correlated with the extruded snacks

height. Thus, a higher spread ratio implied that the snack has expanded more during the extrusion process which would lead to an increase in the height of the snacks. Therefore, Fig. 7 clearly portrays the trend as normal distribution was not expected in the results findings.

Furthermore, the weight of the extruded snacks was strongly correlated to the density (r = 0.966), hardness (r = 0.658), diameter (r = 0.988) and thickness (r = 0.830) of the extruded snacks, but negatively corelated with spread ratio (r = -0.150) and specific volume (r = -0.024) of the corn-coconut extruded snacks.

3.5. Sensory Evaluation Score of Samples

Sensory Composition of Samples is shown in Table 7. The texture of the maize-coconut extrudates indicate that the mean force required to puncture the extruded sample reduced with increased barrel temperature.

Table 7. Sensory Evaluation Score of Samples

Samples	Colour	Texture	Taste	Flavor	Overall Acceptability
NPO	$6.00^{a}\pm2.42$	$5.12^{a}\pm1.90$	$5.88^{abcd}\pm2.43$	$5.68^{a}\pm2.41$	$5.56^{ab}\pm2.28$
BCO	$5.72^{a}\pm1.95$	$5.60^{a}\pm1.87$	$5.96^{abc}\pm2.70$	$5.92^{a}\pm2.48$	$4.92^{ab}\pm2.12$
COA	$5.40^{a}\pm1.96$	$5.76^{a}\pm2.26$	$5.72^{abcd}\pm2.17$	$5.32^{a}\pm2.43$	$5.52^{ab}\pm2.38$
UST	$5.00^{a}\pm1.91$	$5.92^{a}\pm2.25$	$4.96^{bcd}\pm2.47$	$5.28^{a}\pm2.81$	$5.28^{ab}\pm2.48$
YXZ	$4.84^{a}\pm2.09$	$5.68^{a}\pm2.43$	$4.88^{bcd}\pm2.39$	$5.04^{a}\pm2.19$	$5.04^{ab}\pm2.17$
QRW	$5.92^{a}\pm2.12$	$5.64^{a}\pm1.63$	$5.00^{bcd}\pm2.48$	$5.20^{a}\pm1.88$	$5.32^{ab}\pm2.54$
QWU	$5.28^{a}\pm2.30$	$5.88^{a}\pm1.92$	$4.36^{d}\pm2.46$	$5.16^{a}\pm2.70$	$5.64^{ab}\pm2.83$
VST	$5.68^{a}\pm2.54$	$6.40^{a}\pm2.14$	$6.40^{ab}\pm2.08$	$5.24^{a}\pm2.71$	$6.32^{a}\pm1.75$
SOA	$5.24^{a}\pm2.73$	$5.68^{a}\pm2.48$	$4.84^{cd}\pm2.54$	$4.48^{a}\pm2.54$	$4.52^{b}\pm2.12$
ABC	$5.52^{a}\pm1.78$	$5.88^{a}\pm1.74$	$4.80^{cd}\pm2.29$	$5.52^{a}\pm2.00$	$5.84^{ab}\pm2.49$
KSJ	$5.56^{a}\pm1.36$	$5.28^{a}\pm1.69$	$5.64^{abcd}\pm2.43$	$5.36^{a}\pm1.75$	$5.32^{ab}\pm2.49$
SOP	$5.60^{a}\pm1.83$	$5.92^{a}\pm2.08$	$5.84^{abcd}\pm2.19$	$5.60^{a}\pm2.45$	$5.84^{ab}\pm2.37$
FGH	$6.08^{a}\pm2.02$	$5.52^{a}\pm2.33$	$6.84^{a}\pm1.55$	$6.00^{a}\pm2.22$	$5.84^{ab}\pm1.78$

Values are mean ± standard deviation of triplicates. The values with the same letter down a column are not significantly different at $p< 0.05$.

The flavour acceptance of the blended extruded snack food was found between 4.48 - 6.0. The addition of coconut significantly affected the flavour acceptability of maize-coconut snacks. This may be due to higher cooking temperatures (120°C to 150°C), which were key in modifying and eliminating the off flavours to improve their sensory properties (Simons *et al.,* 2015).

The taste of the extruded snacks was also influenced by the lupine incorporation, up to 20 per cent. However, the addition of 40 to 50 per cent of lupine flour significantly decreased the taste of the final product. It resulted in a lower taste score, as Jayasena and Nasar-Abbas (2012) reported. LIU *et al.* (2000) described high-fiber extruded cereal products with low expansion, hard texture, and rough, uneven skins as features that make products unappealing to potential end users.

Overall acceptability scores of the extruded snack demonstrated no significant ($p>0.05$) difference. The overall acceptability results of extruded foods in this study agreed with that of Hall and Johnson (2004). Even though higher colour scores were recorded, the overall acceptability was decreased.

4.Conclusion

This study demonstrates that extrusion parameters, specifically temperature and maize-to-coconut ratios, significantly impact the physicochemical properties and sensory acceptability of maize-coconut extruded snacks. Higher extrusion temperatures led to increased expansion and reduced hardness of the

extrudates, enhancing their sensory appeal. Snacks with higher maize content exhibited more significant expansion and lower hardness, resulting in higher sensory rankings. The proximate analysis revealed that the snacks possess desirable nutritional qualities, with carbohydrate content ranging from 66.36% to 69.40%, protein content from 9.93% to 12.31%, and fat content from 8.90% to 9.16%. Both processing variables and ingredient composition influenced functional properties such as bulk density, emulsion activity index, foam capacity, and oil absorption capacity. Notably, while foam capacity increased significantly, high foam capacity is undesirable in extruded snacks and should be optimized. The colorimetric properties underscore the importance of visual appeal in consumer acceptance. Overall, optimizing extrusion conditions and ingredient ratios is crucial for developing maize-coconut snacks with improved physical characteristics, nutritional value, and consumer acceptability. Future research should focus on refining these parameters to enhance product quality and explore the commercial viability of these snacks.

5.Reference:

Adebowale, O. J. and Komolafe, O. M. (2018). Effect of Supplementation with Defatted Coconut Paste on Proximate Composition, Physical and Sensory Qualities of a Maize-Based Snack. *Journal of Culinary Science & Technology*, 16:1, 40-51, DOI: 10.1080/15428052.2017.1315322.

Alefew, Y. D., Tiruneh, A. T., & Yehuala, T. F. (2024). Optimization of extrusion conditions for development of high-quality rice-lupin-pumpkin based extruded snack food. *Heliyon,* 10(24): e40913. https://doi.org/10.1016/j.heliyon.2024.e40913.

Anon, A. H., Fagbohoun, J. B., Koffi, A. G., Anno, H. F. A. and Kouamé, L. P. (2021). Functional Properties of Composite Flours Produced with Ivorian Taro (Colocasiaesculenta L. CvFouê) Corms Flour and Wheat (Triticumaestivum L.) Flour. GSC Biological and Pharmaceutical Sciences, 15(03): 164–176.

Ape, D., Nwogu, N. A., Uwakwe, E. I. and Ikedinobi, C. S. (2016). Comparative Proximate Analysis of Maize and Sorghum Bought from Ogbete Main Market of Enugu State, Nigeria. *Greener Journal of Agricultural Sciences*, 6 (9): 272-275. *http://doi.org/10.15580/GJAS.2016.9.101516167*

Asare, E.K., Samule, S.D., Emmmanuel, O.A., Esther, S.D., & Agnes, S.B. (2012). Extrusion cooking of rice-groundnut-cowpea mixtures-effects of extruder characteristics on nutritive value and physico-functional properties of extrudates using response surface methodology. *Journal of Food Processing and Preservation*, 36(5), 465-476

Awolu, O.O., Oluwaferanmi, P.M., Fafowora, O.L., & Dseyemi, G.F. (2015). Optimization of the extrusion process for the production of ready-to-eat snack from rice, cassava and kersting's groundnut composite flours. LWT – *Food Science and Technology*, 64(1), 18-24.

Awoyale, W., Maziya-Dixon, B., Sanni, L. O., & Shittu, T. A. (2011). Nutritional and sensory properties of a maize based snack food (kokoro) supplemented with treated distillers' spent grain (DSG). International Journal of Food Science and Technology, 46(8): 1609-1620.

Blejan, A. M., Nour, V., Corbu, A. R., & Codină, G. G. (2025). Corn-Based Extruded Snacks Supplemented with Bilberry Pomace Powder: Physical, Chemical, Functional, and Sensory Properties. *Applied Sciences*, *15*(5), 2468. https://doi.org/10.3390/app15052468.

Chakraborty, S. K., Singh, D. S., Kumbhar, B. K., & Chakraborty, S. (2011). Millet–legume blended extrudates characteristics and process optimization using RSM. *Food and Bioproducts Processing,* **89**(4), 492-499.

Dumchaiyapoom, K., Hannanta-anan, P. and Phongpipatpong, M. (2019). Effect of

extrusion conditions on the physical properties of coconut rice-based extrudates. The 12th TSAE International Conference on Earth and Environmental Science, 2019. doi:10.1088/1755-1315/301/1/012056.

Eke, L. (2025). *Roasted corn, coconut and 'Ube': Proudly Nigerian superfood that can gain UN cultural status.* Business Day, June 1, 2025. https://businessday.ng/life/article/roasted-corn-coconut-ube-proudly-nigerian-superfood-that-can-gain-un-cultural-status/. Accessed on June 2, 2025.

Fang, Q., Hanna, M., & Lan, Y. (2003). Extrusion system components. In: Heldman D. R. Ed., Encyclopedia of Agricultural, Food, and Biological Engineering, (301-305). CRC Press.

Felix-Medina, J.V., Montes-Avila, J., Reyes-Moreno, C. et al. (2020). Second-generation snacks with high nutritional and antioxidant value produced by an optimized extrusion process from corn/common bean flours mixtures. *LWT-Food Science & Technology*,124, 109172.

Grasso, S. (2020) Extruded snacks from industrial by products: a review. *Trends in Food Science & Technology*, 99: 284-294. doi: 10.1016/j.tifs.2020.03.012 Available at https://centaur.reading.ac.uk/89591/.

Gurbuz, Y. (2017). Heat applications in feed and food processing. Proceedings of 72nd The IRES International Conference, Mecca, Saudi Arabia, 23rd-24th June 2017.

Heitman, K., Thomas, S. E., Kelly, O., Fanelli, S. M., Krok-Schoen, J. L., Luo, M., & Taylor, C. A. (2023). Snacks contribute considerably to total dietary intakes among adults stratified by glycemia in the United States. PLOS Glob Public Health 3(10): e0000802. https://doi.org/10.1371/journal.pgph.0000802.

Hess, J. M., Jonnalagadda, S. S. and Slavin, J. L. (2016). What Is a Snack, Why Do We Snack, and How Can We Choose Better Snacks? A Review of the Definitions of Snacking, Motivations to Snack, Contributions to Dietary Intake, and Recommendations for Improvement. Advances in Nutrition, 7:466–75. doi:10.3945/an.115.009571.

Hewlings, S. (2020). Coconuts and Health: Different Chain Lengths of Saturated Fats Require Different Consideration. *Journal of Cardiovascular Development and Disease*, *7*(4), 59. https://doi.org/10.3390/jcdd7040059.

Hoang, N. (2024). Improving Food Texture and Stability Through Emulsion Science. *African Journal of Food Science and Technology,* 15(6): 01-02. DOI: http:/dx.doi.org/10.14303//ajfst.2024.088.

Honerlaw, J.P., Ho, Y.L., Nguyen, X.X.T., Cho, K., Vassy, J. I., Gagnon, D.R., & Djousse, L. (2019). Fried food consumption and risk of coronary artery disease: The million-veteran program. *Clinical Nutrition*, 39: 1203-1208.

Ibe, P. C., Agu, H. O., Ikegwu, T. M., Ishiwu, C. N. and Nwokeke, B. C. (2025). Assessment of sensory properties of optimized wheat-white yam composite cookies using response surface methodology. *International Journal of Food Science and Nutrition,* 10, 2: 12-22.

Inyang, U., Oboh, I. and Etuk, B. (2018). Kinetic Models for Drying Techniques—Food Materials. *Advances in Chemical Engineering and Science*, **8**, 27-48. doi: 10.4236/aces.2018.82003.

James, S., Akosu, N. I., Maina, Y. C., Baba, A. I., Nwokocha, L., Amuga, S. J., Audu, Y., & Omeiza, M. Y. M. (2018). Effect of addition of processed bambara nut on the functional and sensory acceptability of millet-based infant formula. *Food science & nutrition*, *6*(4), 783–790. https://doi.org/10.1002/fsn3.618.

Krishnasree, V., Gopinath, P.P., Mohan, G., Binitha, N.K., Jasna, V.K., Seenath, P., Shamna, N., Sajayan, A. and Sujatha, R. (2023). Optimization of Extruded Snack Enriched with Coconut Inflorescence Sap Honey: A Promising Supplementary Food among Tribals. Asian Journal of Dairy and

Food Research. DOI: 10.18805/ajdfr.DR-2067.

Kwon, K., Park, K. H., & Rhee, K. C. (1996). Fractionation and characterization of proteins from coconut (*Cocos nucifera*). *Journal of Agriculture and Food Chemistry* **44**:1741–1745.

Leonel, M., Freitas, T. S., & Mischan, M. M. (2009). Physical characteristics of extruded cassava starch. Scientia Agricola, 66(4), 486–493. doi:10.1590/S0103-90162009000400009

Li, X. (2021). Effects of Extrusion Cooking on Physical and Nutritional Quality of Puffed Snacks Made from Blends of Barley and Green Lentil Flours. A Thesis submitted to the Faculty of Graduate Studies of The University of Manitoba, Department of Food and Human Nutritional Sciences, University of Manitoba Winnipeg, Manitoba.

Małecki, J., Muszyński, S., & Sołowiej, B. G. (2021). Proteins in Food Systems-Bionanomaterials, Conventional and Unconventional Sources, Functional Properties, and Development Opportunities. *Polymers*, *13*(15), 2506. https://doi.org/10.3390/polym13152506.

Nayak, B., Berrios, J.J., Powers, J.R., & Tang, J. (2011). Effect of extrusion on the antioxidant capacity and color attributes of expanded extrudates prepared from purple potato and yellow pea flour mixes. *Journal of Food Science* 76, C874-C883.

Ndife, J., Abasiekong, K. S., Nweke, B., Linus-Chibuezeh, A., & Ezeocha, V. C. (2020). Production And Comparative Quality Evaluation of Chin-Chin Snacks From Maize, Soybean And Orange Fleshed Sweet Potato Flour Blends. *FUDMA Journal of Sciences, 4 (2), 300 – 307*. DOI: https://doi.org/10.33003/fjs-2020-0402-220.

Norfezah, M.N., Hardacre, A., & Brennan, C.S. (2011). Comparison of waste pumpkin material and its potential use in extruded snack foods. *Food Science and Technology International* 17, 367-373.

Nur-Adibah, L., Nor-Afizah, M., Wan-Zunairah, W.I. and Syed-Muhammad, S.K. (2024). Development of fibre-rich okara-based expanded snack via single screw extrusion. *Food Research* 8 (2): 48 – 56.

Nwadi, O.M.M., Uchegbu, N.N. and Okonkwo, T. M. (2023). Use of Cereals and Egg Products in Extruded Foods: A Review. *Pakistan Journal of Nutrition,* 22: 1-10. 10.3923/pjn.2023.1.10.

Offiah, V., Kontogiorgos, V., & Falade, K. O. (2018). Extrusion processing of raw food materials and by-products: A review. *Critical Reviews in Food Science and Nutrition*, *59*(18), 2979–2998. https://doi.org/10.1080/10408398.2018.1480007.

Okache, T. A., Agomuo, J. K. and Kaida, I. Z. (2020). Production and Evaluation of Breakfast Cereal Produced from Finger Millet, Wheat, Soybean, and Peanut Flour Blend. Research *Journal of Food Science & Quality Control*, 6(2): 9-19.

Okeke, E. C., Ene-Obong, H. N., Uzuegbunam, A. O., Ozioko, A., Umeh, S. I., & Chukwuone, N. (2009). The Igbo traditional food system documented in four states in southern Nigeria. In: Indigenous Peoples' Food Systems: the many dimensions of culture, diversity and environment for nutrition and health (Eds), Food and Agriculture Organization of the United Nations Centre for Indigenous Peoples' Nutrition and Environment, Rome 2009.

Okeke, E.C., Eneobong, H.N., Uzuegbunam, A.O., Ozioko, A.O., & Kuhnlein, H. (2008). Igbo Traditional Food System: Documentation, Uses and Research Needs. *Pakistan Journal of Nutrition,* 7(2): 365-376.

Pathirana, H. P. D. T. H., Lakdusinghe, W. M. K., Yalegama, L. L. W. C., Chandrapeli, C. A. T. D., & Madusanka, J. A. D. (2020). Evaluation of Nutritional Composition of Defatted Coconut Flour Incorporated Biscuits. *CORD*, *36*, 33-39. https://doi.org/10.37833/cord.v36i.427.

Piayura, S. and Itthivadhanapong, P. (2023). The effects of feed moisture and dried coconut meal content on the physicochemical, functional, and sensory properties of gluten-free Riceberry rice flour-based extruded snacks. *Frontiers in Sustainable Food System*, 7: 1194594. https://doi.org/10.3389/fsufs.2023.1194594

Prinyawiwatkul, W., Beuchat, L.R., & Phillips, R.D. (1995), "Modelling the effects of peanut flour, feed moisture content, and extrusion temperature on physical properties of an extruded snack product", International Journal of Food Science and Technology, Vol. 30 No. 1, pp. 37-44.

Rehm, C. D., & Drewnowski, A. (2017). Replacing American Breakfast Foods with Ready-To-Eat (RTE) Cereals Increases Consumption of Key Food Groups and Nutrients among US Children and Adults: Results of an NHANES Modeling Study. *Nutrients*, *9*(9), 1010. https://doi.org/10.3390/nu9091010.

Ruiz-Armenta X. A., Zazueta-Morales, J. de J., Aguilar-Palazuelos, E. et al. (2018). Effect of extrusion on the carotenoid content, physical and sensory properties of snacks added with bagasse of naranjita fruit: optimization process. *CyTA - Journal of Food* 16(1), 172-180.

Sahu, C., Patel, S. and Khokhar, D. (2018). Studies on storability of maize-millet based soy fortified extruded snacks. *International Journal of Agricultural Engineering* 11(Sp. Issue): 46-52, DOI: 10.15740/HAS/IJAE/11.Sp. Issue/46-52.

Sali, A. (2024). Extruded snacks with byproducts of coconut. A Master in Vocation Dissertation in the Department of Traditional Foods and Applied Nutrition, St. TERESA'S COLLEGE (Autonomous), ERNAKULAM Mahatma Gandhi University, Kottayam, Kerala.

Samarajeewa, U. (2024). Coconut: Nutritional and Industrial Significance. IntechOpen. doi: 10.5772/intechopen.1004173.

Serge, E. O., Gu, B. J., Kim, Y. S., & Ryu, G. H. (2011) Effects of feed moisture and barrel temperature on physical and pasting properties of cassava starch extrudate. *Korean Journal of Food Preservation* 18(3), 271–278.

Singha, P., Muthukumarappan, K., & Krishnan, P. (2017). Influence of processing conditions on apparent viscosity and system parameters during extrusion of distiller's dried grains-based snacks. *Food Science and Nutrition,* 6: 101–110.

Sujirtha, N. and Mahendran, T. (2015). Use of Defatted Coconut Flour as a Source of Protein and Dietary Fibre in Wheat Biscuits. *International Journal of Innovative Research in Science, Engineering and Technology,* 4,8: 7344-7352.

Sundaresan, T., Subramaniam, S., Chinnapa, V. and Rajoo, B. (2023). Effect of defatted coconut flour on functional, nutritional, textural and sensory attributes of rice noodles. *International Journal of Food Science & Technology,* 58, 10: 5077-5088**.** https://doi.org/10.1111/ijfs.16606.

Thachil, M. T., Chouksey, M. K., & Gudipati, V. (2014). Amylose-lipid complex formation during extrusion cooking: effect of added lipid type and amylose level on corn-based puffed snacks. *International Journal of Food Science and Technology*, Volume 49, Issue 2, February 2014, Pages 309–316, https://doi.org/10.1111/ijfs.12333.

Tiwari, U., Mary, G., Jaganmohan, R., Alagusundaram, K., & Towari, B.K. (2011). Quality characteristic and shelf-life studies of deep-fried snack prepared from rice brokens and legumes by-product. *Food and Bioprocess Technology*, 4(7), 1172-1178.

Ugwuanyi, R. G., Eze, J. I., & Okoye, E. C. (2020). Effect of soybean, sorghum and african breadfruit flours on the proximate composition and sensory properties of chin-chin. European Journal of Nutrition and Food Safety, 12(1): 85-98.

Ugwuanyi, R. G., Eze, J.I., & Okoye, E.C. (2020). Effect of soybean, sorghum and African breadfruit flours on the proximate composition and sensory properties of chin-

chin. *European Journal of Nutrition and Food Safety,* **12**(1), 85-98.

Vadassery, K., Pratheesh, G. P., Gayathri, M., Binitha, N.K., Jasna, V.K., Seenath, P.K., Shamna, N., Arya, S., & Sujatha, R. (2023). Optimization of Extruded Snack Enriched with Coconut Inflorescence Sap Honey: A Promising Supplementary Food among Tribals. *Asian Journal of Dairy and Food Research* 42(4): 495-503. doi: 10.18805/ajdfr.DR-2067.

Author Contributions:

Conceptualization, TMI; methodology, CCU; software, TMI; validation, HOA; formal analysis, CCU; investigation, CCU; resources, CCU; TMI; writing—original draft preparation, CCU; writing—review and editing, MCE; visualization, HOA; supervision, TMI; project administration, CCU. All the authors pull resources together for the research. All authors have read and agreed to the published version of the manuscript."

Funding:

"This research received no external funding".

Data Availability Statement:

The data for this research can be made available on request.

Acknowledgments:

The authors acknowledge the department of Food Science and Technology, Nnamdi Azikiwe University, Awka for providing the facilities for the research and the university administration for in-kind support.

Conflicts of Interest:

The authors declare no conflict of interest.

CARPATHIAN JOURNAL OF FOOD SCIENCE AND TECHNOLOGY

journal homepage: **http://chimie-biologie.ubm.ro/carpathian_journal/index.html**

Research article

EVALUATION OF WINE PARAMETERS DURING THE MATURATION PROCESS IN DIFFERENT TYPES OF WOOD

Dafina Llugaxhiu Krasniqi[1], Besarta Peci[1], Alush Musaj[1], Bahtir Hyseni[1]✉

[1]Food Engineering and Technology, Faculty of Food Technology, University "Isa Boletini" in Mitrovica, Kosovo

✉bahtir.hyseni@umib.net

https://orcid.org/0000-0002-0470-9274

https://doi.org/10.34302/2025.17.3.15

Article history:
Received
July 26th , 2025
Accepted
November 19th 2025

Keywords
Wine maturation
Wood influence
Microbiological content
Chemical and physical parameters
HPLC

Abstract

This study investigates the influence of various oak types on the microbiological, chemical, and physical properties of wines during maturation. Eight samples were analysed, including Cabernet Sauvignon matured in American, French, Hungarian, and Balkan oak barrels, as well as a young Cabernet Sauvignon, a Vranç matured in Balkan oak, and grape juice. Parameters assessed included microbiological content, sugar levels, alcohol content, glycerol content, pH, acidity, turbidity, and sulfur dioxide (SO_2) levels. Results showed that samples matured in Hungarian oak exhibited higher stability compared to other wood types, while significant discrepancies were observed between declared and measured alcohol levels. Microbiological analyses revealed the presence of *Acetobacter,* yeasts, and molds in several samples, except for the young wine and Vranç, which were microorganism-free. Additionally, turbidity values exceeded acceptable standards across all samples. These findings highlight the influence of wood type and maturation conditions on wine quality, suggesting strategies for optimizing aging processes to ensure product stability and optimal sensory attributes.

1. Introduction

Wine is an alcoholic beverage produced by the fermentation of fresh grapes or grape must (Kelebek et al., 2009). Different grape varieties possess unique vinification characteristics and distinct styles. Additionally, the style of wine is influenced by the geographical environment (Wang et al., 2022). Today, the winemaking industry and global wine consumption represent significant socio-economic markets, with production ranging from 250 to 300 million hectoliters per year over the past two decades (Martin et al., 2020). Wine is primarily composed of 86% water, 12% ethanol, and 1% glycerol and sugars, with 0.4% organic acids. Key components include polyphenols, anthocyanins, tannins, minerals, volatile compounds, and vitamins. Organic acids like tartaric and malic acids come from grapes, while acetic and succinic acids are fermentation byproducts. Sulfites, produced during fermentation, should not exceed 350 mg/L.

Nitrogen compounds, absorbed from nitrate, ammonia, or urea during cultivation, are converted into amino acids such as proline and arginine. These amino acids can form higher alcohols that affect the wine's aroma. Terpenes, although present in small amounts, significantly influence the sensory properties of wine. Polyphenols, especially flavonoids, contribute to wine's color, taste, and bitterness, with tannins affecting bitterness levels. Essential vitamins in wine include vitamins B and C, as well as folic acid. The overall composition and quality of wine depend on the grape variety, production techniques, and interactions between ingredients (Markoski et al., 2016; Evers et al., 2021; Nemzer et al., 2022).

Maturation is a historical practice that has been used for thousands of years by many civilizations. Two fundamental parameters in the maturation process are the quality of the wood barrel and the duration of maturation. Wooden barrels, which are used for 6 to 18 months, incur significant economic costs. The maturation process varies with the type of wine. Red wine aging has two phases: the wood (oxidation) phase and the bottle (reduction) phase. During maturation, wine undergoes numerous physical and chemical changes. Compounds such as phenolic, lactones, aldehydes, and furfuryl compounds are transferred from the wood to the wine. The type and quantity of these substances depend on maturation time, wood type, wood origin, and wood usage. Other changes include the evaporation of volatile components and exposure to natural oxygen, resulting in condensation reactions and the polymerization of flavonoid compounds. These reactions affect the phenolic composition, color, and bitterness of the wine. Compounds may remain in the wood or lees, causing continuous changes during maturation (Alamo-Sanza and Nevares, 2018; Carpena et al., 2020; Pfahl et al., 2021; Jordão and Cosme, 2022).

Given the high consumption of wine today and the significant impact aging has on its characteristics, this study aims to investigate wine parameters, including microbiological and chemical content, and compare these parameters and stability during the maturation process in different types of oak wood. The research aims to investigate the impact of oak wood on wine quality, with a particular emphasis on the crucial role of the type of oak used in the maturation process.

2. Materials and methods

2.1. Materials

2.1.1. Wine samples

This research was conducted in the Faculty of Food Technology laboratory at the University "Isa Boletini" in Mitrovica. For the study, samples were collected from various wineries in the Rahovec region, Kosovo, which we will not disclose by name for confidentiality reasons. Codification and characteristics of the wine samples are detailed in Table 1.

Table 1. Codification and wine characteristics

Samples	Grape variety	Wooden oak	Time of maturation	Alcohol percentage labelling
S1	Cabernet Sauvignon	"American oak"	8 months	14.1%
S2	Cabernet Sauvignon	"French oak"	8 months	14.1%
S3	Pinot Noire	"Balkan oak"	16 months	ND#
S4	Cabernet Sauvignon	"Hungarian oak"	8 months	14.1%

S5	Cabernet Sauvignon	"Hungarian oak"	16 months	16%
S6	Cabernet Sauvignon	"Young wine "	NA*	16%
S7	Vranç	"Balkan Oak"	14 months	ND#
S8	Grape Juice	NA*	NA*	NF^

* NA- Not aged, NF^ - Not Fermented, ND# - Not Declared

2.1.2. Chemicals and reagents

Plate Count Agar (PCA) (#COT090219502) was purchased from Liofilchem. Glucose yeast extract $CaCO_3$ medium (GYC) (#40545) was purchased from Sigma-Aldrich. Yeast Glucose-Chloramphenicol agar (YGC agar) (#620070) was purchased from Liofilchem (Conda, Spain). MRS agar (#69964) was purchased from Sigma-Aldrich. Sodium hydroxide (NaOH) (#3034) was purchased from Lachner, Czech Republic, and other chemicals were of analytical reagent grade.

2.2. Methods

2.2.1. Microbiological analysis

For microbiological analysis, the wine samples were processed immediately after collection. The total counts of bacteria (TBC), number of *Acetobacter* cells (A), *Lactobacillus* cells (L), and yeast and molds (Y/M) were assessed using an optical microscope (N-400M microscope with an achromatic objective, 100X for bacteria and 40X for molds, respectively). The plate dilution method was applied for the quantitative determination of CFU (Colony Forming Units) counts for respective groups of microorganisms in 1 mL of wine. Petri dishes of gelatinous nutritive substrate were inoculated with 1 mL of wine samples (TBC, A, L, and Y/M) in duplicate. For the identification of TCB, PCA was used, and the samples were incubated aerobically at 30°C for 72 hours. *Acetobacter* cells were cultivated on GYC medium and incubated at 30°C aerobically for 48 hours. *Lactobacillus* species were grown on MRS agar and incubated at 37°C for 72 hours in anaerobic conditions. Finally, yeast and molds were cultivated on YGC agar and incubated at 25°C for 5 days. After incubation, the results were collected and expressed in CFU/mL (Kántor *et al.,* 2014).

2.2.2. Sample preparation for chemical characterization

All wine samples were filtered and decanted into laboratory bottles for the analysis of sugar levels, alcohol content, glycerol content, pH, acidity, turbidity, free SO2, total SO2, and stability.

2.2.3. Chromatographic analysis of sugars, glycerol, and alcohol

The sugar content in wine samples was measured using HPLC (LC Shimadzu, Model: RID-20A, Duisburg, Germany) with a Shim-Pack SPR-Ca, 250 x 7.8 mm column, and a refractive index detector at a working flow rate of 0.65 mL/min and 80°C, using distilled water as the mobile phase. The samples were filtered through a 0.45 µm PTFE membrane filter. Each sample was injected twice with a 20 µL injection volume, and the peak was detected. Different concentrations (8, 4, 2, 1, 0.5, 0.25 g/L) of sucrose, glucose, fructose, and glycerol, respectively, were used for standard curve construction, where different concentrations (18, 9, 4.5, 2.25, 1.125, 0.562 g/L) of alcohol were used for standard curve construction. The remaining concentrations of sucrose, glucose, fructose, and glycerol in the samples were determined by comparing their peak areas with those of standard curves. The retention times for sucrose, glucose, fructose, and glycerol were 7.66, 9.17, 11.12, and 13.28 minutes, respectively. For ethanol, the retention time was 13.7 minutes (Figure 1).

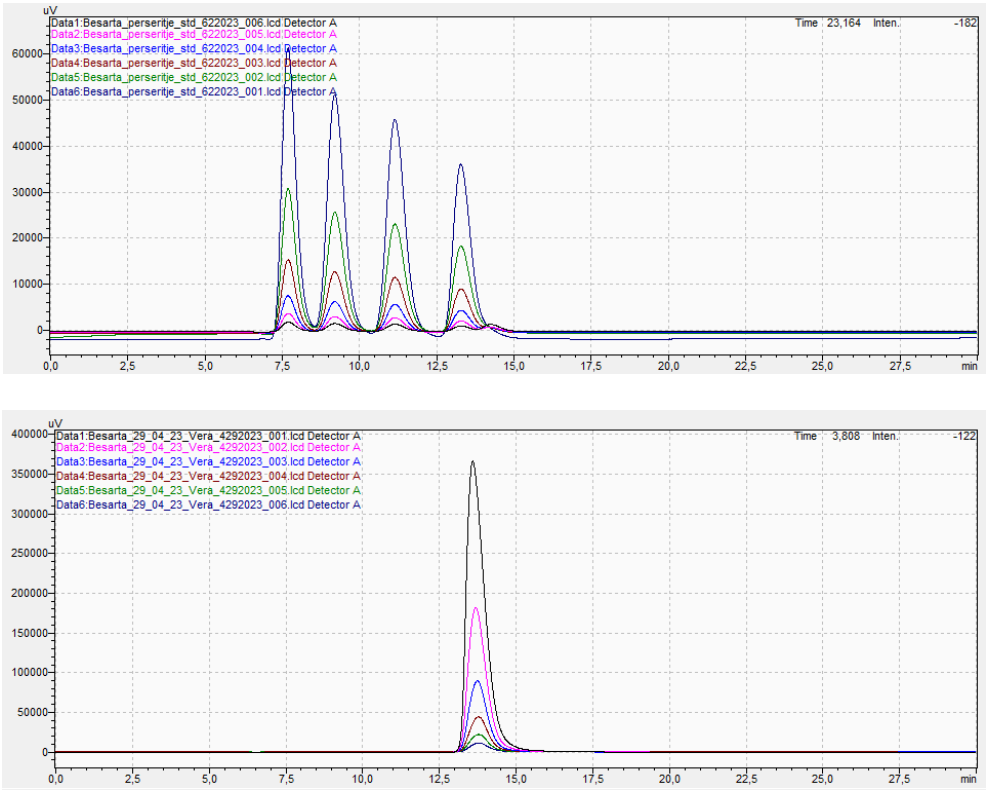

Figure 1. HPLC chromatograms of standards. a) Sucrose, glucose, fructose, and glycerol; b) Ethanol

2.2.4. Measurement of turbidity

Turbidity in wine, measured using a turbidity meter (#ORIONAQ4500, Singapore), is quantified in Nephelometric turbidity units (NTU). This measurement indicates the clarity of the wine, with higher NTU values corresponding to greater turbidity (cloudiness) due to suspended particles.

2.2.5. Measurement of wine protein stability

The stability of the wine was assessed through a series of tests designed to evaluate its resistance to common instabilities based on (Protein Stability in Wine, Virginia Tech, Enology and Fermentation Science protocol). First, a 55% trichloroacetic acid (TCA) solution was prepared. Following this preparation, 8 test tubes were each filled with 10 mL of wine, and 1 mL of the 55% TCA solution was added to each test tube. These test tubes were then mixed in an evaporator. For comparison, another set of 8 test tubes was prepared by adding 10 mL of wine and 1 mL of distilled water to each, and these were also mixed in the evaporator. Both sets of test tubes were placed in a water bath maintained at 80°C for 2 minutes. After 2 minutes, the test tubes were removed from the water bath, and turbidity measurements were conducted on each sample.

2.2.6. pH measurement

The pH was determined using a pH meter (HI2002-01 HANNA Instruments pH meter, USA/Romania) based on the Vinmetrica protocol for wine pH measurement. Firstly, the pH meter was calibrated using a set of pH buffer solutions to ensure accuracy. After calibration, the pH probe was inserted into the wine samples and slowly stirred until the reading on the meter stabilized.

2.2.7. Measuring TA (titratable acidity)

Titratable acidity is determined by titrating a sample with the TA Titrant, which has a standard known concentration (0.133 N) of NaOH according to the Vinmetrica protocol for wine acidity measurement. We add the TA Titrant slowly with stirring until the pH meter reaches the target pH of 7. From the volume of titrant used, the TA value was calculated following the formula:

TA (g/tartaric acid/L) =(V*0.133*75)/S (1)

where V = mL of Titrant needed to reach the endpoint; 0.133 = normality of the Titrant, S = mL sample. The value 75 is the equivalent weight of tartaric acid.

2.2.8. Measurement of total SO_2

Total SO_2 was determined using the Ripper method (Thermo Scientific notes, No. T5 method) and as described in the article by Guerra, M, and Cantos-Villar, E. (2015). Twenty milliliters of wine were transferred into a 250-milliliter Erlenmeyer flask, and 10 milliliters of 1.0 N NaOH were added. After a 10-minute reaction period at a high pH, 5 mL of 1% starch solution and 10 mL of 25% sulfuric acid were added. The sample was then titrated with a 0.01 N iodine solution until a purple color (VI) appeared. The volume of iodine solution spent was recorded. This procedure was repeated for all samples to determine the total SO_2 content. The total SO_2 content was calculated by using the following formula:

$$SO_2 \text{ (mg/L)} = VI \times NI \times 1280 \quad (2)$$

where, VI = Volume of iodine titrant used at the endpoint of the titration (mL), NI = Normality of the iodine titrant (certified or standardized value), 1280 = (32g SO_2/equivalent × 1000 mg/g)/25 mL wine.

2.2.9. Measurement of free SO_2

Free SO_2 was determined using the Ripper method (Thermo Scientific Notes No. T5 method, as described in the article by Guerra, M., and Cantos-Villar, E. (2015). Twenty milliliters of wine were transferred into a 250 mL Erlenmeyer flask, and 5 milliliters of a 1% starch solution and 5 milliliters of a 25% sulfuric acid solution were added. The mixture was titrated with 0.01 N iodine solution until a purple color appeared (VI). The same formula used for determining total SO_2 was applied to calculate the concentration of free SO_2

2.3. Statistical analysis

Most parameters were measured in duplicate, with each value representing the mean of two readings. Statistical analysis was performed to evaluate the relationships between key variables using the Pearson correlation coefficient. This coefficient measures the strength and direction of the linear association between two variables, with values ranging from -1 to +1.

3. Results and discussions

3.1. Microbiological analysis of wine samples

The microbiological performance of wine samples shown in Table 2 reveals that all wine samples were free of total mesophilic bacteria. *Acetobacter* was detected in samples S1, S2, S3, and S4. However, no *Acetobacter* were found in samples S5, S6, S7, and S8. To no surprise, yeasts were detected in several samples, as shown in Table 2. However, no yeasts were found in samples S6, S7, and S8. Molds were detected in samples S2, S4, and S8. We characterized the molds found in samples S2, S4, and S8 under the microscope, identifying them as *Penicillium*, *Penicillium spp*., *Trichoderma*, and *Penicillium cyclopium* (Figure 2). In contrast, no molds were found in samples S1, S3, S5, S6, and S7.

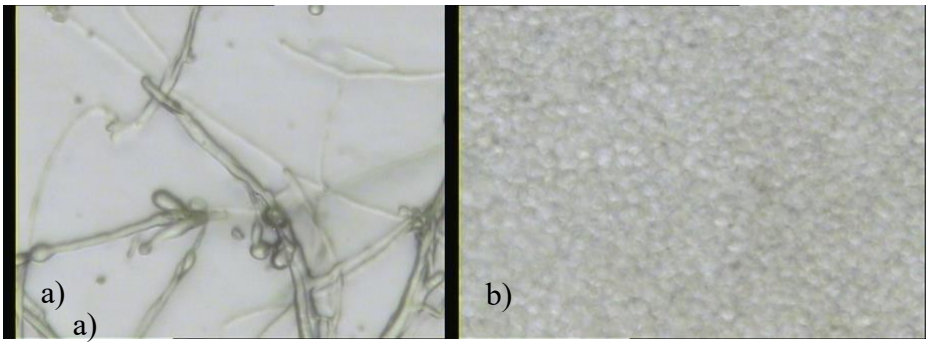

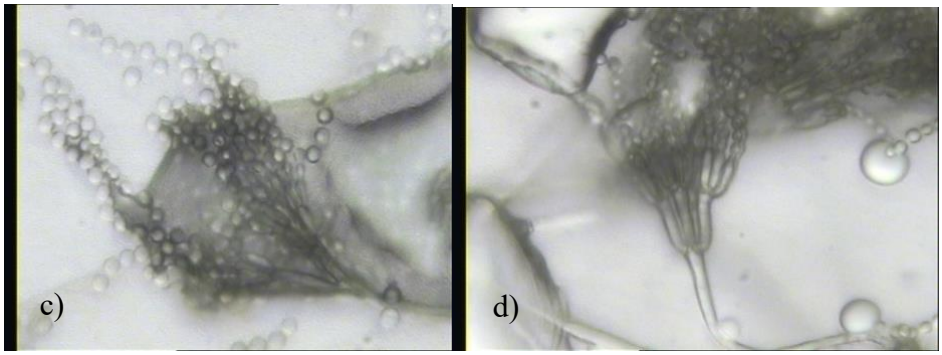

Figure 2. Microscopic examination of Molds in wine samples. a) *Trichoderma*; b) *Penicillium*; c) *Penicillium spp*; d) *Penicillium cyclopium*

All wine samples free of total mesophilic bacteria can be attributed to the acidic nature of wine, with a pH ranging from 3.1 to 3.9, which inhibits the growth of most human pathogenic microorganisms. The combination of high acidity and alcohol content in wine creates a strong antimicrobial environment.

According to literature, a wine composition containing 0.6% tartaric acid, 15% ethanol, and a pH of 3.0 exerts a potent bactericidal effect (Azevedo et al., 2016). The physical and chemical analyses further support these findings, indicating that the majority of wine samples had a pH range of 3.1 to 3.4.

Additionally, the titratable acidity, expressed as tartaric acid, averaged between 0.5% and 0.7% (5-7 g/L tartaric acid). These parameters align with those reported in scientific literature, which likely accounts for the absence of bacteria and Lactobacillus in the wine samples. These bacteria are ubiquitous, adapting well to environments with high levels of sugars and alcohol. Being aerobic and mesophilic, *Acetobacter* can spoil wine, necessitating careful monitoring by winemakers during both production and storage. They are capable of converting ethanol into acetaldehyde and acetic acid, which can lead to wine spoilage (Zgardan et al., 2022). The presence of *Acetobacter* in samples S1, S2, S3, and S4 could be due to exposure to inappropriate temperatures and oxygen during production. High sugar levels after fermentation, combined with the presence of oxygen, may also promote the growth of these bacteria. During fermentation, high concentrations of SO_2 are typically added, which, along with other factors, increases stress on the yeast. This stress arises from anaerobic conditions, reduced levels of nitrogen, lipids, and vitamins, increased acidity, ethanol concentration, and temperature. Despite these challenges, some yeasts can survive the stresses of the fermentation process (Romano et al., 2022). Perpetuini et al. (2021) show that specific yeasts found in wine environments are resistant to potassium metabisulfite and even to cleaning agents used in wine cellars. Based on this, the yeasts present in samples S1, S2, S3, S4, and S5 may be those that have successfully withstood the rigorous conditions of the wine production process.

Molds are ubiquitous and can be found on various surfaces, including the air, the surfaces of grapes, and the wood used for maturation. Common mold genera include *Aspergillus*, *Botrytis*, *Penicillium*, and, to a lesser extent, *Phytophthora*, *Alternaria*, and *Cladosporium*. The presence of mold has a significant impact on the physical, chemical, and sensory properties of wine. Uncontrolled mold proliferation on grapes before harvest can lead to secondary contamination by bacteria and yeasts, potentially causing a condition known as rot. Moreover, mold on grapes can facilitate the spread of infections.

Beyond aesthetic concerns, molds can produce potent sensory metabolites, which play a crucial role in determining wine quality. *Penicillium* is a diverse genus with over 200 known species, many of which grow at low temperatures, below 5°C, earning them the

moniker "cold-weather mold." The primary concern with the presence of molds in grapes or wine is the potential production of mycotoxins. Fugelsang and Edwards (2015) show that Penicillium spp. can produce one or more mycotoxins in grape must. *Trichoderma* spp. are known to cause green mold disease, which can lead to reduced yield without fortification and cause malformation of fruiting bodies. Such malformations negatively impact all parameters of product quality (Zorić et al., 2023). Each isolate of *Penicillium* cyclopium is known to produce a strong musty odor. This species thrives at low temperatures and is likely responsible for food spoilage, even in refrigerators (Mislivec, 1981).

Given the above, the presence of molds in samples S2, S4, and S8 may be attributed to their initial presence on the grapes, which then spread to the surfaces where the wine was produced. Additionally, the conditions in the production environment may have been conducive to mold growth. The molds identified in these samples could negatively impact the quality of the wine and pose potential health risks.

Table 2. Microbiological analysis of wine samples

Sample	*Total bacterial count* CFU/mL	*Lactobacillus* CFU/mL	*Acetobacter* CFU/mL	*Yeasts* CFU/mL	*Molds* CFU/mL
S1	0	0	$4x10^2$	$7x10^2$	0
S2	0	0	$3x10^2$	$2x10^2$	$1x10^2$
S3	0	0	$6x10^2$	$7x10^2$	0
S4	0	0	$10x10^2$	$17x10^2$	$2x10^2$
S5	0	0	0	$2x10^2$	0
S6	0	0	0	0	0
S7	0	0	0	0	0
S8	0	0	0	0	$1x10^2$

3.2. Sugars, glycerol, and alcohol analysis of wine samples

The sugar content measurements are presented in Table 3. According to Law No. 02/L-8 on wines, which classifies wines based on their sugar content, the categories are as follows: a) dry wine: containing no more than 4 g/L of unfermented reducing sugar, and b) semi-dry wine: containing more than 4 g/L but not exceeding 12 g/L of unfermented reducing sugar (Republic of Kosovo. Law No. 02/L-8 on wines). Based on this classification and the sample results, S1, S3, and S7 are categorized as dry wines, while samples S2, S4, S5, and S6 are classified as semi-dry wines. Sample S8, with 103.43 g/L of reducing sugar, is identified as grape juice. Sucrose levels were also measured in the laboratory, showing that all samples, except for S8, have similar sucrose levels. This means they applied the chaptalization process, which involves adding sugar to grape must before fermentation to increase the wine's alcohol content. This practice is often used when the climate is too poor for the grapes to develop sufficient sugar content naturally (Martin, 1990). Figure 3 represents an HPLC chromatogram showing the peaks of sucrose, glucose, fructose, glycerol, and ethanol in wine samples.

Table 3. Measurement of sugars, glycerol, and alcohol in wine samples

Sample	Sucrose (g/L)	Glucose (g/L)	Fructose (g/L)	Glycerol (g/L)	Alcohol (%)
S1	5.75	0	1.51	10.31	13.70
S2	5.79	5.68	1.58	16.35	11.78
S3	4.02	0	1.87	25.91	11.15
S4	5.30	4.05	1.56	15.72	11.86
S5	3.28	3.79	1.37	14.43	13.89
S6	5.08	0	5.00	8.65	13.59
S7	6.94	2.61	1.34	11.14	12.90
S8	0	49.71	53.72	0	0

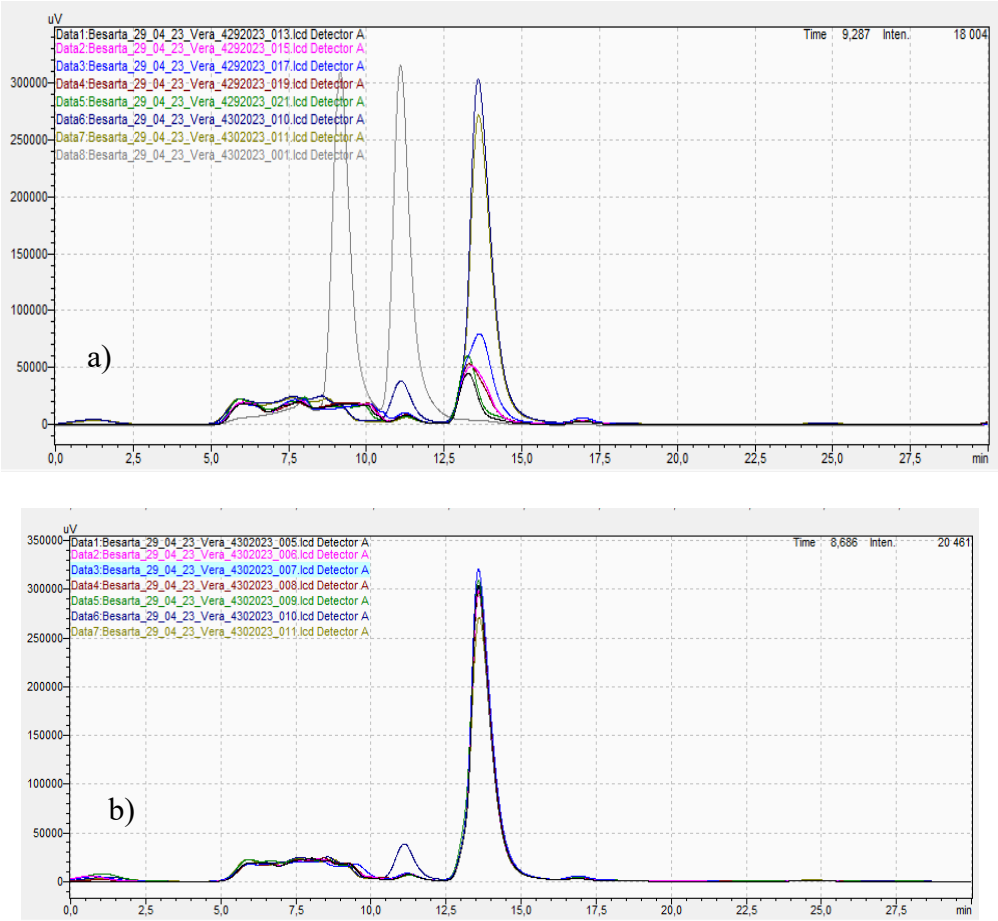

Figure 3. HPLC chromatograms of sugars and ethanol in wine samples. a) HPLC chromatogram of sucrose, glucose, fructose, and glycerol; b) HPLC chromatogram of ethanol.

Glycerol is a sugar alcohol that is the most significant quantitative product in wine after ethanol and carbon dioxide, typically found in concentrations ranging from 1 to 15 g/L. Table

3 shows the results of the alcohol and glycerol content in all samples. Sample S8 does not contain glycerol. The alcohol content ranged from 11% to 13%. Based on the information provided and the results shown in Table 3, it is evident that only sample M6 has a normal glycerol level. In contrast, samples S1, S2, S3, S4, S5, and S7 exhibit higher-than-normal glycerol levels, while sample S8 contains no glycerol. The two key roles of glycerol production in yeast are maintaining redox balance and aiding in the response to hyperosmotic stress. Glycerol production in wine is influenced by several factors, including higher temperatures (20–25°C) that increase glycerol content, especially in red wines compared to white wines. On the other hand, limited oxygen promotes glycerol production, though results vary by yeast strain. Some non-*Saccharomyces* yeasts produce more glycerol under low oxygen conditions. High sugar levels in grape juice, especially from late harvests, lead to increased glycerol as yeast cells accumulate it to balance osmotic pressure. Limited nitrogen in the must increases glycerol production, as does higher sulfur dioxide content. Non-Saccharomyces yeasts, such as *Metschnikowia pulcherrima* and *Lachancea thermotolerans*, often produce more glycerol than *Saccharomyces cerevisiae* and can reduce the ethanol content. These factors can be managed to enhance glycerol production, which affects the wine's texture and sweetness (Scanes et al., 1998). Sample S8 does not contain alcohol, as it is grape juice and has not undergone fermentation. According to Administrative Instruction No. 15/2009 of the Republic of Kosovo, which sets the parameters for the physical-chemical analysis of wine, the minimum natural alcohol content for quality wines with a designated geographical origin is 10.5 vol.% (Administrative Instruction No. 15/2009 of the Republic of Kosovo). Based on this instruction and the sample results, none of the wines have an alcohol content below the required minimum. This confirms that the analyzed wines have the desired strength, ranking them among high-quality wines. It is important to note that most wine samples had their alcohol content declared on the label, as shown in Table 3. However, none of the declared alcohol levels matched the laboratory-measured results. In all cases, the measured alcohol levels were lower than those stated on the labels. A positive Pearson correlation coefficient of 0.55 was observed between glycerol and ethanol, indicating a moderate association between these two variables. A strong positive correlation was observed between sucrose and ethanol, with a coefficient of 0.82, indicating a significant and robust relationship between these two variables.

3.3. Turbidity analysis of wine samples

Turbidity is a crucial parameter in wine production, influencing both the final composition and the aroma of the wine. It measures the total suspended particles in the liquid, which in this case, reflects the clarity and potential quality of the wine. According to the Australian Wine Research Institute, the maximum acceptable turbidity in red wine after filtration is 10 NTU (Duarte et al., 2015). Based on these standards and the results presented in Table 4, it is evident that none of the wine samples exhibit turbidity values within the normal range.

Table 4. Measurement of turbidity in wine samples.

Sample	Turbidity (NTU)
S1	25.2
S2	127
S3	19.5
S4	120
S5	104
S6	33.4
S7	33.0

Table 5. Measurement of wine protein stability in samples

Sample	Samples with TCA (NTU) ±SD	Blank Sample (NTU)±SD
S1	1.85 ±0.056	2.38 ±0.098
S2	9.97± 0.106	10.49± 0.579
S3	2.05 ±0.162	1.53 ±0.388
S4	4.79 ±0.077	9.35 ±0.169
S5	0.91 ±0.042	0.67±0.077
S6	2.83±0.862	1.3 ±0.367
S7	1.66 ±0.325	1.39 ±0.070
S8	2.17±0.021	3.46 ±0.056

3.4. Protein stability analysis of wine samples

The results of protein stability in wine are shown in Table 5. Wine, like many other products, contains proteins primarily derived from grapes. However, proteins can also originate from yeast. Yeast influences the protein composition of wine in two ways: a) by transferring proteins during the yeast autolysis process, and b) by hydrolyzing must proteins through the extracellular protease present in the yeast (Tian and Harrison, 2012). The proteins present in wine are responsible for colloidal instability, leading to the formation of amorphous sediments and haze. Protein haze can develop at high temperatures during storage or transport due to protein self-aggregation. Several factors, including storage or aging temperature, pH, wine protein composition, organic acids, ethanol, phenolic compounds, and sulphate content, influence the formation of this haze. Protein instability can also occur through the mixing (stirring) of otherwise stable wines. While the formation of haze or deposits in wine bottles does not pose a health risk to consumers and does not affect the wine's aroma or taste, it significantly impacts the wine's commercial appeal. This is particularly true for white wines, where visual clarity is crucial for consumer acceptance (Cosme et al., 2020). When the turbidity values are higher for the TCA-treated samples than for the Blank samples, it indicates a potential for instability due to the presence of proteins. Samples S3 and S6 exhibit potential instability. These samples may be unstable due to the factors mentioned above. Other studies suggest that protein instability is not strongly linked to the total protein content in wine. Instead, the molecular characteristics of individual proteins determine their propensity to precipitate. However, the exact proteins responsible for wine turbidity remain uncertain, with contradictory findings in the literature regarding which proteins cause haze and sediment formation. Some researchers have identified a fraction or specific group of proteins that contribute to this instability (Mesquita et al., 2001).

3.5. Chemical analysis of wine samples

The results of the total SO_2 analysis reveal a variation in SO_2 content among the samples, with S1 exhibiting the highest SO_2 concentration and S8 showing the lowest (Table 6). According to Administrative Instruction No. 15/2009 of the Republic of Kosovo, which outlines the wine parameters for physical-chemical analyses, the total SO_2 content should not exceed 160 mg/L (Administrative Instruction No. 15/2009 of the Republic of Kosovo). Based on this standard and the results presented in Table 6, it is evident that all the wine samples have permissible levels of total SO_2, staying well within the established limit.

Regarding the free SO_2 content, sample S4 has the highest concentration at 24.8 mg/L, while samples S3 and S8 have the lowest at 5.6 mg/L (Table 6). According to the same Administrative Instruction No. 15/2009, the maximum allowable free SO_2 content is 30 mg/L (Administrative Instruction No. 15/2009

of the Republic of Kosovo). Based on this standard and the results, we conclude that all the analyzed samples have free SO_2 levels within the permissible range.

A strong positive correlation was also identified between total SO_2 and free SO_2, with a Pearson coefficient of 0.89, implying that as one variable increases, the other tends to increase proportionally.

The results of the pH measurements on the wine samples indicated that there are no significant differences in pH values among the analyzed wine samples (Table 6). As previously mentioned, the typical pH range for wine is between 3.1 and 3.9 (Azevedo et al., 2016). Based on the results, we can confirm that all the wine samples fall within the normal pH range.

Table 6. Chemical analysis of wine samples

Sample	Free SO_2, mg/L ±SD	Total SO_2, mg/L ±SD	pH ±SD	Acidity g/L ±SD
S1	17.6 ± 2.26	52 ± 1.13	3.4 ± 0.098	7.63 ± 2.44
S2	19.2 ± 6.78	40.8 ± 10.18	3.335 ± 0.049	7.2 ± 1.83
S3	5.6 ± 1.13	11.2 ± 0	3.73 ± 0.028	5.6 ± 0.14
S4	24.8 ± 7.9	41.6 ± 4.52	3.575± 0.063	5.6 ± 0
S5	8.8 ± 3.39	12.8 ± 2.26	3.375 ± 0.021	5.85 ± 0.07
S6	11.2 ± 6.78	15.2 ± 5.65	3.345 ± 0.134	5.9 ± 0.14
S7	7.2 ± 3.39	12.8 ± 9.05	3.29 ± 0.070	5.85 ± 0.07
S8	5.6 ± 3.39	7.2 ± 1.13	3.375 ± 0.007	5.15 ± 0.07

The acidity of the wine samples, expressed as tartaric acid, is presented in Table 6. Samples S1 and S2 have higher acidity values, which correlate with lower pH levels, while minor differences in acidity are reported for the remaining samples. According to Law No. 04/-L for wines, the total acidity content expressed as tartaric acid should not be less than 3.5 g/L (Republic of Kosovo, Law No. 02/L-8 on wines). Rajkovic and Sredovic (2009) indicated that the titratable acidity of red wine, expressed in tartaric acid, typically ranges from 4.0 to 8.0 g/L.

A weak negative correlation was found between pH and acidity, with a Pearson coefficient of -0.287, indicating an inverse relationship between these two variables.

4. Conclusions

In conclusion, the microbiological and chemical analyses of the wine samples provide significant insights into the factors that influence wine quality and stability. The absence of total mesophilic bacteria, Lactobacillus, and the presence of *Acetobacter* in specific samples underscore the importance of controlling oxygen exposure and temperature during production to prevent spoilage. The identification of yeasts and molds in some samples highlights the resilience of microorganisms under challenging fermentation conditions, as well as the potential for mold contamination during grape harvesting and wine processing. Chemical analyses, including measurements of pH, acidity, alcohol, glycerol, sugars, and turbidity, indicate that the wine samples largely meet acceptable regulatory standards, thereby ensuring their overall quality. However, discrepancies between the declared and measured alcohol levels, along with the presence of protein instability in some samples, suggest areas where further optimization is needed. Ultimately, this study underscores the importance of rigorous monitoring and control during wine production to ensure its microbiological safety and sensory properties while maintaining adherence to quality standards.

The statistical findings highlight both significant positive and negative associations among the studied parameters, providing insights into their interdependencies.

5. References

Administrative Instruction No. 15/2009 of the Republic of Kosovo. https://auvk.rksgov.net/auvk/repository/docs/A_2009_15_al.pdf,(accesed July, 2023)

Australian Wine Research Institute. https://www.awri.com.au/industry_support/winemaking_resources/storage-and-packaging /pre-packaging-preparation/pre-bottling-wine-adjustments-and-specifications/ (accessed August, 2023) (accessed August, 2023)

Alamo-Sanza, M., Nevares, I. (2018). Oak wine barrel as an active vessel: A critical review of past and current knowledge. Critical Reviews in Food Science and Nutrition, 58(16), 2711–2726.

Azevedo, S., Battaglene, T., Hodson, G. (2016). Microbiologically, wine is a low food safety risk consumer product. *BIO Web of Conferences*, 04003(7),1-6.

Carpena, M., Pereira, A.G., Prieto, M.A., Simal-Gandara, J. (2020). Wine aging technology: Fundamental role of wood barrel. *Foods*, 9(9),1–25.

Cosme, F., Fernandes, C., Ribeiro, T., Filipe-Ribeiro, L., Nunes, F.M. (2020). White wine protein instability: Mechanism, quality control and technological alternatives for wine stabilisation—an overview. *Beverages*, 6(1),1–28.

Duarte, D.P., Oliveira, N., Georgieva, P., Nogueira, R., Bilro, L.(2015). Wine classification and turbidity measurement by clustering and regression models. *Conference of Telecomunicatioin*, 317–320.

Evers, M.S., Roullier-Gall, Ch., Morge, Ch., Sparrow, C., Gobert, A., Alexandre, H. (2021). Vitamins in wine: Which, what for, and how much?. *Comprehensive Reviews in Food Science and Food Safety*, 20(3), 2991–3035.

Fugelsang, K.C., Edwards, Ch.G. (2015). Molds and other microorganisms. in Wine Microbiology. 2nd ed, *SPRINGER*, 52-61.

Free and total SO_2 measurement method https://assets.fishersci.com/TFS-Assets/LPD/Application-Notes/Free%20and%20total%20sulfur%20dioxide%20SO2%20in%20wine%20by%20automatic%20titration.pdf

Jordão, A.M., Cosme, F. (2022). The Application of Wood Species in Enology: Chemical Wood Composition and Effect on Wine Quality. *Applied Sciences*, 12(6),1-23.

Kántor, A., Petrová, J., Kačániová, M. (2014). Chemical and microbiological analysis of red wines during storage at different temperatures. Scientific *Papers Animal Science and Biotechnologies*, 47(2),101–107

Kelebek, H., Selli, S., Canbas, A., Cabaroglu, T. (2009). HPLC determination of organic acids, sugars, phenolic compositions and antioxidant capacity of orange juice and orange wine made from a Turkish cv. Kozan. *Microchemical Journal,* 91(2), 187–192.

Managing pH and TA in wine https://vinmetrica.com/managing-ph-and-ta-in-wine/

Martin, M.E., Grao-Cruces, E., Millan-Linares, M.C, Montserrat-De la Paz, S.(2020). Grape (vitis vinifera l.) seed oil: A functional food from the winemaking industry. *Foods*, 9(10), 1–20.

Martin, G.J. 1990. The chemistry of chaptalization. *Endevour*, 14(3), 137-143

Markoski, M.M., Garavaglia, J., Oliveira, A., Olivaes J, Marcadenti, A. 2016. Molecular properties of red wine compounds and cardiometabolic benefits. *Nutrition and Metabolic Insights*, 9, 51–57.

Mesquita, P.R., Piçarra-Pereira, M.A., Monteiro, S., Loureiro, V.B., Teixeira, A.R., Ferreira, R.B. (2001). Effect of wine composition on protein stability. *American Journal of Enology and Viticulture*, 52(4), 324–330.

Mislivec, Ph.B. (1981). Toxic Species of Penicillium Common in Food. *Journal of Food Protection*, 44(9), 723–726.

Nemzer, B., Kalita, D., Yashin, Y.A., Yashin, Y.I.(2022). Chemical Composition and Polyphenolic Compounds of Red Wines: Their Antioxidant Activities and Effects on Human Health—A Review. *Beverages*, 8(1),1–18.

Pfahl, L., Catarino, S., Fontes, N., Graça, A., Ricardo-Da-silva, J. (2021). Effect of barrel-to-barrel variation on color and phenolic composition of a red wine. *Foods*, 10(7),1-16.

Perpetuini, G., Rossetti, A.P., Battistelli, N., Arfelli, G., Tofalo, R. (2021). Adhesion properties, biofilm forming potential, and susceptibility to disinfectants of contaminant wine yeasts. *Microorganisms*, 9(3), 1–12.

Protein Stability in Wine. Virginia Tech, Enology and Fermentation Science. Retrieved from https://www.enology.fst.vt.edu/downloads/ProteinS.pdf

Rajkovic, M.B., Sredovic, I.D. (2009). The determination of titratable acidity and total tannins in red wine. *Journal of Agricultural Sciences, Belgrade*, 54(3), 223–246.

Romano, P., Braschi, G., Siesto, G., Patrignani, F., Lanciotti, R. (2022). Role of Yeasts on the Sensory Component of Wines. *Foods*, 11, 1–23.

Republic of Kosovo. Law No. 02/L-8 on wines. https://auvk.rksgov.net/legjislacioni/udhezimet-administrative/(accesed, September, 2023)

Scanes, K.T., Hohmann, S., Prior, B.A. (1998). Glycerol Production by the Yeast Saccharomyces cerevisiae and its Relevance to Wine: A review. *South African Journal of Enology and Viticulture*, 19(1),17-24.

Tian, B., Harrison, R. 2012. Pathogenesis-Related Proteins in Wine and White Wine Protein Stabilization. *Intech*, 1-13.

Wang, H., Miao, Y., Xu, X., Ye, P., Wu, H., Wang, B., Shi, X. (2022). Effects of Blending on Phenolic, Colour, Antioxidant and Aroma Components of Cabernet Sauvignon Wine from Xinjiang (China). *Foods*, 11(21):1-17.

Zgardan, D., Mitina, I., Mitin, V., Behta, E., Rubtov, S., Boistean, A, Sturza, R.,. Munteanu. (2022) Acetic Acid Bacteria Detection in Wines by Real-Time PCR. *Scientific Study and Research*, 23(2),179–188.

Zorić, Š.L., Janjušević, L., Djisalov, M., Knežić, T., Vunduk, J., Milenkovic, I., Gadjanski, I. (2023). Molecular Approaches for Detection of Trichoderma Green Mold Disease in Edible Mushroom Production. *Biology (Basel)*. 12(2),1–20.

Acknowledgments

This study was conducted at the Faculty of Food Technology, University ”Isa Boletini” in Mitrovica, Kosovo.

CARPATHIAN JOURNAL OF FOOD SCIENCE AND TECHNOLOGY

journal homepage: **http://chimie-biologie.ubm.ro/carpathian_journal/index.html**

Research article

THE IMPACT OF TYPE OF GRAPE VARIETY ON THE VOLATILE AROMA COMPOUNDS AND SENSORY PROPERTIES OF GRAPE BRANDY IN SOUTH-WEST OF ROMANIA

Felicia Stoica[1], Daniela Doloris Cichi[1]✉, Mira Elena Ionică[1], Mihai Cichi[2]

[1]Horiculture & Food Science Department, Faculty of Horticulture, University of Craiova, Craiova, România

[2]Department of Agricultural and Forestry Technologies, Faculty of Agronomy, University of Craiova, Craiova, România

✉daniela.cichi@edu.ucv.ro

https://orcid.org/0009-0007-8759-6597

https://doi.org/10.34302/2025.17.3.16

Article history:
Received
May 16th , 2025
Accepted
October 19th, 2025

Keywords
Grape distillate;
Neutral/semi-aromatic/aromatic grape varieties;
Aromatic volatile compounds;
Sensory properties.

Abstract

This paper presents the results of a study that examined the impact of grape variety on the aromatic profile and sensory characteristics of distilled beverages produced in the Southwest of Oltenia, Romania, and Podgorica (Montenegro). Six grape varieties were used: neutral (Fetească Regală and Fetească Albă), semi-aromatic (Sauvignon), and aromatic (Tămâioasă Românească, Muscat Ottonel, and Muscat of Alexandria). The pomace brandies were obtained by distilling the grape pomace from the mentioned varieties using a traditional copper still, under identical conditions.

The gas chromatography–mass spectrometry (GC/MS) method was applied to identify 30 aromatic volatile compounds belonging to the groups of alcohols, volatile acids, volatile esters, terpenes, and volatile aldehydes. Sensory evaluation of the distillates was also carried out to determine the typical characteristics of the analyzed brandies.

Alcohol content, fatty acid esters, and terpenic compounds were significantly higher in all brandies obtained from aromatic grape varieties compared to those from neutral or semi-aromatic varieties. A higher average content of 2-phenylethanol was detected in brandy from aromatic variety sample TR (7.19 mg/L in TR) compared to all other brandies.In neutral/semi-aromatic grape brandies, the highest value was found in FR (6.23 mg/L).The linalool content, which contributes significantly to the aroma of roses, anise seeds, grapefruit, lime, and citrus, is significantly higher in brandies from aromatic varieties (0.68 mg/L - TR and 1.15 mg/L - MO) compared to brandies from neutral/semi-aromatic varieties (0.25 mg/L - FR and 0.34 mg/L - S).The research results showed that the grape variety had a significant impact on the aromatic volatile compounds and the sensory properties of the brandy. Sensory analysis supports the chemical determinations, showing that all brandies fall into the category of high-quality spirits.

1.Introduction

The distillates obtained from the fermentation of grape marc exhibit a much more complex chemical composition than the original fruits. Recent advances in analytical techniques and laboratory equipment have enabled a deeper understanding of the biochemical components of natural spirits. Grape marc represents the solid residue resulting from the vinification process, separated from the must, and consists-depending on the grape variety and the vinification technology used-of varying proportions of stems, skins, and seeds (Gheorghiță *et al.,* 2002).

The sensory quality of fresh grape marc distillates is determined exclusively by their volatile aromatic compound composition, which is fundamental to consumer perception.

Volatile aromatic compounds-including alcohols, volatile acids, esters, terpenes, aldehydes, and acetals-serve as key sensory markers and quality indicators in alcoholic beverages (Wei et al., 2018). The varietal aromatic potential of grapes is a major factor influencing the character, quality, and distinctiveness of distillates, especially in those produced from Muscat varieties.

Terpenes compounds represent the primary group of aromatic compounds found in grapes (V. vinifera), wines, and distillates derived from Muscat varieties. The most significant among them are terpineol, linalool, geraniol, nerol and citronellol. These compounds are chiefly responsible for the delicate floral and aromatic notes and constitute the key factors influencing the aroma profile of both aromatic and neutral/semi aromatic varieties (Matijaševic et al., 2019; Cichi et al., 2022).

The alcohol content has a major influence on the quality of the distillate, as it contributes to its body and aromatic complexity. High alcohol values are not beneficial to the quality of distillates (Christoph et al., 2007; Tsakiris et al., 2014). Thus, high alcohol concentrations in distilled beverages are associated with oily, green, cut grass aromas; aromas of grass and herbaceous plants (1-hexanol); and aromas of rose and honey (phenylethyl alcohol), while 1-heptanol is associated with an oily aroma (Soufleros et al., 2004; Matijaševic et al., 2019).

Esters are key compounds that predominantly enhance the pleasant fruity and floral aromas of distilled beverages (Soufleros et al., 2004; Matijaševic et al., 2019). Among them, ethyl esters of medium-chain fatty acids-such as hexanoic, octanoic, decanoic, and dodecanoic acids - are particularly important, as they positively influence the aroma profile by imparting distinct fruity and floral notes (Christoph et al., 2007; Lukic et al., 2011; Tsakiris et al., 2014; Matijaševic et al., 2019). Fatty acids themselves play a crucial role in determining the sensory quality of distilled beverages, acting as precursors for volatile compounds and contributing to aroma development through their association with various aromatic groups, including esters (Christoph et al., 2007; Tsakiris et al., 2014; Matijaševic et al., 2019).

Aldehydes, which form an extensive class of aromatic compounds, are often cited as having a negative impact on the quality of distilled beverages (Lukic et al., 2011). Research shows that total aldehyde levels exceeding 1200 mg/L (especially acetaldehyde) significantly influence the aroma of the distillate and indicate marked oxidation of ethanol during the fermentation process (Soufleros et al., 2004; Plutowska et al., 2010; Lukic et al., 2011).

Acetals, on the other hand, contribute to the aromatic profile of many fruit-based alcoholic beverages, giving them a fine and pleasant taste and bouquet (Cortés et al., 2005; Plutowska et al., 2010).

Distillates obtained from grape marc stand out from other similar products and are highly valued by consumers due to their added value, which lies in the specific production technology closely tied to the history and traditions of a particular country or geographical region (Lukić I. et al., 2011).

In Drăgășani - Vâlcea, there are favorable environmental conditions and a long tradition of vine cultivation and, implicitly, wine and distilled beverage production (Stoica et al., 2019).

Grape marc spirit is a traditional product, obtained mainly from neutral-flavored grape varieties. The use of marc from aromatic varieties to obtain superior natural distillates contributes to enriching the sensory profile of the final product, giving it complex, fruity, and floral aromas. These distillates are distinguished by their finesse, balance, and authenticity, while also reflecting the particularities of the grape variety and the winemaking traditions of the region of origin.

The aim of this study was to analyze the aromatic profile of grape marc distillates obtained from both neutral and aromatic varieties, both autohton and international. In addition, the research aims to clarify the link between the aromatic composition and the sensory qualities of fresh grape marc distillates.

2.Materials and methods

The aim of this study was to determine the chemical composition of distilled beverages obtained from fermented grape pomace from several white grape varieties, including neutral and aromatic types, both native and international, distilled using a traditional still.

2.1. Grape samples.

For this study, six white grape varieties were used, including three neutral or semi-aromatic varieties - Fetească Regală (FR), Fetească Albă (FA), and Sauvignon (S) - and three aromatic varieties - Muscat Ottonel (MO), Muscat of Alexandria (MA), and Tămâioasă românească (TR). Each variety was used for the production of distillates in Romania, particularly in the Oltenia region (southwest of the country).

All six varieties were harvested from a vineyard located on the Olt Hill, in the Drăgășani wine region, Vâlcea County (44°39′40″N 24°15′38″E). This region enjoys a temperate climate, with weak Mediterranean influences in the south and a limited continental influence in the north. The average temperature during the hottest month, July, ranges between 21.5 °C and 22 °C. The characteristics of the climate are well-defined, featuring warm and scorching summers as well as severe winters. During the coldest months, January and February, the average temperature is between -2 °C and -2.3 °C. Temperature records indicate a maximum of 41.3 °C recorded on August 17, 1952, and a minimum of -33.5 °C on January 24, 1942. According to precipitation data, the region experiences a dry period in the summer, while the rest of the year benefits from abundant rainfall, totaling 578 mm annually. The predominant wind directions include north (14.8%), northeast (10.8%), southwest (8.6%), east (8.5%), and northwest (8.2%). Grapes were sampled at optimal technological maturity (21.7-22.2 Brix for neutral/semi-aromatic varieties and 22.5-23.7 Brix for Muscat-type aromatic varieties) between 10 and 15 September 2023.

2.2. Alcoholic fermentation of grape marcs

After harvest, the grapes were transported to the Faculty of Horticulture in Craiova, Department of Horticulture and Food Science. All grapes were vinified separately, and the resulting pomace, after crushing and pressing, was placed in vessels with a capacity of 150 L each. The vessels were filled to 70% of their volume.

Fermentation occurred spontaneously, triggered by the indigenous microflora of wine yeasts, at 20 °C ± 1 °C. The fermentation process was monitored daily, and it continued until the sugar concentration decreased to 4 °Brix.

2.3. Distillation of fermented grape marcs samples

The fermented grape pomace was distilled in a traditional copper still with an agitator, with a capacity of 80 L. Before starting the distillation, the still was sealed to prevent any vapor loss. Uniform and consistent distillations were achieved by gently heating the still at the beginning of the process, increasing the heat during the main flow, and reducing it toward the end. The water temperature in the cooling tank was maintained between 20 °C and 22 °C.

During the distillation of the fermented material, three main fractions were separated: the first fraction (heads), the middle fraction (heart of the distillate), and the tail fraction. The middle fraction was collected as the fresh

distillate. Distillates were stored in dark, tightly sealed bottles at 20 °C for 12 months. All distillates were analyzed using gas chromatography and following the method used by the Laboratory of the Department of Horticulture and Food science and the laboratory of National Institute for Cryogenics and Isotopic Technologies (I.C.S.I. Rm. Valcea).

2.4. Chemical reagents

Ultrapure water, HPLC-grade dichloromethane, methyl 10-undecenoate, anhydrous sodium sulfate, and sodium chloride were purchased from Sigma-Aldrich (Steinheim, Germany). Ultrapure HPLC-grade dichloromethane from Merck (Darmstadt, Germany) was used as the extraction solvent.

2.5. Analysis of the chemical quality parameters of grape brandy

In accordance with the official Romanian legislation regarding sampling methods and the performance of chemical and physical analyses of alcoholic beverages, the following analyses were carried out:

The alcoholic strength by volume was determined after distillation using a pycnometer (Publications Office of the European Union. Commission Regulation (EC) No 2870/2000).

Methanol content was analyzed following the European Community Reference Methods for the analysis of spirits, using gas chromatography (GC) with a flame ionization detector (FID). Methanol was determined by direct injection of the sample into a gas chromatography system (GC 2010 plus, Shimadzu, Japan). As an internal standard, 2-butanol was added to the spirit prior to injection. Methanol was separated using temperature programming on an SPB®-624 capillary column (30 m × 0.25 mm, df 1.40 µm) and detected with an FID detector.

The methanol concentration was quantified relative to the internal standard, using response factors obtained during calibration under the same chromatographic conditions as those used for the analysis of the spirit (Publications Office of the European Union. Commission Regulation (EC) No 2870/2000; SR 184-2:2010).

2.5.1. Extraction and concentration of minor volatile compounds

The volatile compounds were extracted following the method proposed by Raicevic et al., (2022). Fifty milliliters of distillate were mixed with 100 mL of ultrapure water, and 20 mL of the internal standard (methyl 10-undecenoate, 1 mg/L) was added. The mixture was then extracted with 40 mL of dichloromethane. Sodium chloride (10 g) was added, and the solution was stirred magnetically for 30 minutes. The layers were separated in a separatory funnel, and the organic layer was dried over anhydrous sodium sulfate for 2 hours. The extract was concentrated under a nitrogen stream to 1 mL and analyzed directly by GC/MS (Raicevic *et al.,* 2022).

2.5.2. GC/MS Analysis of minor volatile compounds

Quantitative determination of volatile compounds was performed using a gas chromatography system, a VARIAN 450 gas chromatograph GC-FID detector (flame ionization detection) with a set of 275°C temperature for both the column TG-WAXMS 60 m, ID 0.32 mm, film, 0.25 mm, injector temperature 150°C, column temperature 35°C, 3 min stand, climb to 20°C/min, up to 70 to 150°C with 27°/min, stand 2 minutes, climb 200°C, stand 2 minutes, climb to 240°C with 20°C/min and stands 6 min. The carrier gas was helium (1.2 ml/min flow rate). Injection volume is 1 µl. The identification was made by comparing the retention times of standards from the calibration curve.

2.6. Sensory analysis

The sensory evaluation of spirits samples was performed using the Buxbaum (Raicevic et al., 2022) model with a positive score of 20, which is the globally accepted method for the sensory evaluation of spirits. This model is based on five sensory analyses: color, clarity, distinctiveness, aroma, and taste. This is the most common method used in Western Balkan countries (Rankovic *et al*., 2004; Teševic *et al*.,

2005; Vulic *et al*., 2012; Matijaševic et al., 2013; Stoica *et al*., 2019).

The tasting panel consisted of a group of seven tasters, including three authorized evaluators and four unauthorized evaluators. The tasters were asked to evaluate the sensory attributes on a structured scale: color and clarity (maximum 1), distinctiveness (maximum 2), smell (maximum 6), and taste (maximum 10).

The evaluation was carried out in the tasting room of the Faculty of Horticulture of the University of Craiova. All conditions were ensured for a successful evaluation, including: space, air temperature of 22 °C, white light source, tasting utensils, etc. In order to obtain a uniform taste and smell, 30 ml samples of distillate were tasted at 12/16 °C in colorless, transparent, tulip-shaped glasses. The samples were coded and tested in a balanced order to eliminate the first-order transfer effect and evaluated on the same day. Since the institution lacks an ethics committee for the sensory evaluation of products, all participants provided written consent.

The neutral/semiaromatic grape brandy was evaluated before the Muscat-type aromatic grape brandy because of the stronger aroma of the Muscat brandy.

Between samples, water was provided for rinsing the mouth and pieces of bread for mitigating the previous taste.

2.7. Statistical analysis

Experimental data were subjected to One-way ANOVA analysis of variance, followed by the Tukey`s HSD test for $p< 0.05$ in Statgraphics Centurion 18 for Windows, to assess significant differences between the different type of brandy. All data were reported as mean ± standard deviation.

3. Results and discussions

3.1. Volatile compounds of brandy samples

The aromatic profile is a determining factor of the sensory quality of grape marc distillates and is essential for consumer perception. In grape marc distillates obtained from neutral/semi-aromatic and aromatic grape varieties, using combined gas chromatography–mass spectrometry methods (GC/MS), 29 volatile aromatic compounds were identified and quantified. These belong to several classes of chemical substances such as higher alcohols, esters, acids, aldehydes, acetals, and terpenes. Although studies have been conducted on the chemical composition of alcoholic beverages made from fruits and grape marc, only a few investigations have linked this composition to their sensory properties (Cortés, S. et al., 2009; Lukić, I. et al., 2012; Stoica, F. et al., 2019, 2022; Raicevic, D. et al., 2022).

3.1.1. Alcohols

The ethanol concentration (average alcoholic strength by volume) of brandy from semi-aromatic grapes reached 50.37% vol., while the alcoholic strength of brandy from neutral and aromatic grapes did not reach 50% vol. No statistically significant difference was found between the alcohol content of the analyzed brandies.

The methanol content in the analyzed samples ranged from 128.77 g/hL of 100% vol. alcohol to 148.09 g/hL in brandy from neutral/semi-aromatic grapes, and from 163.48 g/hL to 178.3 g/hL in brandy from aromatic grapes. The determined levels for all types of brandy were much lower than those stipulated in European legislation (Regulation (EU) 2019/787) and Romanian spirits law (2008, Ordinance no. 368/2008), where a methanol concentration below 1,000 g/hL of 100% vol. alcohol is indicated. Significant differences were observed only in two of the aromatic brandies (MA and MO) compared to the neutral or semi-aromatic ones (FR, FA, and S). All these values, within the legal limits, indicate that the raw material handling as well as the fermentation and distillation processes were appropriate [Silva et al., 2000; Soufleros *et al*., 2004; Stoica *et al*., 2019].

All methanol content values in the analyzed brandies fall within the same range (95.5–259 g/L) as reported for grape brandy (Rankovic *et al*., 2004; Cortés *et al.,* 2011; Lukic *et al.,* 2012; Milanov *et al*., 2014), but are lower than those reported for other fruit brandies (Silva *et al*., 2000; Soufleros *et al*., 2004, Geroyiannaki *et al*., 2007; Vulic *et al*., 2012; Arrieta-Garay *et al*., 2014).

Regarding higher alcohols, they were quantitatively the most abundant group of volatile compounds, conferring the specific aroma, taste, and basic character of alcoholic beverages (Cortés *et al.,* 2005; Christoph *et al*., 2007). Among all the higher alcohols analyzed (Table 1) in grape brandies, 2-phenylethanol and 1-hexanol had the highest contents.

Table 1. Concentration in alcohols in different types of grape brandies

Compound	FR	FA	S	TR	MA	MO
Ethanol. %vol	49.6±1.05	49.95±0.7	50.37±1.21	49.96±1.27	49.41±0.96	49.80±1.39
Methanol. g/hL of 100% vol. alcohol	132.59±7.46^{c}	128.77±3.79^{c}	148.09±4.44^{bc}	163.48±6.91^{ab}	171.37±6.92^{a}	178.3±9.07^{a}
Aroma compounds-high alcohol. mg/L						
1-hexanol	1.18±0.01^{c}	1.12±0.04^{c}	1.12±0.01^{c}	3.23±0.09^{a}	1.82±0.08^{b}	3.07±0.09^{a}
1-heptanol	0.22±0.03^{bc}	0.11±0.02^{c}	0.12±0.02^{c}	0.81±0.07^{a}	0.31±0.07^{b}	0.15±0.02^{c}
n-octanol	0.18±0.01^{d}	0.23±0.01^{c}	0.28±0.02^{b}	0.36±0.02^{a}	0.20±0.01^{cd}	0.13±0.01^{e}
n-decanol	0.12±0.01^{b}	0.11±0.01^{b}	0.10±0.01^{b}	0.14±0.02^{a}	0.08±0.004^{c}	0.06±0.01^{c}
Benzyl alcohol	n.d.	0.159±0.011	n.d.	n.d.	n.d.	n.d.
2 phenyl-ethyl alcohol	6.23±0.05^{d}	5.85±0.07^{e}	5.78±0.07^{e}	7.19±0.04^{a}	6.91±0.05^{b}	6.38±0.03^{c}
Total high alcohol	8.58±0.57^{c}	7.57±0.06^{d}	7.39±0.02^{d}	11.81±0.29^{a}	9.38±0.26^{b}	9.79±0.13^{b}

Note: Data are presented as mean±SD; n.d.= not detected; Different lowercase letters on the same row indicate significantly different means (HSD Tukey`s test at $p<0.05$) for the type of brandy from different grapevine varieties; Values without lowercase letters indicate that there were no significant differences between the analyzed variants.

A higher average content of 2-phenylethanol was detected in brandy from aromatic variety sample TR (7.19 mg/L in TR) compared to all other brandies. In neutral/semi-aromatic grape brandies, the highest value was found in FR (6.23 mg/L). The results are consistent with other studies (Soufleros *et al*., 2004; Cortés *et al.,* 2011; Lukic *et al.,* 2011; Matijaševic *et al*., 2019).

For hexanol, significant differences were observed between brandies from aromatic grape varieties (TR, MA, MO) and those from neutral/semi-aromatic varieties; MA had a significantly lower content compared to TR and MO. A relatively higher content of 1-hexanol compared to the other brandies was found in the TR distillate (3.23 mg/L). The results agree with the findings of Cacho et al., 2013 and Raicevic D. et al., 2022. Compared to other fruit brandies, 1-hexanol was detected in lower concentrations in the analyzed samples (Lukic et al., 2011; Cortés et al., 2011; Matijaševic et al., 2019), which can be explained by the use of well-ripened grapes and milder pressing during grape processing, probably influencing the good quality of the brandy.

A higher average content of 1-heptanol was found in aromatic brandies compared to those from neutral/semi-aromatic grapes. Higher contents of 1-heptanol and 2-phenylethanol were recorded in the TR and MA aromatic brandies, with significant differences between the two varieties.

3.1.2. Esters

The total ester content in the analyzed distillates differs significantly depending on the grape variety from which the marc was obtained (Table 2).

The results regarding the total volatile esters identified in this study show that their total content in brandies from aromatic grape varieties ranges from 19.9 mg/L in MA brandy (obtained from Muscat of Alexandria) to 23.87 mg/L in brandy obtained from Tămâioasă Românească (TR). Moreover, the total ester content is statistically significantly higher in brandies from aromatic grape varieties than in those from neutral/semi-aromatic varieties

Table 2. Concentration in esters in different types of grape brandies

Compound, mg/L	FR	FA	S	TR	MA	MO
Ethyl butirate	0.193±0.002^{b}	0.146±0.001^{e}	0.142±0.002^{e}	0.233±0.003^{a}	0.17±0.002^{d}	0.187±0.002^{c}
Ethyl lactate	0.42±0.03^{d}	0.34±0.03^{e}	0.32±0.02^{e}	0.64±0.01^{b}	0.56±0.01^{c}	0.78±0.01^{a}
Isoamyl acetate	0.16±0.005^{d}	0.19±0.004^{c}	0.13±0.003^{e}	0.35±0.003^{a}	0.29±0.01^{b}	0.34±0.01^{a}
Ethyl succinate	2.55±0.12^{b}	2.52±0.09^{b}	2.33±0.06^{b}	2.83±0.10^{a}	2.05±0.06^{c}	2.09±0.06^{c}
Ethyl hexanoate	1.99±0.14^{cd}	1.94±0.07^{d}	1.62±0.09^{e}	3.69±0.12^{a}	2.97±0.10^{b}	2.25±0.06^{c}
Ethyl octanoate	2.03±0.09^{d}	1.90±0.07^{d}	2.01±0.08^{d}	5.72±0.06^{a}	5.34±0.07^{b}	4.83±0.07^{c}
Ethyl nonanoate	0.05±0.01^{b}	0.05±0.01^{b}	0.06±0.002^{b}	0.11±0.02^{a}	0.09±0.02^{ab}	0.12±0.03^{a}
Ethyl decanoate	6.45±0.08^{b}	4.90±0.09^{d}	4.98±0.10^{d}	7.18±0.07^{a}	5.73±0.09^{c}	7.21±0.08^{a}
Ethyl dodecanoate	2.79±0.06^{b}	2.83±0.05^{b}	2.73±0.06^{b}	3.11±0.02^{a}	2.76±0.05^{b}	3.00±0.10^{a}
Total esters	16.63±0.26^{d}	14.82±0.14^{e}	14.33±0.13^{f}	23.87±0.09^{a}	19.9±0.12^{c}	20.81±0.08^{b}

Note: Data are presented as mean±SD; Different lowercase letters on the same row indicate significantly different means (HSD Tukey`s test at $p<0.05$) for the type of brandy from different grapevine varieties

The most abundant esters in all samples are the ethyl esters of medium-chain fatty acids. Among these, the highest values are for ethyl decanoate (between 4.90 mg/L - FA and 7.21 mg/L - MO), followed by ethyl octanoate (between 1.90 mg/L - FA and 5.72 mg/L - TR), ethyl dodecanoate (between 2.73 mg/L - S and 3.11 mg/L - TR), and ethyl hexanoate (between 1.62 mg/L - S and 3.69 mg/L - TR). Ethyl decanoate, ethyl hexanoate, and ethyl octanoate provide a pleasant fresh tropical fruit aroma, while ethyl dodecanoate gives a pear aroma and a characteristic fruity aroma (Matias-Guiua *et al*., 2018; Matijaševic *et al*., 2019).

The distillate obtained from MO shows comparative/similar values to those recorded for distillates from the TR variety regarding the content of isoamyl acetate, ethyl nonanoate, ethyl decanoate, and ethyl dodecanoate, with no statistically significant differences between the two brandies in this regard (Table 2).

The distillate obtained from Fetească Regală (FR) marc is also noteworthy for its higher ethyl butyrate content compared to the aromatic varieties MA and MO, with statistically significant differences.

Distillates obtained from FR, FA, and S do not show significant differences regarding the contents of ethyl succinate, ethyl nonanoate, and ethyl dodecanoate (Table 2).

Regarding the ethyl dodecanoate content, no statistically significant differences were observed between distillates obtained from the marc of neutral and semi-aromatic varieties (FR, FA, S) and the distillate obtained from MA. The ethyl dodecanoate content is significantly higher in distillates from TR and MO compared to distillates obtained from marc of neutral and aromatic varieties.

3.1.3. Terpenes

The values of the analyzed terpenes in the examined brandies are presented in Table 3. The results of the investigation showed that the total terpene content is significantly higher in brandies from aromatic grape varieties (1.66 mg/L - MA and 2.49 mg/L - TR) compared to brandies from neutral/semi-aromatic varieties (0.42 mg/L - FR and 0.91 mg/L - S). These results are supported by other studies (Stoica & Heroiu, 2003; Stoica *et al*., 2003; Doneva-Šapceska *et al*., 2006).

Linalool is the main component in all examined samples, in accordance with other research findings (Cacho *et al.,* 2013). It is followed by alpha-terpineol, geraniol, and citronellol. The linalool content, which contributes significantly to the aroma of roses, anise seeds, grapefruit, lime, and citrus, is significantly higher in aromatic brandies (0.68 mg/L - TR and 1.15 mg/L - MO) compared to brandies from neutral/semi-aromatic varieties (0.25 mg/L - FR and 0.34 mg/L - S). This means that the average linalool concentration in aromatic brandies is well above the perception threshold (0.05 mg/L) (Diéguez *et al*., 2003; Raicevic *et al*., 2022). The obtained values are in agreement with other studies (Matijašević *et al.,* 2019; Stoica *et al*., 2022).

A particular feature is observed with alpha-terpineol, which, although present in all

distillates, reaches its highest values in Tămâioasă Românească (TR) brandy. Moreover, in aromatic varieties, for the two Muscats - Muscat of Alexandria and Muscat Ottonel - the dominant terpene is linalool, whereas in Tămâioasă Românească and Sauvignon (in much lower amounts compared to TR), alpha-terpineol is dominant. Alpha-terpineol provides floral aromas, as well as notes of iris and pine forest.

Table 3. Concentrations of the main terpenes in different types of grape brandies

Compund, mg/L	FR	FA	S	TR	MA	MO
α-terpineol	0.12±0.01^{d}	0.24±0.01^{d}	0.40±0.02^{c}	1.19±0.10^{a}	0.52±0.03^{c}	0.67±0.07^{b}
Linalool	0.25±0.01^{e}	0.28±0.004^{e}	0.34±0.01^{d}	0.68±0.01^{c}	0.89±0.03^{b}	1.15±0.01^{a}
Geraniol	0.021±0.003^{e}	0.022±0.004^{e}	0.070±0.002^{d}	0.37±0.003^{a}	0.15±0.01^{c}	0.21±0.001^{b}
Citronellol	0.030±0.002^{d}	0.051±0.001^{d}	0.091±0.002^{c}	0.25±0.01^{a}	0.11±0.01^{c}	0.15±0.01^{b}
Total terpenes	0.42±0.02^{e}	0.59±0.01^{e}	0.91±0.02^{d}	2.49±0.12^{a}	1.67±0.06^{c}	2.19±0.09^{b}

Note: Data are presented as mean±SD; Different lowercase letters on the same row indicate significantly different means (HSD Tukey`s test at $p<0.05$) for the type of brandy from different grapevine varieties

The citronellol content, which together with linalool is one of the most important terpenic compounds, is below 0.10 mg/L in brandies from neutral/semi-aromatic varieties. In brandies from aromatic varieties, the citronellol content ranges between 0.11 mg/L - MA and 0.25 mg/L - TR. These values are in line with those reported by other researchers (Diéguez *et al*., 2003; Cacho *et al*., 2013) (0.07- 43.53 mg/L) and are significantly above the perception threshold (0.018 mg/L).

The geraniol content, with values below 0.37 mg/L in aromatic brandies, will also contribute to floral aromas, especially rose, as its concentration is above the perception threshold (0.13 mg/L).

The presented results confirm the conclusions of (Tsakiris *et al*., 2014; Matijašević *et al*., 2019; Stoica *et al*., 2019, 2022; Raicevic *et al*., 2022), according to which the aroma of brandy from aromatic grapes is directly related to various monoterpenes, such as alpha-terpineol, linalool, nerol, geraniol, and citronellol.

3.1.4. Volatile acids and aldehydes

The values of total fatty acids identified (Table 4) fluctuate within similar ranges in the distillates obtained from aromatic grape varieties (3.60 mg/L - MA and 5.12 mg/L - TR) and those from neutral/semi-aromatic varieties (3.74 mg/L - FR and 5.43 mg/L - S). Regarding medium-chain fatty acids, decanoic, octanoic, dodecanoic, and hexanoic acids were identified in all brandy samples.

Medium-chain fatty acids usually do not have a significant effect on the aroma of distillates due to their relatively high odor perception thresholds, determined at 8 mg/L for decanoic acid and 15 mg/L for octanoic acid (Lukić *et al*., 2011).

In our research, decanoic acid had the highest values in all samples of distillates (neutral/semi-aromatic and aromatic), compared to the other fatty acids. It is followed by octanoic acid, dodecanoic acid, and hexanoic acid, values that are in agreement with findings from other studies (Christoph *et al.*, 2007; Lukić *et al*., 2011, 2012; Matijašević. *et al*., 2019).

The distillate obtained from Tămâioasă Românească recorded the highest contents of octanoic acid and dodecanoic acid, with significant differences compared to the distillates produced both from aromatic varieties and from neutral/semi-aromatic varieties. The distillate obtained from Sauvignon stands out through significantly higher contents of decanoic acid and hexadecanoic acid compared to the other distillates.

Regarding long-chain fatty acids, which together with glycerol contribute to the aroma

and body of the distillate through oiliness and viscosity, hexadecanoic acid (palmitic) shows average values above 0.40 mg/L in all distillate samples (Table 4), which is consistent with other similar research (Lukić *et al*., 2011, 2012; Matijašević *et al.,* 2019; Raicevic *et al*., 2022).

The concentrations of aldehydes in the distillates obtained from neutral/semi-aromatic grape varieties and from aromatic varieties are presented in Table 4. The total content of identified carbonyl compounds is not significantly different between the brandies obtained from aromatic varieties and those obtained from neutral/semi-aromatic varieties.

The main carbonyl compound in distillates, acetaldehyde, is a direct product of alcoholic fermentation and usually represents about 90% of the total aldehyde content (Silva *et al*., 2000; Spaho, 2017).

No significant differences were found between the acetaldehyde contents of the distillates from neutral/semi-aromatic varieties (197.73 mg/L of 100% vol. alcohol - FA and 220.1 mg/L of 100% vol. alcohol - S) and those from aromatic varieties (198.33 mg/L of 100% vol. alcohol - MA and 226.20 mg/L of 100% vol. alcohol - MO). These results are in agreement with those described in the literature (Hernández-Gómez *et al*., 2005; Lukić. *et al*., 2011, 2012; Raicevic *et al*., 2022).

The values determined in this study are significantly lower compared to the official limits for fruit distillates adopted by the European Council (Regulation (EU) 2019/787).

A significantly higher concentration of benzaldehyde was found in the brandy obtained from the aromatically neutral variety (0.27 mg/L-FA), while the other distillates did not differ in terms of their benzaldehyde content. The benzaldehyde content, which contributes to bitter almond, marzipan, and cherry aromas, identified in our study in the grape pomace distillates, is consistent with data reported in the literature (Christoph *et al*., 2007; Cortés *et al.,* 2009; Bortoletto, A.M. *et al*., 2016). Benzaldehyde is not desirable in large quantities, but when present in small amounts, it contributes to the complexity of the aroma.

Table 4. Concentrations of volatile acids and aldehydes in different types of grape brandies

Compund, mg/L	FR	FA	S	TR	MA	MO
			Volatile acids			
Hexanoic acid	0.51±0.02^{c}	0.53±0.02^{c}	0.59±0.05^{bc}	0.77±0.06^{a}	0.58±0.05^{c}	0.69±0.04^{ab}
Octanoic acid	0.76±0.02^{e}	0.82±0.01^{cd}	0.88±0.01^{c}	1.02±0.04^{a}	0.68±0.01^{f}	0.94±0.02^{b}
Decanoic acid	1.61±0.02^{e}	1.94±0.02^{cd}	2.80±0.02^{a}	1.89±0.01^{d}	1.30±0.03^{f}	2.22±0.07^{b}
Dodecanoic acid	0.45±0.03^{e}	0.51±0.02^{d}	0.66±0.01^{c}	0.97±0.02^{a}	0.62±0.02^{c}	0.74±0.01^{b}
Hexadecanoic acid	0.41±0.01^{c}	0.41±0.01^{c}	0.51±0.02^{a}	0.45±0.01^{b}	0.43±0.01^{bc}	0.46±0.02^{b}
Total acids	3.74±0.07^{d}	4.22±0.03^{c}	5.43±0.05^{a}	5.12±0.03^{b}	3.60±0.08^{d}	5.05±0.06^{b}
			Aldehydes			
Acetaldehyde	212.00±12.49	197.73±10,74	220.10±9.90	218.30±7.05	198.33±11.95	226.20±13.35
Benzaldehyde	0.19±0.01^{b}	0.27±0.02^{a}	0.21±0.04^{b}	0.20±0.02^{b}	0.18±0.01^{b}	0.18±0.01^{b}
Furfural	0.15±0.01^{c}	0.30±0.03^{b}	0.52±0.04^{a}	0.31±0.02^{b}	0.47±0.05^{a}	0.18±0.02^{c}
Total aldehydes	212.30±12.41	198.30±10.76	220.79±9.89	218.80±7.09	198.95±12.01	226.56±13.35

Note: Data are presented as mean±SD; Different lowercase letters on the same row indicate significantly different means (HSD Tukey`s test at $p<0.05$) for the type of brandy from different grapevine varieties

The furfural content in the analyzed distillates ranges between 0.15 and 0.52 mg/L, being significantly lower than the perception threshold of this compound, which is 150 mg/L. Significantly lower amounts of furfural were recorded in the distillates from FR and MO. Furfural is a normal constituent of fruits and can be used as an indicator of the natural origin of the distillate; however, increased concentrations may contribute to the appearance of "roasted"

notes in the spirit (Tsakiris *et al*., 2016; Spaho, 2017). These results are in agreement with those reported in the literature (Ranković *et al*., 2004; Tešević *et al*., 2005; Hernández-Gómez *et al*., 2005; Lukić *et al*., 2011; Cacho. *et al*., 2013; Cortés *et al*., 2011; Arrieta-Garay *et al*., 2014; Raicevic *et al*., 2022).

3.2. Sensory analysis

The sensory characteristics of the examined brandies are presented in Table 5.

All distillates obtained from neutral/semi-aromatic or aromatic grape pomace are colorless and clear, exhibiting excellent clarity and being remarkable for the characteristic aromas and flavors of these types of beverages. In the sensory evaluation, all samples received the maximum score (1.0) for color and clarity, reflecting the superior visual quality of the distillates.

From the perspective of *Distinction*, significant differences were recorded only for distllate from TR compared with distillate from FR.

Brandy from aromatic grape varieties stood out with a relative higher average score for aroma (5.78), due to the distinctive character of Muscat-type grape varieties, which impart a pronounced and intensely fruity aroma to the distillate, appreciated by consumers for its olfactory finesse and expressiveness, however, the differences were not statistically significant between the brandies from neutral/semi-aromatic varieties and those from aromatic varieties (Table 5).

Table 5. Sensory analyses of grape brandies (average values _ STD)

Type of grape brandy	Colour (max 1)	Clarity (max 1)	Distintion (max 2)	Odour (max 6)	Taste (max 10)	Total (max 20)
FR	1.0	1.0	1.81±0.04^{b}	5.59±0.17	9.23±0.13^{b}	18.62±0.22^{c}
FA	1.0	1.0	1.83±0.03^{ab}	5.63±0.12	9.37±0.18^{b}	18.83±0.11^{bc}
S	1.0	1.0	1.88±0.04^{ab}	5.70±0.10	9.48±0.07^{ab}	19.07±0.17^{ab}
Averages	1.0	1.0	1.84±0.03	5.64±0.10	9.36±0.09^{B}	18.84±0.02^{B}
TR	1.0	1.0	1.90±0.03^{a}	5.81±0.10	9.77±0.08^{a}	19.49±0.19^{a}
MA	1.0	1.0	1.84±0.02^{ab}	5.75±0.08	9.58±0.11^{ab}	19.18±0.06^{ab}
MO	1.0	1.0	1.86±0.03^{ab}	5.79±0.10	9.68±0.07^{ab}	19.33±0.16^{a}
Averages	1.0	1.0	1.87±0.02	5.78±0.08	9.68±0.07^{A}	19.32±0.13^{A}

Note: Data are presented as mean±SD; Different superscript small letters on the same column indicate significantly different means (HSD Tukey`s test at $p<0.05$) for the type of brandy from different grapevine varieties; different superscript capital letters indicate significantly different means (HSD Tukey`s test at $p<0.05$) for the type of brandy (neutral/semi aromatic and aromatic).

Regarding taste, both types of brandies-those from neutral/semi-aromatic grapes and aromatic grapes-achieved a high average score above 9. The distillates from aromatic grapes were better appreciated, achieving an average score of 9.68, significantly higher compared to the distillates from neutral/semi-aromatic varieties. The distillate from TR stands out in terms of taste, with an average score of 9.77 points.

The average total score obtained by the brandies from aromatic varieties (19.32) was significantly higher compared to the brandies from neutral/semi-aromatic varieties (18.84), most likely due to the greater taste complexity of the distillates from aromatic varieties. It is also noteworthy that there were no significant differences between the average total scores of the distillates from aromatic varieties and the distillate from Sauvignon, indicating similar olfactory–taste qualities of these distillates, as perceived and appreciated by consumers.

These results demonstrate that Romanian brandies produced from grape pomace have an exceptional sensory profile, characterized by an intense and pleasant aroma, high drinkability, and a perfectly balanced harmony between flavor and taste. All these qualities make both types of analyzed brandies-particularly those

from Tămâioasă Românească and Muscat Ottonel-true unique brands, representative of the tradition and specific characteristics of their origin area in southwestern of Romania, in Drăgășani vineyard region.

4.Conclusions

All the analyzed grape marc distillates were produced using the same technology, the difference between them being determined by the grape variety used - three neutral/semi-aromatic grape varieties (Fetească Regală - FR, Fetească Albă - FA, and Sauvignon - S) and three aromatic varieties (Tămâioasă Românească - TR, Muscat of Alexandria - MA, and Muscat Ottonel - MO).

The content of volatile aromatic compounds (higher alcohols, volatile esters, and terpenes) was higher in the distillates obtained from aromatic varieties than in those from neutral/semi-aromatic grape varieties.

A particular characteristic is shown by α-terpineol which, although present in each variety and implicitly in each distillate, reaches the highest levels in the Tămâioasă Românească (TR) distillate. Moreover, in aromatic varieties it can be observed that in the two Muscats - Muscat of Alexandria and Muscat Ottonel - the dominant terpene is linalool, whereas in Tămâioasă Românească the dominant compound is α-terpineol.

The results of the study showed that the grape variety used for producing the distillates influences certain sensory characteristics (smell and taste).

Distillates from aromatic varieties stood out due to a higher average score for aroma, owing to the distinctive character of Muscat-type grape varieties, which impart a pronounced and intensely fruity aroma to the distillate - highly appreciated by consumers for its finesse and expressive olfactory profile.

Sensory analyses showed that all distillates belong to the category of high-quality spirits and exhibited uniform quality. Both types of distillates were distinguished by excellent drinkability, full and balanced flavor, and overall harmony in the sensory profile.

These results indicate a high quality (volatile aromatic compounds and sensory properties) of the analyzed Romanian distillates, and the aromatic ones (TR and MO) could be certified as a new traditional product—a distinctive brand in Romania, comparable to Grappa from Italy.

5.References

Arrieta-Garay, Y., Blanco, P., López-Vázquez, C., Rodríguez-Bencomo, J.J., Pérez-Correa, J.R., López, F., Orriols, I. (2014). Effects of Distillation System and Yeast Strain on the Aroma Profile of Albarinño (Vitis vinifera L.) Grape Pomace Spirits. *Journal of Agricultural and Food Chemistry*, 62, 10552–10560.

Cacho, J., Moncayo, L., Palma, J.C., Ferreiraa, V., Culleréa, L. (2013). Comparison of the aromatic profile of three aromatic varieties of Peruvian pisco (Albilla, Muscat and Torontel) by chemical analysis and gas chromatography-olfactometry. *Flavour and Fragrance Journal*, 28, 340–352.

Christoph, N., Bauer-Christoph, C. (2007). Flavour of Spirit Drinks: Raw Materials, Fermentation, Distillation and Ageing. *Flavours and Fragrances*; Springer: Berlin, Germany, pp. 219–239.

Cichi D.D**.,** Stoica F., Căpruciu R., Cichi M., (2022). Ampelographic and agronomic variability within the 'Tămâioasa românească' cultivar. *Scientific Papers. Series B, Horticulture.* Vol. LXVI, No. 1, 260- 267

Cortés, S., Gil, M.L., Fernández, E. (2005). Volatile composition of traditional and industrial Orujo spirits. *Food Control*, 16, 383–388

Cortés, S., Gil, M. L., Fernández, E. (2009). Chemical affinities between the major volatile compounds present in a grape pomace distillate, *Journal of the Science of Food and Agriculture*, 89, 1221-1226.

Cortés, S., Rodríguez, R., Salgado, J.M., Domínguez, J.M. (2011). Comparative study between Italian and Spanish grape marc spirits in terms of major volatile compounds. *Food Control*, 22, 673–680.

Diéguez, S.C., De La Peña, M.L.G., Gómez, E.F. (2003). Approaches to spirit aroma: Contribution of some aromatic compounds to the primary aroma in samples of orujo spirits. *Journal of Agricultural and Food Chemistry*, 51, 7385–7390.

Geroyiannaki, M., Komaitis, M.E., Stavrakas, D.E., Polysiou, M., Athanasopoulos, P.E., Spanos, M. (2007). Evaluation of acetaldehyde and methanol in greek traditional alcoholic beverages from varietal fermented grape pomaces (Vitis vinifera L.). Food Control, 18, 988–995.

Gheorghiţă, M., Camelia Muntean, Băducă Cîmpeanu, C. (2002). Oenologie 2. Ed. Sitech, Craiova.

Hernández-Gómez, L. F., Úbeda-Iranzo, J., García-Romero, E., Briones-Pérez, A., (2005). Comparative production of different melon distillates: Chemical and sensory analyses. *Food Chemistry*, 90, 115-125.

Lukic, I., Milicevic, B., Banovic, M., Tomas, S., Radeka, S., Peršuric, C. (2011). Secondary Aroma Compounds in Fresh Grape Marc Distillates as a Result of Variety and Corresponding Production Technology. *Food Technology and Biotechnology,*49, 214–227.

Lukic, I., Milicevic, B., Tomas, S., Radeka, S., Peršuric, Đ. (2012). Relationship between volatile aroma compounds and sensory quality of fresh grape marc distillates, *Journal of the Institute of Brewing*., 118, 285–294.

Matias-Guiua, P., Rodríguez-Bencomoa, J.J., Pérez-Correab, J.R., Lópeza, F. (2018). Aroma profile design of wine spirits: Multi-objective optimization using response surface methodology. *Food Chemistry*, 245, 1087–1097.

Matijaševic, S., Todic, S., Beslic, Z., Rankovic-Vasic, Z. (2013). Volatile components of grape brandies produced from Muscat table grapevine (Vitis vinifera L.) cultivars. *Bulgarian Journal of Agricultural Science*, 19, 783–791.

Matijaševic, S., Popovic-Djordjevic, J., Ristic, R., Cirkovic, D., Cirkovic, B., Popovic, T. (2019). Volatile Aroma Compounds of Brandy 'Lozovaca' Produced from Muscat Table Grapevine Cultivars (Vitis vinifera L.). *Molecules*, 24, 2485.

Milanov, G., Beleski, K., Cvetkovic, J., Nedelkovski, D. (2014). Impact of grape variety and technological procedures on the quality of grape brandies. *Agroznanje*, 15, 425–438.

Ordinul nr. 368/2008 - Normele privind definirea, descrierea, prezentarea şi etichetarea băuturilor tradiţionale româneşti, https://legislatie.just.ro/Public/DetaliiDocument/95128

Plutowska, B., Biernacka, P., Wardencki, W. (2010). Identification of Volatile Compounds in Raw Spirits of Different Organoleptic Quality. *Journal of the Institute of Brewing.*, 116, 433–439.

Publications Office of the European Union. Commission Regulation (EC) No 2870/2000 of 19 December 2000 laying down Community reference methods for the analysis of spirits drinks. *Official Journal - EUR*, L333, 20–46.

Raicevic, D., Popovic, T., Dejan, J., Šukovic, D., Pajovic-Ščepanovic, R. (2022). The Impact of Type of Brandy on the Volatile Aroma Compounds and Sensory Properties of Grape Brandy in Montenegro, *Molecules* 2022, 27, 2974. https://doi.org/10.3390/molecules27092974

Rankovic, V., Palic, R., Živkovic, J., Mosic, I., Stankovic, S., Stojanovic, G. (2004) Investigation of the impact of grape cultivars on the grape brandies quality. *Phys. Chem. Technol.*, 3, 61–66.

Spaho, N. (2017). Distillation Techniques in the Fruit Spirits Production. In Distillation—Innovative Applications and Modeling; IntechOpen: London, UK, Chapter 6.

Silva, M.L., Macedo, A.C., Malcata, F.X. (2000) Review: Steam distilled spirits from fermented grape pomace. *Food Science and Technology International*, 6, 285–300.

Soufleros, E.H., Mygdalia Ageliki, S., Natskoulis, P. (2004). Characterization and safety evaluation of the traditional Greek fruit distillate "Mouro" by flavor compounds

and mineralanalysis. *Food Chemistry*, 86, 625–636.

Stoica, F., Muntean, C., Băducă, C. (2019), 2019- Studies on the chemical and sensorial composition of the grape marc narural distillates, *Annals of University of Craiova, Agriculture, Montanology and Cadastru,* Series, vol. XLIX, p.191-196

Stoica, F., Băducă-Cîmpeanu, C., Cichi, D. D., (2022). Comparative behavior of volatile and aromatic compounds of Tămâioasă românească and Muscat Ottonel grape marcs fermented during traditional still distillation, Scientific Papers. Series b, Horticulture. vol. LXVI, no. 2.
https://horticulturejournal.usamv.ro/pdf/2022/issue_2/art25.pdf

Teševic, V., Nikicevic, N., Jovanovic, A., Djokovic, D., Vujisic, L., Vuckovic, I., Bonic, M. (2005). Volatile Components of Plum Brandies. *Food Technology and Biotechnology*., 43, 367–372.

Tsakiris, A., Kallithraka, S., Kourkoutas, Y. (2014). Grape brandy production, composition and sensory evaluation. *Journal of the Science of Food and Agriculture*, 94, 404–414.

Vulic, T., Nikicevic, N., Stankovic, L., Velickovic, M., Todosijevic, M., Popovic, B., Uroševic, I., Stankovic, M., Beraha, I., Teševic,V. (2012). Chemical and Sensorial Characteristics of Fruit Spirits Produced from Different Black Currant (Ribes Nigrum L.) and Red Currant (Ribes Rubrum L.) Cultivars. *Macedonian Journal of Chemistry and Chemical Engineering*, 31, 217–227.

Wei, X.F, Ma, X.L., Cao, J.H., Sun, X.Y., Fang, Y.L. (2018), Aroma characteristics and volatile compounds of distilled Crystal grape spirits of different alcohol concentrations: Wine sprits in the Shangri-La region of China. *Journal of Food Science and Technology*, 38 (Suppl. S1),50–58.